

**Identification of dengue virus (DENV) NS1
protein residues involved in its cellular
secretion and host factors involved in NS1
protein *N*-glycosylation**

Tan Eng Kuan Brandon

Department of Molecular and Biomedical Science

School of Biological Sciences

The University of Adelaide, Australia



THE UNIVERSITY

of **ADELAIDE**

September 2023

Table of Contents

List of Figures/Tables	IX
Abstract	XIII
Declaration	XV
Acknowledgements.....	XVI
Presentations, Publications and Awards during the PhD candidature... 	XVII
Abbreviations.....	XIX
Amino acid abbreviations.....	XXIII
Material Providers	XXV
Chapter 1:	1
1. Introduction:	1
1.1 Dengue.....	2
1.1.1 History and Epidemiology of Dengue	2
1.1.2 Transmission of Dengue virus (DENV)	4
1.1.3 Emergence of Aedes aegypti as an effective disease vector species	5
1.1.4 DENV clinical manifestations	7
1.1.5 DENV pathogenesis.....	8
1.2 Molecular Biology of Dengue virus	9

1.2.1 Genome structure	9
1.2.2 Structural Proteins	10
1.2.2.a Capsid.....	10
1.2.2.b Membrane	11
1.2.2.c Envelope.....	13
1.2.3 Non-Structural Proteins	14
1.2.3.a NS1.....	14
1.2.3.b NS2A	16
1.2.3.c NS2B.....	17
1.2.3.d NS3	18
1.2.3.e NS4A.....	18
1.2.3.f NS4B	19
1.2.3.g NS5	21
1.2.4 DENV replication cycle.....	22
1.2.5 NS1 Maturation and Subcellular Targeting.....	23
1.3 Lipid Rafts	24
1.3.1 Roles of lipid rafts.....	24
1.3.2 Association of DENV NS1 protein with lipid rafts	25
1.4 Glycosylation	26
1.4.1 DENV protein glycosylation	26
1.4.2 Glycosylation and NS1 secretion.....	27

1.5 Host factors.....	29
1.5.1 Host factors and DENV	29
1.5.2 Interaction of DENV NS1 with human host factors	30
1.6 Roles of NS1 in DENV life cycle	32
1.6.1 Roles of NS1 in viral replication and infectious particle production	32
1.6.2 Replication independent characterisation of DENV VP formation	33
1.7 Secreted NS1 (sNS1) and its many roles in DENV pathogenesis.....	34
1.8 The application of APEX peroxidase-catalysed proximity labelling in characterisation of protein microenvironments in situ	40
1.9 The research gap	41
1.9.1 Project Aims	42
Chapter 2:	43
2. Materials and Methods	43
2.1 General Molecular Biology Methods	44
2.1.1 Mini-preparation of plasmid DNA	44
2.1.2 Midi-preparation of plasmid DNA	44
2.1.3 Chemical transformation of competent bacteria with plasmid DNA	45
2.1.4 Diagnostic restriction digest of plasmid DNA.....	45
2.1.5 Agarose gel electrophoresis.....	46
2.1.6 Gel extraction.....	46

2.1.7 DNA Ligation	47
2.1.8 Phosphorylating and annealing HiBiT Oligonucleotides	47
2.1.9 Polymerase Chain Reaction (PCR).....	48
2.1.9.1. Q5® High-Fidelity PCR	48
2.1.9.2 GeneMorph II Random Mutagenesis.....	48
2.1.10 PCR product and DNA fragment purification	49
2.1.11 Plasmid DNA dephosphorylation	49
2.1.12 NEBuilder HiFi DNA Assembly	50
2.1.13 Colony PCR	50
2.1.14 Western Immunoblotting	51
2.1.15 Enhanced Chemiluminescence (ECL) Western Immunoblotting.....	52
2.1.16 LI-COR Fluorescence Western Immunoblotting.....	53
2.1.17 Stripping and reprobing membranes.....	53
2.1.18 Quantification of nucleic acids	54
2.1.19 Production and isolation of SP6 RNA polymerase-derived RNA transcripts	54
2.1.20 RNA extraction	55
2.1.21 Sanger sequencing	55
2.1.22 Graph preparation and statistical analyses.....	56
2.2 Cell culture techniques	56
2.2.1 Cryopreservation of cell lines	56
2.2.2 Resuscitation of frozen cell lines	56

2.2.3 Maintenance of cell lines in culture medium.....	57
2.2.4 Trypan blue-based enumeration of cells.....	57
2.2.5 Transfection of cells.....	58
2.2.5.1 Lipofectamine 2000/ Lipofectamine 3000.....	58
2.2.5.2 DMRIE-C.....	58
2.2.5.3 PEI polyethylenimine	58
2.2.6 HiBiT luciferase reporter assays.....	60
2.2.7 Generation of lentiviruses.....	60
2.2.8 Immunofluorescence.....	61
2.2.9 Confocal imaging microscopy.....	62
2.2.10 Renilla luciferase reporter assays	62
2.2.11 Lentiviral-based trans-complementation assay.....	63
2.2.12 Focus forming assay	64
2.2.13 APEX2 catalysed proximity labelling	65
2.2.13.1 Full length APEX2-NS1 constructs.....	65
2.2.13.2 pIROD-APEX2-NS1 constructs	66
Chapter 3:	67
3. Identification of NS1 secretion impairing via random point mutagenesis and HiBiT luciferase reporter-based assays	67
3.1 Introduction.....	68

3.2 Results	69
3.2.1 PCR-based random point mutagenesis of wildtype DENV-2 NS1 cDNA	69
3.2.2 Screening of bacterial colonies for clones containing the NS1 insert via colony PCR... 70	
3.2.3 HiBiT luciferase reporter-based assay of NS1 protein secretion for mutagenized NS1 expression constructs	71
3.3 Discussion	76
Chapter 4:	79
4. Analysis and Characterization of identified residues within DENV NS1 protein that are essential for its secretion	79
4.1 Analyses of putative secretion-impairing point mutations within DENV-2 NS1 via <i>in silico</i> analyses, Western blotting and high-resolution confocal imaging	80
4.1.1 <i>In silico</i> analyses indicate that the majority of NS1 secretion-impairing mutations are primarily located within the β -ladder domain.....	80
4.1.2 Wildtype NS1 and NS1 secretion-impairing mutants displayed strong colocalisation within the endoplasmic reticulum (ER)	85
4.2 Investigating the effects of these identified NS1 secretion impairing mutations on DENV RNA replication and infectious virus production	89
4.2.1 Selected NS1 secretion-impairing mutants were shown to not support infectious virus production	89
4.2.2 The wildtype full-length DENV-2 reporter virus (pFKDV _s -R2A) did not support DENV RNA replication and thus DENV RNA replication was assessed via utilisation of DENV-2 sub-genomic replicon construct (sgDV _s -R2A).....	91

4.3 Investigating the relationship between impairing NS1 secretion mutations and DENV RNA replication and infectious virus production.....	93
4.4 Western Blot analysis of putative NS1 secretion-impairing mutations	103
4.5 Utilisation of a replication-independent NS1-NS5 polyprotein expression system (pIRO) to further characterise NS1 secretion-impairing mutants.....	107
4.6 Discussion	111
Chapter 5:	117
5. Towards identification of host factors that are associated with NS1 secretion and glycosylation via an APEX2-catalysed proximity labelling approach coupled with LC-MS/MS.....	117
5.1 Emergence of APEX2-based proximity labelling as a powerful in situ approach to map protein microenvironments	118
5.2 How does APEX2-catalysed proximity labelling work?	119
5.3 Utilisation of the established pFKDVs-APEX2-NS1 virus construct for the APEX2-catalysed proximity labelling approach.....	121
5.4 Utilisation of a different APEX2-proximity biotinylation strategy involving the pIROD-APEX2-NS1 expression system.....	129
5.5 Discussion	132
Chapter 6:	136
6. General Discussion and Future Directions	136

Appendices:	146
Appendix I: Buffers, Media and Solutions	147
Appendix II: Primers	152
Appendix III: Antibodies and Dyes	154
Appendix IV: Supplementary Figures	156
Appendix V: Plasmid Maps	161
Appendix VI: DENV-2 NS1 processed DNA/peptide sequences	170
Appendix VII: Published experimental manuscript	172
References	194

List of Figures/Tables

Figure 1.1.2.1 Various transmission cycles of DENV.....	5
Figure 1.1.3.1 Schematic diagram of the main factors that enable <i>Aedes aegypti</i> to be a highly effective diseases vector for dengue and other related arboviruses.....	7
Figure 1.2.1.1 The DENV genome organisation and membrane topology of translated proteins.....	9
Figure 1.2.2.1 The structure of DENV capsid protein.....	11
Figure 1.2.2.2 Different stages of DENV structure and respective pH-dependent conformation of E protein (green) and the predomain (pr) protein (blue) states throughout the life cycle.....	13
Figure 1.2.3.1 The three-dimensional structure of the flavivirus NS1	16
Figure 1.2.4.1 Overview of the DENV replication cycle	22
Figure 1.7.1.1 Schematic diagram of the flavivirus NS1-mediated disease pathogenesis outlining flavivirus NS1-mediated endothelial cell-dependent hyperpermeability and tissues-specific vascular leakage	37
Table 2.2.5.1 Various transfection reagents.....	59
Figure 3.0.1 Schematic diagram of the random mutagenesis-coupled HiBiT luciferase experimental workflow	68

Figure 3.0.2 Workflow of the PCR-based random point mutagenesis approach for generation of NS1-HiBiT expression plasmids containing point mutations within the NS1.....	70
Figure 3.0.3 An example of the colony PCR results following gel electrophoresis.....	71
Figure 3.0.4 Molecular basis of the DENV-2 NS1-HiBiT split luminescent peptide tag assay	72
Table 3.0.5 Brief overview of the Sanger sequencing results depicting the mutation frequency for the selected 100 NS1 secretion-impairing mutant clones	74
Figure 3.0.6 The identification of NS1 mutant clones with impaired NS1 protein secretion..	75
Figure 4.1.1 <i>In silico</i> analyses of the identified NS1 secretion-impaired mutants	81
Figure 4.1.2 Multiple sequence alignment of various NS1	82
Figure 4.1.3 Several NS1 secretion-impairing mutants were not detected intracellularly by Western blotting.....	84
Figure 4.1.4 Identified secretion-impairing mutations within DENV NS1 do not impact its localisation to the ER.....	86
Figure 4.1.5 Identified secretion-impairing point mutations within DENV NS1 do not impact on its localisation to the ER via cell-based population analyses	88
Figure 4.2.1 NS1 secretion-impairing mutations V220D and A248V also prevented infectious virus production	90
Figure 4.2.2 NS1 secretion-impairing mutations V220D and A248V prevent RNA replication activity	92
Figure 4.3.1 Schematic diagram of DENV constructs.....	94
Figure 4.3.2 Workflow of the DENV-based trans-complementation approach	95

Figure 4.3.3 The initial dual transfection trans-complementation approach failed to support robust DENV RNA replication.....	97
Figure 4.3.4 A lentiviral vector-based trans-complementation strategy supports robust DENV RNA replication.....	99
Figure 4.3.5 The majority of NS1 secretion-impairing mutants appeared to be RNA replication incompetent.....	101
Figure 4.4.1 Western blot analysis of NS1 mutants using an anti-HiBiT peptide tag antibody confirmed their secretion-impairing phenotypes	105
Figure 4.5.1 Characterisation of the indicated NS1 mutants within the replication-independent expression system (pIRO) via high resolution confocal imaging and Western immunoblotting.....	108
Figure 4.5.2 Colocalisation studies showed no apparent differences in NS1-NS4B colocalisation among the pIRO-derived NS1 mutants	109
Figure 5.2.1 Diagram illustrating the mechanism of action of the hydrogen peroxide-dependent catalysed proximity labelling approach via the engineered ascorbic acid peroxidase reporter APEX2	120
Figure 5.3.1 Schematic diagram of the APEX2-NS1 mediated proximity biotinylation experimental workflow prior to preparation of biotinylated proteins for mass spectrometry experiments	121
Figure 5.3.2 Characterisation of APEX2-NS1-mediated proximity biotinylation in DENV2 reporter virus-infected cells	123
Figure 5.3.3 Characterisation of APEX2 NS1-mediated proximity biotinylation in DENV2 reporter virus-infected cells via streptavidin-Western blotting	124

Figure 5.3.4 Analysis of the localisation of NS1 and APEX2 biotinylated proteins within DENV reporter virus-infected cells via confocal microscopy	126
Figure 5.3.5 Viral fitness of both APEX2-NS1 glycosylation mutants, N130A and N207A was markedly attenuated in comparison to the wildtype APEX2-NS1	128
Figure 5.4.1 Schematic illustration of the pIROD-APEX2-NS1 catalysed biotinylation experimental workflow	129
Figure 5.4.2 Characterisation of the pIROD-APEX2-NS1 construct and its derivatives bearing the NS1 <i>N</i> -glycosylation mutations via confocal immunofluorescence analysis	130

Abstract

Dengue virus (DENV) is a Flavivirus of the Flaviviridae family of (+) RNA viruses. It is known to cause approximately 390 million infections and 25,000 deaths annually in tropical and sub-tropical areas across the world. DENV infection has a wide spectrum of clinical manifestations ranging from mild fever to severe forms of dengue; formerly referred to as dengue haemorrhagic fever (DHF) and dengue shock syndrome (DSS). The viral NS1 protein is secreted from DENV-infected cells as a soluble hexameric lipoparticle that can induce vascular leakage; an established hallmark of DENV disease pathogenesis. Despite widespread acknowledgement of the importance of NS1 secretion in DENV pathogenesis, the exact molecular features of NS1 that are critical for its secretion from infected cells are not fully characterised. In this study, we employed random point mutagenesis and a luminescent ‘HiBiT’ peptide tag assay approaches to identify NS1 residues that are essential for its efficient secretion. From these approaches, we identified 10 point mutations that correlated with impaired NS1 secretion, with subsequent *in silico* analyses demonstrating that the majority of these mutations are located within the β -ladder domain of NS1. More detailed studies on two of these mutations V220D and A248V, revealed they also abrogated viral RNA replication and infectious virus production. Subsequent analyses of these mutants by confocal microscopy in the context of a DENV non-structural protein expression system revealed a similar but more reticular NS1 localisation pattern, while these mutant NS1 proteins could not be detected by immunoblotting using a conformation specific NS1 monoclonal antibody. Together, these studies demonstrated that the V220D and A248V mutations of NS1 may disrupt multiple functions and properties of the protein, as might occur if it is improperly folded and/or cannot form critical interactions with other proteins or membranes. Next, we sought to identify novel host factors associated with NS1 *N*-glycosylation, an essential post-translational modification of NS1, using an APEX2-based proximity biotinylation labelling approach and quantitative proteomics. Towards this goal,

appropriate virus constructs were generated for wildtype and *N*-glycosylation NS1 mutants. Following the comprehensive testing of a variety of constructs and optimisation of transfection and proximity biotinylation conditions, large scale experiments were conducted, and lysates were prepared for future streptavidin pulldowns and quantitative proteomics analyses. Taken together, these studies employed a combination of random point mutagenesis and sensitive luminescent peptide assays to identify a panel of mutations that impair NS1 secretion activity. A novel proximity labelling-based experimental workflow was also developed and applied towards proteomics-mediated identification of NS1 proximal proteins and how the NS1 protein microenvironment is altered by mutational disruption of NS1 *N*-glycosylation. We propose that NS1 secretion and *N*-glycosylation may represent novel and viable targets for future antiviral drug and attenuated vaccine development.

Declaration

I certify that this work contains no material which has been accepted for the award of any other degree or diploma in my name, in any university or other tertiary institution and, to the best of my knowledge and belief, contains no material previously published or written by another person, except where due reference has been made in the text. In addition, I certify that no part of this work will, in the future, be used in a submission in my name, for any other degree or diploma in any university or other tertiary institution without the prior approval of the University of Adelaide and where applicable, any partner institution responsible for the joint award of this degree.

The author acknowledges the copyright or published works contained within the thesis resides with the copyright holder(s) of those works.

I give permission for the digital version of my thesis to be made available on the web, via the University's digital research repository, the Library Search and through web search engines unless permission has been granted by the University to restrict access for a period of time.

Tan Eng Kuan Brandon

8th September 2023

Acknowledgements

First and foremost, I would like to express my deepest gratitude to both of my supervisors, Dr Nicholas Eyre and Professor Michael Beard, especially Dr Nicholas Eyre for providing me the opportunity to complete my PhD in your esteemed lab. Without both of your esteemed guidance and wisdom on overcoming experimental hurdles, I would have certainly experienced a few unexpected setbacks throughout my current PhD journey. Also, I would like to thank both kindly for being very prompt on providing comprehensive feedbacks on any PhD milestones, conference presentations as well as this given thesis document. Thank you as well to Professor Jill Carr from Flinders' University for continuously conveying her invaluable guidance and experiences throughout my PhD candidature.

Also, a massive thank you as well to past and present members of the Molecular Virology Group; Tom, Steve, Siena, Roman and Rosa for making me feel at home in the lab. Thank you to past and present members of the Viral Pathogenesis Lab, Kylie, Byron, Chuan, Emily, Brooke, Xavier for your moral support on my PhD project. And, also not forgetting past and present members of the Carr Lab, Josh, Evie, Hawraa, Tim, Amy, Val for always persevering with me during weekly lab meetings to talk about my ongoing experimental issues.

And a special thank you to my wonderful loving parents, Mom and Dad and my little brother despite being 8-9 hours away for your continuous weekly moral support and motivations as without them, I would definitely have a hard time to complete my PhD.

And lastly, I would like to thank the University of Adelaide for providing me this golden opportunity to complete my PhD at your esteemed establishment. With the memorable experiences I have obtained throughout my PhD journey, I am relatively confident in facing the upcoming life challenges ahead to become an established medical research scientist.

Thanks.

Presentations, Publications and Awards during the PhD candidature

Presentations:

Brandon E.K. Tan, Michael Beard and Nicholas Eyre. Identification of Dengue virus NS1 protein residues that are essential for its secretion. **Poster**. Lorne Infection and Immunity 2023 Conference

Brandon E.K. Tan, Michael Beard and Nicholas Eyre. Identification of Dengue virus NS1 protein residues that are essential for its secretion. **Oral presentation**. Australasian Virology Society (AVS) 11 2022 Meeting Gold Coast

Brandon E.K. Tan, Michael Beard and Nicholas Eyre. Identification of Dengue virus NS1 protein residues that are essential for its secretion. **Poster**. Australasian Virology Society (AVS) 11 2022 Meeting Gold Coast

Brandon E.K. Tan, Michael Beard and Nicholas Eyre. Identification of Dengue virus NS1 protein residues that are essential for its secretion. **Oral Presentation**. Flinders University Emerging Leaders Showcase 2022

Brandon E.K. Tan, Michael Beard and Nicholas Eyre. Dengue virus NS1 protein: What residue(s) enables it to efficiently exit the cell? **Oral Presentation**. Australasian Virology Society (AVS) Virtual Symposium 2021 Meeting

Brandon E.K. Tan, Michael Beard and Nicholas Eyre. Identification of Dengue virus NS1 protein residues that are essential for its secretion. **Oral Presentation**. Flinders University Emerging Leaders Showcase 2021

Brandon E.K. Tan, Michael Beard and Nicholas Eyre, Identification of Dengue virus NS1 protein residues that are essential for its secretion. **E-poster** . Lorne Infection & Immunity Virtual Conference 2021 Meeting

Publications:

Brandon E.K. Tan, Michael Beard and Nicholas Eyre, “Identification of Key Residues in Dengue Virus NS1 Protein That Are Essential For Its Secretion” *Viruses*, 2023, 15, 1102
<https://doi.org/10.3390/v15051102>

Awards:

2020 University of Adelaide Major Adelaide Graduate Research Scholarship recipient for Doctor of Philosophy program, \$28,092 AUD per annum

Abbreviations

bp	basepair
C	capsid
C°	degree Celsius
CMV	cytomegalovirus
DENV	Dengue Virus
DENV-1	Dengue Virus-1
DENV-2	Dengue Virus-2
DHF	Dengue Haemorrhagic Fever
DMEM	Dulbecco's Modified Eagle Medium
DNA	deoxyribonucleic acid
DPBS	Dulbecco's Phosphate Buffered Saline
DSS	Dengue Shock Syndrome
E	Envelope
ECL	Enhanced Chemiluminiscent
ER	Endoplasmic Reticulum
FCS	Fetal Calf Serum
G	G-force
HEPES acid	4-(2-hydroxyethyl)-1-piperazineethanesulfonic acid

HF	high fidelity
hr	hour
kb	kilobase
kDa	kiloDalton
kg	kilogram
LB	Luria Bertani Broth
µg	Microgram
µl	Microlitres
mg	milligram
MQ	Milli-Q
MOI	Multiplicity of Infection
MW	Molecular Weight
ng	Nanogram
NS	Non-Structural
NS1	Non-Structural 1
NS2A	Non-Structural 2A
NS2B	Non-Structural 2B
NS3	Non-Structural 3
NS4A	Non-Structural 4A
NS4B	Non-Structural 4B
NS5	Non-Structural 5

ORF	Open Reading Frame
PAGE	polyacrylamide gel electrophoresis
PBS	Phosphate Buffered Saline
PCR	Polymerase Chain Reaction
RC	Replication Complex
Rpm	revolutions per minute
Rcf	relative centrifugal force
RF	Replication Form
RNA	ribonucleic acid
RT	room temperature
SDS	Sodium Dodecyl Sulphate
sNS1	secreted NS1
SOB	Super Optimal Broth
SOC	Super Optimal Broth with Catabolite Repression
TAE	Tris base, acetic acid, EDTA
TGN	trans-Golgi network
V	Volts
Vi	virion clusters
VP	vesicle packets
WNV	West Nile Virus
WHO	World Health Organisation

WT

wildtype

YFV

Yellow Fever Virus

ZIKV

Zika virus

Amino Acid Abbreviations

Amino acid table	3 letter code	1 letter code
Alanine	Ala	A
Arginine	Arg	R
Asparagine	Asn	N
Aspartic Acid	Asp	D
Cysteine	Cys	C
Glutamine	Gln	Q
Glutamic Acid	Glu	E
Glycine	Gly	G
Histidine	His	H
Isoleucine	Ile	I
Leucine	Leu	L
Lysine	Lys	K
Methionine	Met	M
Phenylalanine	Phe	F
Proline	Pro	P
Serine	Ser	S

Threonine	Thr	T
Tryptophan	Trp	W
Tyrosine	Tyr	Y
Valine	Val	V

Material Providers

Agilent Technologies	Texas, USA
Becton, Dickinson and company	New Jersey, USA
Bemis Company, Inc.	Wisconsin, USA
Bio-Rad Laboratories	California, USA
Bioline	Luckewande, Germany
Beckman Coulter	California, USA
Cell Signalling Technology	Massachusetts, USA
Corning	New York, USA
Eppendorf	Hamburg, Germany
GeneTex	California, USA
Grenier Bio-One	Kremsmunster, Austria
ibidi GmbH	Grafelfing, Germany
Intron Biotechnology, Inc.	Gyeonggi-do, South Korea
Invitrogen	California, USA
Jackson ImmunoResearch Laboratories	Maryland, USA
Labcon	California, USA
LI-COR Biosciences	Nebraska, USA
Livingstone International	NSW, Australia
Lucigen Corporation	Wisconsin, USA

Macherey-Nagel	Duren, Germany
Merck Millipore	Massachusetts, USA
New England Biolabs	Massachusetts, USA
Promega	Wisconsin, USA
SARSTEDT AG & Co.	Numbrecht, Germany
Sartorius	Gottingen, Germany
Sigma-Aldrich	Missouri, USA
Sorenson BioScience, Inc.	Utah, USA
Thermo Scientific	Massachusetts, USA
Westlab	Melbourne, Australia

Chapter 1

Introduction

1.1 Dengue

1.1.1 History and Epidemiology of Dengue

Dengue has been ever-present since many centuries ago, with recorded symptoms closely resembling dengue fever being listed in an ancient Chinese medical encyclopedia (992 AD), informally published by the Chin Dynasty dating back to 265-420 AD (Murray et al 2013; Gubler 2006). In this archaic-derived encyclopedia, dengue disease was distinctly described as a “water poison” and strongly linked with flying insects which are known today as mosquitoes (Gubler 2006). Epidemics perceived to be dengue due to its similarity in its disease conditions and spread occurred sporadically throughout the Americas, initially starting out in the West Indies (1635), Central America (1699), Philadelphia (1780), and finally in New Orleans (1945) (Gubler 2006; Gubler 1997). As such, the association between the etiology of dengue and its transmission by mosquitoes became more apparent and was officially acknowledged in the 20th century.

As rapid urbanisation started occurring in the 18th and 19th centuries with the gradual expansion of global shipping industry and development of port cities, this also inadvertently provided ideal conditions for the *Aedes aegypti* mosquitoes to breed (Gubler 2006). With shipping vessels being the primary mode of transportation globally, they also indirectly became the breeding grounds for the mosquitoes in close proximity to humans to complete the transmission cycle, leading to the gradual introduction of dengue virus and mosquitoes to formerly inaccessible coastal destinations around the world. Subsequently, during World War II, the expansion of dengue was greatly amplified with the movement of troops in between countries via modern transportation (Murray et al 2013). And with the conclusion of the war, most South East Asian countries were greatly affected by increased transmission of dengue and the presence of multiple dengue serotypes (hyperendemicity), enhancing the emergence of the severe forms of dengue manifestation.

Based on the official reports provided by World Health Organisation (WHO), the global burden of dengue has escalated 30-fold due to massive geographical expansion and development, accelerated global urbanisation, exponential growth of the world population and unprecedented climate change (WHO 2020; WHO 2009). A recent study utilising mathematical models showed a positive correlation between the increase in dengue incidence and rise in global temperatures, potentially enhancing the global spread of dengue (Anwar et al 2019). Currently about 40% of world population are residing in tropical and sub-tropical areas where there is a high risk of dengue transmission (Murray et al 2013). Dengue transmission is now considered to be endemic in more than 100 countries in the Americas, South East Asia, Western Pacific and WHO-associated regions of Africa, with 70% of the actual global burden of dengue solely within Asia (Bhatt et al 2013; Murray et al 2013). Although dengue is known to be relatively widespread in sub-tropical and tropical countries, another study alarmingly predicted that the current rate of climate change would greatly enhance the spread of dengue *Aedes* vectors to continental Europe (Rocklov and Tozan 2019). The World Health Organisation (WHO) predicted that 50-100 million infections occur yearly, while about 500 000 cases of severe dengue and more than 20,000 dengue related deaths were reported annually (WHO 2020; WHO 2009). However, by using cartographic approaches backed with dengue cohort and dengue incidence populational records, it is estimated that there are in fact 390 million dengue infections yearly, approximately three times the dengue burden estimated provided by the World Health Organisation in 2009 (Bhatt et al 2013; WHO 2009).

1.1.2 Transmission of Dengue virus (DENV)

Dengue virus (DENV), a (+) RNA virus of the *Flaviviridae* family is the causative agent of the most widely spread mosquito-borne viral disease in the world, Dengue (Wilder-Smith et al 2010). Currently, there are four DENV serotypes; DENV-1, DENV-2, DENV-3 and DENV-4. Dengue is known to be transmitted by female mosquitoes of the genus *Aedes*, primarily *Aedes aegypti* and *Aedes albopictus* (Ferreira 2012). Transmission of DENV is greatly influenced by several factors such as the inconsistency in preventive measures, massive population growth, rapid urbanisation, and inadequate public infrastructure in place among many others (de los Reyes and Escaner IV 2018).

It has been established that each of the four DENV serotypes is strongly maintained in two notable evolutionary distinct transmission cycles; an ancient sylvatic cycle involving arboreal *Aedes* mosquitoes and non-human primates that has been described in transmission foci in peninsular Malaysia and West Africa and a ubiquitous human cycle where virus is transmitted between humans via an *Aedes* genus vector (Vasilakis et al 2011; Brady and Hay 2020). Also, humans are currently the only known well-documented amplification hosts and reservoir hosts among arthropod-borne viruses (Vasilakis et al 2011). Humans are frequently exposed to sylvatic DENV and cross-species transmission, leading to the sustained circulation of all DENV-1 to DENV-4 lineages today. Thus, it also has been suggested that the circulation of the four known DENV serotypes within the human cycle is possibly derived from multiple independent zoonotic events, with the recent event suggested to date back to approximately 850 years ago (Brady and Hay 2020; Wang et al 2000). Despite intensive ongoing research, there remains many unanswered questions regarding the unknown ecological factors that influences the mediation between human populations and sylvatic cycles and specific features of diseases caused by respective sylvatic DENV strains.

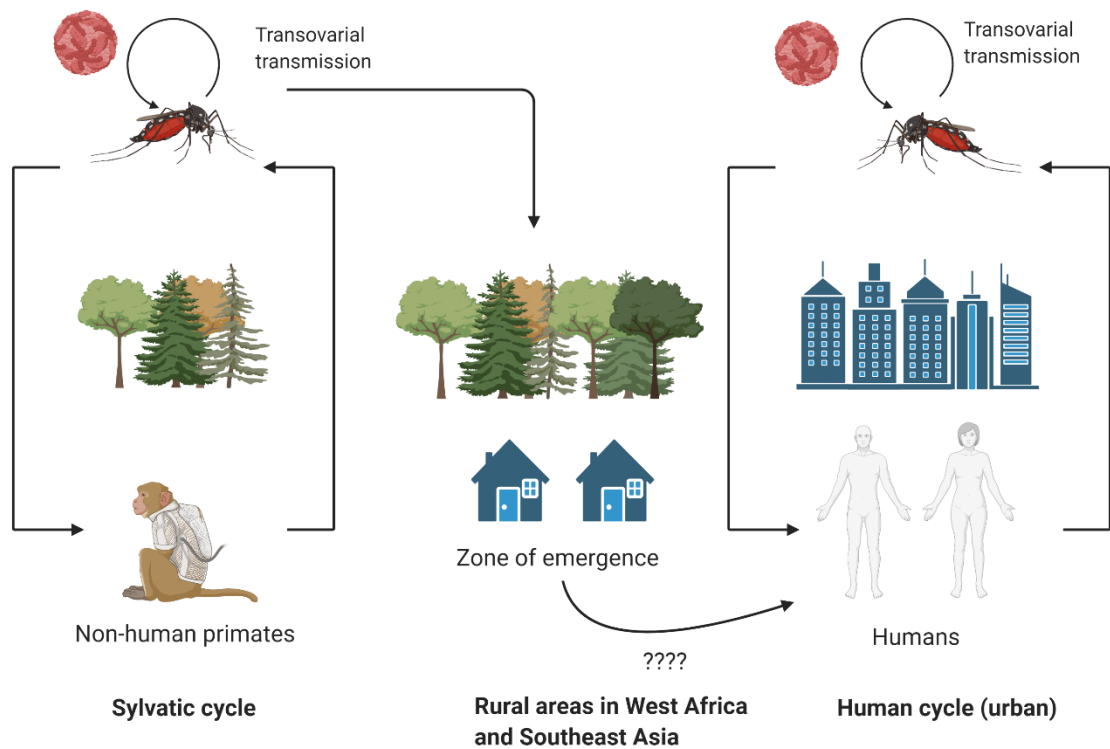


Figure 1.1.2.1 Various transmission cycles of DENV. Sylvatic origins of DENV and the “zone of emergence” where sylvatic cycles interact with human populations in Southeast Asia and West Africa. The human cycle occurs where virus is transmitted among humans via an *Aedes* genus vector. While relatively inefficient, DENV can also persist in several *Aedes* mosquito species via transovarial transmission where DENV-infected mosquitoes transfer the virus to their eggs. Adapted from Vasilakis et al 2011.

1.1.3 Emergence of *Aedes aegypti* as an effective disease vector species

The rise of dengue as one of the rapidly growing infectious diseases with approximately 390 million infections annually can be mostly attributed to the ability of *Aedes aegypti* to thrive in urban environment niches (Brady and Hay 2020). First, *Aedes aegypti* displays adaptable and unpredictable populational kinetics; adult females distribute their eggs heterogeneously across various water-retention container habitats to avoid any form of intraspecific competition as well as increasing the heterogeneity of progeny (Brady and Hay 2020; Colton et al 2003; Reiter 2007). Deposited eggs are desiccation-resistant, enabling them to thrive for long periods of time through harsh and non-ideal conditions. Larval populations develop a form of

behaviour called stacking, where there will be delays in developmental progression from larvae to the pupal stage until resources are deemed sufficient (Ritchie et al 2014). However, as human behaviours and environments effectively provide an optimal habitat for *Aedes aegypti* growth and development all-year long, *Aedes aegypti* can generate massive population sizes within a short period of time to effectively overcome current vector control efforts by humans.

The unique feeding habits of *Aedes aegypti* also make it a highly efficient disease vector. This includes the underlying preferences for human blood which contains essential nutrients required for egg production (Brady and Hay 2020; Canyon et al 1999) as well as the increased frequency of daytime biting events which effectively increase feeding rates per gonotrophic cycle (Harrington et al 2001) and renders vector control approaches like insecticide-treated bed nets ineffective (Brady and Hay 2020; Bhatt et al 2015). Female *Aedes aegypti* mosquitoes have adapted several essential features and behaviours that enable them to prolong their longevity and disseminate arboviruses. This includes minimisation of exposure to harsh environmental conditions by residing in warm and dark areas of human households, laying its eggs in a wide array of containers, and also gradually developing resistance to many known classes of insecticides (Brady and Hay 2020; Moyes et al 2017).

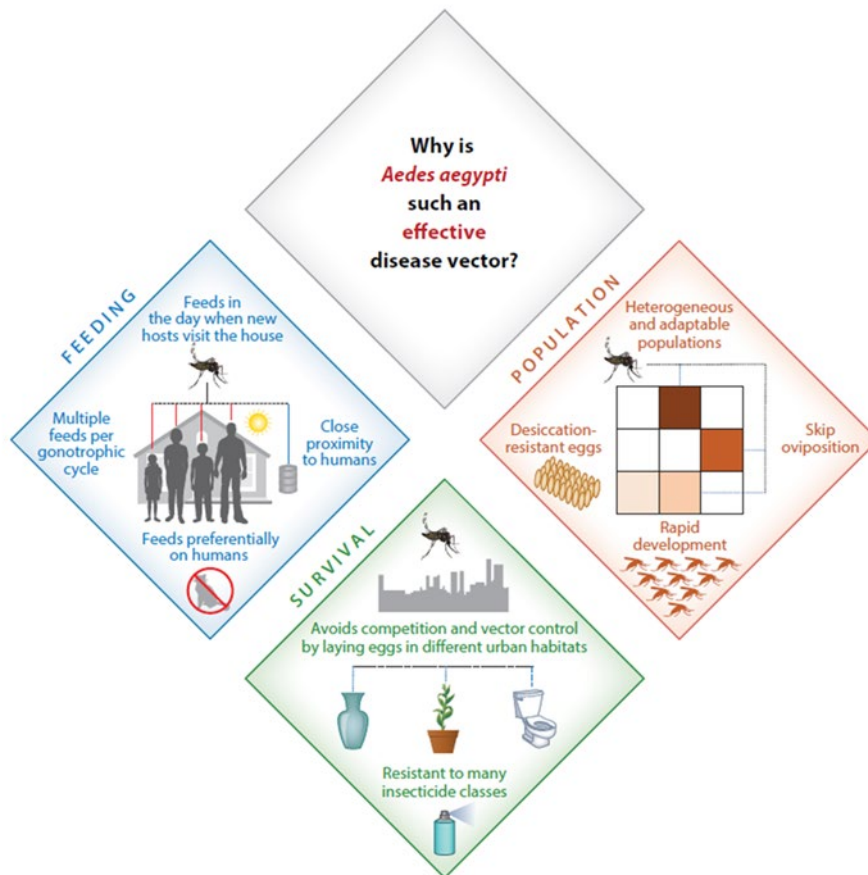


Figure 1.1.3.1 Schematic diagram of the main factors that enable *Aedes aegypti* to be a highly effective disease vector for dengue and other related arboviruses. Adapted from Brady and Hay 2020.

1.1.4 DENV clinical manifestations

Following the bite of a DENV-infected female mosquito and an incubation period between 2-7 days, disease symptoms can manifest, and this is followed by three main phases: an initial febrile phase, a critical phase and, a spontaneous recovery phase (Simmons et al 2012).

Approximately 75% of DENV infection cases are normally asymptomatic and patients that do develop symptoms suffer from a self-limiting debilitating disease known as the classical dengue fever (DF) that is characterised by muscle pain, high fever, and rashes during the febrile phase (Simmons et al 2012; Glasner et al 2018). However, a small cohort of patients unfortunately progress to develop potentially lethal forms of severe disease known as dengue haemorrhagic fever (DHF), which is characterised by vascular leakage of blood plasma and in

some instances dengue shock syndrome (DSS), where low blood pressure and haemorrhage occurs which can potentially result in a circulatory collapse (Simmons et al 2012; Glasner et al 2018; Bhatt et al 2013). The passing of the critical phase is synonymous with a great improvement in the patient's symptoms, known as the recovery phase in which adult patients, may experience fatigue for several weeks onwards following recovery.

1.1.5 DENV pathogenesis

The risk factors for severe dengue disease have been identified as age, DENV strains, high body mass index, gender, genetic variants of human major-histocompatibility-complex class I-related sequence B and pre-exposure to heterotypic strains of DENV (Simmons et al 2012; Anders et al 2011; Hung et al 2005). When one is infected with a DENV strain of a particular serotype (e.g., DENV-2), homotypic antibodies against this DENV serotype are produced and can provide life-long immunity against DENV strains of the same serotype. However, these generated antibodies do not confer complete protection against heterotypic serotypes (e.g., DENV-1, DENV-3, DENV-4). People who are subsequently infected with another DENV serotype often experience more severe dengue clinical symptoms and also increase the risk of developing severe dengue. The underlying phenomenon is known as antibody-dependent enhancement (ADE), which has been extensively studied for many viruses, and particularly dengue viruses (Mady et al 1991). ADE in dengue occurs when heterotypic, non-neutralising antibodies derived from a primary DENV infection bind to DENV particles during a subsequent heterotypic DENV infection (Whitehead et al 2007; Mady et al 1991). The resulting generated antibody-virus complex facilitates the secondary infection by attaching to cells expressing Fc receptors on their cell surface such as macrophages and dendritic cells. This culminates in enhanced viral replication and spread, which can potentially lead to an increased risk of severe symptoms of dengue.

1.2 Molecular Biology of DENV

1.2.1 Genome structure

DENV is a small, enveloped virus possessing a positive-strand RNA genome that is approximately 11kb in length (Lescar et al 2018). The ~11kb (+) RNA genome encodes a single open reading frame (ORF) that is flanked by 5' and 3' untranslated regions (UTR) and encodes a single viral polyprotein that is approximately 3400 amino acids in length. This single viral polyprotein encodes 3 structural proteins, capsid protein (C), membrane protein (M), and envelope protein (E) and 7 non-structural proteins, NS1, NS2A, NS2B, NS3, NS4A, NS4B and NS5 (Scaturro et al 2015; Bartenschlager and Miller 2008). Following the synthesis of polyprotein by the host translational machinery, this polyprotein is co- and post-translationally cleaved by viral and host proteases into the respective individual proteins.

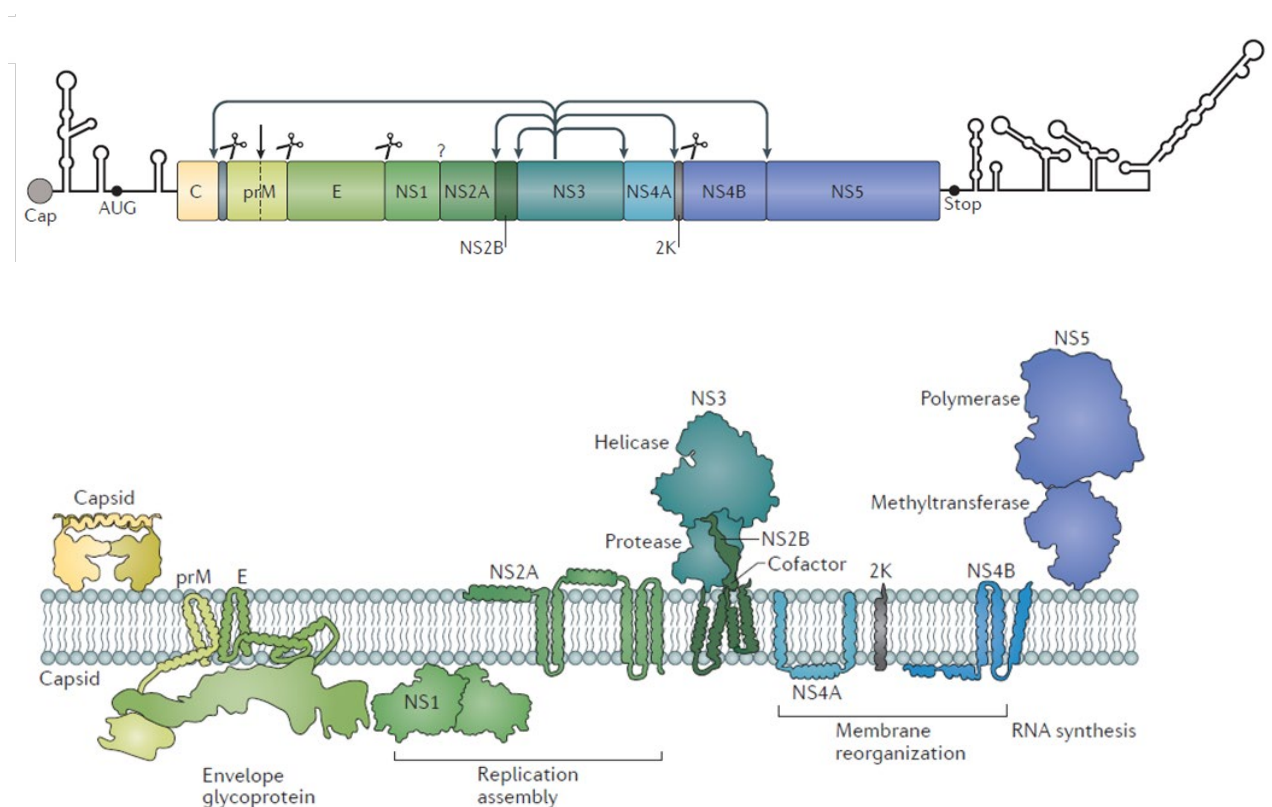


Figure 1.2.1.1 The DENV genome organisation and membrane topology of translated proteins. A schematic representation of the DENV genome and respective mature viral

proteins. The DENV genome is 11kb in size, type-1 capped at the 5' end and the large single ORF is flanked by 5' and 3' UTRs. The ORF encodes a polyprotein that is cleaved by cellular signal peptidases (scissors symbols) and viral NS2B/3 protease (arrow symbols). Adapted from Neufeldt et al 2018.

1.2.2 Structural Proteins

1.2.2.a Capsid

The highly basic 12 kDa mature DENV capsid protein forms homodimers in solution (Byk and Gamarnik 2016). Three-dimensional structures of WNV and DENV capsid proteins were resolved by crystallography and nuclear magnetic resonance (NMR) respectively. Structural studies indicate that the monomer consists of four alpha helices ($\alpha 1$ to $\alpha 4$) and a seemingly unstructured N-terminal domain with a high density of positive charges (Scaturro et al 2014). The helices $\alpha 2$ and $\alpha 4$ of one capsid monomer are antiparallel to the helices $\alpha 2$ and $\alpha 4$ of the neighbouring capsid monomer, with the two interfaces constituting the majority of the capsid dimer contact surface (Byk and Gamarnik 2016). Mutagenesis studies revealed that $\alpha 4$ - $\alpha 4'$ helix interaction is important for stability of protein, dimer formation and infectious virus production. Intriguingly, it has also been suggested that the $\alpha 4$ - $\alpha 4'$ region interacts with viral RNA whilst both the hydrophobic cleft and apolar $\alpha 2$ - $\alpha 2'$ region interact with ER membranes (Ma et al 2004). Also, functional analysis has demonstrated that basic residues within the N-terminus of the DENV capsid protein assist in the formation of viral particles and RNA binding (Byk and Gamarnik 2016). In regard to the host factors that regulate nucleocapsid assembly, a proteomics approach successfully identified 16 proteins that interact with the DENV capsid, including a RNA helicase of the helicase superfamily 2, DEAD (Asp-Glu-Ala-Asp) Box Helicase 3 (DDX3X) (Kumar et al 2018). Several studies have indicated that

DDX3X is an antiviral protein, as overexpression of DDX3X results in the inhibition of viral replication while siRNA knockdown of DDX3X expression led to an increase in infectious DENV titres (Kumar et al 2018; Soulat et al 2008; Schroder et al 2008).

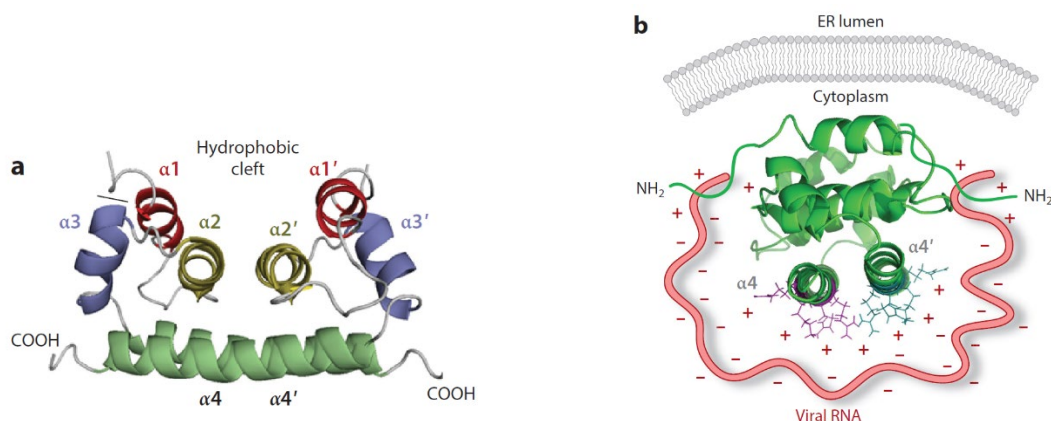


Figure 1.2.2.1 The structure of DENV capsid protein. a) Capsid homodimer (α and α') and four α -helices as shown: $\alpha 1$ (red), $\alpha 2$ (yellow), $\alpha 3$ (blue) and $\alpha 4$ (green) and the hydrophobic cleft. **b)** Proposed model of capsid protein interactions with ER membranes and viral RNA via $\alpha 2$ - $\alpha 2'$ and $\alpha 4$ - $\alpha 4'$ regions respectively. The unstructured N-terminal region (NH_2) also potentially interacts with viral RNA. Adapted from Byk and Gamarnik 2016.

1.2.2.b Membrane

Following translation of the DENV polyprotein and liberation of the individual viral proteins by viral and host proteases, the mature M protein is initially synthesised in a pre-protein form called the precursor-membrane glycoprotein (prM) which is 166 amino acids in length (Li et al 2008; Nasar et al 2020). The prM protein consists of the N-terminal domain with a pre-domain (found in immature virus), M-domain, stem region and the C-terminal transmembrane region, which consists of the α -helical domain (MH) and two transmembrane domains, MT1 and MT2 (Li et al 2008; Zhang et al 2003). Cleavage of prM by the host resident protease Furin liberates the N-terminal 91 “pr” residues upon maturation, leaving

behind the ectodomain (residues 92 to 130) and the transmembrane region (residues 131 to 166) of M in the virion (Li et al 2008). The pr protein comprises seven β strands that are displayed in an antiparallel manner, stabilised by three disulfide bonds (Li et al 2008). The β -barrel structure of the pr peptide conceals the fusion loop of the E protein, preventing fusion of immature virus with the host membrane. The acidic conditions within the trans-Golgi network (TGN) promote conformational change to expose the Furin cleavage site, enabling cleavage of prM protein by Furin (Yu et al 2009). Following cleavage, pr peptide remains non-covalently associated with the E protein fusion loop until the mature virus is released to the extracellular milieu, where the pr is released at neutral pH.

A novel interaction between claudin-1 and prM protein has been identified (Gao et al 2010). Derived from a family of tight junction membrane proteins, claudin-1 has been shown to be upregulated during the early stages of a DENV infection and enhances efficient DENV entry into cell, possibly by functioning as a DENV entry receptor/co-receptor. In contrast, the DENV capsid protein interestingly mediates downregulation of claudin-1 expression upon DENV infection (Gao et al 2010). In another prM-focused study, site-directed mutagenesis studies revealed that the MH domain of prM is involved in assembly and entry of DENV (Hsieh et al 2011). Proline substitutions of several residues within the C-terminus of MH domain greatly impeded the production of virus-like particles (VLPs), assembly, spread and infectivity of virions in cell culture, strongly indicating the importance of the MH domain in the DENV life cycle. Also, several highly conserved residues within the MH domain when substituted with alanine were shown to regulate prM protein cleavage, maturation of DENV particles and DENV entry (Hsieh et al 2014).

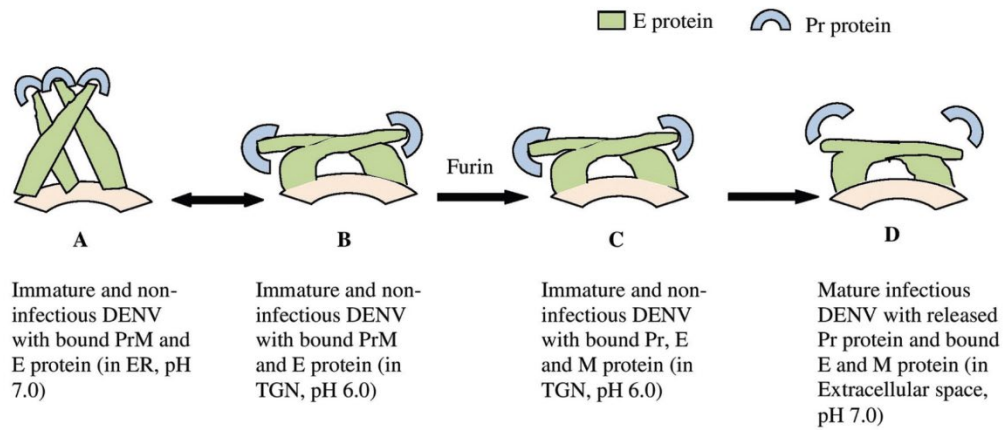


Figure 1.2.2.2. Different stages of DENV structure and respective pH-dependent conformation of the E protein (green) and the predomain (pr) protein (blue) states throughout the life cycle. Adapted from Roy and Bhattacharjee 2021.

1.2.2.c Envelope

E-protein is a major surface glycoprotein that is normally involved in viral internalisation into host cells via endocytosis (Nasar et al 2020). The DENV E protein is comprised of a C-terminal transmembrane anchor domain and an ectodomain connected by a stem region. The ectodomain constitutes approximately the first 400 amino acids and is made up of three different structural β -barrel domains, D-I, D-II and D-III (Slon Campos et al 2017; Modis et al 2004). The β -barrel-like structure D-I resides within the centre of a mature E monomer and is flanked on one side by an elongated finger-like structure, D-II containing the fusion peptide loop at its distal end (Slon Campos et al 2017; Mukhopadhyay et al 2005; Modis et al 2004). D-III is an immunoglobulin (Ig)-like domain thought to possess putative receptor-binding sites and is located on the other side of D-I, connected via a single polypeptide linker. Within an E dimer, the fusion peptide from one E monomer is concealed between D-I and D-III of the adjacent E monomer (Mukhopadhyay et al 2005). E protein undergoes *N*-linked glycosylation at asparagine residues 67 and 153 located in D-II and D-I respectively (Mondotte et al 2007). Glycosylation site N67 is unique to DENV and is proposed to interact

with one of the host cell receptors, DC-SIGN whereas glycosylation site N153 is highly conserved among most flaviviruses (Pokidysheva et al 2006; Mondotte et al 2007; Yap et al 2017). The fusion peptide is important for virus entry and endosomal membrane fusion (Kuhn et al 2002). At neutral pH, dimerization of E proteins positions the fusion loop into the hydrophobic pocket of adjacent E monomer, which in turn avoids premature exposure of the fusion loop to endocytosis of virions by a new cell. Within the acidic endosome, the pH-dependent hinge located at the DI-DIII interface enables the E dimer to readily dissociate and rearrange into a trimeric form which acts as a pre-fusion intermediate that promotes membrane fusion (Modis et 2004; Yap et al 2017).

1.2.3 Non-Structural Proteins

1.2.3.a NS1

NS1 is a 48 kDa non-structural glycoprotein that is multifunctional and can be identified either as a membrane-linked (mNS1) dimeric species associated with vesicular compartments within the cell or a secreted extracellular hexameric species (sNS1) (Muller and Young 2013; Winkler et al 1988; Mason 1989; Brandt et al 1970). Intracellular mNS1 plays an important role in virus replication as it has been greatly observed to co-localise and interact with components of the viral replication complexes (Mackenzie et al 1996; Lindenbach and Rice 1997). On the other hand, the sNS1 is a lipoprotein hexameric particle with its central core packed with lipid components resembling those of plasma-derived high-density lipoproteins (HDLs), which are involved in vascular homeostasis. In a recent cryo-EM study, sNS1 has been demonstrated to interact with and bind to HDLs, forming a NS1-HDL complex upon its dissociation into NS1 dimeric units onto the surface of the lipoprotein particle (Benfrid et al 2022). This NS1-HDL complex has been shown to be essential in inducing the production of

inflammatory cytokines in human macrophages and it was also demonstrated that levels of NS1-HDL complexes were distinctly elevated in the plasma samples of DENV-infected patients.

Advances in X-ray crystallography and cryogenic electron microscopy have enabled determination of the high-resolution 3D crystal structures of the DENV NS1 dimer (**Figure 1.2.3.1; left**) and hexamer (**Figure 1.2.3.1; right**) (Akey et al 2014). The DENV NS1 dimer consists of monomers with 3 prominent domains, a small N-terminal hydrophobic β -roll domain (amino acids position 1 to 29) formed by disulphide linkages between two β -hairpins, the Wing domain (amino acids position 38-151) flanked by two connector subdomains (amino acids position 30-37 and 152-180) and a β -ladder domain comprised of a core β -sheet domain featuring 18-antiparallel β -strands that are arranged like rungs of ladder throughout the length of the dimer (amino acids 181-352) (Akey et al 2014; Akey et al 2015). The connector subdomain of the Wing domain and the β -roll domain form a protrusion that results in one face of the NS1 dimer being hydrophobic that is thought to mediate the association of the NS1 dimer with the ER membrane and replication complex in part via interactions with two other non-structural proteins NS4A and NS4B (Scaturro et al 2015; Akey et al 2015; Akey et al 2014). Three β -roll domains are predicted to face the interior of the hexamer, interacting with the central lipid cargo core (Scaturro et al 2015; Muller et al 2012; Gutsche et al 2011). In both mNS1 and sNS1 species, the distal tips of the β -ladder and the Wing domain disoriented loops contain protruding *N*-glycosylation sites (amino acid positions 130 and 207) that face outwards, enabling them to be exposed to the solvent environment (Akey et al 2015; Akey et al 2014). Also, in a recently published cryo-EM study, recombinant DENV sNS1 has interestingly shown that in addition to conventional stable hexamers, majority of the sNS1 population exists predominantly in either 'loose' or 'stable' tetrameric forms, with their differences based on the organisation of the N-terminal derived elongated β -sheet and β -roll domains (Shu et al 2022). Given sNS1 is known to contribute to DENV pathogenesis, it remains ambiguous if these recently discovered sNS1 forms are pathogenic. Regardless, these

new discoveries will hopefully contribute towards novel therapeutic and vaccine design strategies to overcome severe forms of dengue.

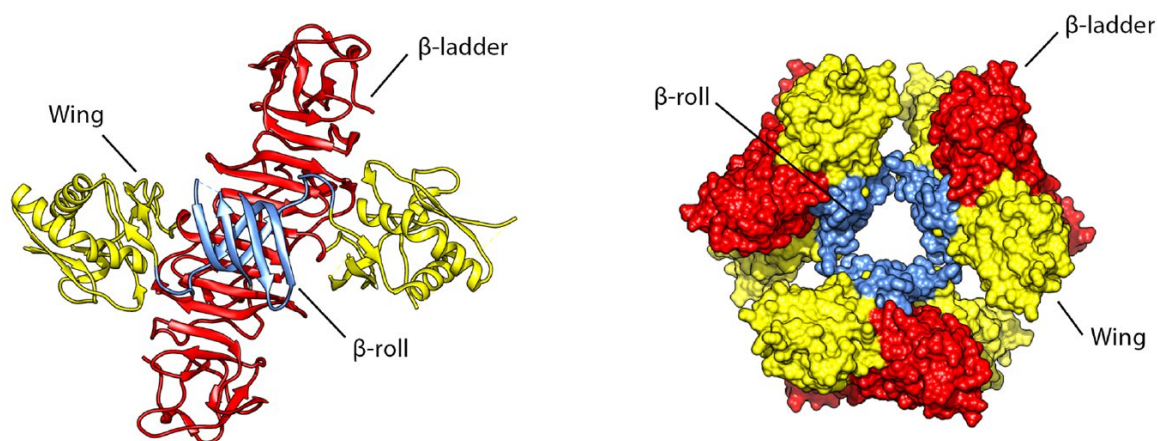


Figure 1.2.3.1 The three-dimensional structure of the flavivirus NS1. The DENV NS1 dimer (left) and hexamer (right) structures with the color-coded Wing (yellow), β -roll (blue) and the β -ladder domains (red) respectively. Taken from Scaturro et al 2015.

1.2.3.b NS2A

NS2A is a 22kDa highly hydrophobic transmembrane protein, with biochemical analysis demonstrating that the NS2A protein features five integral transmembrane segments that span the lipid bilayer of the ER membrane and one segment that associates with the luminal side of the ER membrane without transversing the lipid bilayer (Xie et al 2014; Xie et al 2013).

Following the translation of the polyprotein, both termini of NS2A are processed differently; N-terminus in the ER lumen is cleaved by an undefined membrane-bound host protease while the C-terminus is cleaved in the cytoplasm by the viral NS2B-NS3 protease (Xie et al 2013).

NS2A has been demonstrated to be involved in viral RNA replication, virus assembly, membrane remodelling and antagonism of the host immune response (Shrivastava et al 2017; Xie et al 2014). Mutagenesis studies also identified several amino acid residues within TMS1

and TMS2 transmembrane regions of DENV NS2A protein to be essential for virus-induced cytopathic effects (CPE) (Wu et al 2017). Also, several interactions of DENV NS2A with the 3' UTR, prM, E and NS3 were further established and were shown to be involved in the recruitment of synthesised viral RNA, C-prM-E polyprotein and NS2B-NS3 protease to virion assembly site (Xie et al 2019). Following the recruitment activity, C-prM-E polyprotein is subsequently cleaved by NS2B-NS3 and host signalase to produce respective mature C, prM and E proteins.

1.2.3.c NS2B

NS2B is a 14 kDa (130 amino acid) membrane-associated hydrophobic protein that acts as a cofactor for the NS3 protease (Liu et al 2017; Falgout et al 1991). Topological studies on NS2B via NMR spectroscopy identified four transmembrane helices, while the non-helical conserved region between the $\alpha 2$ and $\alpha 3$ was shown to be involved in the NS2B cofactor activity (Li et al 2015). This highly dynamic conserved domain is likely to form β -strands with the NS3 protein, to drive formation of the NS2B-NS3 complex. Additionally, a study also reported that polyubiquitination of NS3 promotes the recruitment of NS2B protein to form the NS2B/3 protease complex, which in turn proteolytically cleaves the antiviral protein STING within the ER to inhibit activation of the host innate immune response (Liu et al 2017). In contrast, an ER-resident protein SCAP can directly compete with NS2B for binding to STING as well as diminishing polyubiquitylation activity of NS3, which eventually suppresses amplification of DENV infection (Liu et al 2017). Intriguingly, the DENV NS2B protein has been implicated in targeting the cytosolic DNA sensor cyclic GMP-AMP synthase (cGAS) for lysosomal degradation, subsequently leading to inhibition of type I interferon production as a result of the inactivation of the cGAS/STING sensing pathway during DENV infection (Aguirre et al 2017).

1.2.3.d NS3

NS3 is a 72 kDa protein that has been extensively studied among DENV proteins and possesses several known enzymatic functions (Sampath et al 2006). The N-terminal protease domain together with its cofactor NS2B is responsible for the proteolytic activity of NS3 and cleaves multiple sites within the DENV polyprotein (Benarroch et al 2004). The C-terminal domain of NS3 can be divided into three domains and possesses three different enzymatic activities; a nucleoside 5' triphosphatase (NTPase) activity, RTPase activity and helicase activity. ATP-driven NS3 helicase activity is responsible for unwinding the viral dsRNA, releasing +ssRNA. NS3 RTPase activity is important for cleaving the phosphoric anhydride bond (γ - β) of 5'-triphosphorylated viral RNA, which is required for capping of 5'UTR of viral RNA (Nasar et al 2020).

1.2.3.e NS4A

NS4A is a small 16 kDa hydrophobic protein whose exact role in the viral replication cycle remains poorly understood (Miller et al 2007). The proposed membrane topology model of NS4A features an N-terminal region, three transmembrane domains (TMD1, TMD2, TMD3) and a C-terminal tail. NS2B-3 protease generates the N-terminal of NS4A within the cytoplasm. The last 23 amino acid residues within the C-terminal domain of NS4A encodes a signal sequence (the 2K fragment), enabling the translocation of adjacent NS4B into the ER lumen. Once NS4B has been translocated, the 2K fragment is proteolytically cleaved from the N-terminal of NS4B by the NS2B-3 protease on the cytosolic side of the ER membrane whereas the C-terminal domain of NS4B is generated by host signalase within the ER lumen (Miller et al 2007). Proteolytic removal of 2K fragment is essential for cytoplasmic membrane alterations to form virus-induced structures which are likely to harbour the viral RC.

Intriguingly, the first 50 amino acid residues of the cytosolic-derived N-terminal domain of NS4A (N50 region) interacts with vimentin, a component of type III intermediate filaments

(IFs) that is known to be redistributed in infected cells during virus infections (Teo and Chu 2014). siRNA-mediated gene knockdown of vimentin has been shown to lead to an unusual, dispersed distribution of RCs in DENV-infected cells, which suggests a crucial role of the vimentin scaffolding network in concentrating and localising RCs at the perinuclear region, thus promoting efficient viral RNA replication (Teo and Chu 2014). It also has been reported that DENV NS4A forms oligomers, as such that introducing mutations to conserved residues, E50A and G67A within the first transmembrane domain of NS4A (TMD1) affect NS4A oligomerisation, folding and stability, leading to attenuated viral replication (Stern et al 2013; Lee et al 2015). Recently, DENV mutagenesis studies which focused on 37 residues within NS4A identified multiple residues that are essential for DENV replication, interactions with other DENV proteins, stability of NS4A and biogenesis of DENV replication organelles (Cortese et al 2021). Given the involvement of NS4A in the aforementioned essential roles within the DENV life cycle, NS4A remains an attractive promising target for novel antiviral strategies.

1.2.3.f NS4B

NS4B is a large hydrophobic 27 kDa protein (Miller et al 2006). NS4B resides within the ER of infected cells until its recruitment to viral replication complex events via recruitment by NS4A. Based on the established NS4B membrane topology model generated by Miller and colleagues in 2006, the C-terminal region consists of three transmembrane domains with the C-terminal tail located in cytoplasm, whereas the N-terminal region is localised in the ER lumen. NS4B colocalises with NS3 and dsRNA, both known components of the flavivirus RC (Paul and Bartenschlager 2013). NS4B interacts with and binds to subdomains 2 and 3 of NS3 via its cytoplasmic loop, enhancing NS3 helicase activity to greatly reduce the affinity of NS3 for single stranded RNA (Zou et al 2015). Through a replication-based screening approach, a known receptor antagonist, SDM25N, was shown to impede DENV RNA replication (van

Cleef et al 2013). Despite identifying single amino acid substitutions, P104L and F164L within NS4 protein that confer resistance to SDM25N replication-inhibition activity was speculated that SDM25N may interfere with the interferon-suppressive activity of NS4B, as NS4B is known to impede interferon signalling by restricting activation of signal transducer and activator of transcription 1 signals (van Cleef et al 2013; Munoz-Jordan et al 2003). A cellular protein, stress-associated ER protein 1 (SERP1) was identified and characterised as a novel host factor for DENV-2 NS4B, and that is involved in the DENV life cycle (Tian et al 2019). Overexpression of SERP1 inhibited virus production and RNA replication at the viral RNA replication stage although overexpression of NS4B in SERP1-expressing cells interestingly rescued the viral replication activity inhibited during SERP1 overexpression (Tian et al 2019). These results suggest that SERP1 is an antiviral protein that restrict DENV-2 infection and may be potentially considered as a novel anti-DENV target. Additionally, from a large-scale cell-based anti-DENV2 screen and medicinal chemistry effort, a highly potent DENV inhibitor, JNJ-A07 was identified and revealed to have nanomolar to picomolar antiviral activity against various clinical DENV isolates (Kaptein et al 2021). JNJ-A07 displays a relatively high barrier to drug-resistance and importantly, JNJ-A07 resistant variant featuring three point mutations within NS4B were shown to be highly attenuated in mosquito cells implying that transmission of JNJ-A07 resistance may be of limited concern. Additional studies indicated NS4B as the molecular target of JNJ-A07 as it blocks the *de novo* formation of the NS3-NS4B complexes which are needed for viral replication, possibly by promoting a conformational change of the NS4B cytosolic loop and thus impairing the NS3-NS4B interaction in the process. Recently in a follow-up study, another related highly potent DENV inhibitor of JNJ-A07, JNJ-1802 was discovered to exhibit improved preclinical safety profiles and shown to reduce DENV infection of all four DENV serotypes in mouse models (Goethals et al 2023). Likewise, with JNJ-A07, JNJ-1802 also blocks the *de novo* formation of the NS3-NS4B complexes only, possibly by direct binding to NS4B prior to its association with NS3 or indirectly which remains unclear.

1.2.3.g NS5

Located at the C-terminal portion of the DENV polyprotein, NS5 is the largest (103 kDa) and most highly conserved of the flaviviral proteins (Liu et al 2010). NS5 consists of two domains, C-terminal domain and N-terminal domain connected by a flexible linker (Lu and Gong 2013). The C-terminal region of NS5 has been long known to contain motifs characteristic of all RNA-dependent RNA polymerases (RdRps) (Brinton 2002). The N-terminal NS5 region contains a methyltransferase domain (**MTase**), which possesses guanine N7 methyltransferase, guanylyl-transferase and ribose 2'O-methyltransferase activities; all of which are important for sequential methylation of the viral 5' RNA cap structure (Liu et al 2010; Brinton 2002). The NS5 RdRp domain is involved in the transcription/replication of the viral genome (Potisopon et al 2014). NS5 RdRp synthesises RNA in three main phases; *de novo* initiation, transition and elongation. NS5-MTase activity has been shown to regulate the efficiency of RdRp activity by increasing the affinity of priming nucleotide ATP upon *de novo* initiation phase as well as promoting a higher catalytic efficiency of the polymerase during the elongation phase. As part of the human innate antiviral response, the type 1 interferon (IFN) pathway acts to induce activation of antiviral effector cells and restricts viral replication (Ashour et al 2009). DENV NS5 was shown to block the IFN signalling pathway by binding to STAT2 and promoting its degradation (Ashour et al 2009). Following binding of type I IFN to its IFNAR receptor and subsequent signalling events, STAT2 forms a complex with STAT1 and IFN regulatory factor 9 to form the transcription factor complex ISGF3 which translocates to the nucleus and binds to interferon-stimulated response element (ISRE) DNA sequences to drive increased levels of expression of a number of proteins involved in generating an antiviral state within the cell, ultimately inhibiting viral replication. In contrast to DENV NS2A and DENV NS5, NS4A and NS4B appear to inhibit IFN

signalling by preventing STAT1 phosphorylation (Ashour et al 2009; Munoz-Jordan et al 2003).

1.2.4 DENV replication cycle

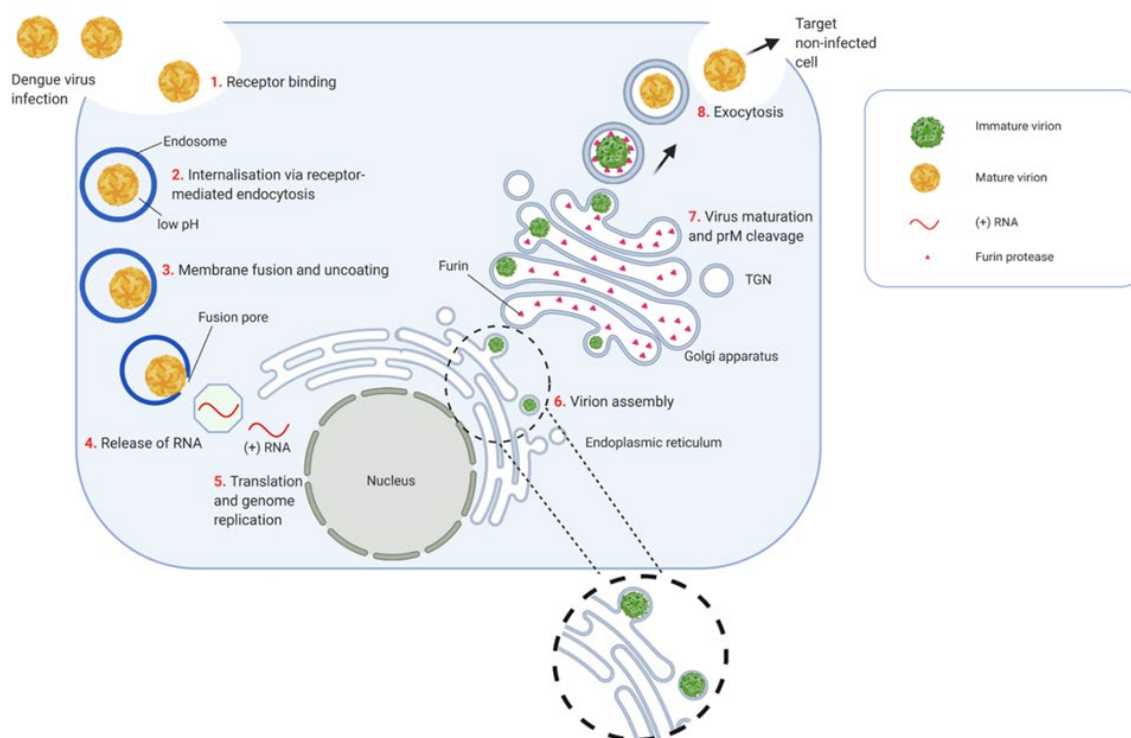


Figure 1.2.4.1 Overview of the DENV replication cycle. The DENV replication cycle begins when mature virions bind to not fully defined receptors such as DC-SIGN and heparin sulphate are internalised via clathrin-mediated endocytosis. Acidification of the endosome induces fusion of the viral envelope with the endosomal membrane, leading to release of DENV nucleocapsid into the cytosol. Uncoating and disassembly of the nucleocapsid occurs, liberating the (+) RNA genome that is translated into a single DENV polyprotein that is subsequently processed co- and post- translationally by viral and host-derived proteases. Non-structural DENV proteins promote endoplasmic reticulum (ER) modification, forming sites of viral genome replication. Following replication of the viral RNA via a negative strand intermediate and the activity of the NS5 RNA-dependent RNA polymerase, newly synthesised (+) RNA genomes are encapsidated. Newly formed nucleocapsid buds into the lumen of ER, collecting a lipid bilayer containing envelope proteins (prM/E), forming immature virions. The immature virions and sub-viral particles are transported through the

trans-Golgi network (TGN) as part of the maturation step where host resident protease Furin cleaves the non-infectious immature particles to generate infectious mature virus particles. Mature virions are eventually released via exocytosis.

1.2.5 NS1 Maturation and Subcellular Targeting

After DENV polyprotein translation at the rough ER, the newly generated polyprotein will then be co- and post-translationally cleaved by viral and host cellular proteases (Watterson et al 2016). Following this, the NS1-NS2A fragment is immediately translocated into ER lumen via a signal peptide sequence located at the C-terminus of the E protein (Watterson et al 2016; Falgout et al 1989). Once the signal peptide sequence is removed by resident host signal peptidase and cleavage of the NS1-NS2A fragment junction occurs by an undefined protease, the NS1 monomer is glycosylated via addition of high mannose carbohydrates before rapidly dimerising, generating a moderate hydrophobic surface, that mediates NS1 interaction with the ER membrane (Watterson et al 2016; Winkler et al 1989; Nowak et al 1989; Winkler et al 1988). After incorporation of high mannose carbohydrate moieties within NS1 glycosylation sites mediated by ER-derived oligosaccharyl transferase complex (OTC), NS1 is then targeted to three distinct sites: A significant fraction of the NS1 population is targeted to viral replication sites while a second population is targeted to the plasma membrane. The remaining NS1 dimer population is trafficked to the Golgi where it associates with “specialised lipid rafts”, obtaining a lipid cargo prior to formation of a NS1 hexamer which undergoes additional NS1 *N*-glycan processing (Winkler et al 1988; Winkler et al 1989; Flamand et al 1999; Khromkyh et al 1999). This additional NS1 glycan processing involves conversion of the high mannose carbohydrates moieties into more complex sugars by resident host glycosidases and glycotransferases (Pryor and Wright 1994; Watterson et al 2016). NS1 is then secreted out from DENV-infected host cell into the bloodstream of infected individuals, predominantly as a soluble NS1 hexameric particle (Gutsche et al 2011; Somnuk

et al 2011). However as discussed above, recent studies have shown that secreted NS1 can be found in tetrameric and hexameric states (Shu et al 2022), and additionally secreted NS1 associates with high density lipoprotein (HDL) such that the surface of the HDL features 2-4 NS1 dimeric rods (Benfrid et al 2022). Further studies may be needed to reconcile which form(s) of secreted NS1 is predominant in the blood of DENV-infected individuals and most significant to vascular damage and other pathogenic effects.

1.3 Lipid rafts

1.3.1 Roles of lipid rafts

Within the exoplasmic leaflet regions of cellular bilayer membranes, ‘lipid rafts’ or sphingolipid-cholesterol rafts are specialised micro-domains that are heavily enriched with sphingolipids and cholesterol (Simon and Ikonen 1997; Ikonen 2001). In this asymmetric bilayer membrane, sphingolipid and glycosphingolipid (subtype of glycolipids) head groups are predominantly enriched in the exoplasmic leaflet and cytoplasmic leaflet, respectively, with the cholesterol filling the void under the head groups, condensing and packaging the sphingolipids into rafts (Simon and Ikonen 1997; Smaby et al 1996; Ikonen 2001). These micro domains can selectively exclude or incorporate plasma membrane proteins on the cell for endocytosis, cholesterol homeostasis, signal transduction and transcytosis across endothelial cells (Ikonen et al 2001; Noisakran et al 2008**b**). Lipid rafts are notably common sites for virus-host cell interactions as many viruses including Epstein-Barr virus (Coffin III et al 2003), human immunodeficiency virus (HIV) (Manes et al 2000), and Hepatitis C virus utilise these rafts for viral assembly, formation of viral replication complexes (Aizaki et al 2004), viral entry and evasion from host immune responses (van der Goot and Harder 2001). Despite knowing that lipid rafts are heavily involved in virus-host cell interactions, and

especially in flavivirus replication, their exact role(s) remains poorly characterised (Noisakran et al 2008b).

1.3.2 Association of DENV NS1 protein with lipid rafts

In regards to the association of NS1 with lipid rafts, Noisakran et al (2008b) performed multicolour immunofluorescence labelling and a flotation gradient centrifugation assay to determine a potential interaction of DENV NS1 with lipid rafts during a DENV-infection. A small fraction of NS1 was associated with low-density fractions containing CD55, a raft-resident protein, while the majority of NS1 was detected within high density fractions containing CD71, a non-raft associated transmembrane protein. Further analysis via multicolour immunofluorescence labelling of DENV-infected HEK-293T cells strongly supported the plasma membrane as the location of NS1-raft association given strong co-localisation of NS1 with raft-associated molecules, CD55 and ganglioside GM1 on the cell surface. These findings suggest the possibility of the involvement of raft associated NS1 and lipid rafts in viral RNA replication.

Recently, it was demonstrated that DENV NS1-induced macrophage activation via TLR-4 increases the concentration of lipid rafts on the plasma membrane, thus promoting attachment of DENV particles to non-infected cells and enhancing DENV infection in the process (Coelho et al 2021). Apolipoprotein AI (ApoA1) is a key component of high-density lipoproteins (HDL) and has been observed to be significantly downregulated in DENV-infected patients (Coelho et al 2021; Feingold 2015). Interestingly, ApoA1-mediated depletion of lipid rafts markedly decreases DENV particle attachment to the cell surface, demonstrating the importance of lipid rafts in DENV infection as well as highlighting the capability of ApoA1 to inhibit DENV infection by depleting lipid rafts (Coelho et al 2021).

1.4 Glycosylation

1.4.1 DENV protein glycosylation

Glycosylation is the enzymatic incorporation of complex oligosaccharide structures to proteins or lipids and involves a vast network of host glycosidases and glycotransferases within the ER and Golgi network (Varki et al 2015; Yap et al 2017). Viruses are heavily reliant on host cell glycosylation machinery to glycosylate their respective proteins, and in many instances glycosylation of viral proteins has been shown to be essential for the infectivity, stability, and antigenicity of several viruses, such as HIV and Influenza virus (Doores 2015; Medina et al 2013). Interestingly, glycosylation has also been exploited by viruses as a mechanism to evade effective immune recognition of underlying viral protein sequences by host antibodies, highlighting the importance of glycosylation modifications in viral immune evasion (Yap et al 2017).

In DENV, only the prM/M, E and NS1 proteins are currently known to be *N*-glycosylated. (Flamand et al 1999; Chambers et al 1990; Winkler et al 1989; Winkler et al 1988). The E protein undergoes *N*-linked glycosylation at two asparagine residues, N67 and N153 while the NS1 protein is *N*-glycosylated on N130 and N207 residues (Flamand et al 1999; Chambers et al 1990; Winkler et al 1989; Winkler et al 1988). The prM/M protein on the other hand is only known to be glycosylated at N69, although it has been proposed to have additional glycosylation sites at N7, N31 and N52 (Yap et al 2017; Courageot et al 2000).

Following the cleavage of the NS1-NS2A junction by an undefined protease in the ER, glycosylation of DENV NS1 occurs where high mannose carbohydrates moieties are added to asparagine residues at 130 and 207 (Pryor and Wright 1994; Winkler et al 1988). In the Golgi, additional NS1 glycan modification occurs, such that a complex-type sugar is incorporated onto N130 glycan, while the high mannose moiety on N207 remains (Pryor and Wright 1994). *N*-glycosylation on NS1 has been widely shown to be essential in multiple NS1 functions throughout the DENV life cycle. Mutating either N130 or N207 glycosylation sites within

DENV NS1 appeared to impede virus growth, thus reducing mouse DENV neurovirulence (Crabtree et al 2005). The alteration of both *N*-linked glycosylation sites within NS1 interestingly resulted in generation of genetically unstable mutant viruses containing several additional non-silent mutations that did not display viral-induced cytopathic effect (CPE). Also, Tajima and colleagues in 2008 demonstrated that mutation of asparagine residue at 130 failed to generate viable virus in both mammalian and mosquito cells while in contrast, mutation of asparagine residue at 207 did not impede viral growth in mammalian cells. Recently, a study utilising plaque assays and indirect immunofluorescence assay approaches showed that ablation of NS1 asparagine residue 130 led to a significant reduction in NS1 protein expression while both E and NS1 protein expressions were not detected following ablation of NS1 asparagine residue 207 (Fang et al 2023). Neurovirulence appeared to be significantly attenuated in mice following 4-days post infection with a DENV strain containing NS1-deletion mutation, indicating that the N130 *N*-glycosylation site may be an essential locus in promoting viral neurovirulence. These latest findings underline the importance of NS1 *N*-linked glycosylation modifications in regard to DENV pathogenicity and hopefully provides a foundation for development of novel effective live attenuated dengue vaccines (Fang et al 2023).

1.4.2 Glycosylation and NS1 secretion

Although there have been many studies on the effects of *N*-linked glycosylation on flavivirus NS1 secretion, the findings have varied considerably. In early studies, it was shown that ablation of one or both glycosylation sites did not impact on NS1 dimerization and secretion, although the mutation of N207 led to a reduction of NS1 secretion and NS1 dimer stability (Winkler et al 1989, Pryor and Wright 1994). Thus, the effect of disruption of glycosylation of NS1 secretion is believed to be linked with the stability of the NS1 oligomer itself. Indeed, DENV-2 infected cells treated with tunicamycin, an antibiotic compound that inhibits *N*-linked glycosylation further confirmed that the absence of *N*-glycosylation was exclusively

responsible for the instability of NS1 oligomers rather than modifications of the polypeptide backbone in NS1 non-glycosylated mutants (Winkler et al 1989; Pryor and Wright 1994).

Furthermore, NS1 secretion was observed to be significantly reduced when DENV-infected cells were treated with *N*-linked glycosylation inhibitors, swainsonine and 1-deoxymannojirimycin (Flamand et al 1999). Additionally, a Yellow Fever Virus non-glycosylated mutant lacking the N130 glycan displayed decreased virus production and reduced cytopathic effects as well as impaired NS1 secretion activity in SW13 human adrenal carcinoma cells (Muyaert et al 1996; Somnuk et al 2011). However, it has been suggested that the discrepancies between these two studies may relate to the treatment of DENV-infected cells with swainsonine and 1-deoxymannojirimycin as well as mutation of YFV N130 glycan which diminished viral infectivity thereby indirectly affecting the release and accumulation of secreted NS1 in the extracellular environment (Somnuk et al 2011).

Fascinatingly, it has been demonstrated that the DENV NS1 N130 glycan is essential for stabilisation of secreted NS1 whereas the N207 glycan promotes stability of the extracellular protein and its secretion (Somnuk et al 2011). NS1 protein levels of a single glycosylation mutant, N207Q and a double glycosylation mutant, N130Q/N207Q, were significantly reduced in the supernatant in comparison to wildtype, while secretion of NS1 remained unaffected for the N130Q single mutant. This observation may be hypothetically attributed to two potential scenarios: Firstly, the transport of NS1 away from the perinuclear region may be affected thereby impairing NS1 secretion (Crabtree et al 2005). Another possibility is that the ablation of N207 glycan might compromise the stability of secreted NS1 as a result of the potential misfolding of NS1, thus impacting efficiency of NS1 secretion (Somnuk et al 2011). Recently, a related study by Wang et al (2019) indicated that the DENV NS1 N130 glycan was essential for NS1 protein secretion whereas the N207 glycan was dispensable for both NS1 stability and secretion, contrasting with the results of the earlier study by Somnuk

et al 2011). However, the contrasting results obtained could be attributed to the clear differences in NS1 purification strategies and signal sequences utilised in these studies (Somnuk et al 2011; Wang et al 2019).

1.5 Host factors

1.5.1 Host factors and DENV

Viruses are known to manipulate host cell membranes and machineries to generate subcellular niches that support viral RNA replication, virus assembly and suppress or evade anti-viral immune responses (Carpp et al 2014). For example, atlastins (ATLs) are ER-resident proteins involved in a variety of cellular processes such as endosomal transport, autophagy activity and lipid droplet formation and DENV has been shown to exploit and manipulate ATLs in the formation of viral replication organelles (ROs) and the process of infectious particle production (Neufeldt et al 2019). As another example, DENV NS2B3 protease can inhibit cGAS-STING signalling, which is otherwise involved in the detection of virus-induced host dsDNA release from mitochondria by the cGAS sensor and subsequent activation of STING to elicit antiviral immune responses via interferons and interferon-stimulating genes (ISGs) expression (Bhattacharya et al 2023; Aguirre et al 2017; Aguirre et al 2012; Yu et al 2012). Accordingly, DENV can effectively evade and suppress activation of cGAS-STING signalling to impair antiviral immune responses during DENV infection. The studies described above are a few of many such examples of DENV-host interactions that facilitate the viral life cycle and drives viral pathogenesis. Given the inherent limited coding capacity of RNA virus genomes and the importance of viral manipulation of host proteins and machinery for viral replication cycles and pathogenesis, most viral proteins have evolved to efficiently interact with many different host factors towards facilitation of different aspects of viral replication and spread (Carpp et al 2014).

1.5.2 Interaction of DENV NS1 with human host factors

Immunoprecipitation and proteomics-based approaches enabled identification of human heterogeneous nuclear ribonucleoproteins (hnRNP) C1/C2, which are involved in mRNA binding, as DENV NS1-interacting partners in DENV-infected HEK293T cells (Noisakran et al 2008a). Although the current nature of the interaction between NS1-hnRNP C1/C2 and NS1 and its biological significance remains elusive, it has been suggested that the structural motifs within hnRNP C1/C2 may associate or interact with NS1 directly or indirectly through other viral/host proteins or DENV RNA prior to formation of the replication complex. This notion was implied based on an earlier related study demonstrating that the hnRNP C1 protein interacts with poliovirus RNA and several viral protein precursors, in which are essential for poliovirus replication activity (Brunner et al 2005; Noisakran et al 2008a). Several years later, the same research group led by Noisakran et al 2008a applied similar affinity purification in tandem with mass spectrometry approaches to successfully identify thirty-six novel host proteins as DENV NS1 interacting partners in DENV-infected human hepatocellular carcinoma (HepG2) cells (Dechtawewat et al 2016). These novel NS1 interacting partners were found to be involved in a range of biological processes ranging from signal transduction to cell cycle progression, with the majority of them involved in cellular metabolism and modification. Among them, the statistically significant DENV interacting partners from mass spectrometry analyses, human NEK2, TAO1 and COG1 were subsequently confirmed to interact with DENV NS1 via co-immunoprecipitation and colocalisation assays. The interactions of both TAO1 and NEK2 with DENV NS1 are thought to be involved in DENV particle while interaction of COG1 protein with NS1 possibly enabled NS1 *N*-glycosylation and NS1 transport to the trans-Golgi network within DENV-infected cells. Thus, additional research of these host proteins in the involvement of these identified NS1-host factor interactions in a DENV infection remains imperative.

Recently, a global DENV NS1 protein interactome analysis successfully elucidated an extensive network of DENV NS1 interactions with human host dependency or restriction factors during DENV replication (Hafirassou et al 2017). Follow-up functional RNAi screening identified a number of host dependency factors and host restriction factors for which silencing their expression decreased or increased viral production, respectively. Several of the host dependency factors that were identified were consistent with earlier findings while this study also identified two novel host factors, the CCT complex and RACK1, that were deemed to be essential for DENV replication (Hafirassou et al 2017; Marceau et al 2016; Savidis et al 2016). Components of the OST complexes were also further identified as host factors that interacted with NS1, and they were postulated to regulate DENV protein function and glycosylation activity. Importantly, the OST complex was also confirmed to be essential for DENV replication as siRNA-mediated silencing of its subunits impaired DENV infection. The importance of this interaction was further demonstrated via experiments involving a well-characterised NGI-1 *N*-linked glycosylation inhibitor which was shown to decrease DENV and ZIKV NS1 glycosylation and impair NS1 secretion, consistent with earlier study by Pryor and Wright 1994. Therefore, pharmacological inhibition of the OST complex via NGI-1 treatment potentially presents a novel opportunity to reduce spread of DENV infection and disease severity in relation to secretion of NS1 and associated DENV disease pathogenesis (Hafirassou et al 2017).

1.6 Roles of NS1 in DENV life cycle

1.6.1 Roles of NS1 in viral replication and infectious particle production

NS1 is involved in regulation of early viral RNA replication events (Youn et al 2013; Khromykh et al 1999; Lindenbach and Rice 1997; Mackenzie et al 1996). Early studies have shown that members of the *Flaviviruses* genus, Yellow Fever Virus (YFV), Kunjin virus (KUNV) and West Nile Virus (WNV) in which NS1 has been deleted are incapable of viral replication (Scaturro et al 2015; Khromykh et al 1999; Lindenbach and Rice 1997). However, an established functional trans-complementation assay can be utilised to efficiently rescue NS1-lacking viruses via ectopic expression of NS1 from heterologous flaviviruses (Scaturro et al 2015; Lindenbach and Rice 1997). A DENV-based trans-complementation system utilising a full-length infectious DENV genome reporter construct with a partial in-frame deletion within NS1 gene (Δ NS1) was also successfully developed to characterise the roles of NS1 in the DENV life cycle, and interestingly demonstrated that NS1 secretion is dispensable for viral RNA replication and infectious virus production (Scaturro et al 2015; Fischl and Bartenschlager 2013).

NS1 has been established to have an important role in viral RNA replication, given its inherent participation in the formation of the viral replication complex (Youn et al 2013; Lindenbach and Rice 1997; Mackenzie et al 1996). Scaturro et al 2015 utilised a full length DENV genome luciferase reporter construct to determine the impact of 46 NS1 point mutants of conserved sites that were predicted to be essential in NS1 folding activity within the DENV life cycle. Indeed, approximately half of the cohort of NS1 selected mutations within the wing domain and β -ladder domain resulted in complete abrogation of DENV RNA replication activity. Among these, replication deficient NS1 mutants were mutations within the conserved cysteine residues, which has previously been demonstrated by Fan et al 2014 to be critical to viral RNA replication and viral spread.

NS1 was also identified as a crucial determinant for infectious virus production (Scaturro et al 2015). This study identified a group of residues (S114, W115, D180, T301) that when substituted with alanine via an alanine scanning mutagenesis approach led to a significant decrease in production of infectious DENV particles with very minimal effects on RNA replication activity. It was suggested that this inherent impairment of infectious DENV production might be potentially due to the disruptions of NS1 interactions with DENV structural proteins. Additionally, follow-up co-immunoprecipitation experiments demonstrated a significant reduction in the interactions of both S114A and W115A point mutants with all the DENV structural proteins. Although D180A and T301A mutations caused a loss of interaction with the capsid protein, they retained the established interactions of NS1 with the remaining structural proteins, potentially indicating that NS1 has an essential role in infectious particle production that is independent of its association with envelope glycoproteins. Thus, the underlying molecular mechanisms involved in the specific roles of NS1 in infectious virus production remain poorly understood.

1.6.2 Replication independent characterisation of DENV VP formation

Early studies demonstrated that DENV infection induces endoplasmic reticulum-derived membrane rearrangements and gives rise to various distinct morphologies including convoluted membranes and clustered ER membrane invaginations known as vesicle packets (VPs); the likely site of viral RNA replication (Welsch et al 2009; Mackenzie et al 1996). While the 3D morphological architecture of DENV and ZIKV viral replication sites have been well-characterised, the underlying mechanisms involved in VP formation have been fundamentally challenging to investigate (Cerikan et al 2020; Cortese et al 2017; Welsch et al 2009; Mackenzie et al 1996). For instance, the study of candidate viral and host proteins potentially involved in VP formation was difficult to disseminate from their involvement in other aspects of RNA replication when using replication-competent viral system.

To overcome this barrier, a replication-independent viral NS polyprotein expression-based system termed “pIRO” was developed and utilised by Cerikan et al 2020. Interestingly, it was revealed that RNA elements within the 3’ UTR and not the 5’ UTR together with the DENV NS1-5 polyprotein was necessary for formation of DENV VPs. Valuable insights into the underlying mechanisms involved in VP formation can be greatly explored using the recently established pIRO system and this may evidently facilitate the development of urgently needed antiviral drugs that can disrupt DENV and ZIKV RNA replication.

1.7 Secreted NS1 (sNS1) and its many roles in DENV pathogenesis

NS1 is secreted from DENV-infected cells as a soluble hexameric lipoparticle (Young et al 2000; Librarty et al 2002). Secreted NS1 has been shown to be involved in a variety of extracellular functions associated with severe DENV infections, since early studies documented its detection at elevated levels in the plasma of DENV-infected patients. It has been established that sNS1 and the plasma membrane associated NS1 are involved in DENV immune evasion through a wide range of mechanisms such as the activation or inhibition of complement pathways and even generation of autoantibodies that cross-react with non-infected endothelial cells and platelets leading to endothelial dysfunction; one of the signature hallmarks of flavivirus disease pathogenesis (Muller and Young 2013; Avirutnan et al 2011; Avirutnan et al 2010; Falconar 2007; Falconar 1997).

As described earlier, a distinctive hallmark of flavivirus disease pathogenesis is the disruption of endothelial integrity (Watterson et al 2016; Avirutnan et al 2006). Plasma leakage occurs after the disruption of endothelial cell barrier integrity subsequently leading to haemorrhage and fluid loss which are strongly linked with DENV infections (Yin et al 2013). Both sNS1

and NS1 have been shown to be able to induce human complement activation (Watterson et al 2016; Avirutnan et al 2006). sNS1 initiation of complement activation has been demonstrated to lead to the generation of SC5b-9 complexes which subsequently induce inflammatory cytokine production and also induce vascular leakage in a subset of dengue infected patients (Avirutnan et al 2006). Additionally, sNS1 derived from DENV, Yellow Fever virus (YFV) and West Nile virus (WNV) can also inhibit the classical and lectin complement activation pathways by associating with and promoting the degradation of an opsonin, C4b by complement-derived protease C1s, leading to protection from complement-dependent neutralisation (Avirutnan et al 2006; Avirutnan et al 2010).

In addition to its roles in triggering endothelial permeability leading to vascular leakage via generation of autoantibodies and the inhibition or activation of complement pathways, sNS1 has also been identified as a pathogen-associated molecular pattern (PAMP) that can activate the pattern recognition receptor (PRR), Toll-like receptor 4 (TLR-4) to induce the expression of high levels of vasoactive chemokines and cytokines such as IL-6 and IL-1 β from human peripheral blood mononuclear cells (PBMCs), subsequently leading to vascular leakage (Beatty et al 2015; Modhiran et al 2015). Importantly, pre-treatment of endothelial cells with a blocking anti-TLR-4 antibody successfully inhibited sNS1-mediated vascular leakage, indicating that sNS1-mediated TLR-4 activation directly leads to vascular leakage.

Accordingly, inhibition of NS1-TLR-4 interactions has been strongly proposed as a viable therapeutic strategy to potentially disrupt the pathogenic activity of sNS1 in promoting vascular leakage in DENV-infected individuals. Interestingly, a subsequent study demonstrated that apart from TLR-4, sNS1 has also been implicated in activation of both Toll-like receptor 2 (TLR-2) and Toll-like receptor 6 (TLR-6) signalling pathways leading to induction of chemokines and cytokines in DENV-infected PBMCs (Chen et al 2015).

Furthermore, survivability rates in DENV-2 infected TLR-6 KO mice were shown to increase significantly compared to wildtype controls, suggesting that the sNS1-TLR-6 interaction axis is important in pathological immune responses during DENV infection. Thus, the major

TLR(s) implicated in the detection of NS1 during an infection is somewhat controversial given the contrasting findings from these above studies (Modhiran et al 2015; Chen et al 2015). However, it has been suggested in a subsequent study by Modhiran et al 2015 that the differences may be attributable to mis-folding and/or contamination with TLR-2/TLR-6 ligands of the commercially available NS1 utilised in the study of Chen et al 2015.

DENV NS1 has also been shown to directly disrupt the integrity of the endothelial glycocalyx layer (EGL) responsible for regulation of endothelial barrier function of human pulmonary microvascular endothelial cells (Puerta-Guardo et al 2016). The sNS1-mediated activation of cellular enzymes, including cathepsin L, has been demonstrated to promote degradation and shedding of components of the EGL layer, leading to the disruption of its integrity and eventually endothelial hyperpermeability (Puerta-Guardo et al 2016). Furthermore, a cohort of NS1 proteins from 5 different flaviviruses including DENV was shown to be able to trigger endothelial barrier dysfunction and hyper permeability *in vivo* in a tissue-specific manner (Puerta-Guardo et al 2019). Unlike the NS1 proteins of the flaviviruses, only DENV NS1 was able to induce hyperpermeability *in vitro* in pulmonary endothelial cells as well as trigger vascular leakage in all evaluated organs in mice. These findings indicate that each respective flavivirus NS1 protein is able to promote endothelial dysfunction and trigger vascular leakage in a tissue-specific manner that distinctly reflects the unique disease pathogenesis of the respective flavivirus infections (Puerta-Guardo et al 2019). Of note, a murine-derived NS1 monoclonal antibody (IG5.3) which exhibits high cross-reactivity towards DENV and ZIKV NS1 proteins, was subsequently shown to prevent DENV NS1-mediated cell barrier integrity disruption for all NS1 tested species including WNV and ZIKV in a variety of disease-relevant human cell lines such as umbilical endothelial cells (HUVEC) and microvascular endothelial cells (HMEC-1) (Modhiran et al 2021). 80% survivability rate was also observed in murine lethal challenge model for DENV following therapeutic treatment with IG5.3. Overall, the findings suggests that IG5.3 monoclonal antibody with its demonstrated

inhibition of multi-flavivirus NS1 activity can be considered as novel antiviral development (Modhiran et al 2021).

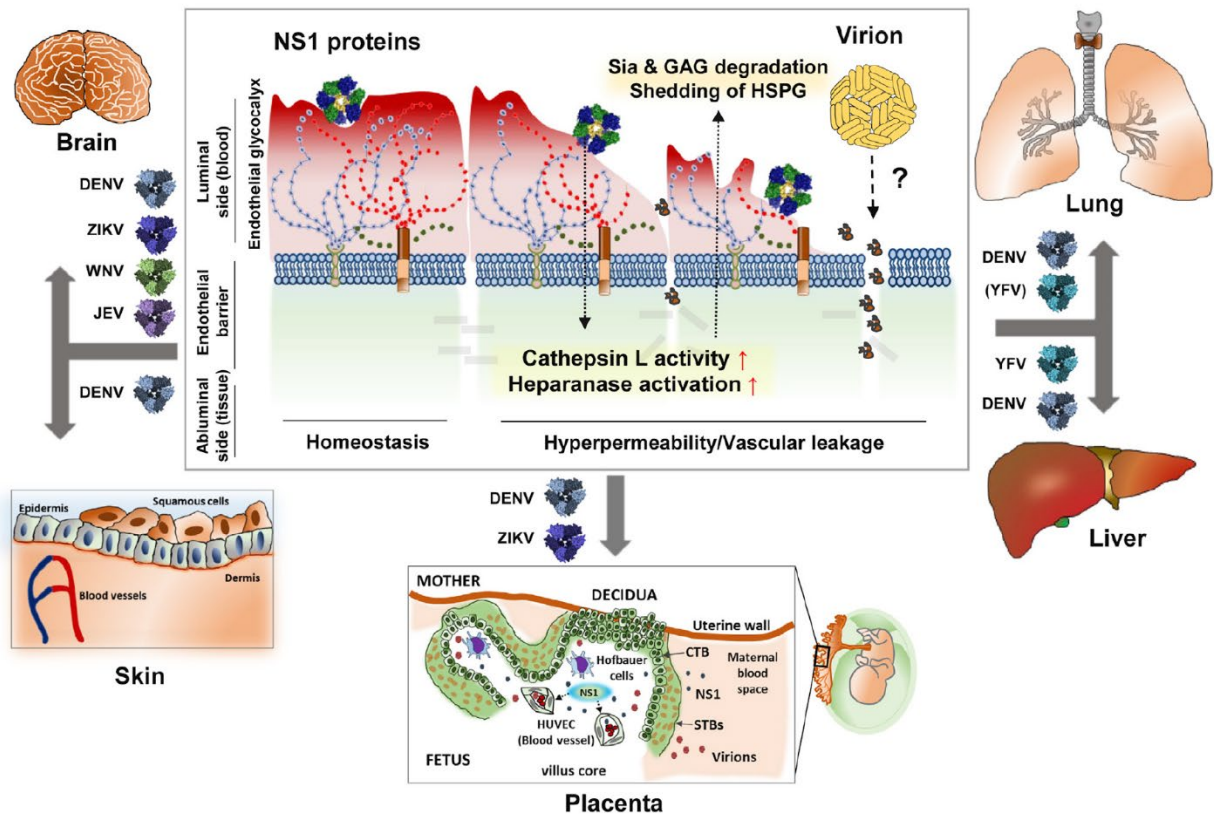


Figure 1.7.1.1 Schematic diagram of flavivirus NS1-mediated disease pathogenesis outlining flavivirus NS1-mediated endothelial cell-dependent hyperpermeability and tissues-specific vascular leakage. Infection with flaviviruses (DENV, WNV, ZIKV, YFV, JEV) leads to the secretion of soluble viral NS1 protein which directly triggers endothelial hyperpermeability and vascular leakage associated with disruption of the endothelial glycocalyx layer (EGL) responsible for regulation of barrier function within endothelial cells. The study by Puerto-Guardo and colleagues (2019) described an endothelial cell-type dependent increase in hyperpermeability and vascular leakage mediated by different flavivirus NS1 proteins that reflects the disease pathogenesis of respective flavivirus infections. DENV NS1 increases the permeability of endothelial cells derived from various tissues, lung, skin, umbilical vein, brain, and liver as shown. ZIKV NS1 appeared to induce endothelial dysfunction of brain-derived endothelial cells and umbilical vein endothelial cells, reflecting severe congenital and neurological defects associated with ZIKV. JEV and WNV NS1 only disrupt the barrier function of brain-derived endothelial cells, consistent with the encephalitic

and neurotropic nature of JEV and WNV disease. YFV NS1 increases the endothelial permeability of lung and liver endothelial cells, consistent with systemic and hepatic pathology of YFV infection. Adapted from Puerto-Guardo et al 2019.

Also, DENV NS1 mutagenesis and transendothelial electrical resistance (TEER) studies revealed that two NS1 domains, the wing and the β -ladder domain are essential for NS1-mediated endothelial dysfunction (Biering et al 2021). The NS1 wing domain is suggested to be essential for initial attachment to cells, while the β -ladder is important for activation of downstream events needed to initiate DENV, ZIKV and WNV NS1-mediated endothelial dysfunction. A NS1-targeting monoclonal antibody, 2B7 has been shown to confer protection against NS1-mediated pathogenesis of multiple flaviviruses including DENV and results suggest that 2B7 can concurrently antagonise cellular interactions of both NS1 wing and β -ladder domains, supporting the proposed potential to treat multiple flavivirus infections with a single therapeutic strategy targeting flavivirus NS1 via the disease-neutralizing 2B7 antibody (Beatty et al 2015; Biering et al 2021). In NS1 chimera studies, residues from position 91 to 93 (**GDI**) within the DENV NS1 wing domain were shown to be essential for tissue-specific NS1 endothelial cell binding, as exchanging the DENV-GDI with WNV-EKQ via NS1 site-directed mutagenesis led to a reduction in the binding capacity of NS1 to human pulmonary microvascular endothelial cells (HPMECs) *in vitro*, as well as a reduced induction of vascular leakage in an *in vivo* mouse model of localised leak (Lo et al 2022). Additionally, TEER studies utilising DENV-WNV NS1 chimeras containing either the DENV wing or β -ladder domain were unable to exhibit TEER reduction values to a similar extent to that of the wildtype DENV NS1, suggesting that both of these DENV-derived domains are essential for the ability of DENV NS1 to cause HPMEC hyperpermeability. Taken together, these findings also appeared to be consistent with earlier studies that reported that the NS1 wing domain is involved in NS1-endothelial cell binding while the β -ladder domain is involved in triggering NS1-mediated endothelial hyperpermeability (Lo et al 2022; Biering et al 2021). Although the

underlying mechanism(s) involved in endothelial cell binding by the **GDI** motif of the NS1 wing domain remains unclear, an improved understanding of the exact features and importance of NS1 wing and β -ladder domains in flavivirus pathogenesis can hopefully pave the way for novel antiviral therapies and strategies (Lo et al 2022). In this context, β -D-glucan derived from fruiting bodies (FR) of the fungus *Agaricus subrufescens* that has been broadly applied for its anti-tumoral and immunomodulatory therapeutic properties, and its sulfated derivatives (FR-S), were identified as promising anti-DENV agents that may target NS1 (de Sousa et al 2022). In *in vitro* experiments, FR-S was shown to significantly inhibit both DENV and ZIKV replication in human monocytic cells as well as inhibit NS1 binding activity to HPMECs. FR-S also significantly reduced DENV NS1-mediated vascular leakage in the mouse dermis and reduce mortality and morbidity in an *in vivo* mouse model of dengue localised leak syndrome, suggesting that these glycans bind to NS1 to prevent its subsequent interactions with host endothelial cells leading to downstream events pertaining to viral pathogenesis. These promising findings support additional studies of FR-S and other known or novel sulfated glycans as potential novel antiviral candidates that may limit flavivirus pathogenesis via interference with NS1-mediated vascular leakage (de Sousa et al 2022).

1.8 The application of APEX peroxidase-catalysed proximity labelling in characterisation of protein microenvironments in situ

When it comes to defining essential components of cellular processes, organelles, and machinery, specifically involving imaging of cellular morphological structures at nanometer resolution, electron microscopy (EM) today remains the undisputed conventional methodology to go to (Kalocsay 2019; Martell et al 2012). This normally involves the application of traditional standard antibody-based detection approaches; however, this has been gradually displaced with the introduction of genetically encoded tags like horseradish peroxidase (HRP) which conveniently do not require tedious processing steps that will induce degradation of cellular structures of interest as the former (Martell et al 2012). Thus, there is a need for techniques that can be applied to imaging relevant structures at high resolution and characterising the components of these structures in an unbiased manner.

The development of an engineered plant ascorbate peroxidase (APX) known as APEX, and improved variants of the reporter enzyme represents a significant breakthrough in exploration of protein localisation by electron microscopy and protein microenvironments by proximity labelling-coupled proteomics approaches, respectively. APEX was initially developed as an EM tag that can be actively expressed in all known cellular compartments and still retain its enzymatic activities even following harsh EM fixation processes (Martell et al 2012). APEX was utilised to map the proteome of the human mitochondrial matrix and also successfully uncovered 31 novel proteins linked to the human mitochondria (Rhee et al 2013).

Interestingly, this group successfully developed a much-improved variant of this APEX tag, “APEX2” which has been shown to display improved resistance to high hydrogen peroxide concentrations, thermal stability and heme binding (Lam et al 2015). Since its development, APEX2 has been widely used in tandem with immunofluorescence analysis in several published protein colocalisation studies including in DENV and Hepatitis C virus studies (Eyre et al 2017a; Eyre et al 2017b). Another APEX2-based study also successfully utilised a combination of APEX2 proximity biotinylation and stable isotope labelling by amino acids in

cell culture (SILAC) to establish a mitochondrial intermembrane space proteome map of 127 proteins with >94% specificity, including identifying several newly uncharacterised mitochondrial proteins in the process (Hung et al 2014). Utilisation of these newly developed proximity labelling techniques coupled with proteomics approaches have enabled further investigations of biological processes previously known to be inaccessible and limited. Despite so, further development and engineering of these tools is needed to fully maximise the potential of these tools in terms of improving spatiotemporal specificity of interaction networks as well as obtaining more comprehensive interactome maps of interest.

1.9 The research gap

sNS1 has been strongly associated with DENV disease pathogenesis since its detection in significantly high levels in the blood of DENV-infected patients (Alcon et al 2002). As described earlier, the pathogenic activity of sNS1 comprises a variety of extracellular roles ranging from elicitation of autoantibodies to the activation or inhibition of complement pathways, of which all leads to the disruption of endothelial barrier integrity, causing vascular leakage in the process (Modhiran et al 2015; Watterson et al 2016; Puerta-Guardo et al 2016 Avirutnan et al 2006; Avirutnan et al 2010). Several NS1 mutagenesis studies have identified residues within the NS1 that are important for its roles in DENV RNA replication, infectious virus production, DENV pathogenic activity and NS1 secretion as well. However, despite the importance of NS1 secretion in DENV disease pathogenesis, the exact molecular determinants of NS1 that are essential for its efficient secretion remain poorly characterised.

Hypothesis: Key residues in DENV NS1 protein are crucial for its secretion and thus could be potential targets for antiviral strategies

1.9.1 Project Aims

AIM 1: To identify key residues of the DENV NS1 protein that are crucial for its secretion via high throughout mutagenesis and sensitive luciferase-based detection assays

Aim 1.1 To identify NS1 point-mutations that result in impaired NS1 secretion as determined via sensitive luciferase assays

Aim 1.2 To visualise the locations of these NS1 key mutations on established NS1 dimer and hexamer 3D structures via *in silico* analyses

AIM 2: Functional characterisation of these DENV NS1 secretion-impaired mutants with respect to roles of NS1 in the DENV replication cycle

Aim 2.1 To evaluate the viral fitness of selected NS1 secretion-impaired point mutants in supporting DENV RNA replication and infectious virus production

Aim 2.2 To characterise selected NS1 secretion-impairing mutants in the context of a replication independent DENV NS1-5 polyprotein expression system (pIRO-D)

AIM 3: Identifying host factors associated with DENV NS1 N-glycosylation

Aim 3.1 To perform proof of concept experiments involving validation of APEX2-NS1 biotinylation activity in the context of viral infection and NS1-5 polyprotein expression via immunofluorescence and Western blotting experiments

Aim 3.2 To optimise and prepare NS1-proximal biotinylated protein samples for LC-MS/MS analyses

Chapter 2

Materials and Methods

2.1 General Molecular Biology Methods

2.1.1 Mini-preparation of plasmid DNA. For preparation of each plasmid clone, a single isolated bacterial colony obtained from transformation was selected and picked from an LB agar plate containing appropriate antibiotic (Ampicillin at 100 µg/mL or Kanamycin at 50 µg/mL) (See **Appendix I: Buffers, Media and Solutions**) and inoculated into a 14mL polypropene centrifuge tube containing 5-10 mL of Luria Broth supplemented with 0.1% ampicillin (100µg/mL). Inoculants in tubes were incubated overnight with shaking on a 37°C incubator. Inoculants were then briefly centrifuged for 15 minutes at 5, 000 x g at room temperature (RT). Following centrifugation, supernatants were discarded and inactivated with sodium hypochlorite, while pelleted bacteria were processed for plasmid DNA extraction using a Macherey-Nagel NucleoSpin® Plasmid QuickPure kit as per manufacturer's instructions. Where appropriate, purified plasmid DNA was analysed via diagnostic restriction digest as described below (See **2.1.4 Diagnostic restriction digest of plasmid DNA**).

2.1.2 Midi-preparation of plasmid DNA. Single bacterial colonies derived from the transformation process (See **2.1.3 Chemical transformation of competent bacteria with plasmid DNA**) were picked from LB plates containing antibiotic with a sterile pipette tip and inoculated into 200 mL of LB supplemented with 100 µg/mL ampicillin and cultured overnight at 37°C with agitation. Plasmid DNA was purified using the NucleoBond® Xtra Midi kit (Macherey-Nagel) as per manufacturer's instructions for medium scale preparation of plasmid DNA. Following the elution step, plasmid DNA concentration was quantified using a NanoDrop Spectrophotometer (Thermo Fisher) instrument (See **2.1.18 Quantification of nucleic acids**). However, for low copy plasmids like the pFKDVs series that are relatively

difficult to culture due to their inherent instability, for each clone, a 10 mL starter LB culture was set up by selecting a single small isolated bacterial colony from the LB-Amp agar plate and cultured at 37°C with agitation for 5-6 hours. Following 5-6 hours of culturing at 37°C, the entire 10 mL starter LB culture was then subsequently transferred into a larger LB culture (250-500 mL) supplemented with ampicillin and cultured overnight at 37°C with agitation.

2.1.3 Chemical transformation of competent bacteria with plasmid DNA. 10-100 ng of plasmid DNA was mixed into 25-50 µL aliquots of high efficiency 5-alpha chemically competent *Escherichia coli* cells (New England BioLabs). Competent cells were then incubated on ice for 30 minutes before undergoing heat-shock at 42 °C for 30 seconds. Heat-shocked cells were incubated in super optimal broth supplemented with glucose (SOC) with agitation at 37°C for 1 hour. Following incubation, 100 µL of transformed competent cells were then plated onto agar plates containing appropriate antibiotics and incubated overnight at 37°C.

2.1.4 Diagnostic restriction digest of plasmid DNA. To perform a diagnostic restriction digest of plasmid DNA, 400-700 ng of plasmid DNA, 1 µL of each respective restriction enzyme (New England BioLabs), 2 µL of 10X CutSmart® Buffer (New England BioLabs) and nuclease-free H₂O added up to a final volume of 20 µL were prepared in a PCR tube, mixed, and incubated overnight at 37°C. Digested plasmid DNA was then mixed with 6X Purple/Blue Loading Dye (New England BioLabs) and subjected to agarose gel electrophoresis (See **2.1.5 Agarose gel electrophoresis**).

2.1.5 Agarose gel electrophoresis. To prepare 1% agarose gels, 1g of agarose powder (Bioline) was dissolved in 100 mL of 1 X TAE buffer by heating up using a microwave. Then, 5 μ L of RedSafe® Nucleic Acid Staining Solution (Intron Biotechnology) was added and mixed gently before pouring into a gel tray with an appropriate well comb size of interest. Following hardening of gel, the well comb was removed, and the gel was placed and immersed within a Mini-Sub Cell® GT Agarose Gel Electrophoresis System (Bio-Rad) containing 1 X TAE buffer. Following this, plasmid DNA samples of interest were mixed with 6X Purple / Blue Loading Dye (New England Biolabs) to a 1 X final concentration of loading dye. Plasmid DNA samples and diluted 1 kb DNA ladder mix (containing 6X Loading Dye and nuclease-free H₂O) were loaded into wells and electrophoresis was subsequently performed at 100V for 60 minutes. Following electrophoresis, gels were visualised using a ChemiDoc® MP Imaging System (Bio-Rad) via accompanying Imaging Lab software using appropriate settings for RedSafe. To validate integrity of *in vitro* transcribed RNA transcripts as detailed below in **2.1.19 Production and isolation of SP6 RNA polymerase-derived RNA transcripts**, the agarose gel electrophoresis tanks and combs were thoroughly rinsed with ethanol and autoclaved H₂O and fresh agarose solution was made with autoclaved H₂O for each respective gel.

2.1.6 Gel extraction. Following agarose gel electrophoresis, bands of interest from agarose were excised with a sterile scalpel blade on a NovaLine® Standard UV Transilluminator box. Excised agarose fragments containing DNA fragments of interest were purified using a Macherey-Nagel Nucleospin® Gel and PCR Clean-up kit as described in the manufacturer's instructions. In brief, 100 μ L of binding buffer was added to each 50 mg of agarose gel fragment and incubated at 60°C for 10 minutes with mixing and vortexing. Once the agarose gel was fully dissolved, the mixture was transferred to a column and centrifuged at 11, 000 x g for 1 minute. Wash solution containing ethanol (500-700 μ L) was added to column and

centrifuged at 11, 000 x g for 1 minute. Following this, the flow-through was discarded and columns were centrifuged again at 11,000 x g for 1 minute. For elution, either pre-warmed TE buffer or nuclease-free H₂O was added to the column and incubated at RT for 1 minute, before centrifuging columns at 11, 000 x g for 1 minute. Purified samples of interest were analysed for DNA concentration and purity (A₂₆₀/A₂₈₀ ratio; ~1.8 for DNA) using a NanoDrop Spectrophotometer (Thermo Fisher) instrument before storing purified samples at -20°C.

2.1.7 DNA Ligation. Plasmid vector DNA (50 ng) and DNA inserts of interest were mixed thoroughly at a molar ratio of 3:1 for ligation reactions involving restriction enzyme cloning. For T4 DNA ligation, ligation reactions consisting of insert DNA and vector DNA, 1 µL of T4 DNA ligase (New England BioLabs) and 2 µL of 10 X T4 ligase buffer (New England BioLabs) were prepared in nuclease-free H₂O to a final volume of 20 µL. Ligation mixes were subsequently incubated at RT for 10 minutes or overnight at 14°C before transforming the mix into competent bacterial cells (See **2.1.3 Chemical transformation of competent bacteria with plasmid DNA**). For Quick Ligation, a reaction containing the restriction enzyme digested vector DNA (50 ng), DNA insert, 10 µL of 2 X Quick Ligase Reaction Buffer (New England BioLabs), 1 µL of Quick Ligase and nuclease-free H₂O to a final volume of 20 µL was thoroughly mixed, vortexed, and incubated at RT (25°C) for 5 minutes before transforming the mix into competent bacterial cells.

2.1.8 Phosphorylating and annealing HiBiT Oligonucleotides. A PCR tube containing 10 X T4 ligase buffer (New England BioLabs), 1 µL of each complimentary oligonucleotide (See **HiBiT TOP FWD** and **HiBiT BOT REV primers** in **Appendix II: Primers**), 1 µL of T4 Polynucleotide Kinase (PNK) and nuclease-free H₂O added to a final volume of 20 µL was prepared. The protocol was set up and run as follows: Step 1: 37°C for 30 minutes, Step 2:

95°C for 5 minutes, Step 3: 70°C for 10 minutes. Following this, the mix was then allowed to cool for 1 hour at RT. Following this, an aliquot of the sample was diluted in nuclease-free H₂O (1 in 40) before ligating the diluted oligo duplex and 50-100 ng of digested plasmid DNA of interest (See **2.1.7 DNA Ligation**). The ligation mix was then transformed into competent bacterial cells as detailed above (See **2.1.3 Chemical transformation of competent bacteria with plasmid DNA**).

2.1.9 Polymerase Chain Reaction (PCR).

2.1.9.1. Q5® High-Fidelity PCR (New England BioLabs) was utilised for high fidelity PCR amplifications of gene fragments for molecular cloning purposes. PCR reactions were set up as 25 µL reactions on ice containing 12.5 µL of Q5® High-fidelity 2X Master Mix, 1.25 µL of each 10 µM forward/reverse primer (See **Appendix II: Primers**), 100-200 ng of template DNA and remaining nuclease-free H₂O to 25 µL. PCR reactions were then performed using a S1000® Thermal Cycler (Bio-Rad) with the appropriate thermal cycling conditions [Step 1: 98°C for 30 seconds, Step 2: 95°C for 10 seconds, Step 3: 64-72°C (as appropriate for a given oligonucleotide pair) for 30 seconds, Step 4: 72°C for 50 seconds, Step 5: Repeat Steps 2-4 for 30X, Step 6: 72°C for 1 minute 30 seconds, Step 7: Hold at 4°C].

2.1.9.2. GeneMorph II Random Mutagenesis. (Agilent Technologies) was utilised for the random PCR-based point mutagenesis to generate NS1 mutant clones. PCR reactions were set up in 50 µL volumes containing 250-500 ng of DNA template, 1 µL of Mutazyme II DNA Polymerase (2.5 U/ µL), 250ng of each forward/reverse primer, 5 µL of 10 X Mutazyme II reaction buffer, 1 µL of 40 mM dNTP mix and nuclease-free H₂O to a final volume of 50 µL. PCR reactions were performed using a S1000® Thermal Cycler (Bio-Rad) as described above with appropriate thermal cycling conditions [Step 1: 95°C for 2 minutes, Step 2: 95°C for 30 seconds, Step 3: 64-72°C for 30 seconds (depending on the T_m of the given primers), Step 4: 72°C for 1 minute and 30 seconds, Step 5: Repeat Step 2-4 for 30X, Step 6: 72°C for 2

minutes, Step 7: Hold at 4°C]. Following PCR, PCR products were purified as detailed below in **2.1.10 PCR product and DNA fragment purification**.

2.1.10 PCR product and DNA fragment purification. Where appropriate, such as following PCR-based random point mutagenesis, PCR products were subsequently incubated with 2 µL of *DpnI* enzyme (New England BioLabs) for 2 hours at 37°C to remove plasmid DNA template which may contaminate downstream reactions. PCR products were purified using a Macherey-Nagel Nucleospin® Gel and PCR Clean-up kit, as detailed above in **2.1.6 Gel extraction**. Similarly for overnight *XbaI* linearisation reactions to generate templates for *in vitro* RNA transcription (See **2.1.19 Production and isolation of SP6-derived RNA transcripts**), digested products were immediately purified using the Macherey-Nagel Nucleospin® Gel and PCR Clean-up kit and eluted in 11-13 µL of pre-warmed nuclease-free H₂O.

2.1.11 Plasmid DNA dephosphorylation. To reduce vector religation prior to Gibson Assembly reactions (See **2.1.12 NEBuilder HiFi DNA Assembly**), restriction digested cloning vectors were subjected to dephosphorylation via the addition of 2 µL of 10 X Antarctic Phosphatase Reaction Buffer (New England BioLabs) and 2 µL of Antarctic Phosphatase (New England BioLabs) in a total volume of 20 µL. The Antarctic Phosphatase reaction protocol was performed using a S1000® Thermal Cycler (Bio-Rad) according to manufacturer instructions [Step 1: 37°C for 30 minutes, Step 2: 80°C for 2 minutes, Step 3: Hold at 4°C]. Agarose gel electrophoresis (See **2.1.5 Agarose gel electrophoresis**) was performed before gel extraction of the digested and dephosphorylated plasmid DNA fragment of interest where as indicated.

2.1.12 NEBuilder HiFi DNA Assembly. The NEB Builder HiFi DNA Assembly Cloning Kit (New England BioLabs) was employed for various cloning reactions. Reactions were set up on ice as per manufacturer's instructions and consisted of 50 ng of digested plasmid DNA, insert DNA PCR products (DNA molar ratio of vector: insert = 1:2 as recommended for 2-3 fragments assembly), 10 μ L of the NEB Builder HiFi DNA Assembly Master Mix and nuclease-free H₂O added to a final volume of 20 μ L per reaction. Reactions were conducted using a S1000® Thermal Cycler (Bio-Rad) as followed [Step 1: 50°C for 1 hour, Step 2: Hold at 4°C]. 2 μ L of NEBuilder HiFi DNA reaction generated products were subsequently transformed into competent cells, as described above (See **2.1.3 Chemical transformation of competent bacteria with plasmid DNA.**).

2.1.13 Colony PCR. Colony PCR was performed as follows. Following transformation, individual colonies were randomly selected and picked with a sterile pipette tip and dipped into a sterile PCR tube containing 5 μ L of nuclease-free H₂O. The given pipette tip was then streaked onto a grid-labelled LB agar plate supplemented with ampicillin (100 μ g/mL) and incubated overnight at 37°C. PCR master mixes were prepared such that each reaction comprised of 0.25 μ L of GoTaq® DNA Polymerase (Promega), 1 μ L of 10mM dNTP mix (Promega), 10 μ L of 5X Green GoTaq® Reaction Buffer (Promega), 1 μ L of each 20 μ M primer specific for insert of interest and nuclease-free H₂O to a final volume of 50 μ L. These master mixes of 45 μ L/tube were distributed to each PCR tube containing bacterial remnants for each random colony. PCR reaction was then performed with the following conditions [Step1: 95°C for 2 minutes, Step 2: 95°C for 1 minutes, Step 3: 62-70°C for 1 minute, Step 4: 72°C for 1 minute and 45 seconds, Step 5: Repeat Step 2-4 for 30 cycles, Step 6: 72°C for 5 minutes, Step 7: Hold at 4°C if left overnight]. PCR products were separated on an agarose gel at 100V for 1 hour and immediately visualised on a NovaLine® Standard UV Transilluminator box to check for the presence of the insert of interest. When the specific

insert was confirmed to be present, the corresponding bacterial colony on the grid-labelled LB agar plate was selected for Mini-preparation of plasmid DNA as described above (See **2.1.1 Mini-preparation of plasmid DNA**).

2.1.14 Western Immunoblotting. Huh-7.5 cells were seeded at 1×10^5 cells/well in a 12-well plate (Corning) in 1 mL of Dulbecco's Modified Eagle Medium containing HEPES (Invitrogen) supplemented with 1% penicillin-streptomycin and 10% foetal bovine serum (FBS). Following culture for 24 hours, 1 μ g of DNA was transiently transfected into cells using 3 μ L of Lipofectamine 3000 and P3000 reagent (2 μ L of P3000 per 1 μ g of DNA) (Thermo Fisher) (See **2.2.5 Transfection of cells**). At 48-hours post-transfection, supernatant samples were collected. Following washing with 1 X PBS of remaining cell monolayers, 100-150 μ L of NP-40 lysis buffer containing protease inhibitor cocktail (See **Appendix I: Buffers, Media and Solutions**) was dispensed to each well. Lysates were harvested and homogenised by passing through a 25-gauge needle with a 1cc/mL syringe (Terumo). The supernatant and lysate samples were centrifuged at 10,000 x g at 4°C for 10-15 minutes. SDS PAGE 4 X reducing or non-reducing buffer (See **Appendix I: Buffers, Media and Solutions**) were added to samples to achieve a 1 X final concentration of loading buffer. Samples were boiled at 95°C for 5 minutes on a heating block or S1000® Thermal Cycler (Bio-Rad) before being loaded onto a 10-well /15-well 4-20% Mini PROTEAN® TGX precast gel (Bio-Rad) along with a Precision Plus Protein® Kaleidoscope® Prestained Protein Standards (Bio-Rad) protein ladder. Samples were subjected to electrophoresis at 100V for 60-65 minutes using a Mini PROTEAN® Tetra cell (Bio-Rad) in running buffer (See **Appendix I: Buffers, Media and Solutions**). Two types of protein transfer were utilised. The first involves conventional 'wet transfer' where a membrane sandwich (sponge: paper: gel: nitrocellulose membrane: paper: sponge) was constructed and proteins were transferred at 100V for 60-70 minutes in a Mini PROTEAN® 3 cell (Bio-Rad) tank system containing a

magnetic stirrer and ice pack submerged in Transfer buffer to prevent overheating of the setup (See **Appendix I: Buffers, Media and Solutions**). The other involves semi-dry transfer utilising a Trans-Blot Turbo Transfer System (Bio-Rad), where a sandwich (Bio-Rad mini-size paper stacks: mini-size nitrocellulose membrane: gel: mini-size paper stacks) was constructed as per manufacturer's instruction. Proteins were transferred to nitrocellulose membranes for 5-7 minutes via the Mixed MW 1.3A program. Following protein transfers, membranes were blocked with 5% skim milk in TBS, as detailed below.

2.1.15 Enhanced Chemiluminescence (ECL) Western Immunoblotting. Following the transfer step, nitrocellulose or PVDF membranes were incubated in Ponceau S stain for 5 minutes prior to blocking the membrane with 5% skim milk in TBS (See **Appendix I: Buffers, Media and Solutions**) for an hour with gentle agitation. The membrane was then incubated with monoclonal 4G4 primary antibody hybridoma supernatant appropriately diluted (1 in 10) (See **Appendix III: Antibodies and Dyes**) in TBS-T solution (See **Appendix I: Buffers, Media and Solutions**) containing 5% skim milk and incubated overnight with gentle agitation at 4°C. TBS-T washes were performed for 5 x 5 minutes each before incubating the membrane with goat anti-mouse secondary antibody HRP conjugate (Invitrogen) (See **Appendix III: Antibodies and Dyes**) appropriately diluted (1 in 10,000) in TBS-T containing 5% skim milk for 1 hour at RT with gentle agitation. Following the secondary antibody incubation, a second round of TBS-T washes was carried out for 5 x 5 minutes prior to incubation with an enhanced chemiluminescent (ECL) SuperSignal® West Femto Maximum Sensitivity Substrate (Thermo Scientific) solution prepared via mixing of the ECL components at a 1:1 ratio and subsequent 5 minutes incubation in the dark. Following this, membranes were imaged using a ChemiDoc® MP Imaging System instrument (Bio-Rad) and associated Imaging Lab software (Bio-Rad).

2.1.16 LI-COR Fluorescence Western Immunoblotting. Following protein transfer, nitrocellulose membranes were subjected to protein staining using the Revert® 700 Total Protein Stain Pack Insert (LI-COR, USA) stain before imaging the membranes using an Odyssey® CLx Imaging System (LI-COR, USA). Following a destaining step with a LI-COR destaining solution, membranes were then blocked with 5% skim milk in 1 X TBS for 60 minutes at RT with gentle agitation. The membrane was then incubated with 5 mL per membrane of monoclonal 4G4 primary antibody diluted (1 in 10) or anti-HiBiT peptide tag antibody diluted (1 in 1000) (See **Appendix III: Antibodies and Dyes**) in TBS-T solution (See **Appendix I: Solutions, Buffers and Media**) containing 5% skim milk at 4°C overnight with gentle orbital shaking. TBS-T washes were performed for 5 x 5 minutes each prior to incubation of membranes with secondary antibodies (See **Appendix III: Antibodies and Dyes**) appropriately diluted in TBS-T solution and 5% skim milk for 1 hour with gentle agitation in the dark at RT. Following the incubation in the dark, TBS-T washes were carried out for 6 x 5 minutes in the dark before imaging the membranes using an Odyssey® CLx Imaging System (LI-COR, USA) and the default 700nm/800nm channel.

2.1.17 Stripping and reprob ing membranes. To confirm similar loading of protein for the Western blot performed using the Enhanced Chemiluminescence (ECL) Western blotting method, blots were stripped and re-probed with anti- β - actin antibody. Stripping of bound primary and secondary antibodies was performed by incubating the membrane in freshly made stripping buffer (See **Appendix I: Solutions, Buffers and Media**) for 30 minutes at 50-60°C with agitation. 2 x 10 minutes TBS-T washes were subsequently performed followed by blocking of membrane for 60 minutes with gentle agitation in 5% skim milk in 1 X TBS. The membrane was then incubated in anti- β actin mouse monoclonal antibody (Sigma Aldrich) (1 in 10,000) (See **Appendix III: Antibodies and Dyes**), appropriately diluted in TBS-T containing 5% skim milk solution overnight at 4°C with gentle orbital shaking. TBS-T

washes, secondary antibody incubation and imaging of the blots following ECL application were performed as previously detailed above in **2.1.15 Enhanced Chemiluminescence (ECL) Western Immunoblotting**.

2.1.18 Quantification of nucleic acids. DNA or freshly prepared *in vitro* RNA transcripts were quantified using a NanoDrop Spectrophotometer (Thermo Fisher) instrument based on the 260/280 absorbance ratio. Where possible, concentrations of plasmid DNA samples were adjusted to 1 µg/µL before storing at -20°C. RNA samples were aliquoted into sterile nuclease-free 1.5 mL tubes or PCR tubes before storing at -80°C (RNA) to prevent multiple freeze thaw cycles that would potentially affect RNA integrity.

2.1.19 Production and isolation of SP6 RNA polymerase-derived RNA transcripts.

Plasmid DNA of interest (pFKDVs and pFKsgDVs series) was linearized overnight at 37°C with *Xba*I before purifying using a Nucleospin® Gel and PCR Clean-up kit (Macherey-Nagel) (See **2.1.10 PCR product and DNA fragment purification**). Purified linearised DNA template was then utilised to transcribe RNA via the SP6 RNA polymerase promoter reaction using an SP6 mMessage mMachine® Kit (Thermo Fisher). SP6 reactions were set up at RT in a 20 µL/ volume reaction containing 4.5 µL of purified linearised template (0.1-1 µg with, 1.5 µL of SP6 GTP, 10 µL of 2 x SP6 NTP/CAP, 2 µL of enzyme mix, and 2 µL of 10 x SP6 reaction buffer (Ensure this is added last in the reaction setup). Following brief vortexing, SP6 reactions were incubated at 37°C for 3 hours. Following the 3 hours incubation process, 1 µL of TURBO DNase (Thermo Fisher) was added and samples were mixed and incubated at 37°C for 15 minutes before proceeding to RNA isolation as detailed below (See **2.1.20 RNA extraction** below).

2.1.20 RNA extraction. SP6 RNA polymerase-derived *in vitro* transcribed RNA samples were transferred to nuclease-free 1.5 mL microcentrifuge tubes prior to the addition of 1 mL of TRI reagent® (Sigma-Aldrich). Samples were mixed by pipetting and incubated for 5 minutes at RT. 200 µL of chloroform was then added and tubes were shaken vigorously for 15 seconds, incubated for 5 minutes at RT and centrifuged at 12,000 x g for 25-30 minutes at 4°C. Following centrifugation, three separate layers will be very apparent: a lower pink organic phase, a middle interphase (DNA) and a clear aqueous phase (RNA) at the top. The clear aqueous phase containing RNA was transferred into a new 1.5 mL nuclease-free tube. 500 µL of isopropanol was added and mixed to precipitate the RNA before being centrifuged at 12,000 x g at 4°C for 30 minutes. Following centrifugation, the supernatant was removed without disturbing the RNA pellet of the tube (normally translucent in appearance but sometimes cannot be seen) at the bottom. RNA pellets were washed once with 1 mL of 75% ethanol (prepared in nuclease-free H₂O) before centrifuging at 7,000 x g at 4°C for 5 minutes. RNA pellets were then resuspended and dissolved in pre-warmed nuclease-free H₂O and RNA concentrations were quantified using a NanoDrop Spectrophotometer (Thermo Fisher) instrument (See **2.1.18 Quantification of nucleic acid**), before immediately storing at -80°C.

2.1.21 Sanger sequencing. To sequence cloned plasmid DNA constructs, a minimum of 500-700 ng of plasmid DNA was added to a mixture containing 1 µL of 10 µM of oligonucleotide (forward/ reverse) and nuclease-free H₂O to a total volume of 13 µL. Sequencing samples were generally prepared for both forward and reverse sequencing of PCR-amplified inserts for each clone. Samples were packaged into a ziplock bag and submitted to the Australian Genomic Research Facility (AGRF) for Sanger sequencing and resulting sequence chromatograms were analysed using the SnapGene® software (ver.7.0) or Benchling® software.

2.1.22 Graph preparation and statistical analyses. Schematic diagrams were created and using the online-tool platform, Biorender®. All graphs were generated, and statistical analyses performed using the GraphPad Prism 9 software, as described.

2.2 Cell culture techniques

2.2.1 Cryopreservation of cell lines. For long-term storage of cells in liquid nitrogen, cells at approximately 80-90% confluency with low passage number were stringently washed with 1 X PBS, trypsinised, resuspended in complete DMEM after 5 minutes of trypsinisation, and centrifuged at 200 x g for 10 minutes. Following centrifugation, supernatants were aspirated, and cells were resuspended in complete DMEM before the addition of an equal volume of filter-sterilised 2 X freezing mix (50% (v/v) DMEM, 30% (v/v) FBS, 20% (v/v) DMSO). Aliquots of 1ml cell suspensions were then transferred into cryopreservation vial tubes (Sigma-Aldrich) and placed into a Mr Frosty® Freezing Container (Thermo Fisher) containing fresh isopropanol and immediately transferred to the nearest -80°C freezer for 48-72 hours, before moving these vials into liquid nitrogen for long-term storage.

2.2.2 Resuscitation of frozen cell lines. Cryovials containing frozen cells were thawed rapidly in a 37°C water bath. Once fully thawed, cells were transferred into a 15 mL centrifuge tube (Corning) and centrifuged at 200 x g for 10 minutes. Supernatants were discarded and pelleted cells were resuspended in complete DMEM before being transferred to 25cm², 75cm² or 175cm² tissue culture flasks (Corning) containing prewarmed complete DMEM and incubated at 37°C in a 5% CO₂ humidified incubator.

2.2.3 Maintenance of cell lines in culture medium. 293FT and Huh-7.5 cell lines were maintained in complete DMEM with HEPES supplemented with 10% foetal bovine serum (FBS) and 1% penicillin-streptomycin. Huh-7.5 cell lines expressing DENV NS1-HiBiT, NS1-SmBiT and NS1-HiBiT KDEL constructs were maintained in complete DMEM which was further supplemented with blasticidin (5 µg/mL) for selection. Huh-7.5 cells stably expressing the T7 RNA polymerase (Huh-7.5 + T7 RNA pol) for the pIRO-derived experiments were also maintained in complete DMEM further supplemented with puromycin dihydrochloride (3 µg/ µL) (Sigma-Aldrich) for selection. Cells were cultured in 0.2 µM vented-cap tissue culture flasks (25 cm², 75 cm², 175 cm²) (Corning) in a 37°C, 5% CO₂ humidified incubator. At 70-80% confluency, cells were subsequently passaged by removing culture media, washing with PBS and incubating with a minimal volume of Trypsin-EDTA solution at 37°C for a maximum of 5 minutes before resuspending the cells in complete DMEM. Cells were sub-cultured at a ratio of 1:5 or 1:6 and transferred into new tissue culture flasks. When needed, cell density in cell suspensions was enumerated with a Neubauer Improved haemocytometer (Livingstone) as detailed below (See **2.2.4 Trypan blue-based enumeration of cells** below).

2.2.4 Trypan blue-based enumeration of cells. Before seeding cells, 50 µL of inactivated trypsinised cells that has been resuspended in complete DMEM was transferred to a 1.5 mL centrifuge tube containing 150 µL of Trypan Blue stain solution (1 in 4) and subsequently mixed by pipetting. 10 µL of this mixture was loaded into one chamber of a Neubauer Improved haemocytometer (Livingstone International, Australia). Using an inverted microscope with a 10X objective lens, the number of live cells were counted as per 5 x 1mm² square. Cell concentrations were calculated as follows: Total cells/ mL = Cells counted x Dilution factor x 10, 000.

2.2.5 Transfection of cells. For transfections, cells were seeded (96-well: 1.5×10^4 cells/well, 24-well: 4×10^4 cells/well, 12-well: 1×10^5 cells/well, 8-well imaging glass bottom chamber μ -slide (ibidi GmbH, Germany): 2×10^4 cells/well, 6-well: 3×10^5 cells/well, 100mm plates: 8.8×10^6 cells/well) and cultured overnight at 37°C.

2.2.5.1. Lipofectamine 2000 / Lipofectamine 3000. At 24-hours post-seeding, contents in Tube A (100 μ L of reduced serum medium, Opti-MEM (Thermo Fisher), X μ g of DNA and X μ L per X μ g of P3000 reagent (Lipofectamine 3000 only) were mixed together by pipetting with contents in Tube B (100 μ L of Opti-MEM, X μ L of Lipofectamine 2000/ Lipofectamine 3000 transfection reagent) and incubated for 5 minutes (Lipofectamine 3000) or 15 minutes (Lipofectamine 2000) at RT. Following the incubation, 100 μ L of the mixture was added dropwise to the seeded cells and returned to culture at 37°C. At 3-4 hours post-transfection, the media was aspirated and replaced with fresh complete DMEM and returned to culture at 37°C.

2.2.5.2. DMRIE-C. At 24-hours post seeding of cells in a 6-well plate, media was aspirated, cells were washed once with PBS and cells were transfected with 1 mL of Opti-MEM mixture containing 6 μ L of DMRIE-C transfection and 5 μ g RNA before returning to culture for 4 hours at 37°C. At 4-hours post transfection, media containing transfection mixtures were aspirated and replaced with 2 mL of complete DMEM and returned to culture at 37°C.

2.2.5.3. PEI polyethylenimine. As similar to the Lipofectamine transfection protocol described above, contents of both Tube A (50 μ L of Opti-MEM, X μ L of PEI reagent [1 μ g/ μ L]) and Tube B (50 μ L of Opti-MEM, X μ g of DNA) were mixed together by pipetting and incubated for 10 minutes at RT. 100 μ L of the mixture was added dropwise to the seeded cells and returned to culture at 37°C without replacing the media following 3-4 hours post transfection as per the manufacturer's instructions.

Table 2.2.5.1 Various transfection reagents

The transfection protocol was scaled accordingly based on their surface area as shown below:

	Tube A	Tube B
Lipofectamine 2000 (Thermo Fisher)		
Opti-MEM	100 μ L	100 μ L
DNA	6-well- 5 μ g 12-well- 2 μ g 24-well- 0.5 μ g	
Lipo 2000 reagent		6-well- 3-5 μ L 12-well- 3 μ L 24-well- 0.6-1 μ L
Lipofectamine 3000 (Thermo Fisher)		
Opti-MEM	100 μ L 8-well chamber slide- 25 μ L	100 μ L 8-well chamber slide- 25 μ L
DNA	6-well- 5 μ g 8-well chamber slide- 0.5 μ g 12-well- 2 μ g	
P3000 reagent	2 μ L per 1 μ g of DNA	
Lipo 3000 reagent		6-well- 6 μ L 8-well chamber slide- 0.6 μ L 12-well- 3 μ L
DMRIE-C (Thermo Fisher)		
Opti-MEM	6-well- 1 mL	
DMRIE-C	6-well- 6 μ L	
RNA	6-well- 5 μ g	
PEI Prime linear polyethylenimine (Sigma-Aldrich)		
Opti-MEM	50-200 μ L	50-200 μ L
DNA		6 well- 2 μ g 100mm plate- 9 μ g
PEI reagent (1 μ g/ μ L)	6 well- 9 μ L 100mm plate- 42 μ L	

2.2.6 HiBiT luciferase reporter assays. Huh-7.5 cells were seeded in 12-well plates or 24-well plates (Corning) and cultured overnight at 37°C. Cells were transiently transfected with purified uncharacterised NS1 expression clones using Lipofectamine 2000 transfection reagent (See **2.2.5 Transfection of cells**) and returned to culture at 37°C before a media change at 4-hours post-transfection. At 48-hours post-transfection, supernatant samples were collected and centrifuged at 3,000 x g for 5 minutes to remove dead cell debris before transferring to a new 1.5 mL microcentrifuge tube containing 2 X Passive Lysis Buffer (Promega) at 1:1 ratio. 1 X Passive Lysis Buffer (150 µL per well for 12-well plates and 100 µL per well for 24-well plates) was then added to cell monolayers and incubated for 5 minutes before harvesting the lysate samples. 10-20 µL of each supernatant or lysate sample was transferred to wells of a 96-well white microplate before the addition of 50 µL of Nano-Glo® HiBiT Lytic Buffer containing diluted LgBiT protein (1:100) and Nano-Glo® HiBiT Lytic Substrate (1:50) (Promega) derived from a Nano-Glo® HiBiT Lytic Detection System kit (Promega). Luciferase signals were detected using the Glomax® Discover Microplate Reader (Promega) as per the manufacturer's instructions.

2.2.7 Generation of lentiviruses. HEK 293FT cells were seeded in 6-well trays at 3.5×10^5 cells/well and cultured overnight. Cells were then transfected using Lipofectamine 2000 as per manufacturer's instructions as earlier described above in **2.2.5 Transfection of cells**. In brief, Tube A (100 µL of Opti-MEM, 3 µL of Lipofectamine 2000) and Tube B (100 µL of Opti-MEM, 0.7 µg of proviral plasmid DNA of interest, and 0.7 µg each of packaging plasmids psPAX2 and psMD2.G) were thoroughly mixed by pipetting and incubated for 15 minutes at RT. The transfection mixture was then added dropwise to cells and cells were returned to culture at 37°C. Within 4-hours and 24-hours post transfection, media was aspirated and replaced with 2mL of complete DMEM. At 48-hours post-transfection, supernatant containing lentiviruses was collected and transferred into 15 mL centrifuge tube

(Corning) and stored at 4°C. To each well, 2 mL of complete DMEM was then added and cells were returned to culture at 37°C. At 72-hours post transfection, lentivirus-containing media was again collected from cells and pooled together with previously collected media in their respective tube. Lentivirus-containing pooled supernatants were then centrifuged at 500 x g for 5 minutes to pellet and remove cell debris. Supernatants were then transferred to a new tube and filtered using a Minisart® 0.45 µM syringe yellow filter (Sartorius). Alternatively, lentivirus preparations were then aliquoted into screw cap tubes and stored at -80°C. 500 µL of filtered lentivirus was mixed with 1 mL of fresh complete DMEM (1 in 3 dilution) and 8 µg/mL of polybrene (Merck Millipore) and applied to semi-confluent target Huh-7.5 cells following removal of their media. Transduced Huh-7.5 cells were cultured for 3 days at 37°C in a 5% CO₂ humidified incubator before antibiotic selection with blasticidin (5 µg/mL) (Sigma Aldrich) to select for stably transduced cells. In some instances, transduced cells were immediately used for experimentation without selection such as in trans-complementation experiments (See **2.2.11 Lentiviral-based trans-complementation assay** below).

2.2.8 Immunofluorescence. Cells were seeded (See **2.2.5 Transfection of cells**) and left to culture overnight at 37°C. For 8-well coverslip glass bottom chamber µ-slides (ibidi GmbH), slides were pre-coated with 0.2% (w/v) gelatin (Sigma-Aldrich) for an hour at RT before seeding of cells. Cells were transiently transfected using Lipofectamine 2000 (Thermo Fisher) or Lipofectamine 3000 (Thermo Fisher) transfection reagents and appropriate plasmid DNA constructs of interest as detailed in **2.2.5 Transfection of cells**. At 4-hours post-transfection, media was aspirated and replaced with fresh DMEM. At 24-hours post-transfection, transfected cells were washed with PBS solution before being fixed with 200 µL of ice-cold methanol: acetone (1:1) by incubating for 5 minutes at 4°C. The fixative was then aspirated, and cells were washed with PBS solution before blocking wells with 100 µL of 5% (w/v) bovine serum albumin (BSA) in PBS for 30 minutes at RT. Blocking solution was then

removed before incubating the fixed cells with 100 μL /well of appropriately diluted primary antibody in PBS/1% BSA (See **Appendix III: Antibodies and Dyes** for further details). Primary antibody was then removed, and cell monolayers were washed with PBS prior to incubation with 100 μL /well of Alexa Fluor 488-conjugated secondary antibody (See **Appendix III: Antibodies and Dyes**) diluted in 1%BSA-PBS for 2 hours in the dark at 4°C. The secondary antibody was then removed, and monolayers were washed once with PBS before incubating cells with 100 μL /well DAPI diluted in PBS to 1 $\mu\text{g}/\text{mL}$ (1 in 1000) (See **Appendix III: Antibodies and Dyes**) for 10 minutes in the dark at RT. The DAPI solution was removed before replacing with 200 μL /well of PBS. Samples were imaged immediately or stored in the dark at 4°C for less than 2 weeks before imaging.

2.2.9 Confocal imaging microscopy. Following fluorescently staining of samples as described in **2.2.8 Immunofluorescence**, samples were imaged with a ZEISS LSM 880 Fast Airyscan confocal fluorescence microscope by utilising a C Plan-Apochromat 63X oil immersion objective and 2.5X Zoom (Flinders Microscopy and Microanalysis, Flinders University, South Australia, Australia). Confocal images were acquired at 1024 x 1024 pixels, processed, and analysed using an in-built ZEN Blue (version 3.2) software (ZEISS). Colocalisation analysis was carried out by measuring Pearson's correlation coefficient of each cell (>20-25 cells per group). Colocalised pixels of images were highlighted using the 'Colocalisation' tool of the software following setting conservative thresholds that were consistent across all analysed images.

2.2.10 Renilla luciferase reporter assays. Huh-7.5 cells were seeded in 12-well plates at 6.5×10^4 cells/well and returned to culture overnight. As lysates were harvested at multiple timepoints (4hr [a measurement of input RNA], 24hr, 48hr, 72hr and, where indicated 96hr), 4-5 individual 12-well plates with duplicate/ triplicate for each transfection were prepared for

each respective timepoint (1 plate per timepoint). At 24-hours post-transfection, media was aspirated, cells were washed once with PBS and cells were transiently transfected with 500 μ L of Opti-MEM media containing 2.4 μ L of DMRIE-C (Thermo Fisher) reagent and 2 μ g of RNA for each well and returned to culture for 4 hours at 37°C. At 4-hours post-transfection, media was aspirated and replaced with complete DMEM, with the exception of plates for the 4hr timepoint, for which 100 μ L of 1 X Renilla luciferase lysis buffer (Promega) was dispensed to each well. For all the other plates at the time of harvest, transfected cells were washed once with PBS before the addition of 100 μ L of 1 X Renilla luciferase lysis buffer. Plates containing lysate samples were wrapped in parafilm and stored at -20°C in zip lock bags. Following the final timepoint of the experiments, all stored plates were thawed on an orbital shaker with gentle agitation for 15 minutes before harvesting the lysates. 10-20 μ L of respective lysates were transferred into wells of a 96-well white microplate before the automated addition of 50 μ L of the Renilla Luciferase Assay Reagent (Promega) mix containing the fully thawed Renilla Luciferase Assay buffer and Renilla Luciferase Assay Substrate (1:100) and measurement of luminescence using a GloMax® Discover System (Promega) instrument. For this, the default Renilla Luciferase Assay System protocol (Promega) was utilised (50 μ L Renilla Luciferase Assay Reagent per well with luminescence integrated over 10 seconds with a 2-second delay between wells).

2.2.11 Lentiviral-based trans-complementation assay. Lentivirus preparations were thawed from -80°C (See **2.2.7 Generation of lentiviruses**) and used to transduce semi-confluent Huh-7.5 cells in 6-well plates. Following 3 days of culture, lentivirally transduced cells were reseeded into 12-well plates. Following trypsinisation, cells were resuspended in 3 mL of complete DMEM. Next, 350 μ L of cell suspension was transferred into wells of a 12-well plate before subsequently adding 650 μ L of complete DMEM to each well. Given that we were performing timepoint experiments (4hr, 24hr, 48hr, 72hr, 96hr), cells were placed into 5

separate 12-well plates in duplicates or triplicates with each plate for respective time points (See **2.2.10 Renilla luciferase reporter assays** above). Following 24-hours, a master mix comprised of 500 μ L of Opti-MEM, 2.4 μ L of DMRIE-C and 2 μ g of RNA for each well was prepared to transiently transfect seeded Huh-7.5 cells with RNA transcripts of pFKsgDVs-R2A- Δ NS1 or pFKDVs-R2A- Δ NS1 as indicated. At 4-hours post-transfection, media was aspirated, cell monolayers were washed with PBS and 1 mL of complete DMEM were added to each well. Once the final timepoint 12-well plate was collected, all -20°C stored plates were thawed and placed on an orbital shaker with gentle agitation for 15 minutes at RT. 10-20 μ L of lysate sample was then transferred to wells of a 96-well white microplate before detection of *Renilla* luciferase activity with the GloMax® Discover System as described above (See **2.2.10 Renilla luciferase reporter assays** above).

2.2.12 Focus forming assay. Prior to performing the focus-forming unit (FFU) assays, virus-containing supernatants were collected at indicated timepoints, cleared of cells and debris by centrifugation for 10-15 minutes and stored at -80°C. To determine the viral titres, Huh-7.5 target cells were seeded into 96-well plates at 2×10^4 cells/well a day prior to the infection. Seeded cells were inoculated with 40 μ L/well of serially diluted virus-containing supernatants. Cells were then cultured for 3 hours before removing viral-inoculum, washed with PBS and returning to culture in complete DMEM (150 μ L per well) for 72 hours at 37°C. Cells were then washed with PBS and fixed with ice-cold acetone: methanol (1:1) fixative for 15 minutes at 4°C. Infected cell foci were enumerated following indirect immunofluorescent labelling of the DENV capsid protein using mouse anti-capsid monoclonal antibody (6F3.1, diluted 1 in 1% BSA/PBS) and conjugated secondary antibody (Alexa Fluor 488, diluted 1 in 400 in 1% BSA/PBS) as described above in **2.2.8 Immunofluorescence** (See **Appendix III: Antibodies and Dyes**). Virus infectivity was

expressed as focus forming units (FFU)/mL with the given formula; $\text{FFU/mL} = 25 \times \text{number of foci counted} \times \text{dilution factor}$).

2.2.13 APEX2 catalysed proximity labelling.

2.2.13.1. Full length APEX2-NS1 constructs. Huh-7.5 cells were seeded into 6-well plates at 1×10^5 cells/well and returned to culture overnight. Cells were then washed once with PBS and transfected by addition of 1 mL of Opti-MEM mixture containing 6 μL of DMRIE-C transfection reagent and 5 μg RNA, and cells were then returned to culture for 4 hours at 37°C (See **2.2.5 Transfection of cells.**). At 4-hours post-transfection, transfection mixtures were aspirated and replaced with 2 mL/well of complete DMEM and returned to culture for 3 days. At 4-days post-transfection, transfected cells were trypsinised for 5 minutes before reseeding into the desired cell culture plates for proof-of-concept experiments: 12-well plates for Western blotting, 48-well plates / 8-well coverslip glass bottom chamber μ -slides (ibidi GmbH) that were pre-coated with 0.2% (w/v) gelatin for 60 minutes for immunofluorescence. For reseeding of cells to perform Western blotting, 250 μL of cell suspension and remaining 1.5 mL of DMEM were added each well of a 12-well plate and returned to culture overnight at 37°C . To confirm the transfection efficiency prior to biotinylation, 40 μL of cell suspension and 60 μL of complete DMEM were transferred to a 96-well plate for immunofluorescence validation (See **2.2.8 Immunofluorescence**). As for the confocal immunofluorescence experiment, 30 μL of cell suspension and 70 μL DMEM were transferred to the gelatin pre-coated 8-well coverslip glass bottom chamber μ -slides and returned to culture overnight at 37°C .

At 7-days post-transfection (Western blotting) or 5-days post-transfection (immunofluorescence), cells were incubated with 450 μL (WB) or 120 μL (IF) of 500 μM biotin phenol in complete media for 30 minutes at 37°C , as described (Hung et al 2016). Following a 30-minute incubation with biotin phenol, 5 μL (WB) or 1.3 μL (IF) of 30%

hydrogen peroxide (Sigma-Aldrich) was then added to cells and samples were continuously agitated for 1 minute. The media was then immediately aspirated from cells and cell monolayers were washed 3 times with 400 μ L (WB) or 130 μ L (IF) of quencher solution (See **Appendix I: Buffers, Media and Solutions** for further details). For Western blotting, cells were washed with PBS once before the addition of 150 μ L RIPA lysis buffer supplemented with protease inhibitor cocktail. Lysates were homogenised, centrifuged, and mixed with Western loading buffer, as detailed above in **2.1.14 Western Immunoblotting**. For immunofluorescence analysis, cells were immediately fixed with ice-cold acetone-methanol fixative (1:1) and fluorescently stained with primary Ab anti-NS1 4G4 (Mozzy Mabs) and secondary antibody anti-mouse IgG Alexa Fluor 488 conjugate (Invitrogen) mixed with Cy3-streptavidin (Jackson ImmunoResearch Laboratories, USA) and DAPI (Sigma-Aldrich) (See **Appendix III: Antibodies and Dyes**) as detailed above in **2.2.8 Immunofluorescence**.

2.2.13.2. pIROD-APEX2-NS1 constructs. For pIROD-APEX2-NS1 biotinylation experiments, Huh-7.5 cells stably expressing the T7 RNA polymerase (Huh-7.5 + T7 RNA pol) (See **2.2.3 Maintenance of cell lines in culture medium**) were seeded into 100mm culture dishes (Corning) and cultured overnight at 37°C. At 48-hours post-seeding to ensure the cells reached a confluency of 85-90%, cells were transiently transfected with wildtype pIROD-APEX2-NS1 and its derivative plasmids utilising PEI linear polyethylenimine transfection reagent (Sigma-Aldrich) and returned to culture overnight at 37°C as per manufacturer's instructions (See **2.2.5 Transfection of cells**). At 24-hours post-transfection, transfected cells were biotinylated as detailed above in **2.2.13.1. Full length APEX2-NS1 constructs**.

Chapter 3

Identification of NS1 secretion-impairing mutations via random point mutagenesis and HiBiT luciferase reporter- based assays

3.1 Introduction

Since its discovery in the 1970s, the flavivirus NS1 protein has been widely recognised to be essentially important in the flavivirus lifecycle in terms of viral replication and infectious virus production (Plaszczyc et al 2019; Scaturro et al 2015; Muller and Young 2013; Youn et al 2013; Lindenbach and Rice 1997; Mackenzie et al 1996). Aside from these key roles, it is also known to be secreted from DENV-infected cells as a soluble hexamer where it is involved in a variety of extracellular pathogenic functions. Notably, NS1 has been characterised as a pathogen-associated molecular pattern (PAMP) which activates Toll-like receptor 4 (TLR-4) to initiate release of inflammatory chemokines and cytokines or initiate a massive “cytokine storm” that disrupts endothelial cell integrity leading to vascular leakage, a distinctive hallmark of flavivirus disease pathogenesis notably for DENV (Watterson et al 2016; Modhiran et al 2015; Lin et al 2005). NS1 has also been demonstrated to promote degradation of components lining the endothelial glycocalyx-like layer (EGL) of human pulmonary endothelial cells known to regulate endothelial barrier function (Puerta-Guardo et al 2016). Although it is established that NS1 is secreted to subsequently perform a variety of extracellular functions related to vascular damage and immune evasion, the exact molecular details of which NS1 residues and domains are involved in its efficient secretion activity remains poorly characterised.

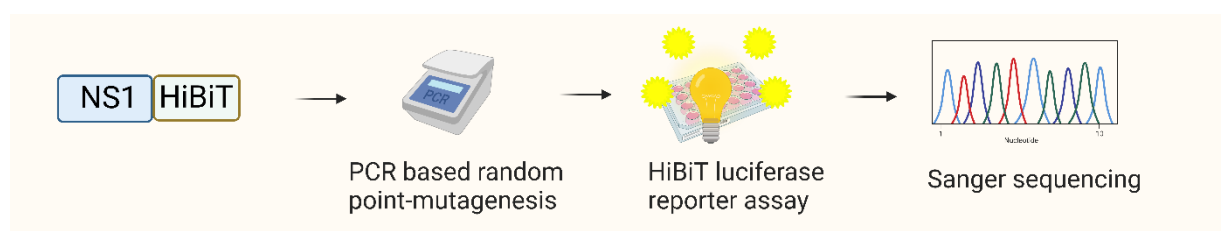


Figure 3.0.1 Schematic diagram of the random mutagenesis-coupled HiBiT luciferase experimental workflow. Wildtype DENV-2 NS1 was subjected to PCR-based random point mutagenesis before incorporating the potentially mutagenized NS1’ cDNA PCR product into a lentiviral expression plasmid construct containing the C-terminal HiBiT tag. Seeded Huh-

7.5 cells were transiently transfected with the indicated NS1 expression plasmids and supernatant and lysates were harvested at 48-hours post-transfection. Extracellular-to-intracellular NS1 luminescence activity ratios were measured for each respective NS1 clone. Identified NS1 clones bearing mutation(s) that impacted NS1 secretion activity by more than 50% relative to wildtype NS1-HiBiT controls were submitted for Sanger sequencing.

3.2 Results

3.2.1 PCR-based random point mutagenesis of wildtype DENV-2 NS1 cDNA

To generate an extensive library of NS1 point mutants, we capitalized on a recently established cloning strategy (**Figure 3.0.2**) after attempting several relatively inefficient strategies in which contamination of DENV infectious clone (pFK-DVs) plasmid DNA was finally revealed to be the root of the underlying problems. In brief, this cloning strategy initially involved digesting the pFK-DVs plasmid containing the synthetic full-length DENV-2 genome with *Bam*HI-HF and *Kas*I restriction enzymes overnight to obtain a DNA fragment containing wildtype DENV-2 NS1 cDNA. The purified excised NS1 cDNA was then amplified via Q5 HiFi PCR before subjecting 250ng of the *Dpn*I-treated purified NS1 PCR products to PCR-based random point mutagenesis (Agilent). This was subsequently followed by HiFi DNA Assembly (Gibson Assembly) of dephosphorylated *Bam*HI/ *Xho*I-digested pLenti6 HiBiT plasmid and mutagenized NS1' PCR products, to ultimately generate a large pool of pLenti6-NS1'HiBiT mutant clones.

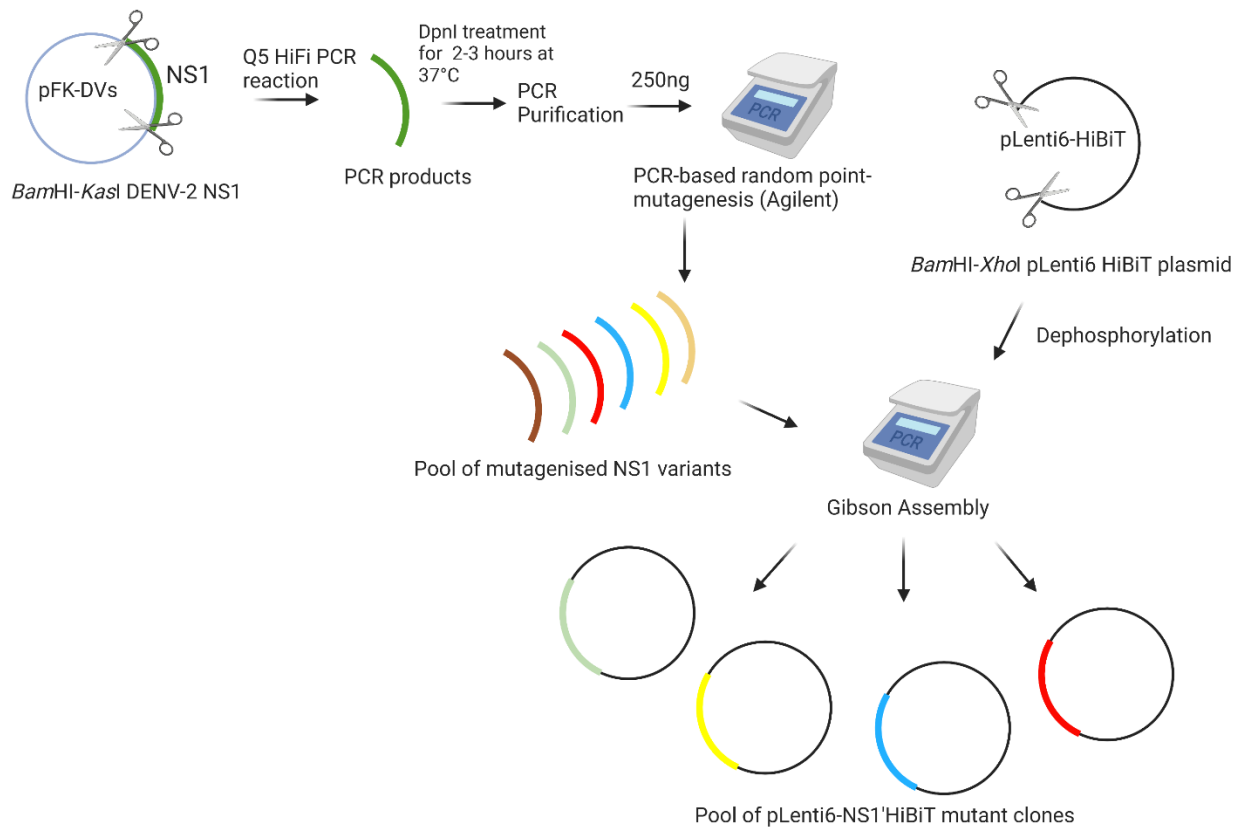


Figure 3.0.2 Workflow of the PCR-based random point mutagenesis approach for generation of NS1-HiBiT expression plasmids containing point mutations within the NS1.

3.2.2 Screening of bacterial colonies for clones containing NS1 insert via colony PCR

By utilising the cloning strategy described above, Gibson Assembly generated products were chemically transformed into competent *Escherichia coli* cells (New England BioLabs) before randomly selecting bacterial colonies for colony PCR-mediated screening to identify clones that harbour an uncharacterised NS1 cDNA insert. Of 300 bacterial colonies screened via colony PCR, 173 of them were confirmed to harbour the NS1 insert (**Figure 3.0.3**) and were subsequently processed for plasmid DNA propagation and extraction.

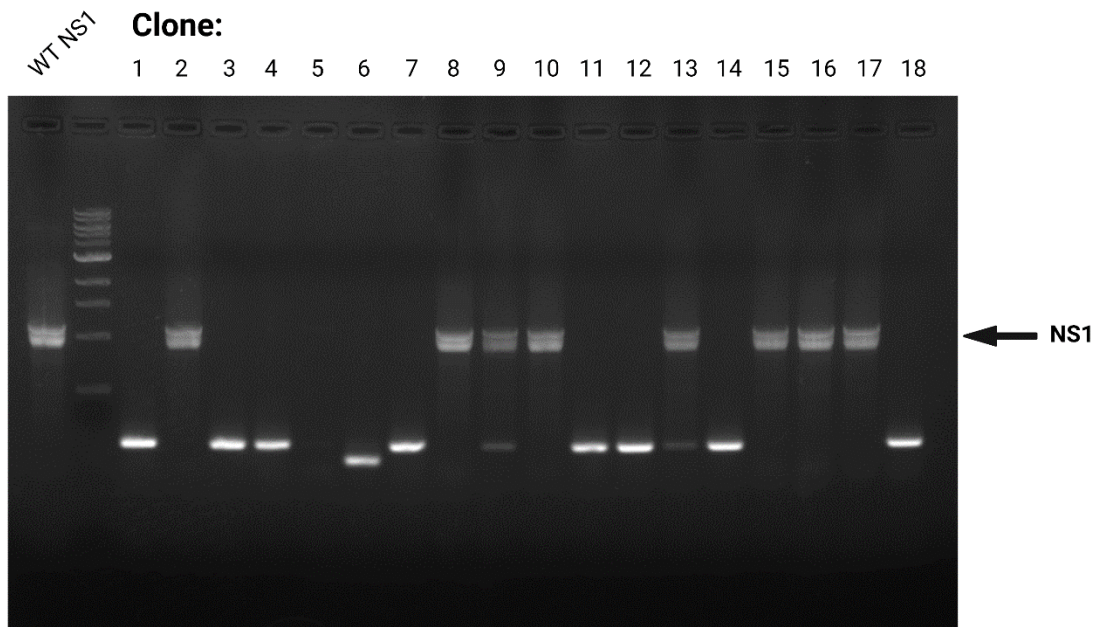


Figure 3.0.3 An example of the colony PCR results following gel electrophoresis.

Individual isolated colonies were randomly selected, spotted onto a gridded LB agar plate containing ampicillin, and dipped into a PCR tube of nuclease free water. PCR reagents were added, and PCR was performed prior to analysis via agarose gel electrophoresis to verify the presence of the NS1 insert. Following the confirmation of the presence of the NS1 insert, the corresponding bacterial colonies were cultured overnight and processed for plasmid DNA extraction for the upcoming HiBiT luciferase reporter-based assays.

3.2.3 HiBiT luciferase reporter-based assays of NS1 protein secretion for mutagenized NS1 expression constructs

We next sought to identify NS1 mutant clones that displayed impairment in NS1 secretion efficiency based on extracellular-to-intracellular measurement of NS1-HiBiT luminescence ratio via HiBiT luciferase reporter-based assays. Luciferase activity was determined based on the quantification of HiBiT-tagged proteins in respective cell lysates and supernatant samples using the Nano-Glo® HiBiT Lytic Detection System (Promega). This lytic luciferase detection system works on the basis that the HiBiT fragment will spontaneously associate with its complementary partner, the LgBiT protein (Schwinn et al 2018) (**Figure 3.0.4**). When in close proximity, these split luciferase peptide fragments will associate together to generate a complemented reporter enzyme, ‘NanoBiT’ that is capable of generating a high intensity

luminescence signal in the presence of the furamazine substrate. The degree of luminescence activity produced is directly proportional to the quantity of HiBiT-tagged protein found in samples of interest.

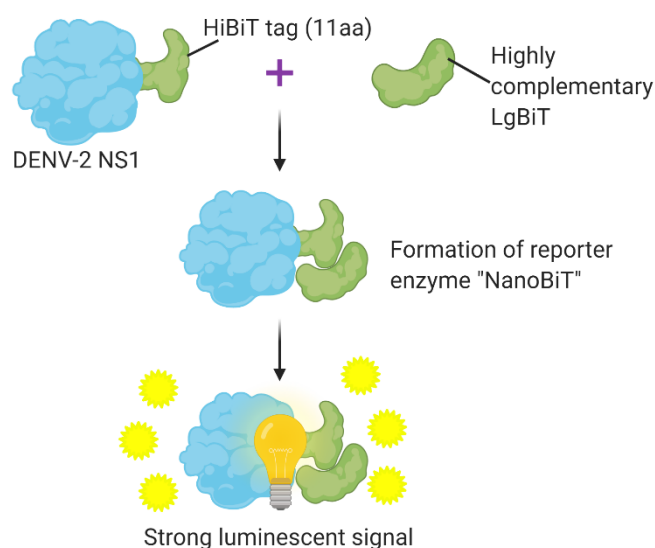


Figure 3.0.4 Molecular basis of the DENV-2 NS1-HiBiT split luminescent peptide tag assay. The protein of interest DENV-2 NS1 has been engineered to feature a HiBiT split luciferase tag that is highly complementary to its binding partner LgBiT. When in close proximity to each other, these complementary split fragments will associate together to form the ‘NanoBiT’ reporter enzyme that is capable of generating a strong luminescent signal in presence of the furimazine substrate. This schematic diagram has been adapted from the Nano-Glo® HiBiT Lytic Detection System (Promega).

To identify NS1 clones that harbour point mutation(s) that significantly impair NS1 secretion, Huh-7.5 human hepatocellular carcinoma cells were seeded into 24-well plates and were transiently transfected with uncharacterised NS1-HiBiT expression clones, before extracellular and intracellular samples of each NS1 clone were collected at 48-hours post-transfection. Lytic buffer containing LgBiT protein and furamazine substrate derived from the Nano-Glo® HiBiT Lytic Detection System (Promega) kit was added to respective

extracellular and intracellular samples before measurement of luciferase activity. For this, all 173 purified NS1 clones were probed for their extracellular and intracellular NS1 levels via the HiBiT luciferase reporter-based assay. The HiBiT luciferase assays revealed numerous mutagenized NS1 clones with distinctively altered ratios of extracellular-to-intracellular NS1 luminescence activities (**Figure 3.0.6A**). As expected, the wildtype NS1-HiBiT generated almost equivalent luciferase activity in the intracellular and extracellular samples across each independent luciferase experiment. The NS1-SmBiT construct (negative control) displayed negligible levels of NS1 luminescence, which closely resembled to that of untransfected parental Huh-7.5 cells, consistent with the established SmBiT peptide's weak affinity for the LgBiT protein (Dixon et al 2016; Schwinn et al 2018). Additionally, an NS1-HiBiT construct with a C-terminal ER-retention motif, KDEL exhibited intracellular NS1 luminescence activity that was markedly higher than that of its corresponding extracellular NS1 samples, highlighting its expected utility as a positive control for inhibition of NS1 secretion activity.

Extracellular-to-intracellular NS1 luminescence ratios were determined for the 173 NS1 clones to identify any potential clones bearing mutation(s) that impact upon NS1 secretion activity (**Figure 3.0.6 B**). Approximately 100 clones out of 173 were confirmed to possess mutation(s) that may have a significant impairment in NS1 secretion. These 100 NS1 clones were submitted for Sanger sequencing to determine the mutation(s) associated with this NS1 secretion impairment phenotype. Sanger sequencing results interestingly revealed varying mutation frequencies among these cohort of NS1 mutant clones as shown (**Table 3.0.5**).

Table 3.0.5 Brief overview of the Sanger sequencing results depicting the mutation frequency for the selected 100 NS1 secretion-impairing mutant clones.

Mutation frequency (1 indicates 1 point mutation per clone)	No. of NS1 clones
1	16
2	24
3	18
>4	42

Total :100 NS1 clones

To simplify further characterisation of these NS1 secretion-impairing mutants in subsequent studies, only NS1 mutant clones bearing a single coding point mutation(s) were considered for subsequent experiments. Accordingly, 10 NS1 mutants, E139K, S152L, D180Y, V220D, A248V, T283A, L298W, C313S, I335T, and R336S were selected for subsequent *in silico* analyses. On a side note, although two other NS1 mutants, W210L and W232R, were shown to display a greater than 50% decrease in NS1 secretion efficiency as well as bearing a single coding mutation(s), they were excluded from this study given that their luminescence activities closely resembled those of wildtype NS1-HiBiT and parental Huh-7.5 cells respectively (**Figure 3.0.6 B**).

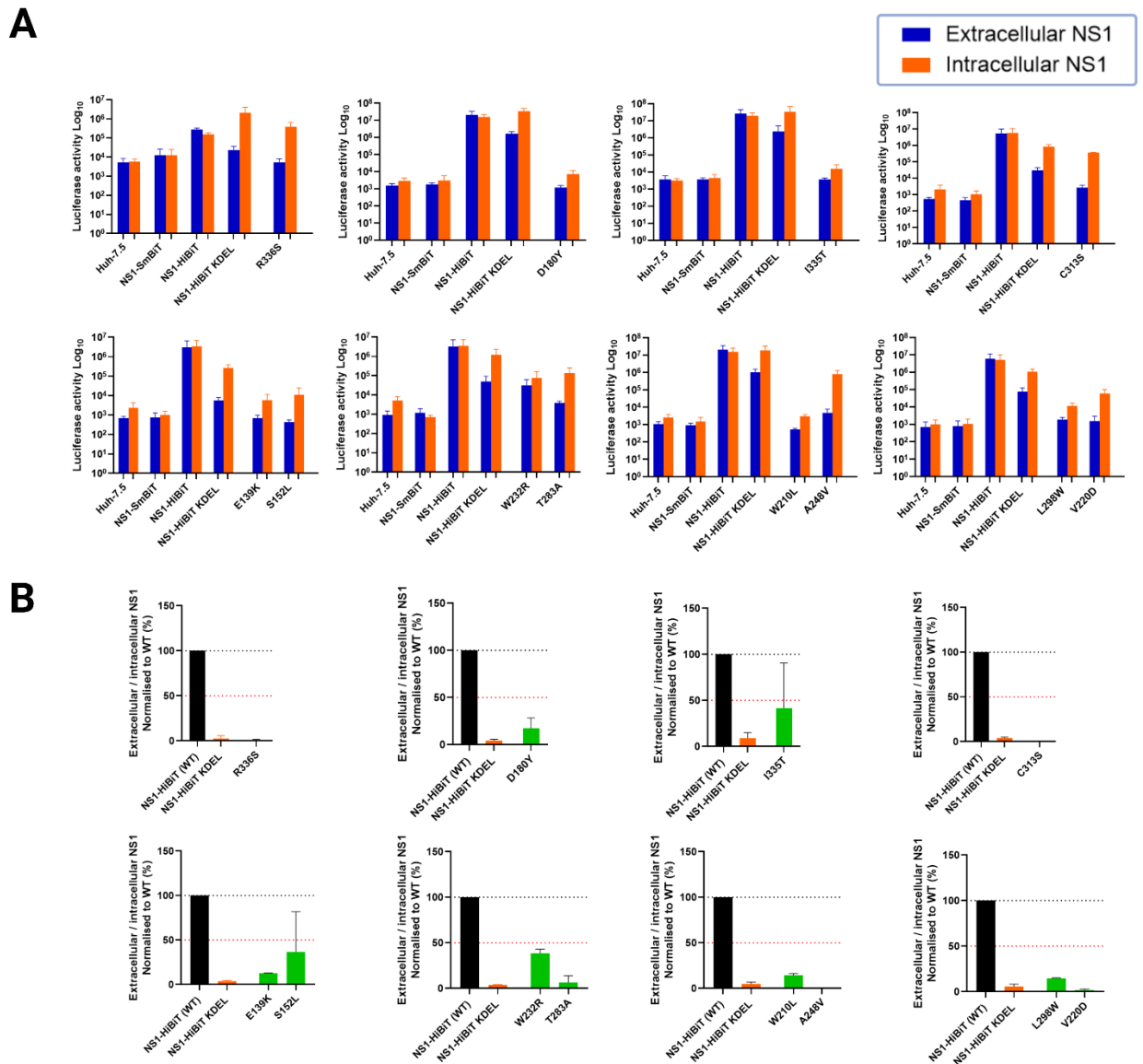


Figure 3.0.6 The identification of NS1 mutant clones with impaired NS1 protein secretion. (A) Raw luciferase values of each indicated NS1 clones. Lysates and supernatants were harvested from Huh-7.5 cells that were transfected with NS1-SmBiT (negative control), NS1-HiBiT (wildtype), NS1-HiBiT KDEL (positive control for intracellular NS1 retention) or indicated mutagenized NS1-HiBiT expression clones and probed for their luciferase activity via the Nano-Glo® HiBiT Lytic Detection System. Orange bars represent intracellular samples (lysate), while blue bars represent extracellular samples (supernatant). Data for mutagenized clones are only depicted for those selected clones that encoded a single amino acid substitution and displayed a >50% reduction in the ratio of the extracellular-to-intracellular NS1 luciferase activity. Data are presented as raw luciferase activity (relative light units [RLU]) means \pm SD of duplicates for each group, from two

independent experiments. **(B) Normalised extracellular-to-intracellular NS1 luminescence ratios of the indicated NS1 clones.** Extracellular-to-intracellular NS1 luminescence ratios were subsequently determined for each sample in (A) and expressed as percentage of wildtype NS1-HiBiT values. Black bars represent wildtype NS1-HiBiT, orange bars represent NS1-HiBiT KDEL, while the green bars represent the NS1-HiBiT point mutants as shown. A black dotted line is indicated at 100% secretion efficiency and a red dotted line is indicated at 50% secretion efficiency. Data are presented as means \pm SD of duplicates for each group, from two independent experiments. Adapted from Tan et al (2023).

3.3 Discussion

Several recent mutagenesis studies have identified NS1 residues that are essential to the roles of NS1 in the DENV lifecycle in terms of viral RNA replication, infectious virus production and NS1 secretion (Scaturro et al 2015; Plaszczyca et al 2019). Despite this, the exact molecular features of NS1 that are critical for its secretion activity remain poorly understood. To address this current gap in knowledge, we aimed to generate a comprehensive library of NS1 point mutants through the utilisation of random PCR-based point mutagenesis. This NS1 mutant library was then subjected to a HiBiT luciferase reporter-based assays to assess the extracellular-to-intracellular NS1 luminescence ratio of each clone within the library. NS1 clones that exhibited more than a 50% decrease in NS1 secretion efficiency were then submitted for Sanger sequencing to identify the mutation(s) associated with the NS1 secretion impairment phenotype. Together, the combination of high throughput mutagenesis and the split luciferase peptide tag reporter-based assay enables elucidation of NS1 residues and domains that are critical in DENV NS1 secretion.

Initially, there were several challenges in generating the NS1 mutant library, ranging from unacceptably low rates of PCR-based random point mutagenesis to inefficient cloning of the mutagenized NS1 into the expression construct. However, these underlying issues were

eventually resolved after several troubleshooting steps. Following the PCR-based mutagenesis reaction, newly mutagenized NS1 was cloned into the lentiviral expression construct containing the HiBiT tag via Gibson Assembly as conventional restriction cloning was unsuccessful after several attempts. In contrast, transformation of the Gibson Assembly generated products into competent bacteria cells yielded a large number of bacterial colonies. Next, we also decided to incorporate colony PCR as part of our confirmational step to ensure that the bacterial colonies chosen for the next step harboured the NS1 insert. Approximately half of the clones that were screened via colony PCR indeed harboured the NS1 insert. While simple and cost efficient, it is likely that colony PCR-based screening may have potentially failed to identify many clones possessing the NS1 insert due to the possibilities of bacterial debris inhibiting the given PCR reactions (Lee and Cooper 1995). In spite of this, a large cohort of 173 clones with potentially mutagenized NS1 inserts was generated for subsequent analysis via HiBiT luciferase reporter-based assays.

The HiBiT luciferase reporter-based assays successfully identified 100 out of possible 173 NS1 clones to have a more than >50% decrease in their NS1 secretion efficiency based on the extracellular-to-intracellular NS1 luminescence ratio. We subsequently sequenced these 100 NS1 clones to identify the mutation(s) associated with the apparent impairment in NS1 secretion efficiency. Unfortunately, approximately 90% of these NS1 clones contained more than a single coding point mutation(s), so we focused on those clones that featured a single coding point mutation and also resulted in a marked decrease in NS1 secretion efficiency. Despite several attempts to optimise the PCR-based mutagenesis rates to our ideal frequency of one point mutation per clone, many of the identified NS1 clones contained multiple mutations that could not be unentwined from each other. For example, a higher DNA template concentration for PCR-based mutagenesis did not appreciably reduce the observed mutation rate (not shown) despite expectation of reduced mutation rates as targets amplified from

higher concentration of template would undertake less duplications than targets from a lower template concentration. Future studies of this nature may potentially benefit from random point mutagenesis approaches that feature more precisely controlled mutation rates.

In summary, we have successfully utilised a combination of high throughput random point mutagenesis and sensitive luciferase reporter-based expression assay approaches to identify a sizeable cohort of NS1 clones bearing mutation(s) associated with NS1 secretion efficiency. Despite unexpected challenges in regard to the high mutation frequency of these NS1 secretion-impairing clones, we successfully identified 12 NS1 clones bearing single point mutations for further analyses. In summary, we have developed a rapid, unbiased and relatively inexpensive approach to identify NS1 secretion-defective mutants. This approach may be further refined and adapted for further studies of flavivirus NS1 protein secretion and that of other secreted proteins for which the determinants of secretion efficiency are poorly characterised.

Chapter 4

Analysis and characterization of identified residues within DENV NS1 protein that are essential for its secretion

4.1 Analyses of putative secretion-impairing point mutations within DENV-2 NS1 via *in silico* analyses, Western blotting and high-resolution confocal imaging

4.1.1 *In silico* analyses indicate that the majority of NS1 secretion-impairing mutations are primarily located within the β -ladder domain

To map and visualise the locations of these NS1 secretion impairing mutations within the domains of the established NS1 dimer and hexamer structures, *in silico* modelling analyses were conducted (**Figure 4.1.1**). Interestingly, most of the NS1 secretion impairing mutations were mapped to the β -ladder domain (V220D, A248V, T283A, L298W, C313S, I335T, R336S), while two mutations flanking the 2nd connector sub-domain (S152L and D180Y) interlinking the Wing domain and β -ladder domain and one mutation within the Wing domain (E139K) were also identified. No NS1 secretion impairing mutations were mapped to the remaining regions of NS1; the β -roll domain and the 1st connector sub-domain while the two corresponding *N*-glycosylation sites (N130 and N207) within NS1 also did not feature on sites that were identified as important to NS1 secretion. However, as the mutant library was not exhaustive, it is important to note that many residues and motifs within NS1 may not have been randomly mutagenized and assessed for their importance to NS1 secretion in the original screen.

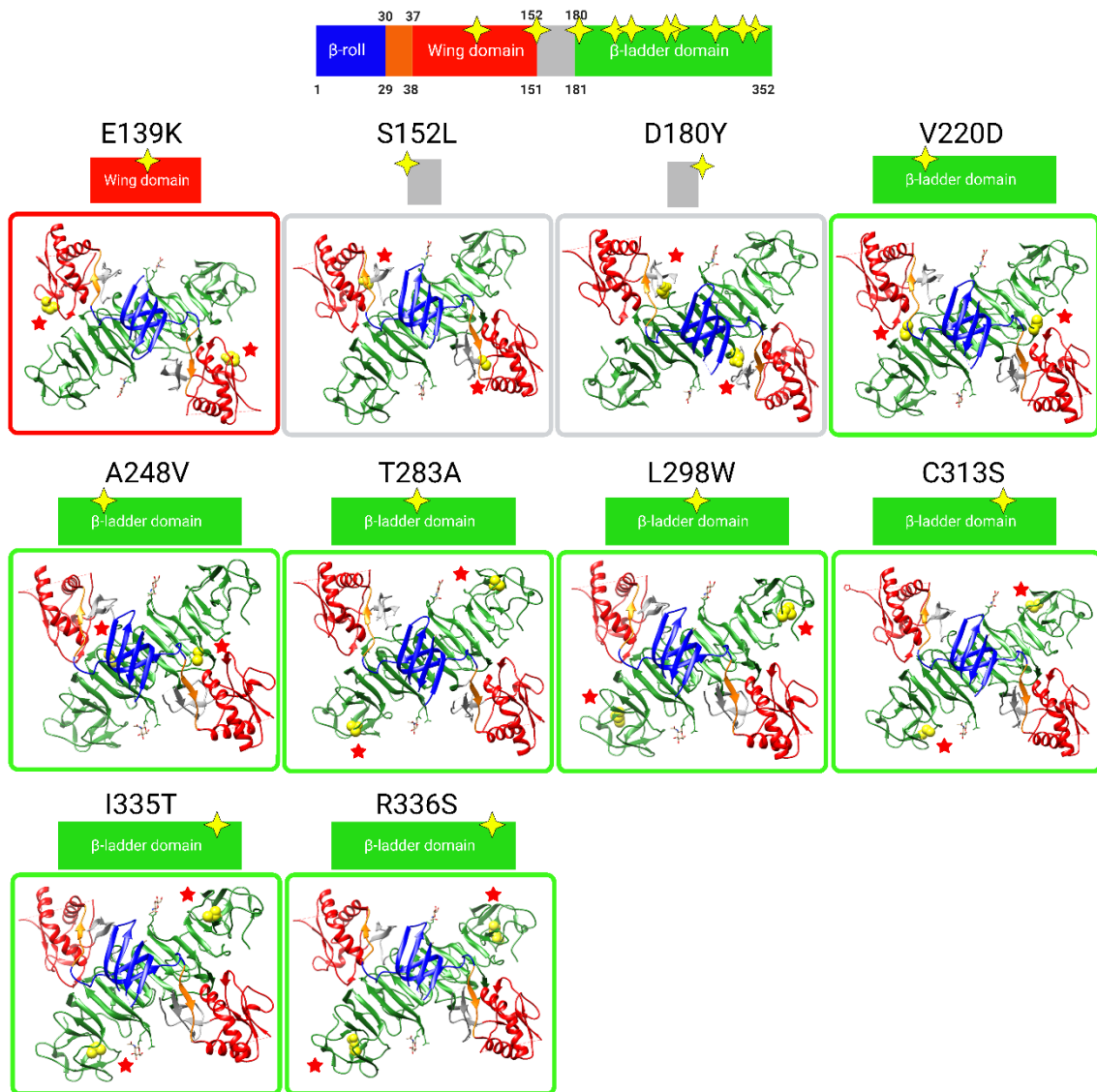


Figure 4.1.1. *In silico* analyses of the identified NS1 secretion-impaired mutants. The location of the 10 selected NS1 secretion-impaired mutants identified were visualised on the three-dimensional structure of NS1 dimer (Protein Data Bank entry 4O6B), with mutant residues portrayed as van der Waals spheres in yellow and indicated with red stars for easier visualisation. From left to right, the β -roll, 1st connector, Wing, 2nd connector and β -ladder are highlighted in blue, orange, red, grey and green, respectively. These *in silico* analyses were carried out using UCSF® Chimera software ver.1.13.1. Adapted from Tan et al 2023.

To further understand whether the identified secretion influencing NS1 residues were relatively conserved amongst different DENV serotypes and related flaviviruses, an alignment of NS1 amino acid residues of all DENV serotypes, West Nile virus (WNV) and Yellow Fever virus (YFV) was carried out (**Figure 4.1.2**). Alignment results showed that most of the

residues corresponding to the NS1 secretion impairing point mutations within the β -ladder domain are highly conserved across DENV serotypes and closely related flaviviruses, YFV and WNV. Similarly, D180 within the 2nd connector sub-domain is highly conserved across NS1 sequences for different DENV serotypes and related flaviviruses.

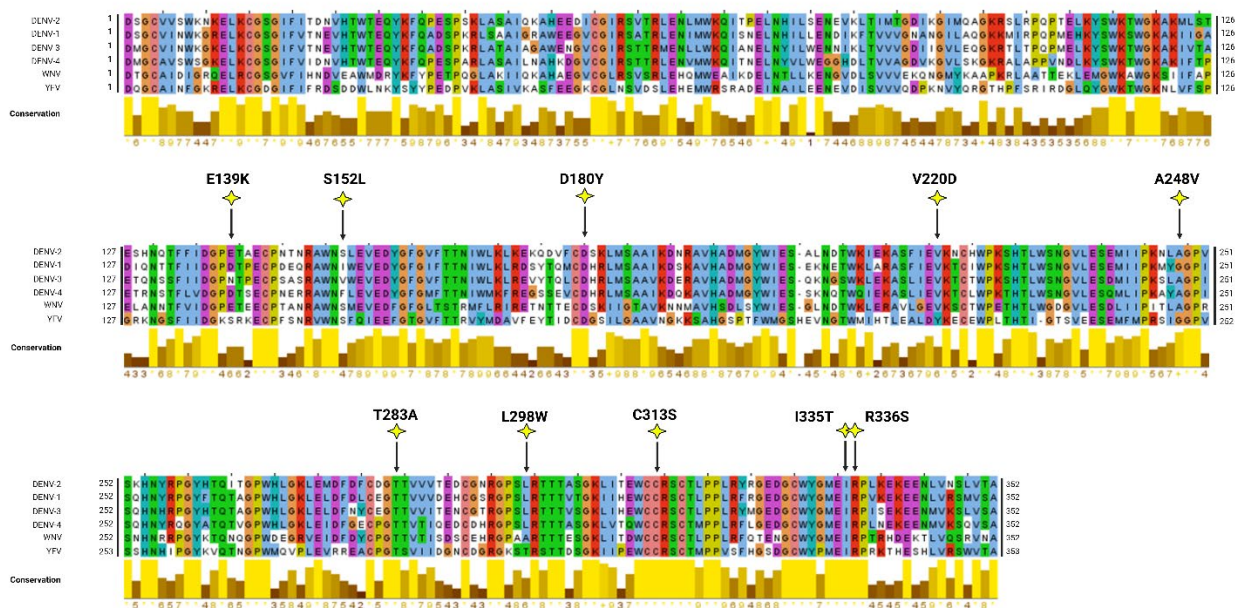


Figure 4.1.2. Multiple sequence alignment of various NS1. Alignment of NS1 amino acid sequences of representative isolates from different DENV serotypes and two related flaviviruses (West Nile virus [WNV], Yellow Fever virus [YFV]) was performed using the in-built ClustalW algorithm in Jalview®. The graphical displays below the alignments show the relative amino acid conservation across the various NS1 sequences, with yellow indicating the highest degree of conservation across the sequences. The positions of the mutated residues are indicated as yellow stars within the NS1 amino acid sequence alignment.

As our current strategy of identifying of NS1 secretion-impairing mutants was exclusively based on luciferase readout values, we decided to also investigate the NS1 secretion activity of these NS1 mutants via Western blotting using a conformation specific anti-NS1 monoclonal antibody ‘4G4’ (**Figure 4.1.3 A**). Intracellular DENV-2 NS1 was strongly detected for wildtype NS1-HiBiT, KDEL-tagged NS1-HiBiT in cell lysates, including the

E139K, D180Y and V220D NS1-HiBiT mutants (**Figure 4.1.3 A**). The other NS1 mutants S152L, A248V, L298W and I335T appeared to be weakly expressed intracellularly, while T283A, C313S and R336S NS1 mutants could not be detected by Western blotting. Extracellular DENV-2 NS1 protein was only readily detected in the wildtype NS1-HiBiT, E139K, S152L and D180Y supernatant samples, while NS1-HiBiT KDEL was not detected in supernatant samples, consistent with its expected retention in the ER.

To further investigate whether weak or undetectable expression of NS1 mutants observed in these Western blotting experiments could be potentially attributed to inefficient transfection, lysates and supernatant samples derived from these experiments were also probed for intracellular and extracellular NS1 expression levels respectively, via the HiBiT luciferase reporter assays (**Figure 4.1.3 B**). Intracellular NS1-derived luciferase activities were markedly higher than their corresponding extracellular NS1 values for the majority of these mutants, including those NS1 mutants (T283A, C313S and R336S) that were undetectable by Western blotting. This indicates that the underlying difficulties in detecting the expression of these mutants by Western blotting cannot be simply attributed to low transfection efficiency. Additionally, the extracellular and intracellular DENV-2 NS1 Western blotting signals for each respective NS1 mutant with the exception of T283A, C313S and R336S, were also quantified prior to determining the extracellular-to-intracellular NS1 luminescence ratio (**Figure 4.1.3 C**). As expected, the given NS1 mutants displayed an impairment in NS1 secretion efficiency, which is largely consistent with the initial results from earlier HiBiT luciferase reporter assays.

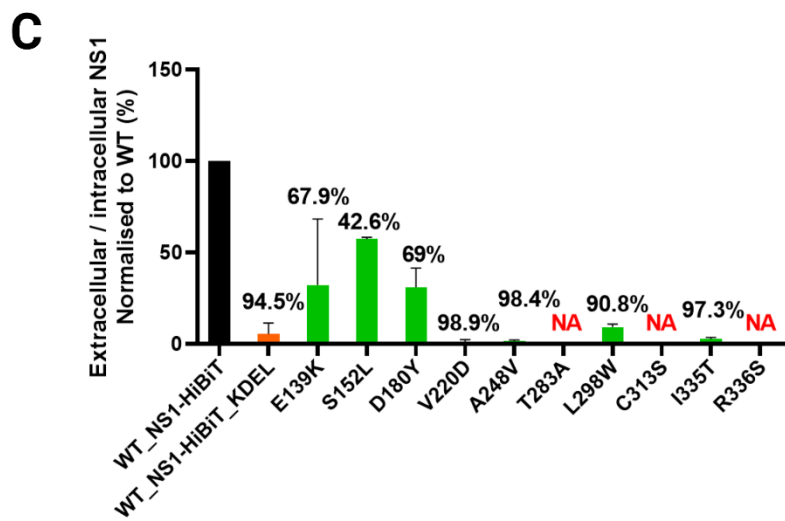
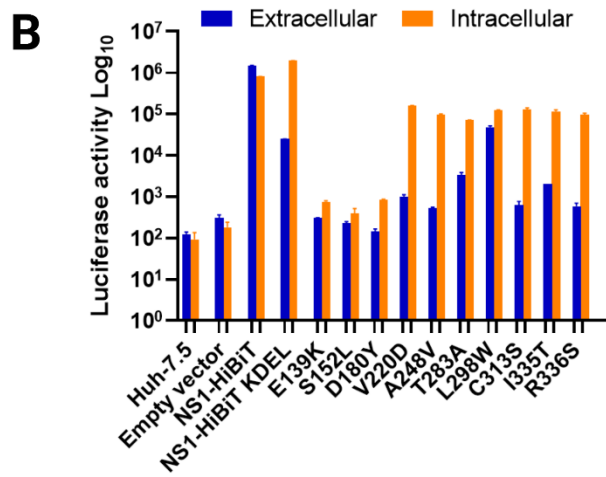
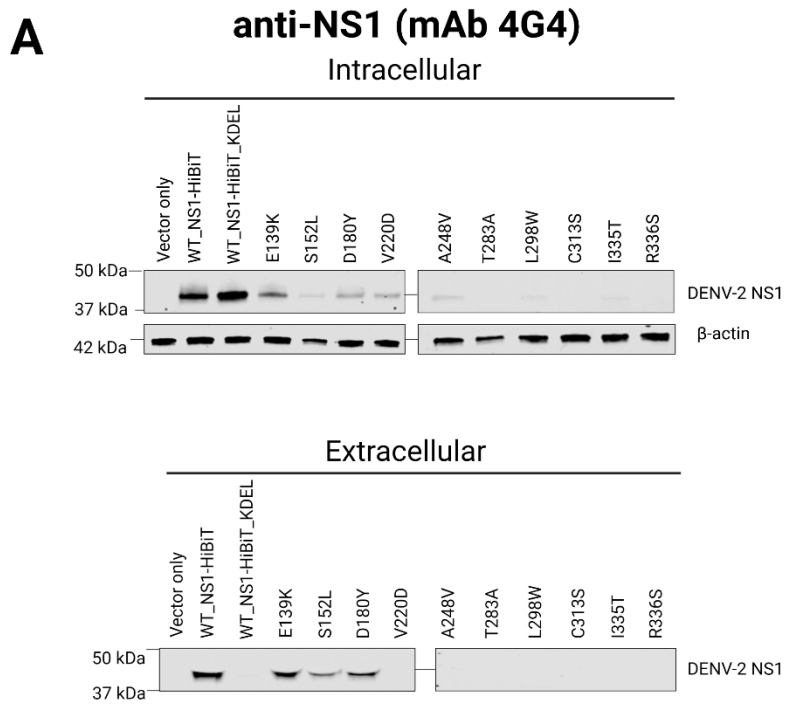


Figure 4.1.3 Several NS1 secretion-impairing mutants were not detected intracellularly by Western blotting. (A) Intracellular and extracellular expression levels in transiently transfected 293FT cells. Cell lysates following addition of NP-40 lysis buffer and supernatant were harvested from transfected 293FT cells at 48-hours post-transfection, before subjecting to SDS PAGE and immunoblotting to probe for DENV2-NS1 and β -actin. (B) Detection of HiBiT-tagged in supernatant and lysates samples that were also similarly utilised for Western immunoblotting. Aliquots of the samples utilised and derived from (A) were also assayed for their luminescence activity via the HiBiT luciferase reporter assays. (C) Relative expression levels of extracellular-to-intracellular NS1 were expressed as a percentage of the wildtype NS1. Data are means \pm SD from two independent replicate, with values above each bar indicating a decrease in NS1 secretion efficiency as a percentage of wildtype values. Also, NS1 mutants, T283A, C313S and R336S were excluded from Western signals quantification analyses given the inability to detect and visualise them by Western blotting as shown in **Figure 4.1.3 A**.

4.1.2 Wildtype NS1 and NS1 secretion-impairing mutants displayed strong colocalisation with the endoplasmic reticulum (ER)

NS1 is thought to participate in membrane rearrangements of the ER via its interaction with DENV NS4A and NS4B and it colocalises with double stranded RNA (dsRNA) within ER derived VPs that are known to house viral RNA replication events (Eyre et al 2017a; Scaturro et al 2015; Welsch et al 2009; Grief et al 1997; Mackenzie et al 1996). Thus, we sought to investigate whether the identified NS1 secretion-defective mutants also displayed altered localisation profiles with regards to the ER. For this, we transiently transfected Huh-7.5 cells with the NS1-HiBiT expression constructs bearing the respective mutations and assessed the localisation of NS1 with regards to the ER by high resolution confocal imaging. Of note, we also utilised a highly cell-permeable IRaZolve-ER Blue@dye (REZOLVE Scientific, Australia) fluorogenic dye to label the ER in fixed Huh-7.5 cells to compliment NS1 staining for the NS1-ER colocalisation analyses as shown (**Figure 4.1.4**).

All the NS1 mutants, including the negative control NS1-SmBiT and the positive control for intracellular retention, NS1-HiBiT KDEL displayed DENV-2 NS1 staining patterns that closely resembled those of the wildtype NS1-HiBiT (**Figure 4.1.4**). NS1 (white in individual panels and green in merged panels) and ER-specific fluorescent dye (white in individual panels and red in merged panels) signals indicated strong colocalisation in all groups, as distinctly highlighted by separate visualisation of colocalised signals (white; right panels).

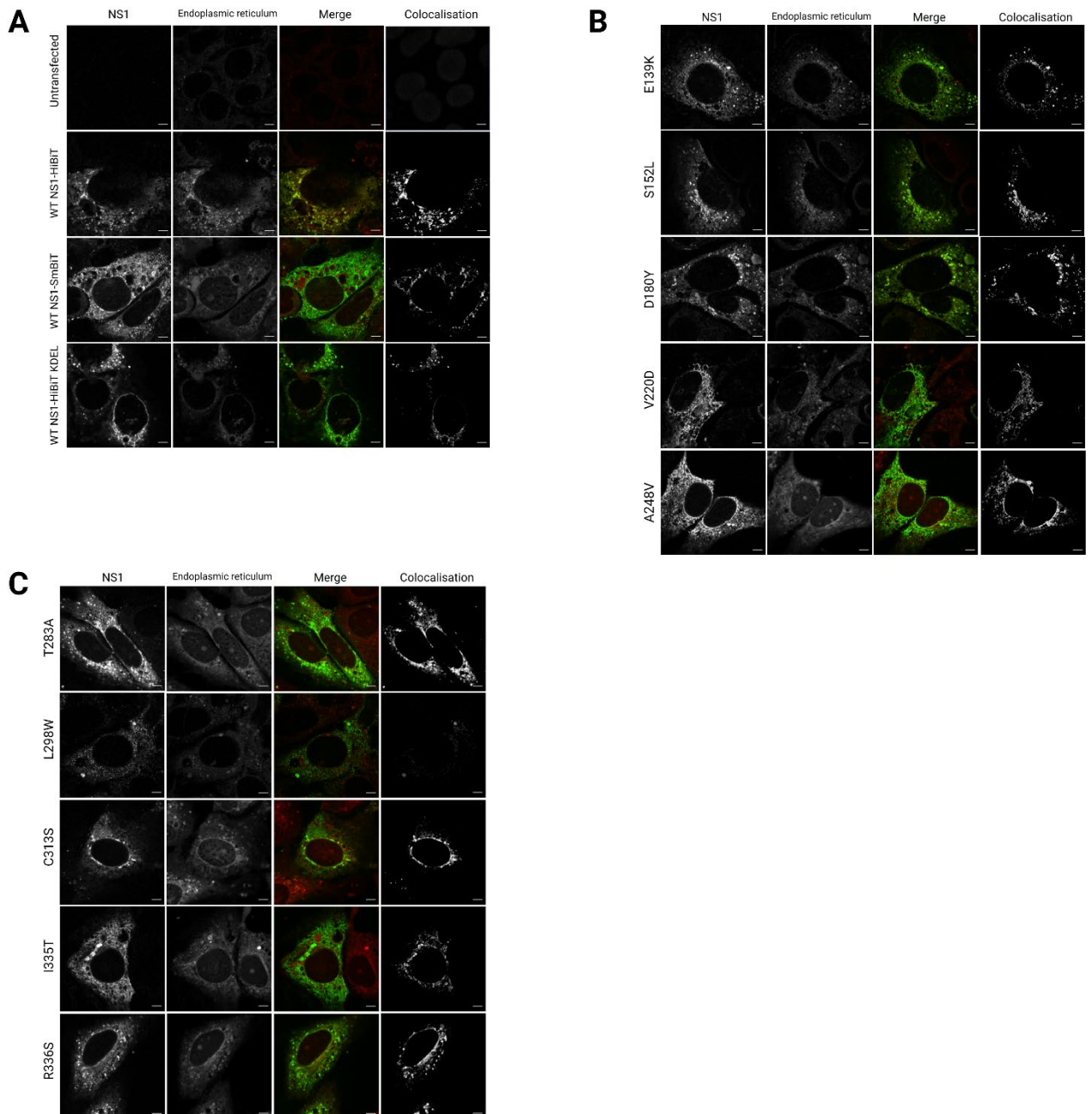


Figure 4.1.4 Identified secretion-impairing mutations within DENV NS1 do not impact its localisation to the ER. Huh-7.5 cells were transiently transfected with DENV NS1 expression constructs bearing the respective NS1 secretion-impairing mutations and cultured overnight before cell-fixation and fluorescent labelling. NS1 proteins (white; left column), endoplasmic reticulum (white; second column from the left), merged images (third column) and NS1-ER colocalised pixels (white; fourth column) are indicated and displayed in (A), (B) and (C); (scale bars, 5 μ m). Adapted from Tan et al 2023.

Additionally, confocal tile scan images were also acquired to quantify colocalisation signals between NS1 and ER for all groups (Figure 4.1.5 A,B,C). All mutants displayed Pearson's correlation coefficient values between 0.5-0.9 which is indicative of strong colocalisation activity between NS1 and the endoplasmic reticulum. Furthermore, colocalisation analysis across 20-25 cells/group showed no significant differences between the individual mutant groups in comparison to the wildtype NS1 or wildtype KDEL-tagged NS1 (Figure 4.1.5 D), indicating that none of the identified mutations appeared to disrupt or alter localisation of NS1 to the ER.

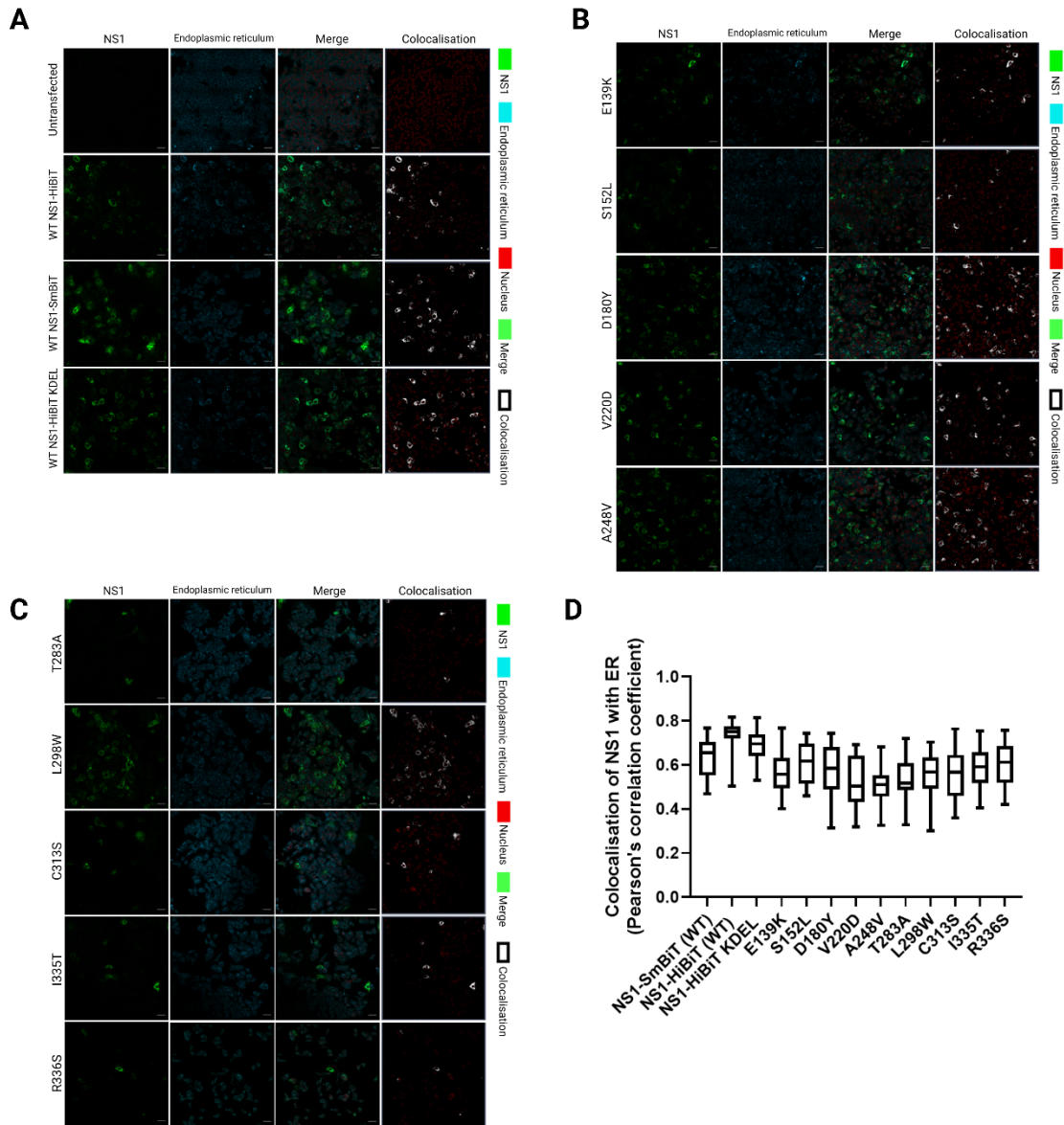


Figure 4.1.5 Identified secretion-impairing point mutations within DENV NS1 do not impact on its localisation to the ER via cell based population analyses. Huh-7.5 cells were transiently transfected with DENV NS1 expression constructs bearing respective NS1 secretion-impairing mutations and cultured overnight prior to fixation and immunostaining processes. Following these steps, cells were immunostained for NS1 protein (green; first column), endoplasmic reticulum (blue; second column) and nuclei (red). Merged images (third column) and NS1-ER colocalised pixels (white; fourth column) are indicated in (A), (B) and (C); (scale bars, 50 μ m). (D) Colocalisation between ER and NS1 signals (Pearson's correlation coefficient) was measured for 20-25 cells per sample group. Box & whiskers plot indicates median values, 25th to 75th percentiles, maximum and minimum values (n = 22-25 cells/group). Unpaired student t-tests between wildtype NS1-SmBiT and each mutant dataset indicated no significant differences (P > 0.05).

4.2 Investigating the effects of these identified NS1 secretion impairing mutations on DENV RNA replication and infectious virus production.

4.2.1 Selected NS1 secretion-impairing mutants were shown to not support infectious virus production

Given that both V220D and A248V mutations were shown to impair NS1 secretion efficiency, we decided to investigate the influence of these mutations on the DENV replication cycle via a reverse genetics approach. Additionally, we also chose to compare the effects of these two selected mutations to those of two glycosylation mutations, N130A and N207A which have been previously shown to impact NS1 secretion (Wang et al 2019; Fan et al 2014; Somnuk et al 2011). The selected mutations (N130A/ N207A/ V220D/ A248V) were individually incorporated into the full length DENV-2 construct (pFKDVs) via site-directed mutagenesis (Fishl and Bartenschlager 2013). Huh-7.5 cells were transiently transfected with *in vitro* RNA transcripts of respective constructs and culture supernatants were subsequently harvested at 24hr, 48hr, 72hr, 96hr and 120hr. Viral infectivity of supernatants was then determined by focus forming unit (FFU) assays. As shown, both V220D and A248V mutations prevented infectious virus production across all the timepoints (**Figure 4.2.1**). Somewhat surprisingly, both N130A and N207A mutants were associated with moderate increases in infectious virus production, compared with the wildtype DENV virus as shown.

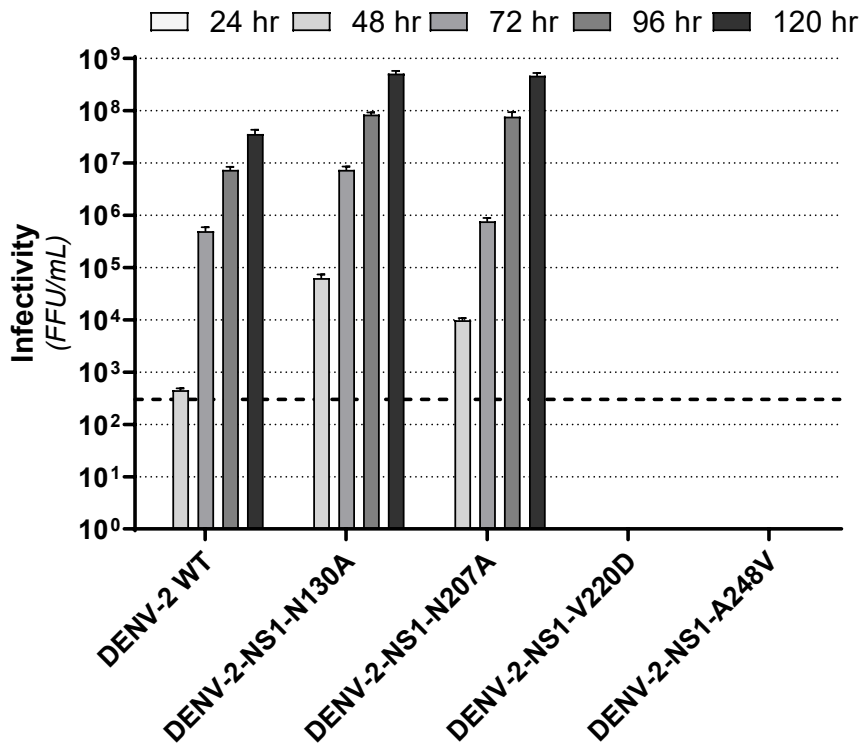


Figure 4.2.1 NS1 secretion-impairing mutations V220D and A248V also prevented infectious virus production. Infectious virus production by Huh-7.5 cells following transient transfection with wildtype DENV-2 RNA transcripts or derivatives containing NS1 secretion-impairing mutations (V220D or A248V) or *N*-linked glycosylation mutations (N130A or N207A), as indicated. Culture supernatants were harvested at indicated timepoints from 24hr, 48hr, 72hr, 96hr and 120hr. Infectivity of viral particles within supernatants was determined by focus forming unit (FFU) assay. Data are presented as means \pm SD from three independent replicates. The dashed line in black indicates the limit of detection for the infectivity assay. Taken from Tan et al 2023.

4.2.2 The wildtype full-length DENV-2 reporter virus (pFKDVs-R2A) did not support DENV RNA replication and thus DENV RNA replication was assessed via utilisation of DENV-2 sub-genomic replicon construct (sgDVs-R2A).

With the availability of an established full-length DENV-2 reporter construct encoding a *Renilla luciferase* reporter gene (pFKDVs-R2A), we decided to investigate the influences of these NS1 secretion-impairing mutations on the DENV replication cycle (Fischl and Bartenschlager 2013). Following incorporation of these point mutations into the pFKDVs-R2A via site-directed mutagenesis (SDM), *in vitro* RNA transcripts were transcribed and transfected into Huh-7.5 cells. Lysates were harvested at 4hr, 24hr, 48hr, 72hr and 96hr for measurement of raw luciferase activity and were normalised to values of the 4hr timepoint, which serves as a readout of input RNA levels following transfection.

However, despite multiple efforts to validate these given constructs, including via restriction digest, Sanger sequencing of the *Renilla luciferase* reporter gene (not shown), and their employment in transfection studies, negligible luciferase activity was observed for all selected constructs (not shown), suggesting the presence of unknown mutation(s) in the parental pFKDVs-R2A construct may have rendered this genome replication defective.

With the availability of a wildtype *Renilla luciferase* reporter encoding sub-genomic replicon construct (sgDVs-R2A), we investigated the potential impact of NS1 mutations on DENV RNA replication and translation by incorporation of these selected mutations (N130A/ N207A/ V220D/ A248V) into the sgDVs-R2A construct (Fischl and Bartenschlager 2013). While N130A and N207A mutants displayed replication kinetics that were similar to that of the wildtype sub-genomic replicon, the V220D and A248V mutants displayed gradually declining luciferase activities that closely reflected those of the replication defective ‘GND’ negative control (**Figure 4.2.2**).

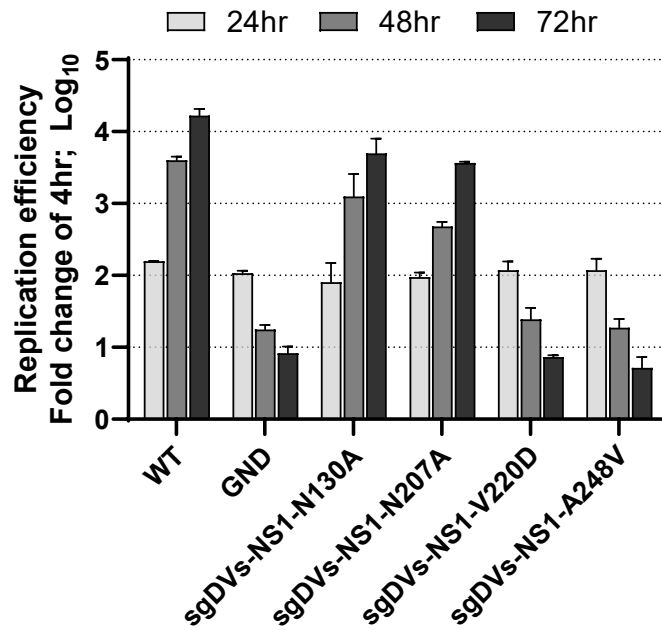


Figure 4.2.2 NS1 secretion-impairing mutations V220D and A248V prevent RNA replication activity. Replicative fitness of NS1 mutants in the context of a sub-genomic replicon construct encoding a *Renilla luciferase* reporter gene (sgDVs-R2A). *In vitro* transcribed RNA for the indicated constructs were transiently transfected into Huh-7.5 cells. Luciferase activities were measured for lysates harvested at 4hr, 24hr, 48hr and 72hr. Luciferase values were expressed as a fold change relative to the average values for the 4hr timepoint (a measurement of input RNA) for each respective construct. A replication-deficient lethal mutation within NS5 (GND) that disrupts NS5 RNA-dependent RNA polymerase activity was included as a negative control. Data are presented as means \pm S.D from three independent replicates (n =3). Taken from Tan et al 2023.

4.3 Investigating the relationship between impairing NS1 secretion mutations and DENV RNA replication and infectious virus production

Several studies have demonstrated that other members of the Flavivirus genus, Kunjin virus, West Nile virus and Yellow Fever virus that without their NS1 failed to replicate but can be evidently rescued when NS1 is ectopically trans-complemented by expression of full-length protein (Scaturro et al 2015; Youn et al 2013; Young et al 2013; Khromykh et al 1999; Lindenbach and Rice 1997). In the context of DENV NS1, a DENV-based trans-complementation system was developed by Scaturro et al (2015) and employed to demonstrate that DENV NS1 secretion is not essential for its roles in DENV RNA replication and infectious virus production. In this study, we sought to adapt this established trans-complementation system for our investigations into the impact of our NS1 secretion-impairing mutants of interest on DENV RNA replication and infectious virus production when trans-complemented.

The full length DENV-2 strain 16681 (pFKDVs-R2A) (**Figure 4.3.1 A**) and a derivative sub-genomic reporter DENV-2 replicon (pFKsgDVs-R2A) both containing a *Renilla luciferase* sequence gene (R2A) (**Figure 4.3.1 B**), were the starting basis of these trans-complementation studies (Scaturro et al 2015; Fischl and Bartenschlager 2013). For this, a 97 codon in-frame deletion within NS1 (Δ NS1) was successfully incorporated into the pFKDVs-R2A and pFKsgDVs-R2A constructs by HiFi DNA Assembly (New England BioLabs) to generate trans-complementation pFKDVs-R2A- Δ NS1(**Figure 4.3.1 C**) and pFKsgDVs-R2A- Δ NS1 constructs (**Figure 4.3.1 D**). Also, a lethal mutation within the DENV NS5 RNA-dependent RNA polymerase affecting viral RNA replication activity “GND” was also incorporated into these constructs as negative controls (**Figure 4.3.1 E**).

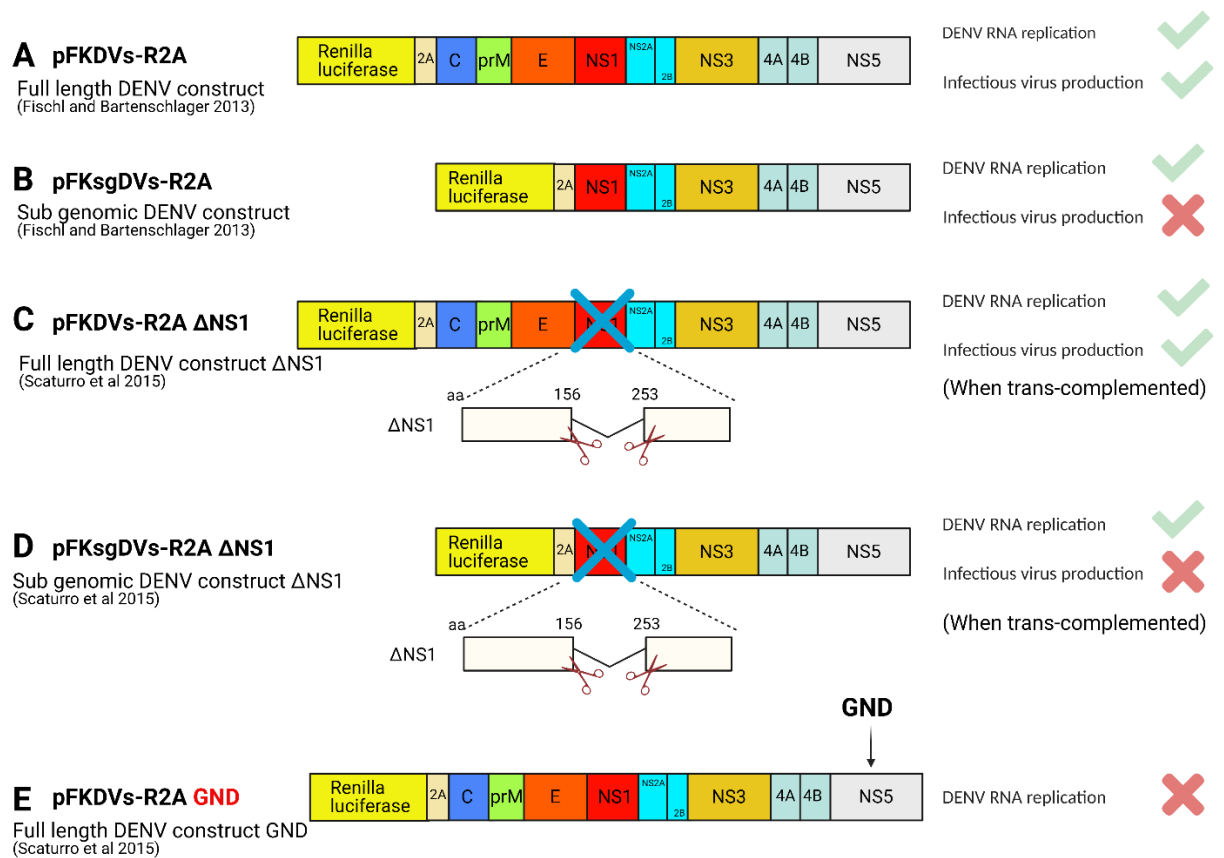


Figure 4.3.1 Schematic diagram of DENV constructs. In this trans-complementation approach, a 97 codon in-frame deletion within NS1 (Δ NS1) was incorporated into established DENV constructs, pFKDVs-R2A (A) and pFKsgDVs-R2A (B) via HiFi DNA Assembly (New England BioLabs), thereby generating pFKDVs-R2A Δ NS1 (C) and pFKsgDVs-R2A Δ NS1 (D) respectively. A known replication-deficient lethal mutation within NS5 “GND” that disrupts its RNA-dependent RNA polymerase activity, e.g. as shown in (E) was also included into both (C,D) trans-complementation constructs. Scissors symbols indicate the deletion of codons position GND between 156-253 of NS1 (Δ NS1-156-253).

To provide some context of the overall trans-complementation approach, a SP6 promoter located upstream of the 5' UTR of DENV full length and sub-genomic replicon constructs that feature a large deletion in NS1 enables the generation of *in vitro* transcribed RNA transcripts via SP6 RNA polymerase transcription reactions. These viral RNA transcripts can then be delivered into cells of interest that heterologously express NS1 or NS1 mutants of interest to determine viral RNA replication and infectious virus production activity. In the

case of the sub-genomic replicon constructs, viral RNA replication is only assessed via measurement of *Renilla luciferase* enzyme-derived signals from the *Renilla luciferase* sequence gene cassette incorporated into the 5' end of the viral genome (R2A). On the other hand, assessing infectious virus production entails transducing naïve seeded cells with supernatants containing infectious virus particles and their subsequent application to naïve NS1-expressing cells for evaluation of luminescence signals (**Figure 4.3.2**).

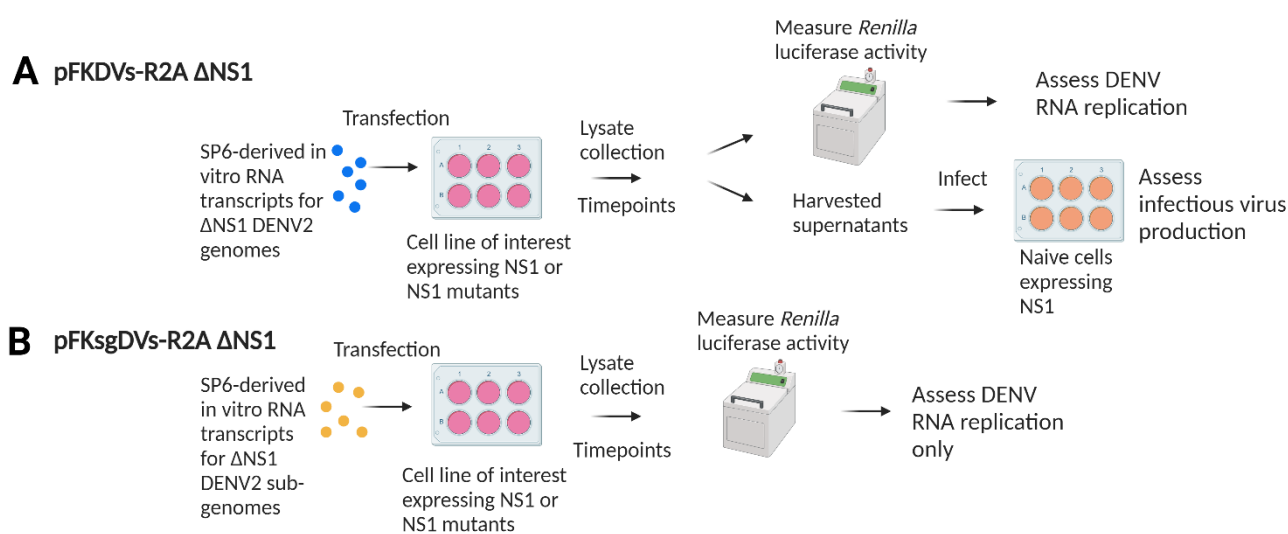


Figure 4.3.2 Workflow of the DENV-based trans-complementation approach. (A, B) *In vitro* RNA transcripts generated from respective linearised DVs-R2A Δ NS1 constructs via SP6 RNA polymerase-driven transcription reactions are transfected into an NS1-expressing cell line of interest (Huh-7.5 cell lines stably expressing full length wildtype NS1, wildtype NS1 C-terminally fused with a KDEL motif or NS1 featuring 1 of 10 identified NS1 secretion impairing mutations). At appropriate timepoints (4hr, 24hr, 48hr, 72hr, 96hr), lysates are harvested to measure luciferase activity generated via the *Renilla luciferase* gene (R2A) to assess DENV RNA replication activity. Additionally, supernatants containing infectious virus particles collected prior to harvesting of lysates are utilised to infect naïve wildtype NS1-expressing cells before measuring luciferase activity to assess infectious virus production.

In our initial trans-complementation experiments, we applied a dual transfection approach. In brief, this involved transiently transfecting Huh-7.5 cells with the NS1 DNA expression constructs of interest, before subsequently transfecting the DNA-transfected cells with RNA transcripts for the sub-genomic replicon construct bearing a Δ NS1 deletion (pFKsgDV_s-R2A Δ NS1) (**Figure 4.3.1 D**, **Figure 4.3.3 A**). Doubly transfected Huh-7.5 cells were then harvested at indicated timepoints from 4hr to 96hr, before assessing DENV RNA replication levels via luciferase assays (**Figure 4.3.3 B**). Following normalisation of raw luciferase values to the 4hr timepoint of respective groups, the mutant NS1-HiBiT R336S and positive control NS1-HiBiT KDEL in most timepoints displayed low luciferase activities that closely matched those of the negative control (**Figure 4.3.3 C**). The wildtype NS1-HiBiT appeared to display steady luciferase levels from 24hr to 72hr timepoints before a rapid decline in luciferase activity at the final timepoint of 96hr. With these unconvincing results, the initial double transfection trans-complementation approach was deemed unsuccessful, as both wildtype NS1-HiBiT and NS1-HiBiT KDEL were expected to support DENV RNA replication. While low overlapping DNA/RNA transfection efficiencies may explain the observed low luciferase activities, the modest improvements in these efficiencies that could be potentially be achieved by further optimisation of transfection conditions suggested that another alternative trans-complementation strategy was needed.

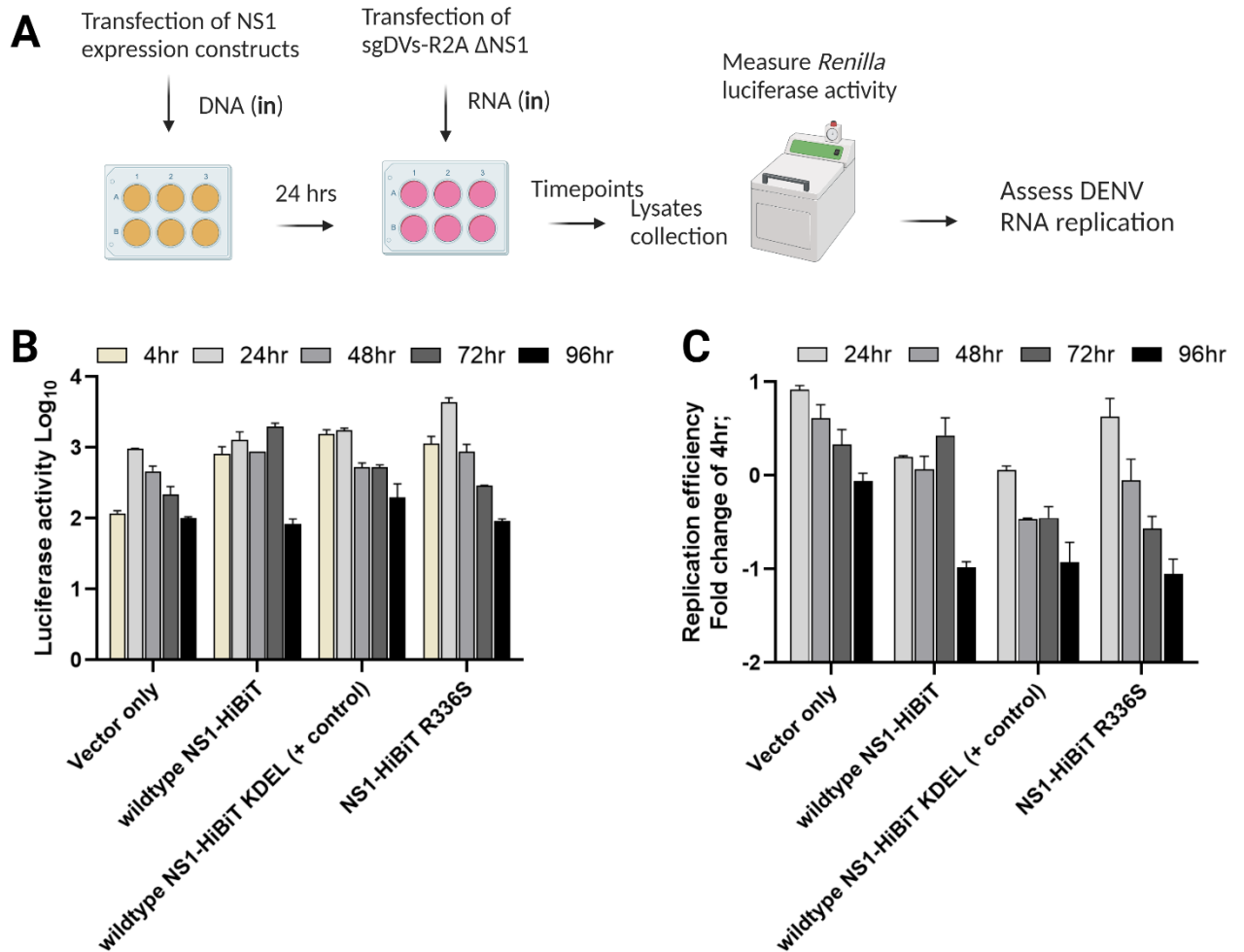


Figure 4.3.3 The initial dual transfection trans-complementation approach failed to support robust DENV RNA replication. (A) Schematic diagram of the dual transfection trans-complementation experimental approach. Seeded naïve Huh-7.5 cells were transiently transfected with NS1 expression constructs (empty vector, wildtype NS1-HiBiT, wildtype NS1-HiBiT bearing an ER retention motif “KDEL”, NS1 secretion-impairing mutant NS1-HiBiT R336S). At 24-hours post-transfection, cells were transfected with RNA transcripts of the FKsgDVs-R2A Δ NS1. Lysates were subsequently harvested at 4hr, 24hr, 48hr, 72hr and 96hr timepoints to determine DENV RNA replication via luciferase assays. (B) Raw luciferase values of indicated timepoints for each indicated group. (C) Replicative fitness of wildtype NS1 and NS1 mutant in the context of a sub-genomic replicon construct bearing a Δ NS1 (pFKsgDVs-R2A Δ NS1). For each respective construct, raw luciferase values were measured and expressed as a fold change relative to average values for the 4hr timepoint (a measurement of input RNA transfection) to assess efficiency of viral replication. Data are presented as means \pm SD of duplicates for each group from a single experiment.

Next, we attempted to utilise a lentiviral-based trans-complementation approach. In this first instance, this involved generating replication-defective lentivirus vectors for each indicated expression construct, which includes a negative control construct, wildtype trio of NS1-HiBiT, untagged NS1, NS1-HiBiT KDEL (+ control) and a mutant NS1-HiBiT R336S (**Figure 4.3.4 A**). Generated lentiviruses were then utilised to transduce Huh-7.5 cells. Following 3 days post-transduction, the confluent lentivirally transduced cells were reseeded and cultured overnight. *In vitro* RNA transcripts of the sub-genomic replicon construct bearing the Δ NS1 deletion (pFKsgDVs-R2A Δ NS1) were then transfected into these newly reseeded Huh-7.5 cells before harvesting of lysates at respective timepoints as indicated.

In contrast to previous results from **Figure 4.3.3**, the wildtype untagged NS1 and NS1-HiBiT KDEL displayed a sequential increase in associated luciferase values from 24hr to 72hr before a slight decrease at the 96hr timepoint (**Figure 4.3.4 B**). The other wildtype NS1-HiBiT construct displayed steadily increasing luciferase values from the 24hr timepoint to the 96hr timepoint. Mutant NS1-HiBiT R336S surprisingly displayed luciferase activity kinetics that closely resembled both negative controls, with initial luciferase activity at the 24hr timepoint closely reflecting that of the wildtype constructs, before markedly declining in subsequent timepoints. Regardless of the results for the mutant NS1 R336S, the lentiviral-based trans-complementation approach appeared to be a promising strategy which was backed by demonstration that all the wildtype NS1 constructs displayed expected and robust replication kinetics across all timepoints. Thus, the lentiviral-based trans-complementation strategy was employed in subsequent experiments.

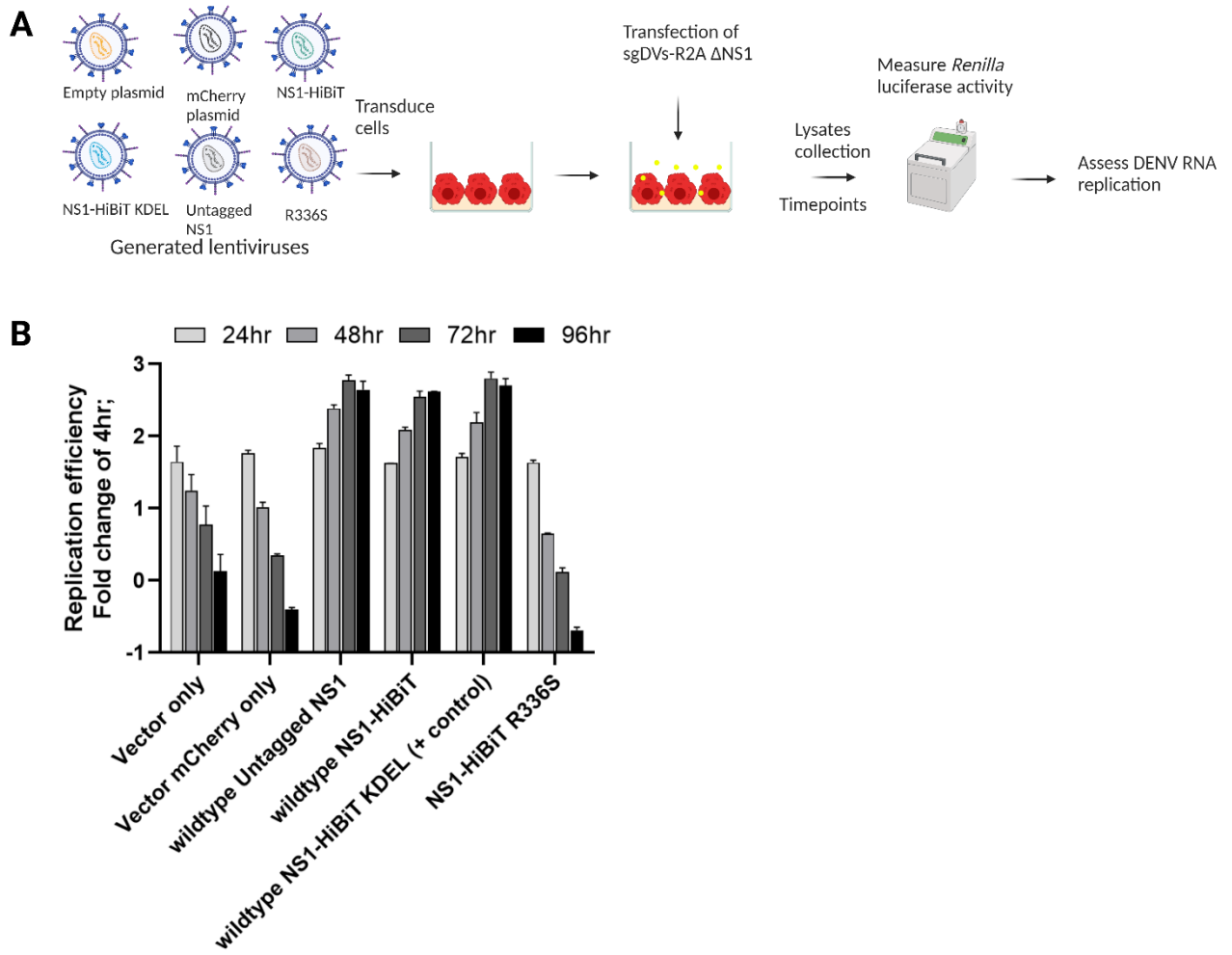


Figure 4.3.4 A lentiviral vector-based trans-complementation strategy supports robust DENV RNA replication. (A) Schematic diagram of the lentiviral vector-based trans-complementation approach. Huh-7.5 cells were transduced with lentiviruses for the indicated NS1 expression constructs (empty vector only [- control], empty vector with mCherry [- control], wildtype untagged NS1, wildtype NS1-HiBiT, wildtype NS1-HiBiT KDEL and a mutant NS1-HiBiT R336S). At 72-hours post-transduction, lentiviral vector transduced Huh-7.5 cells were reseeded before subsequent transfection with FKsgDVs-R2A RNA transcripts. Lysates were harvested at multiple timepoints (4hr, 24hr, 48hr, 72hr, 96hr) before measuring luciferase activities. (B) Replicative fitness of wildtype NS1 variants and the indicated NS1 mutant in the context of a sub-genomic replicon construct bearing a Δ NS1. For each transfection condition, raw luciferase values were measured and expressed as a fold change relative to average values for the 4hr timepoint (measurement of input RNA) to assess efficiency of viral replication. Data are presented as means \pm SD of duplicates from a single experiment (n=1).

Next, lentiviruses were prepared for the remaining 10 NS1 mutants of interest (E139K, S152L, D180Y, V220D, W232R, A248V, T283A, L298W, C313S, I335T) and, together with the previously generated lentiviruses (**Figure 4.3.4**), were subsequently utilised to transduce naïve Huh-7.5 cells (**Figure 4.3.5 A**). Following 72-hours post-transduction, lentivirally transduced cells were reseeded, before being transiently transfected with FKsgDVs-R2A Δ NS1 RNA transcripts. Lysates were harvested at two timepoints, 4hr and 72hr, before determining RNA replication efficiency via measurement of luciferase activity.

The wildtype untagged NS1, NS1-HiBiT and NS1-HiBiT KDEL constructs displayed largely consistent replication levels at the 72hr timepoint, as previously shown in **Figure 4.3.4 B**. However, all of the NS1 mutants, with the exception of E139K, appeared to display replication levels that closely resembled those of the negative controls, possibly indicating these NS1 mutants may not support viral RNA replication (**Figure 4.3.5 B**). At the 72hr timepoint, only the NS1 mutant E139K exhibited a replication efficiency that was comparable to that of the wildtype untagged NS1 and NS1-HiBiT KDEL constructs. This trans-complementation assay was repeated, and this yielded similar results (not shown). Hence, these trans-complementation studies demonstrated that, with the exception of E139K, all the NS1 mutants appeared to cause a ‘lethal’ defect in viral RNA replication. While we intended to also perform these trans-complementation experiments in the context of the full-length DENV construct bearing a Δ NS1 deletion (pFKDVs-R2A Δ NS1), the replication-defective phenotypes displayed by the vast majority of these NS1 mutants undermined the rationale for such follow-up studies of the impact of these mutations on infectious virus production.

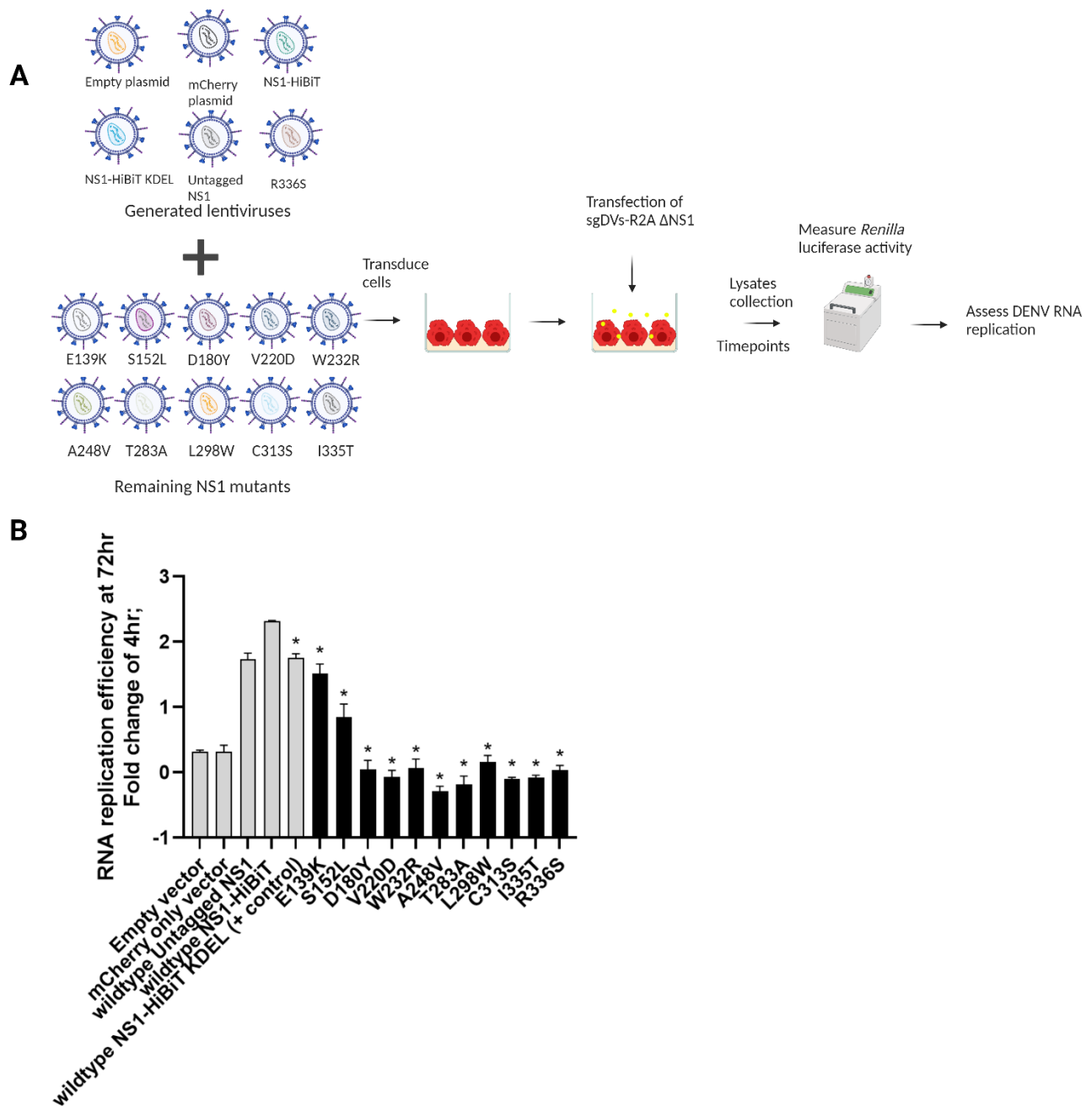


Figure 4.3.5 The majority of NS1 secretion-impairing mutants appeared to be RNA replication incompetent. (A) Schematic diagram of the lentiviral vector-based trans-complementation approach. Seeded Huh-7.5 cells were transduced with generated lentiviruses for expression constructs as indicated empty vector only [- control], empty vector with mCherry [- control], wildtype untagged NS1, wildtype NS1-HiBiT, wildtype NS1-HiBiT KDEL and 11 NS1 secretion impairing mutants [E139K, S152L, D180Y, V220D, W232R, A248V, T283A, L298W, C313S, I335T, R336S]. At 72-hours post-transduction, lentiviral vector transduced Huh-7.5 cells were reseeded before transfection with RNA transcripts of FKsgDVs-R2A. Lysates were harvested at two timepoints only (4hr, 72hr) before measuring RNA replication activity. (B) Replicative fitness of wildtype NS1 variants and NS1 mutants in the context of a sub-genomic replicon construct bearing a Δ NS1. For each respective

expression construct, raw luciferase values were measured and expressed as a fold change relative to average values for the 4hr timepoint (measurement of input RNA) to assess RNA replication efficiency. Data are presented as means \pm SD from three independent replicates. Significance between wildtype NS1-HiBiT and NS1 mutants was calculated using unpaired student's t-test (T-test) (*, $p < 0.05$). Wildtype NS1 variants and negative controls are portrayed as grey bars while the NS1 secretion-impairing mutants are portrayed as black bars.

4.4 Western Blot analysis of putative NS1 secretion-impairing mutations

Given difficulties in detection of several NS1 mutant proteins by Western blotting using the anti-NS1 mAb '4G4' (See **Appendix IV: Supplementary Figures: SF4.1, SF4.2**), we postulated that since this specific antibody recognises a mature NS1 protein conformation that is disrupted by the selected NS1 mutations rendering them undetectable by Western blotting using this '4G4' antibody.

With that in mind, we performed additional Western blotting studies using a commercially available anti-NS1 monoclonal antibody (GeneTex) (See **Appendix IV: Supplementary Figures: SF4.3**). Unfortunately, intracellular NS1 proteins could not be reliably detected using this antibody, including for NS1-HiBiT and KDEL-tagged NS1-HiBiT protein lysates. Total-protein staining (LI-COR) and reprobing using an anti- β -actin antibody (housekeeping gene) confirmed equivalent loading of respective lysate samples. Further optimisation of Western blotting conditions using this anti-NS1 monoclonal antibody enabled detection of intracellular NS1 in wildtype NS1-HiBiT and KDEL-tagged NS1-HiBiT lysates while all NS1 mutants appeared to be weakly detected (See **Appendix IV: Supplementary Figures: SF4.3**). Additionally, utilisation of a stronger lysis buffer, RIPA lysis buffer instead of NP-40 lysis buffer did not impact upon the inability to detect these NS1 mutant proteins such that these results closely reflected those of the '4G4' Western blotting results.

Likewise with the previous anti-NS1 '4G4' analyses, a small-scale immunofluorescence analysis was performed to further determine if 'GT4212' anti-NS1 monoclonal antibody (GeneTex) was able to detect NS1 proteins. Huh-7.5 cells were transiently transfected with the wildtype NS1-HiBiT, wildtype KDEL-tagged NS1-HiBiT and a NS1 mutant NS1-HiBiT R336S known to be successfully detected with the anti-NS1 '4G4' antibody via immunofluorescence but not by Western blotting. Both wildtype and mutant NS1-HiBiT R336S were well-expressed and specifically detected, especially the R336S mutant which had a much stronger NS1 expression labelling intensity than the wildtype KDEL-tagged NS1-

HiBiT and wildtype NS1-HiBiT (See **Appendix IV: Supplementary Figures: SF4.4**). Thus, this result showed that the ‘GT41212’ anti-NS1 monoclonal antibody (GeneTex) was able to detect the wildtype NS1, wildtype KDEL-tagged NS1-HiBiT and a selected NS1 mutant R336S by immunofluorescence but failed to do so by Western blotting, consistent with the reactivity and utility of anti-NS1 ‘4G4’ antibody for detection of these NS1 variants.

In a final attempt to detect those NS1-HiBiT mutant proteins via Western blotting, we employed a newly available anti-HiBiT peptide tag antibody (Promega). As previously described, respective NS1 expression constructs were transiently transfected into Huh-7.5 cells before subjecting the harvested cell lysates and supernatant samples to SDS-PAGE and Western blotting. The wildtype NS1-HiBiT, KDEL-tagged NS1 and mutant NS1-HiBiT proteins were all readily detected in their intracellular lysate samples (**Figure 4.4.1 A**). While readily detected, all mutant NS1-HiBiT proteins appeared to be expressed at much lower levels than their wildtype and KDEL-tagged NS1 counterparts. In regards to the corresponding supernatant samples, wildtype NS1-HiBiT was strongly detected while the KDEL-tagged NS1-HiBiT was detected at distinctly lower levels, consistent with its expected KDEL-directed intracellular retention activity. As expected for the NS1 secretion-impaired mutants, all NS1-HiBiT mutants were detected at markedly reduced levels in their supernatant samples, with parallel analysis of the HiBiT luciferase activity in lysate and supernatant samples largely reflecting these phenotypes (**Figure 4.4.1 B**).

Quantitative analysis of the Western blot signals to determine the normalised extracellular-to-intracellular NS1-HiBiT ratios confirmed the NS1 secretion-impairing phenotypes that were observed in the original (**Figure 3.0.6**) and Western blot-parallel HiBiT luciferase assays (**Figure 4.4.1 C**). Taken together, the Western blot studies using an anti-HiBiT peptide tag antibody successfully enabled detection of all mutant proteins and confirmed their secretion-impaired phenotypes as seen and indicated with the initial HiBiT luciferase assays (**Figure 3.0.6**).

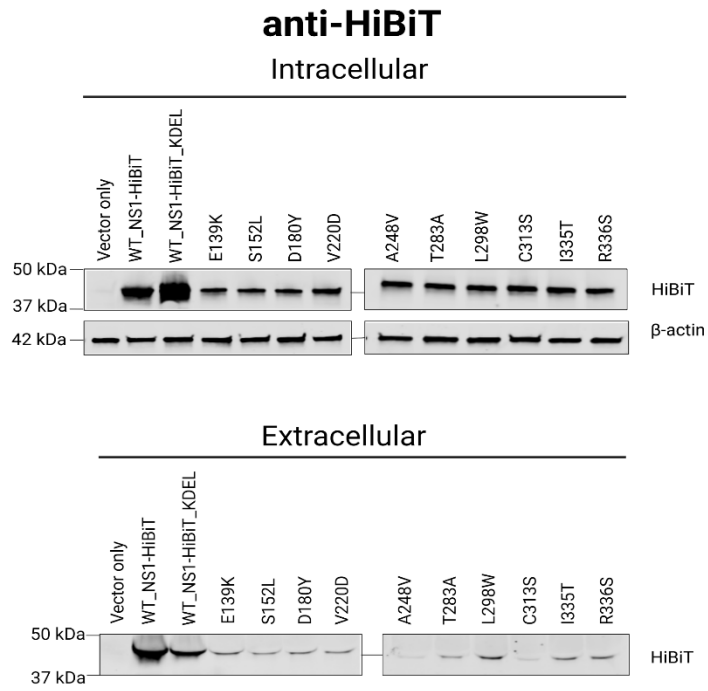
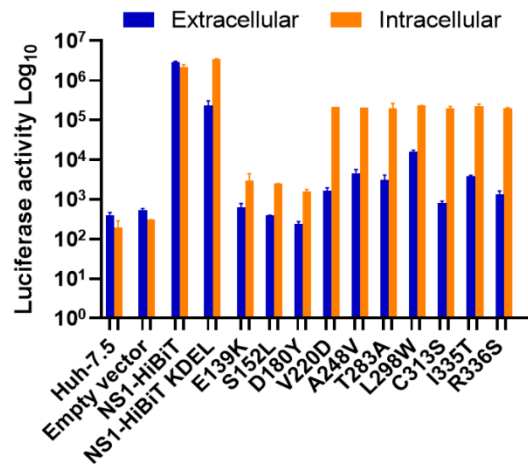
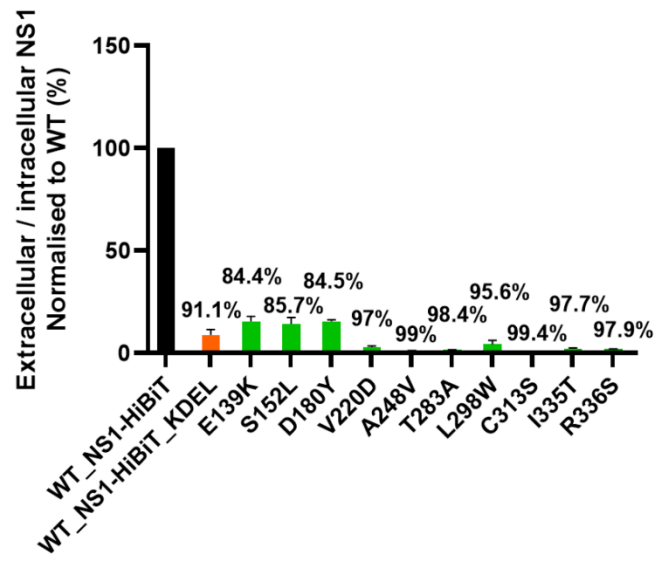
A**B****C**

Figure 4.4.1 Western blot analysis of NS1 mutants using an anti-HiBiT peptide tag antibody confirmed their secretion-impairing phenotypes. (A) At 48-hours post-transfection, cell lysates (intracellular) and supernatants (extracellular) were harvested from Huh-7.5 cells that had been transiently transfected with the indicated NS1-HiBiT expression constructs, prior to subjecting samples to SDS-PAGE and Western blotting to detect DENV NS1 using an anti-HiBiT peptide tag antibody. β -actin was also detected in parallel as a protein loading control for lysate samples. (B) Cell lysates and supernatant samples that were used in the Western blotting (A) were also analysed via HiBiT luciferase assays. Orange bars represent lysate samples, while blue bars represent supernatant samples. (C) Quantitative analysis of Western blotting data obtained using the anti-HiBiT antibody (Promega). Extracellular-to-intracellular NS1-HiBiT mutant protein levels were expressed as a percentage of values for the respective wildtype control samples. Black bars represent NS1-HiBiT point mutants, orange bars represent NS1-HiBiT KDEL, while green bars represent NS1-HiBiT point mutants, as indicated. Data are means \pm SD from two independent replicates, with the values above each error bar indicating %-decrease in NS1 secretion efficiency compared to the wildtype values. Taken from Tan et al 2023.

4.5 Utilisation of a replication-independent NS1-NS5 polyprotein expression system (pIRO) to further characterize NS1 secretion-impairing mutants

Given that the NS1 secretion-impaired mutants V220D and A248V appeared to be replication incompetent (**Figure 4.2.2**), we also investigated the impact of these mutations on NS1 localisation and secretion by employing a newly established replication-independent expression system termed “pIRO” (plasmid-induced replication organelle formation) that give rises to the biogenesis of VPs that morphologically resemble VPs generated in infected cells (Cerikan et al 2020). Like in previous experiments (**Figure 4.2.1**; **Figure 4.2.2**), we individually incorporated our mutations of interests, N130A, N207A, V220D and A248V into the pIRO expression construct using site-directed mutagenesis. To determine if these point mutations would alter the colocalisation staining pattern between NS1 and NS4B, we transiently transfected Huh-7.5 cells stably expressing the T7 RNA polymerase with the wildtype and mutant pIRO expression constructs prior to fixation, immunofluorescent staining of NS1 and NS4B and subsequent analyses by high resolution confocal imaging (**Figure 4.5.1 A**).

Interestingly, all the pIRO-D mutants displayed similar NS1 and NS4B staining patterns in comparison to the wildtype pIRO-D, although the typical juxtannuclear NS1- and NS4B-positive foci appeared to be less frequently observed for the N130A, V220D and A248V mutants (**Figure 4.5.1 A**). Additionally, intracellular NS1 in pIRO-D V220D and A248V transfected cell lysates was not readily detected by Western blotting analysis (**Figure 4.5.1 B**). This was unexpected as our previous results using NS1 overexpression alone (**Figure 4.1.3**) demonstrated that the same mutant NS1 proteins were detectable intracellularly, albeit at low levels when expressed in regard to the NS1-HiBiT expression constructs. In contrast, intracellular NS1 was readily detected for the wildtype pIRO-D, pIRO-D N130A and pIRO-D N207A mutants (**Figure 4.5.1 B**). Similarly extracellular NS1 was also readily detected in the

supernatants of the cells transfected with wildtype, pIRO-D N130A and N207A mutants. As expected, *N*-glycosylation mutants N130A and N207A displayed an appreciable decrease in their molecular weight that was consistent with the loss of the glycans of these given sites. DENV NS3 was also distinctly detected at similar levels in the lysates of the wildtype and all four pIRO-D mutants, indicating similar transfection efficiencies and NS protein expression levels across all pIRO-D derived transfected Western blotting samples as shown.

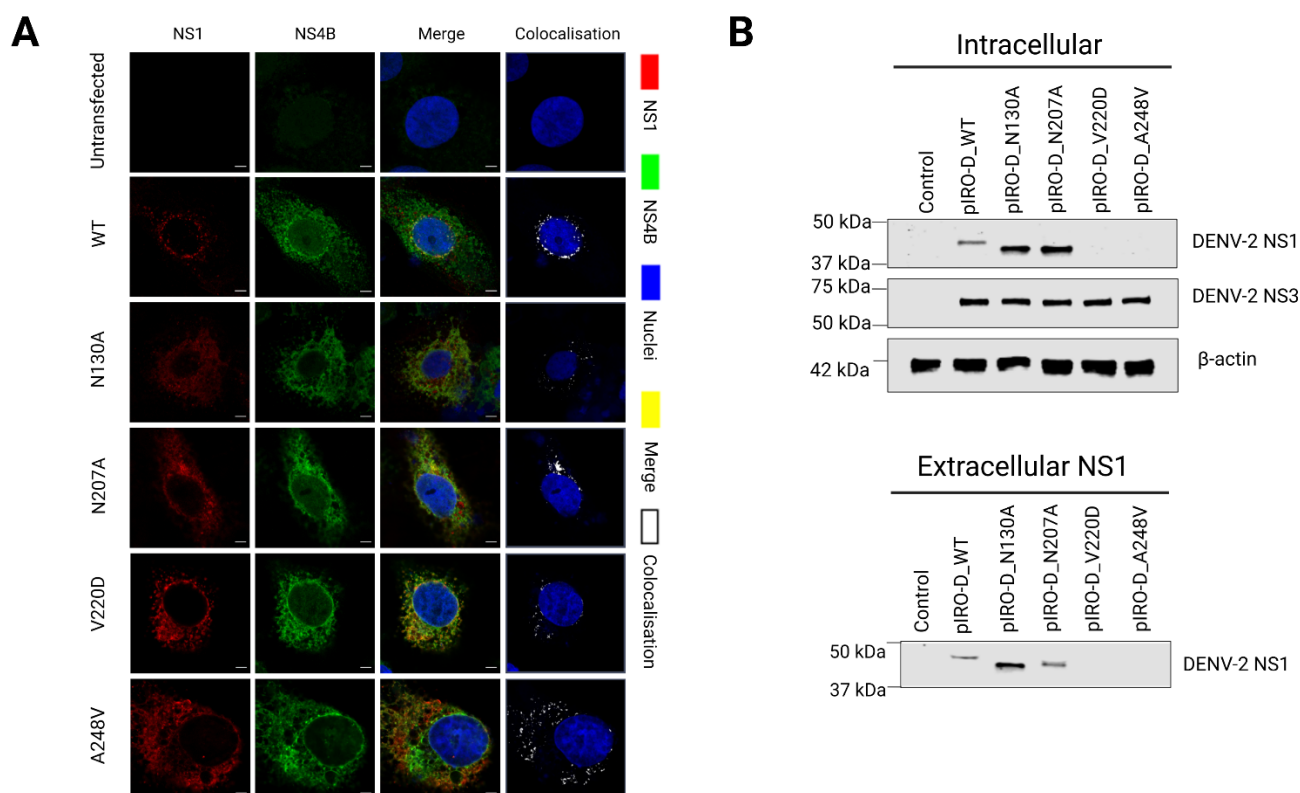


Figure 4.5.1 Characterisation of the indicated NS1 mutants within the replication-independent expression system (pIRO) via high resolution confocal imaging and Western immunoblotting. (A) Huh-7.5 cells expressing T7 RNA polymerase were transfected with the pIRO expression constructs containing the indicated NS1 mutations (N130A/ N207A/ V220D/ A248V) and cultured overnight before fixation and fluorescent labelling with NS1-, NS4B-specific antibodies. Confocal images of NS1 proteins (red, left column), NS4B proteins (green, second column from the left), nuclei (blue, third column), and colocalisation panels (white, fourth column) are portrayed. Scale bars are 5 μ m in length

as shown. **(B)** Western blotting analysis of the pIRO-derived NS1 mutants. Naïve Huh-7.5 cells were transiently transfected with the pIRO-derived expression constructs as described in **(A)**. At 48-hours post-transfection, supernatants (extracellular) and cell lysates (intracellular) were collected and subjected to SDS PAGE and Western blotting using antibodies against NS1, NS3, and β -actin as indicated.

Tile scan images of the wildtype and all four pIRO-D mutant groups were also captured to determine if there were significant alterations in their NS1-NS4B colocalisation across a large number of cells (**Figure 4.5.2 A**). Interestingly, colocalisation analyses showed no significant difference in the NS1-NS4B colocalisation status for all the four pIRO-D mutants in comparison to the wildtype pIRO-D (**Figure 4.5.2 B**), indicating that these NS1 secretion impairing mutations possibly did not result in distinctive changes in the colocalisation of the NS1 protein with NS4B.

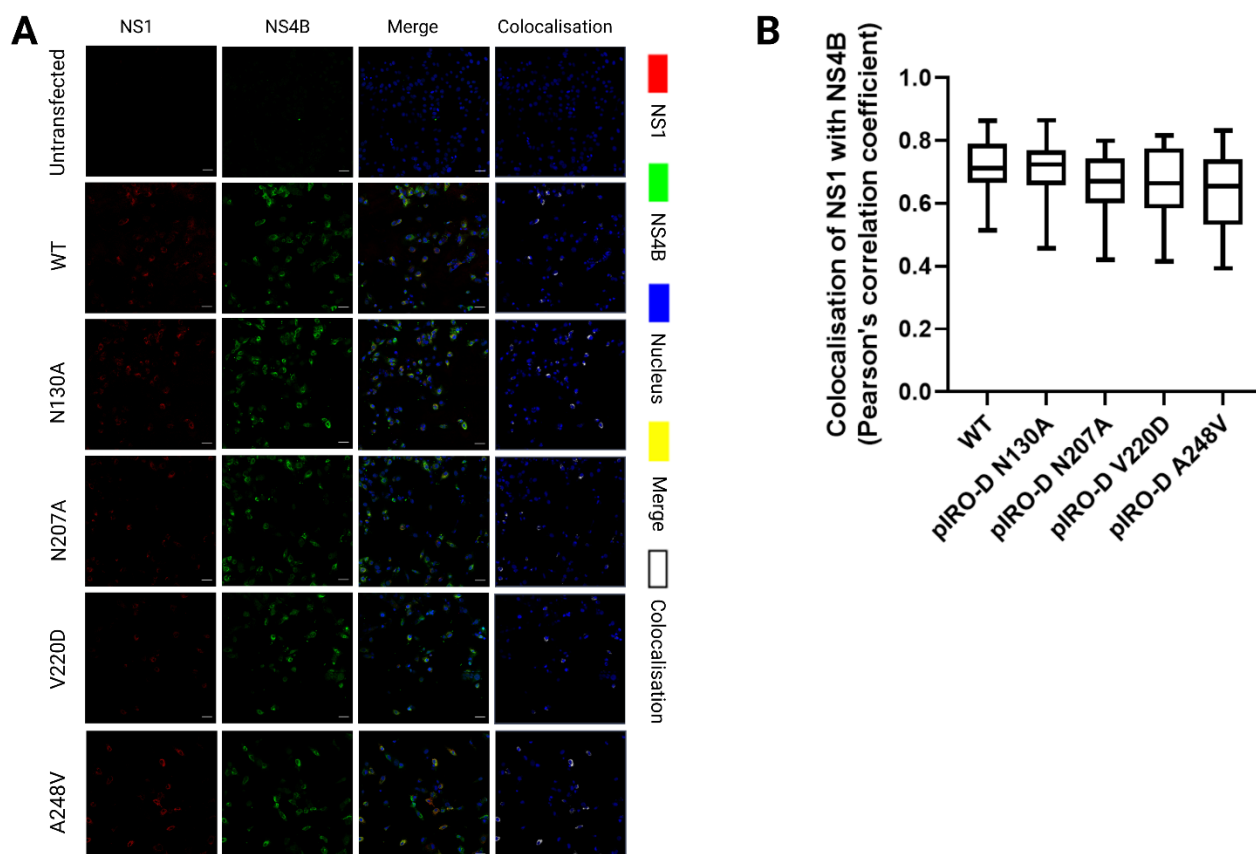


Figure 4.5.2 Colocalisation studies showed no apparent differences in NS1-NS4B colocalisation among the pIRO-derived NS1 mutants. (A) Huh-7.5 cells were transiently transfected with pIRO expression constructs containing respective NS1 single point mutations (N130A/ N207A/ V220D/ A248V) and cultured overnight prior to fixation and immunostaining. Confocal tile scan images of NS1 proteins (red, first column), NS4B proteins (green; second column from left), nuclei (blue, third column) and colocalisation panels (white; fourth column). Confocal images were obtained using a 63X objective; scale bar 5 μm . (B) Quantification of colocalisation between NS1 and NS4B for >30 NS1/NS4B-positive cells per group via Pearson Correlation Coefficients. The box and whiskers plot indicates median values, 25th to 75th percentiles, maximum and minimum values (n= 30-35 cells per group).

4.6 Discussion

Following successful identification of a small panel of NS1 secretion-impairing mutants via high throughput mutagenesis and luciferase reporter-based assays in Chapter 3, we next sought to further characterise these NS1 mutants. By utilising *in silico* analyses to determine the locations of these NS1 secretion-impairing mutations, we revealed that majority of these mutations mapped to the β -ladder. Additional NS1 secretion impairing mutations were identified in the 2nd sub connector domain and the Wing domain. While the β -ladder is the largest domain of the NS1 crystal structure and thus provides more coverage for the introduction of mutations by the error prone DNA polymerase during the PCR-based random point mutagenesis, previous studies have also implicated the β -ladder domain as a critical determinant of NS1 secretion (Plaszczyca et al 2019). Multiple sequence alignments for representative isolates of the four DENV serotypes, WNV and YFV provided an overview of the degree of conservation of each secretion influencing residues and this revealed that most of the mutations that mapped to the β -ladder domain are highly conserved among the DENV serotypes. This suggests that these residues may be important determinants of NS1 secretion efficiency or NS1 folding for a broad range of DENV serotypes and related flaviviruses.

And in the context of our NS1 secretion studies, Plaszczyca et al (2019) similarly identified a cohort of NS1 secretion-impairing mutations; D136A within the Wing domain and W311A, P319A, P320A, E334A, R336A within the C-terminal of the β -ladder domain. Consistent with our study, our analyses also identified Arg-336 as a key determinant of NS1 secretion as its mutation (R336S) similarly impaired NS1 secretion efficiency in our HiBiT-tagged expression system. Additionally, in a related study, Arg-336 has also been described to be important for viral RNA replication, hinting that this residue is essential for the multifaceted

functions of NS1 and perhaps correct NS1 maturation and/or interactions may be disrupted by such mutations (Scaturro et al 2015). Notably, several of the NS1 secretion-impairing mutations that we identified in this study, E139K, C313S and I335T mapped in close proximity to the NS1 secretion-impairing mutations that were also identified by Plaszczyca et al (2019); D136A, W211A, E334A and R336A. This interpretation suggests that the β -ladder domain and perhaps the Wing domain are essential for NS1 secretion activity, and the solvent-exposed nature of these sites within the domains may potentially mediate NS1 interactions that are important for its secretion.

Interestingly, NS1 protein was not readily detected in the lysates or supernatants for several NS1 mutants when probed by Western blotting using the conformation specific anti-NS1 '4G4' antibody. Initially, we considered that this may be attributable to inefficient transfection. However, this seemed unlikely as many of the mutant NS1 proteins that were undetectable by Western blotting nonetheless displayed robust HiBiT luciferase assay values in the same lysates or supernatants that were used for Western blotting. Somewhat surprisingly, many of these NS1 mutant proteins were readily detected by immunofluorescence and confocal imaging when cells were labelled using the same conformation specific '4G4' antibody. While it could be potentially considered that these one or more of NS1 mutations directly disrupt the epitope within NS1 which recognises the anti-NS1 '4G4' antibody, it is also possible that such mutations may disrupt correct NS1 folding and/or maturation to render the NS1 mutant protein unrecognisable by the antibody.

We attempted to troubleshoot the indicated challenges in Western blot detection of several NS1 mutant proteins by utilising different lysis buffers, cell lines and alternative commercial anti-NS1 antibodies (monoclonal and polyclonal antibodies) but unfortunately this did not enable improved detection of mutant NS1 protein. Eventually, we acquired a newly available

anti-HiBiT peptide tag antibody and this indeed enable reliable detection of all NS1 mutant proteins. These anti-HiBiT Western blotting results confirmed the secretion-impaired phenotypes of these mutants that were initially identified by early HiBiT luciferase assays. However, it was interesting to note that the mutants that were most readily detected by anti-NS1 '4G4' Western blotting (**Figure 4.1.3A**) were associated with lower HiBiT luciferase values (**Figure 4.1.3B**). Thus, it is possible that the accessibility of the HiBiT tag at the C-terminus of the NS1 may be enhanced by certain NS1 mutations and that this is another potential readout of changes in NS1 conformation that could be explored in future follow-up studies.

Subsequent studies involving high resolution confocal imaging revealed some interesting observations. These defined NS1 secretion impairing mutations did not appear to cause distinctive changes in the localisation of NS1 protein or its colocalisation with the ER. This indicates that the impaired secretion of these NS1 mutant proteins cannot be attributed to the gross mislocalisation of the protein. More detailed analyses are needed to further determine whether these mutations induce more subtle changes in NS1 localisation that were not observed in this study. Additionally, these NS1 mutant proteins were successfully detected by high resolution confocal imaging not by Western blotting using the '4G4' antibody, which suggests that the recognition of NS1 mutant proteins by the '4G4' NS1 antibody is perhaps more susceptible to the processing steps involved in Western blotting such as boiling and lysis in strong detergents, as compared to the less destructive steps involved in immunofluorescence. Future analysis of NS1 mutant protein localisation utilising anti-NS1 antibodies that recognise linear epitopes may help to resolve and validate whether these mutations indeed alter NS1 localisation within cells.

Given the multiple roles of NS1 in the DENV life cycle, we decided to investigate whether these newly identified NS1 secretion-defective mutations would have any impacts on DENV RNA replication and infectious particle production. Firstly, we employed a sub-genomic replicon system to determine if our mutations impacted upon viral RNA replication. Interestingly, the selected V220D and A248V mutations appeared to prevent DENV RNA replication, suggesting that these highly conserved residues are essential to multiple roles of NS1. However, in contrast, both *N*-glycosylation mutants exhibited DENV RNA replication and infectious virus production that were comparable to the wildtype DENV, which is reasonably consistent with previous studies (Crabtree et al 2005; Fan et al 2014).

To investigate whether NS1 secretion is dispensable for roles of NS1 in the DENV replication cycle, we also adapted an established DENV-based trans-complementation system in our studies. Initially, we attempted a double transfection trans-complementation approach, but this appeared to be unsuccessful as the wildtype NS1-HiBiT and positive control NS1-HiBiT KDEL failed to display luciferase activities and kinetics that would be expected for robust DENV replication. This may be attributable to low DNA/RNA transfection efficiencies and a small proportion of cells that were successfully co-transfected with both NS1 DNA expression plasmid and DENV Δ NS1 RNA that are needed for viral replication. To improve the efficiency of NS1 transgene delivery, we utilise a lentiviral-based trans-complementation approach. In contrast to the double transfection approach, the wildtype NS1 and the positive control NS1-HiBiT KDEL expressing cells displayed expected high luciferase activities compared to the controls. However, most of the NS1 mutants appeared to be replication incompetent, which is arguably not surprising given that most of these mutated residues are highly conserved among the DENV serotypes and may be essential for multiple critical roles of NS1 in the DENV life cycle.

Given that the NS1 secretion-impaired mutants V220D and A248V appeared to be replication incompetent, we employed a recently established T7-based replication-independent expression system termed ‘pIRO’ (plasmid-induced replication organelle formation) known to promote biogenesis of VPs in the absence of viral RNA replication (Cerikan et al 2020). Interestingly, heterologously expressed NS1-V220D and NS1-A248V displayed localisation patterns and ER colocalisation profiles that were largely undistinguishable to those of the wildtype NS1, once again suggesting that the observed impairment of NS1 secretion is not directly attributable to the mislocalisation of protein. When heterologously expressed in the context of an NS1-NS5 polyprotein via T7 RNA polymerase, both V220D and A248V mutants remained strongly colocalised with NS4B, indicating that the established NS1-NS4B interaction may not be severely disrupted or compromised. This possibility was taken into consideration, given previous studies have demonstrated that NS1 may have a key role in the stabilisation and rearrangements of membranous viral replication complexes, via its interaction with NS4A and NS4B (Youn et al 2013; Young et al 2013; Scaturro et al 2015; Plaszczyca et al 2019). However, further studies are required to comprehensively determine whether interactions of NS1 with NS4A and NS4B are indeed disrupted by these given mutations.

In summary of this chapter, we have further investigated the impact of these NS1 secretion-impairing mutations on the roles of NS1 in the DENV life cycle. We have shown that majority of these highly conserved mutated residues are located within the β -ladder domain with several mutations found nearby a motif that has recently been identified as important for NS1 secretion (Plaszczyca et al 2019). Initially, we had difficulties in detecting majority of these NS1 mutants by Western blotting using a conformation-specific antibody, suggesting that most of these mutations may disrupt NS1 folding or maturation. However, with the utilisation of an anti-HiBiT peptide tag antibody based on earlier HiBiT luciferase assays.

confirmed the secretion-impairing phenotypes displayed by these NS1 mutants. Of note, we demonstrated that the selected NS1 mutants, V220D and A248V were unable to support DENV RNA replication and infectious virus production. This was consistent with the relatively high conservation of the residues among DENV serotypes. Lastly, we also utilised a T7-derived replication independent expression system to characterise NS1-V220D and NS1-A248V, showing localisation profiles and NS4B colocalisation which were comparable to the wildtype NS1, although the failure to detect these mutant NS1 proteins by Western blotting suggests that they are not appropriately processed and/or folded in this NS1-NS5 polyprotein expression system that has been shown to recapitulates the viral NS protein expression and membrane rearrangements that occur during viral infection.

Chapter 5

**Towards identification of host factors that are associated
with NS1 secretion and glycosylation via an APEX2-
catalysed proximity labelling approach coupled with LC-
MS/MS**

5.1 Emergence of APEX2-based proximity labelling as a powerful in situ approach to map protein microenvironments

Cellular processes are known to be heavily regulated by proteins and their interactions with RNA, DNA, and other proximal proteins (Qin et al 2021). As such, elucidating these biological interaction networks is essential to understanding the majority of biological processes and their impairment has been associated with an array of human diseases including immune disorders and cancers. According to Scott and Pawson (2009), to truly comprehend these underlying biological processes, we require three key parameters; the overall constitution of the given protein network, its organisation within the space and its evolution over time (Lobingier et al 2017; Scott and Pawson 2009). Traditional approaches such as yeast two-hybrid screens and affinity purification-coupled mass spectrometry have been greatly utilised to investigate molecular interactions (Qin et al 2021). In particular, affinity purification has been utilised in tandem with mass spectrometry to greatly enhance interrogation of protein-protein interactions (Lobingier et al 2017; Gavin et al 2006). However, these approaches have their limitations as many such protein interaction assays have organelle specificity restrictions and the inability to elucidate interaction networks while concurrently capturing a snapshot of these interactions as they occur both spatially and temporally (Qin et al 2021; Lobingier et al 2017).

Proximity labelling (PL) was developed as a complementary solution to capture the temporal and spatial snapshot of a protein's interaction networks, while preserving its molecular environment (Lobingier et al 2017; Kim and Roux 2016). PL-based applications utilise engineered enzymes namely biotin ligases (BioID, BioID2, TurboID), horseradish peroxidase (HRP) and the engineered ascorbic acid peroxidase derived from plants (APEX2) which is known for its fast-labelling kinetics (Lobingier et al 2017; Lam et al 2015; Martell et al 2012). By capitalising on its relatively short labelling duration of < 1 minute, APEX-based PL

approaches have successfully been utilized in many interactome studies involving processes such as GPCR signalling, Wnt activation and p38 mitogen-activated protein kinase (MAPK) isoforms in cardiomyocytes (Qin et al 2021; Grainger et al 2019; Paek et al 2017; Dumont et al 2019).

Here, we sought to adapt this recently established APEX2 proximity biotinylation approach combined with mass spectrometry (LC-MS/MS) to capture and generate an interactome map of APEX-tagged DENV-2 NS1 and how its interactions and microenvironments is altered by several mutations that disrupts its *N*-glycosylation (Hung et al 2016).

5.2 How does APEX2-catalysed proximity labelling work?

APEX2 peroxidase catalytically converts a small molecule substrate, biotin phenol into a short-lived radical species that diffuses from the APEX2 active site and covalently tags neighbouring endogenous proteins that are in proximity, preferentially at their surface exposed tyrosine residues or other electron-rich moieties (Martell et al 2012). The APEX2 labelling radius is limited to approximately 20 nm, as these short-lived radicals will react with water molecules or other endogenous radicals leading them to rapidly decay as they slowly move away from the APEX2 active site (Kalocsay 2019). To put it in simple context, the labelling radius of these PL enzymes like APEX2 can be analogously described as a contour map, in which the reactant concentration is at the highest at the PL enzyme active site and gradually decreases nanometer by nanometer away from the source (Hung et al 2016; Qin et al 2021).

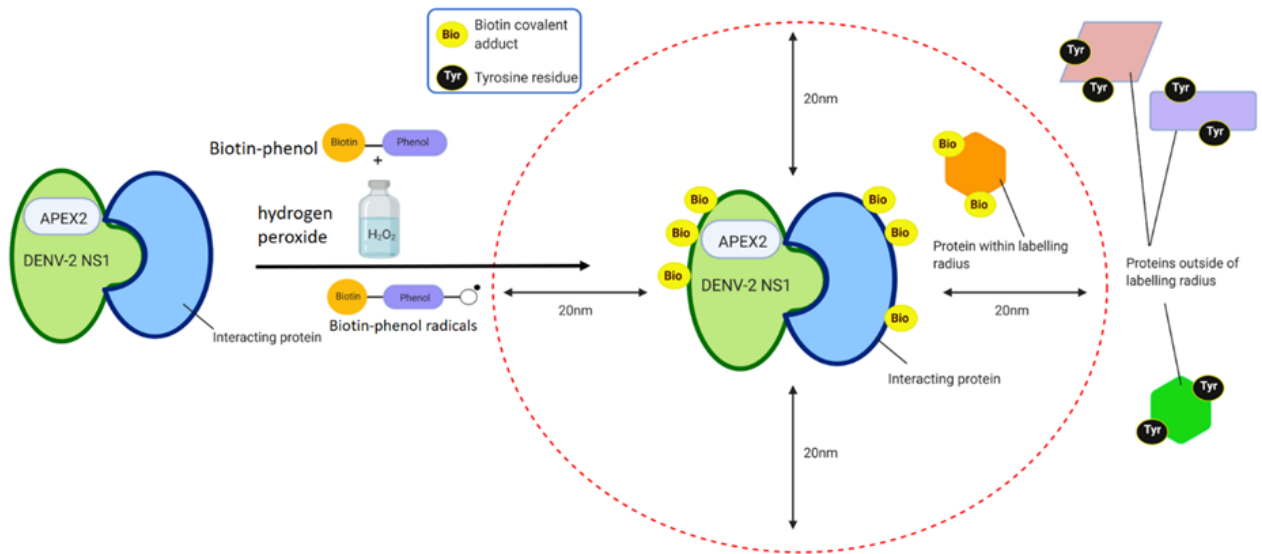


Figure 5.2.1 Diagram illustrating the mechanism of action of the hydrogen peroxide-dependent catalysed proximity labelling approach via the engineered ascorbic acid peroxidase reporter APEX2. Protein of interest “DENV-2 NS1”(light green) is fused with APEX2 (light blue) and transiently or stably expressed in cells using NS polyprotein expression systems or engineered viral genomes. In the presence of hydrogen peroxide (H₂O₂) and biotin-phenol, the APEX2 will proceed to catalyse the oxidation of biotin-phenol substrate, leading to the production of short-lived biotin phenoxyl radicals. These radicals will covalently tag any neighbouring endogenous proteins preferentially on their surface-exposed tyrosine residues (“Tyr”) or electron-rich amino acid moieties by forming biotin covalent adducts (“Bio”)(yellow). The APEX2 labelling is normally limited to a radius of approximately 20 nm from the APEX2. Thus, proteins located outside the described proximity labelling radius will not be covalently tagged, as illustrated above.

5.3 Utilisation of the established pFKDVs-APEX2-NS1 virus construct for the APEX2-catalysed proximity labelling approach

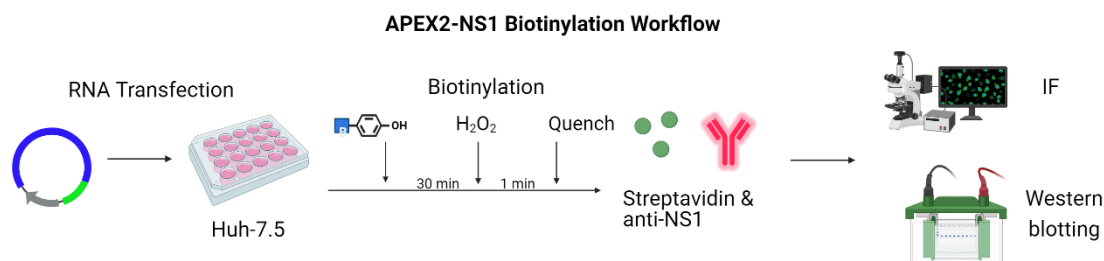


Figure 5.3.1 Schematic diagram of the APEX2-NS1 catalysed biotinylation experimental workflow prior to preparation of biotinylated proteins for mass spectrometry experiments. Generated *in vitro* RNA transcripts from the APEX2-derived constructs were utilised to transfect Huh-7.5 cells. At 7-days post transfection, cells were incubated with biotin phenol for 30 minutes prior to the addition of H₂O₂ for 1 minute to initiate the APEX2-catalysed biotinylation reaction. Media was aspirated and the biotinylation reaction was quenched and cells were washed with quencher solution before proceeding to fixation and fluorescent labelling of NS1 and biotinylated proteins for analysis by microscopy analysis. For Western blotting experiments, cells were lysed and subjected to SDS-PAGE and Western blotting to detect NS1 and biotinylated protein of interest.

To identify novel or known host factors that are associated with DENV NS1 *N*-glycosylation using the APEX2-catalysed proximity labelling approach in tandem with mass spectrometry, we first incorporated the N130A and N207A mutations individually or together into a full length DENV2 construct containing an APEX2-tagged NS1 (pFKDVs-APEX2-NS1) via site-directed mutagenesis (Eyre et al 2017a). The pFKDVs-APEX2-NS1 virus has been successfully utilised in APEX2-based electron microscopy imaging analyses and have been shown to support viral RNA replication and infectious virus production (Eyre et al 2017a). As well as the wildtype APEX2-NS1 virus construct, a self-cleaving APEX2 “2A-APEX2-2A”

construct (2A self-cleaving peptides flanking the APEX2 tag that is located upstream of DENV structural genes) will serve as a control for virus-encoded but non-specific biotinylation activity. In addition, a mutant APEX2-NS1 N130A, mutant APEX2-NS1 N207A and a double mutant APEX2-NS1 N130A N207A (in later experiments) will serve as experimental samples moving forward.

To validate the expression and functionality of these APEX2 constructs, we performed a simple Western blotting experiment to ensure that the biotinylation process is functioning as expected. As described in **Figure 5.3.1**, RNA transcripts derived from the APEX2-NS1 constructs were transfected into Huh-7.5 cells. Following 7-days post-transfection, cells were biotinylated prior to the addition of RIPA lysis buffer before harvesting and subjecting the lysates to SDS-PAGE and Western blotting. A variety of protein bands of different molecular weights were detected using streptavidin throughout the lanes of all APEX2 construct expressing groups, indicating that these constructs supported H₂O₂-dependent biotinylation activity (**Figure 5.3.2**). These biotinylated proteins were most strongly detected between the 25-76 kDa range for the wildtype APEX2-NS1 and both APEX2-NS1 glycosylation mutants while a more sporadic spread of biotinylated proteins was observed for the non-targeted control 2A-APEX2-2A. In parallel, DENV-2 NS1 proteins were also readily detected in the lysates of all of the APEX2-expressing viral constructs by Western blotting. As expected, wildtype APEX2-NS1 displayed a greater apparent molecular weight than untagged NS1 encoded by the 2A-APEX2-2A virus, consistent with the addition of the approximately 28 kDa APEX2 protein to NS1. Also, N130A and N207A APEX2-NS1 proteins displayed a slightly lower apparent molecular weight than wildtype APEX2-NS1, consistent with the absence of the glycans on the mutated asparagine residues 130 and 207.

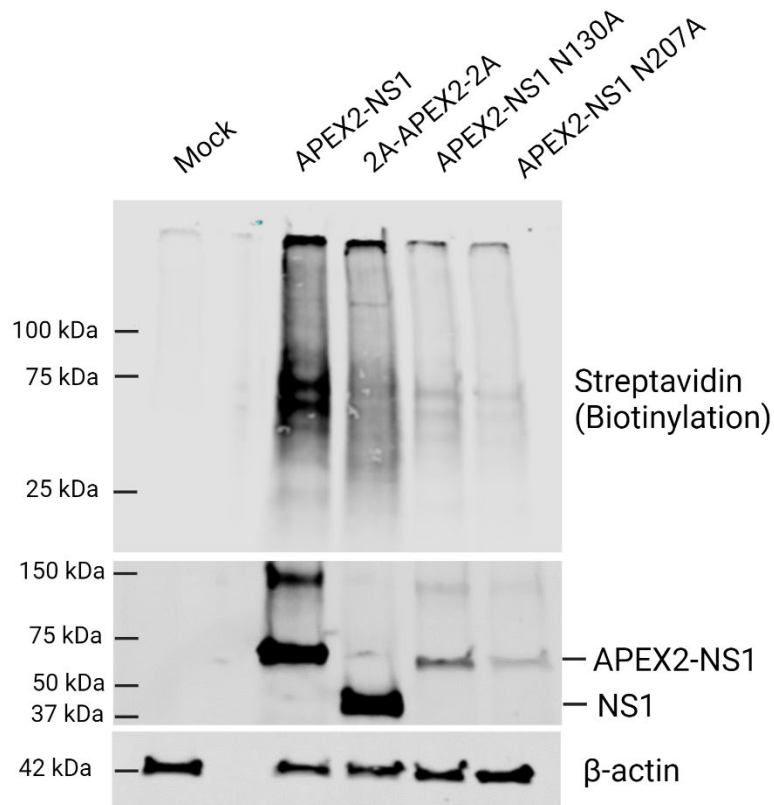


Figure 5.3.2 Characterisation of APEX2-NS1-mediated proximity biotinylation in DENV2 reporter virus-infected cells. Huh-7.5 cells were transfected with RNA transcripts derived from respective FK-DVs viral APEX2 constructs of wildtype APEX2-NS1, 2A-APEX-2A [control for non-specific biotinylation] or APEX2-NS1 glycosylation mutants, N130A and N207A. At 7-days post-transfection, cells were incubated with biotin phenol for 30 minutes prior to the addition of H₂O₂ for 1 minute to initiate the APEX2-catalysed biotinylation reaction. Following the 1-minute incubation with H₂O₂, media was quickly aspirated and the biotinylation reaction was quenched with quencher solution three times before adding the RIPA lysis buffer to lyse cells before harvesting and subjecting the lysates to SDS-PAGE and Western blotting. NS1 and biotinylated proteins were detected using a conformation specific anti-NS1 ‘4G4’ antibody and streptavidin fluorescent conjugate (LI-COR), respectively. β-actin levels were also detected in parallel as a loading control for the experimental samples as shown.

Following these promising preliminary proximity biotinylation results experiments, we then proceeded to perform more comprehensive streptavidin-Western blotting experiments, which also included replicates of each experimental sample omitting either H₂O₂ or biotin phenol substrate to further confirm the specificity of the biotin phenol (BP) and H₂O₂-dependent APEX2 reaction (Hung et al 2016). Similar to the preliminary experiments, biotinylated protein bands of different molecular weight were readily detected in the lysates of the APEX2-NS1 expressing virus infected cells following biotinylation with both H₂O₂ and biotin phenol substrate (**Figure 5.3.3**). No protein bands were observed in the mock-transfected lysate samples as well as those where either the H₂O₂ or biotin phenol substrate were omitted. Intracellular NS1 protein was readily detected in all of the APEX2-based lysate samples including the APEX2-NS1 glycosylation mutants, N130A and N207A.

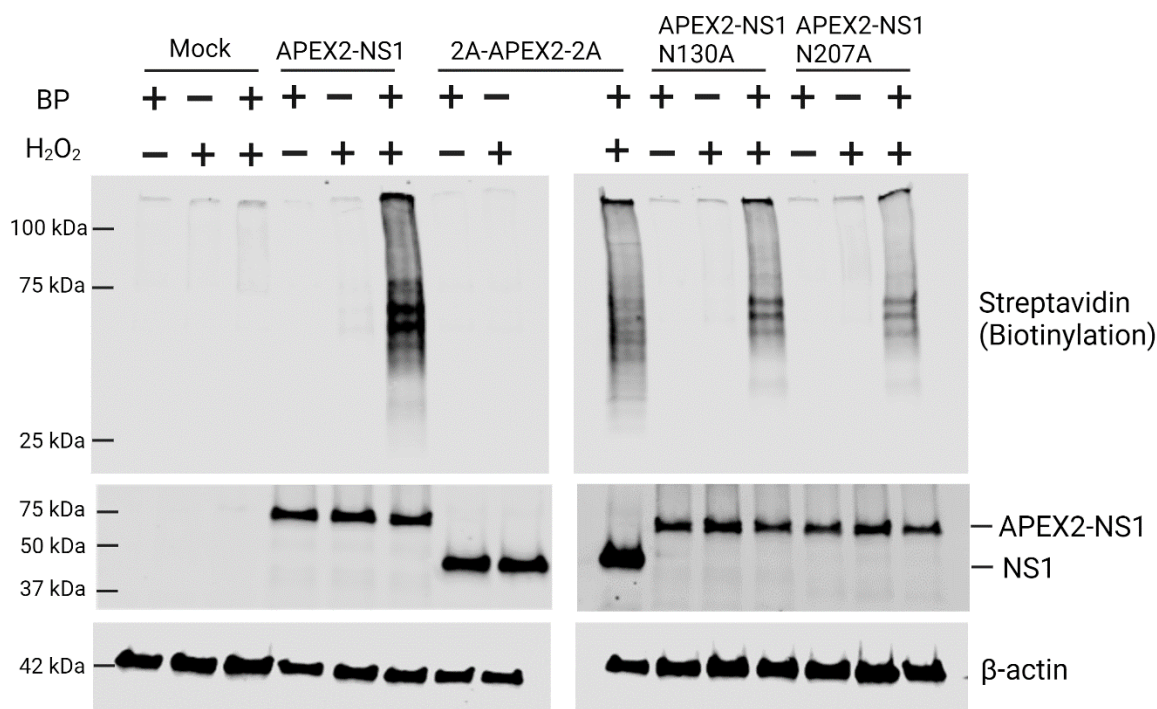


Figure 5.3.3 Characterisation of APEX2 NS1-mediated proximity biotinylation in DENV2 reporter virus-infected cells by streptavidin-Western blotting. Huh-7.5 cells were transfected with in vitro transcribed viral RNA for the respective constructs of wildtype

APEX2-NS1, 2A-APEX-2A [control for non-targeted biotinylation activity] or APEX2-NS1 glycosylation mutants, N130A and N207A. In parallel, samples where the hydrogen peroxide or biotin phenol was omitted were included as negative controls as shown. At 7-days post-transfection, cells were incubated with pre-warmed biotin phenol for 30 minutes before the addition of H₂O₂ for 1 minute to initiate the APEX2-catalysed biotinylation reaction. Following the 1-minute H₂O₂ incubation, media was immediately aspirated and biotinylation reactions were quenched with three quencher solution washes before cell lysis. Harvested lysates were subjected to SDS-PAGE and Western blotting to probe for NS1 and biotinylated proteins using a conformation specific anti-NS1 '4G4' antibody and streptavidin fluorophore conjugate (LI-COR), respectively. β -actin levels were also detected in parallel as a loading control for the experimental samples, as indicated.

Next, we also performed confocal immunofluorescence analysis to validate the APEX2-NS1 viral constructs and the specificity of proximity biotinylation. At 5-days post-transfection of RNA transcripts into Huh-7.5 cells, transfected cells were biotinylated in the presence of H₂O₂ and biotin phenol substrate, before being fixed and fluorescently labelled with anti-NS1 antibody and a streptavidin fluorophore conjugate (Jackson ImmunoResearch). Both APEX2 glycosylation mutants displayed relatively similar biotinylation staining patterns to that of the wildtype APEX2-NS1, although the APEX2 mutant N207A biotinylation staining intensity appeared to be distinctly weaker than that of the wildtype APEX2-NS1 virus and N130A mutant (**Figure 5.3.4**). On the other hand, the positive control 2A-APEX2-2A biotinylation staining pattern was intense and distributed throughout the whole cell, consistent with its expected non-targeted biotinylation activity. Of note, both APEX2-NS1 glycosylation mutants and the 2A-APEX2-2A control that features non-tagged NS1 demonstrated NS1 staining patterns that were deemed indistinguishable to that of the wildtype APEX2-NS1.

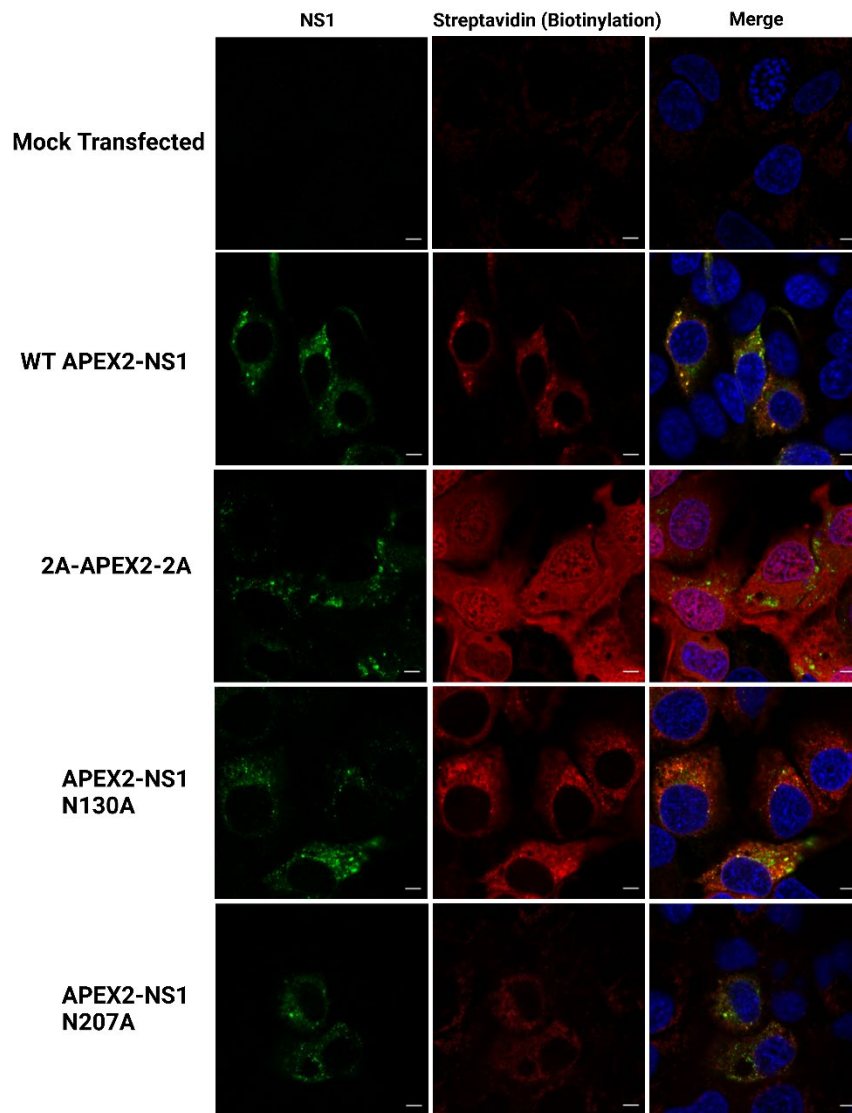


Figure 5.3.4 Analysis of the localisation of NS1 and APEX2 biotinylated proteins within DENV reporter virus-infected cells via confocal microscopy. Huh-7.5 cells were transfected with *in vitro* transcribed RNA transcripts of the respective reporter viruses for wildtype APEX2-NS1, 2A-APEX2-2A [control for non-targeted biotinylation] or APEX2 NS1 glycosylation mutants, N130A and N207A. At 5-days post-transfection, cells were processed for APEX2-mediated proximity biotinylation, before undergoing cell fixation and fluorescently labelled with anti-NS1 ‘4G4’ antibody and a streptavidin fluorescent Cy3-conjugate (Jackson ImmunoResearch Laboratories) to probe for DENV-2 NS1 and biotinylated proteins respectively. NS1 proteins (green, left column), biotinylated proteins (red, second column) and merged images (third column) are as displayed. Scale bars are 5 μm .

Given that our APEX2-derived constructs bearing the NS1 glycosylation mutations (N130A or N207A) were newly generated, we proceeded to determine their viral fitness in comparison to the wildtype APEX2-NS1 virus construct via focus-forming unit assay. Culture supernatants were harvested from RNA-transfected cells at 6 different timepoints (24hr, 48hr, 72hr, 96hr, 120hr, 144hr) and utilised to determine infectivity of viral particles generated within supernatants via focus forming unit assay. Infectivity was only detected at low levels within the first 96hr post-transfection for both APEX2-NS1 glycosylation mutants compared to the wildtype APEX2-NS1 virus for which infectivity was observed at the 72hr timepoint and increase notably at 120hr and 144hr post-transfection (**Figure 5.3.5**). Viral particle production for both APEX2-NS1 glycosylation mutants was approximately 10-fold lower than that of the wildtype APEX2-NS1 virus throughout the time course. Interestingly, 2A-APEX2-2A displayed infectious virus production levels that were markedly higher than that of the corresponding wildtype APEX2-NS1 virus throughout the time course. Given that the viral fitness of the APEX2-NS1 glycosylation mutants appeared to be markedly attenuated in comparison to the wildtype APEX2-NS1, we considered that this attenuated viral fitness would likely affect the subsequent biotinylation experiments and quantitative comparisons between the viral and host factors that are being identified in close proximity to the APEX2-tagged NS1. Thus, we have considered an alternative strategy to manoeuvre around the inherent differences in viral fitness of these given APEX2-NS1 viruses.

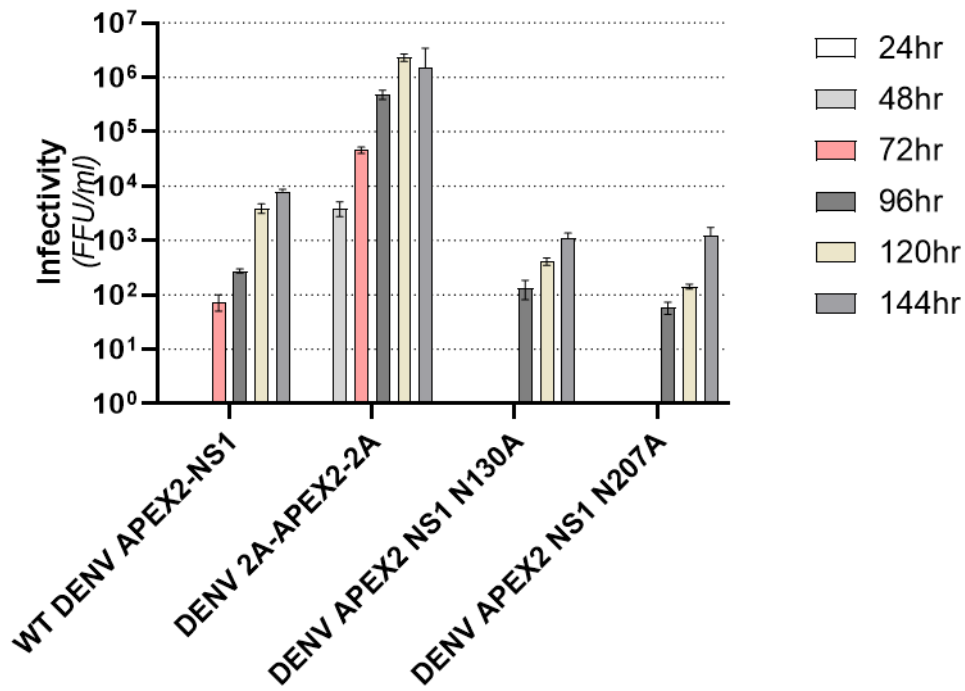


Figure 5.3.5 Viral fitness of both APEX2-NS1 glycosylation mutants, N130A and N207A was markedly attenuated in comparison to the wildtype APEX2-NS1. Seeded Huh-7.5 cells were transiently transfected with *in vitro* transcribed RNA transcripts of wildtype DENV-2 APEX2-NS1, 2A-APEX2-2A or the APEX2-NS1 derivatives bearing *N*-glycosylation mutations (N130A or N207A) as indicated. Culture supernatants were harvested at the indicated timepoints. Infectivity of viral particles within supernatants was determined by focus forming unit (FFU) assay. Data are presented as means \pm SD from three independent replicates.

5.4 Utilisation of a different APEX2-proximity biotinylation strategy involving the pIROD-APEX2-NS1 expression system

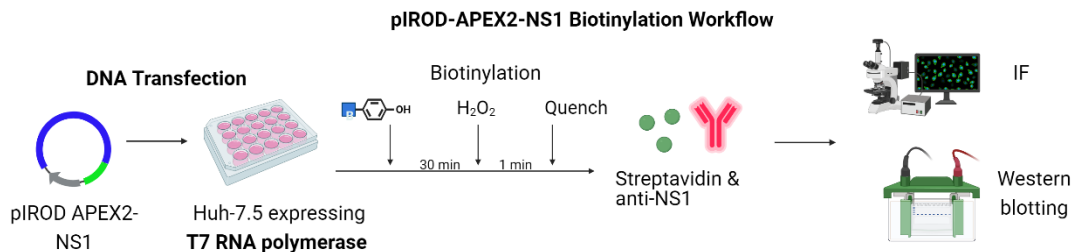


Figure 5.4.1 Schematic illustration of the pIROD-APEX2-NS1 catalysed biotinylation experimental workflow. Wildtype pIROD-APEX2-NS1 and its derivatives pIRO-APEX2-NS1 glycosylation mutants N130A and N207A were transiently transfected into Huh-7.5 cells stably expressing T7 RNA polymerase (Huh-7.5 + T7 RNA pol). At 24-hours post-transfection, transfected cells were processed for APEX2-mediated proximity labelling before either performing immunofluorescence analysis or streptavidin-based Western blotting.

Given that both APEX2-NS1 N130A and N207A mutants displayed attenuated viral fitness in comparison to wildtype APEX2-NS1, we decided to apply the APEX2 biotinylation strategy to the replication-independent NS polyprotein expression system termed pIRO (Cerikan et al 2020). First, we incorporated the wildtype APEX2-NS1, mutants APEX2-NS1 N130A, APEX2-NS1 N207A and double mutant APEX2-NS1 N130A N207A (which was generated at a later stage of the project) into the pIRO expression construct via site-directed mutagenesis. We proceeded to perform immunofluorescence analysis and Western blotting to validate these newly generated pIROD-APEX2-derived expression constructs.

For immunofluorescence analysis, we transfected seeded Huh-7.5 cells + T7 RNA pol cells were transfected with the pIROD-APEX2 constructs before proximity biotinylation at 24-hours post-transfection. Cells were then fixed and fluorescently labelled with anti-NS1 antibody and a streptavidin-fluorophore conjugate (Jackson ImmunoResearch). Confocal immunofluorescence analysis results showed strong NS1 and biotinylation signals for the pIROD-APEX2 glycosylation mutants, N130A and N207A that were comparable to that of the wildtype pIROD-APEX2-NS1 (**Figure 5.4.2**). Subsequent Western blotting studies following proximity biotinylation experiments also revealed comparable biotinylation levels and APEX2-NS1 banding patterns between the wildtype pIROD-APEX2-NS1 and pIROD-APEX2 glycosylation mutants, N130A and N207A (not shown).

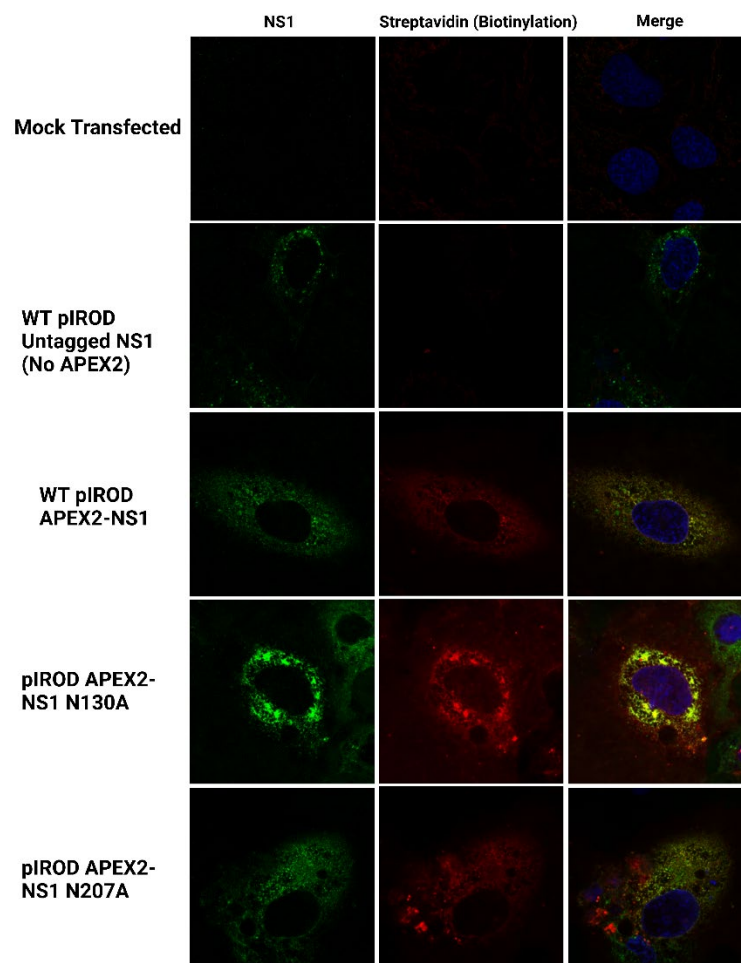


Figure 5.4.2 Characterisation of the pIROD-APEX2-NS1 construct and its derivatives bearing the NS1 *N*-glycosylation mutations via confocal immunofluorescence analysis.

Huh-7.5 cells stably expressing the T7 RNA polymerase (Huh-7.5 + T7 RNA pol) were transfected with plasmid DNA of the wildtype pIROD-APEX2 NS1, wildtype untagged pIROD (No APEX2 tag) or pIRO-APEX2-NS1 derivatives bearing NS1 glycosylation mutations, N130A and N207A, as indicated. At 24-hours post-transfection, cells were biotinylated in the presence of biotin phenol substrate and H₂O₂ before undergoing fixation and fluorescent labelling with anti-NS1 '4G4' antibody and streptavidin Cy3-fluorophore conjugate (Jackson ImmunoResearch Laboratories) to probe for DENV-2 NS1 and biotinylated proteins respectively. NS1 (green, column), biotinylated proteins (red, second column) and merged images (third column) are as displayed. DAPI-stained nuclei (blue) are also depicted in the merged images.

Following successful validation of proximity biotinylation activity displayed by these pIROD-APEX2-NS1 constructs, we proceeded to optimise the experimental approach in terms of transfection efficiency and cell density in a large-scale format towards preparation of samples for LC-MS/MS. A more cost-efficient transfection reagent, PEI linear polyethylenimine (Sigma-Aldrich) was to be employed for these large-scale experiments. We initially transfected Huh-7.5 T7 cells with an eGFP expression construct and cultured overnight before assessing transfection efficiency via fluorescence microscopy. This showed that approximately 40-50% of cells were successfully transfected under these conditions (not shown).

Further optimisation of PEI-mediated DNA transfection was then performed to improve transfection efficiency and minimise cell toxicity. This was performed using the eGFP expression plasmid but also involved testing using the plasmids of the intended proteomics (mock transfected, pcDNA-NES APEX2 [non-targeted biotinylation], wildtype pIROD-APEX2 NS1, pIROD-APEX2 NS1 N130A, pIROD-APEX2 NS1 N207A, double mutant pIROD-APEX2 NS1 N130A N207A). Following this, we proceeded to conduct the APEX2-mediated proximity biotinylation (in triplicates for each group) and harvested the lysates for

pulldown of biotinylated NS1 proximal proteins of interest and analysis via quantitative label-free LC-MS/MS. Unfortunately, these experiments could not be completed within the timeframe of this Ph.D. candidature and other members of the laboratory will process these given samples for streptavidin pulldown and mass spectrometry analysis as initially described.

5.5 Discussion

To better understand the biological functions of a protein of interest, it is important to elucidate the molecular networks or interactions between the target protein and associated proximal proteins within its microenvironment. One of the most common approaches to identify the given protein components of a specific compartment or pathway of interest involves utilising affinity purification strategies in tandem with mass spectrometry (Hung et al 2016; Lobingier et al 2017; Gavin et al 2006). However, this strategy has many limitations ranging from failure to identify transient or weaker protein interactions resulting in false negatives to obtaining false positive interactions due to artifacts of detergent lysis and/or density centrifugation steps involved in sample preparation (Hung et al 2016). As a result of this, proximity labelling approaches have been successfully developed in recent years to provide an alternative avenue to overcome these given experimental challenges.

One of the prominent established proximity labelling methods involves utilising an engineered ascorbic acid peroxidase (APEX2) tag to capture a temporal and spatial snapshot of the molecular proximal environment of a target protein of interest (Martell et al 2012; Hung et al 2014; Hung et al 2016; Lam et al 2015). With its distinctive advantages such as its rapid biotinylation labelling kinetics which occurs within a minute, we seek to capitalise on

this approach to identify novel or known host factors associated with NS1 *N*-glycosylation and glycan-dependent interactions. Initially, we utilised an established full length DENV2 construct containing an APEX2- tagged NS1 that has been successfully applied in APEX2-based electron microscopy imaging analyses and has been shown to support viral RNA replication and infectious virus production (Eyre et al 2017a). We performed proof of concept experiments to validate the expression and biotinylation activity of 5 groups consisting of the mock transfected cells, wildtype APEX2-NS1, a self-cleaving 2A-APEX2-2A construct that serves as a experimental control for non-targeted APEX2 biotinylation and two APEX2-NS1 glycosylation single mutants, N130A and N207A.

Confocal immunofluorescence analyses showed comparable localised proximity biotinylation signals displayed by both wildtype and mutant APEX2-NS1 proteins in infected cells, indicating that the tagging of APEX2 to NS1 as well as the incorporation of these NS1 glycosylation mutations to NS1 did not fully compromise overall biotinylation processes. Additionally, there appeared to be strong colocalisation of NS1 and biotinylated proximal proteins within the cytoplasmic perinuclear vesicles that are thought to predominantly reflect DENV replication complexes (Mackenzie et al 1996; Grief et al 1997; Welsch et al 2009; Acosta et al 2014). This suggests that the incorporation of the APEX2 peroxidase tag as well as the introduction of NS1 glycosylation mutations did not also affect the proteolytic processing of NS1 by viral and host proteases and its localisation to putative replication complexes. On the contrary, biotinylated 2A-APEX2-2A proteins were observed in a diffuse pattern throughout the cytoplasm and nucleus, which is expected to reflect its non-targeted biotinylation activity.

Western blotting analysis following APEX2-proximity biotinylation also revealed distinctive comparable biotinylation levels and intensity between the wildtype APEX2-NS1, and both

APEX2-NS1 N130A and N207A glycosylation mutants. 2A-APEX2-2A also showed comparable biotinylation levels and interestingly, more biotinylated proximal proteins of a range of apparent molecular weights were detected compared to that of the wildtype APEX2-NS1, likely reflecting its non-targeted biotinylation activity and greater replicative fitness. However, we also interestingly discovered that the viral fitness of both APEX2-NS1 glycosylation mutants was markedly attenuated in comparison to the wildtype APEX2-NS1 virus. This was relatively unexpected as we previously showed that the incorporation of both NS1 glycosylation mutations into a full length DENV construct (pFKDVs) and a sub-genomic replicon construct (pFKsgDVs-R2A) displayed infectious particle production and replication kinetics that closely resembled the wildtype NS1. Although it is challenging to pinpoint the exact causation of viral attenuation this mutation induced, it is apparent that wildtype NS1 is less functionally sensitive to these NS1 glycosylation mutations than APEX2-tagged NS1. Further studies are required to determine the exact effects of the APEX2 insertion in NS1 and the described NS1 glycosylation mutations. Nevertheless, we were concerned the distinctly reduced replicative fitness of these APEX2-NS1 *N*-glycosylation mutants would potentially complicate our quantitative analyses of NS1 proximal protein maps following LC-MS/MS analysis.

As we had successfully utilised the replication independent expression system termed pIRO in our recent characterisation of several NS1 mutants in a manner that is independent of the potentially complicating effects of altered viral replicative fitness, we decided to adapt the pIRO expression system in our NS1 APEX2 biotinylation experiments (Cerikan et al 2020). Using this approach, we observed comparable biotinylation levels, intensities, and banding patterns to that of wildtype pIROD-APEX2 NS1 for both NS1 glycosylation mutants in Western blotting experiments. Similarly, immunofluorescence and confocal analysis also revealed similar and expected NS1 localisation and biotinylated protein localisation patterns

between groups. We then proceeded to perform our APEX2 biotinylation experiments in a large-scale format to generate sufficient lysates for pulldown experiments of biotinylated NS1 proximal proteins in preparation for LC-MS/MS analysis. Initially, we encountered substantial cell cytotoxicity events following transfection of Huh-7.5 T7 cells with the wildtype or mutant pIROD-APEX2 NS1 expression constructs as well as with our mock transfected cells. This involved considerate optimisation of pIROD construct plasmid DNA transfection conditions to enable cost-effective, efficient, and non-toxic transfection of viral NS protein expression to maximise the yield, meaningfulness, and relevance of streptavidin-captured biotinylated proteins.

In summary, to identify known or novel host factors associated with NS1 glycosylation activity, we developed an optimised APEX2-catalysed based proximity labelling approach that was to be utilised in tandem with quantitative LC-MS/MS analysis. In this work, we have successfully demonstrated APEX2-dependent biotinylation of NS1 proximal proteins of wildtype and mutant APEX2-NS1 groups via immunofluorescence analysis and Western blotting (Hung et al 2016). Upon discovering that the N130A and N207A mutant APEX2-NS1-expressing viruses were markedly attenuated in comparison to the wildtype APEX2-NS1 virus, we applied APEX2-NS1 biotinylation strategy to the 'pIRO' NS1 protein expression system. With this pIROD-APEX2 NS1 system, we also observed APEX2 biotinylation of NS1 proximal proteins for the wildtype and mutant pIROD APEX2 NS1 groups. However, considerable optimisation of pIRO-D plasmid DNA transfection conditions were required to ensure high transfection efficiency and minimal cytotoxicity. The generated APEX2-biotinylated lysates will be used for pulldown experiments of biotinylated NS1 proximal proteins and analysis by mass spectrometry. Taken together, these studies will hopefully provide novel or known insights into the proteome microenvironment of NS1 and also the given relationship of NS1 *N*-glycosylation.

Chapter 6

General Discussion and Future Directions

Dengue virus (DENV) remains one of the most rapidly spreading arthropod viral diseases worldwide, with the incidence of dengue infections increasing approximately 30-fold within the past 50 years due to massive population growth, rapid urbanisation, and recent unprecedented global warming (WHO 2020; Wilder-Smith et al 2010; WHO 2009; Gubler 2002). DENV is transmitted by female *Aedes* mosquitoes predominantly of the *Aedes aegypti* and *Aedes albopictus* species and is responsible for the highest disease burden among all flaviviruses, affecting more than 380-400 million people and responsible for approximately 25,000 deaths annually (Guzman and Harris 2015; Bhatt et al 2013). Given that approximately 40% of the current world population mainly resides in sub-tropical and tropical areas, it is also predicted that increasing global temperatures due to climate changes will amplify the spread of Dengue *Aedes* vectors to non-tropical areas of continental Europe and North America (Murray et al 2013; Rocklov and Tozan 2019). To date, there are no specific antiviral therapies that have been approved for treatment of DENV infection. Furthermore, the only approved dengue vaccines on the market, Dengvaxia® and TAK-003 are currently associated with considerable safety concerns regarding their applicability and administration due to their potential contribution towards antibody-dependent enhancement (ADE) of subsequent DENV infections (Wichmann et al 2017; Flasche et al 2016; WHO 2016; Osorio et al 2014). In this context, administration of Dengvaxia® is only recommended to only individuals that are 9-45 years of age and most importantly have at least one prior history of dengue infection (WHO 2020). Accordingly, there remains an urgent need for the development of novel and effective antiviral strategies in the form of treatments and vaccines.

One of the 10 proteins of DENV, NS1 is a 48-kDa non-structural glycoprotein that predominantly exists as a membrane associated dimeric species (mNS1) or a secreted hexameric NS1 lipoparticle (sNS1) (Muller and Young 2013; Mason 1989; Winkler et al

1988; Brandt et al 1970). mNS1 is important in viral RNA replication while sNS1 is strongly linked with DENV disease pathogenesis of severe DENV infections (Mackenzie et al 1996; Lindenbach and Rice 1997; Young et al 2000; Libraty et al 2002). Since its discovery in the serum of DENV-infected patients, sNS1 has been strongly implicated in an array of extracellular functions, which includes inducing a cytokine storm leading to vascular leakage through the activation of TLR-4, elicitation of auto-antibodies leading to endothelial dysfunction and also the degradation of the endothelial glycocalyx-like layer (EGL) known to regulate endothelial barrier function leading to disruption of its integrity (Puerta-Guardo et al 2016 ;Beatty et al 2015; Modhiran et al 2015; Yin et al 2013; Falconar 2007; Young et al 2000; Falconar 1997). Despite many studies that demonstrate the impact of NS1 secretion on DENV disease pathogenesis, the underlying molecular determinants associated with aspects of NS1 secretion remained poorly characterised. Thus, this project aimed to enhance our understanding of the key residues or motifs within the DENV NS1 protein that influence NS1 secretion activity. It also aimed to develop a proximity biotinylation approach to identify NS1 proximal proteins in the context of viral non-structural protein expression and typical DENV-induced membrane rearrangements as well as the impact of mutational disruption of NS1 *N*-glycosylation on these NS1-proximal proteins. From these studies, it was hypothesised that an improved understanding of the viral and host determinants of NS1 secretion and *N*-glycosylation may reveal targets of antiviral therapies and attenuated vaccine design.

As detailed in Chapter 3, we proceeded to utilise a combination of high throughput mutagenesis and a sensitive luminescent peptide tag assay to successfully identified several NS1 residues that are essential for its secretion (Tan et al 2023). While this approach enabled the identification of NS1 secretion impairing mutants, we were unable to fully optimise the desired PCR-based mutagenesis rates and, as a result, the vast majority of clones contained

more than one single coding point mutations. Accordingly, we focussed our attention on selecting those clones bearing single coding point mutation that resulted in >50% decrease in NS1 secretion efficiency for subsequent studies. Conversely, we also missed the opportunity to sequence those NS1 clones that displayed a near-normal NS1 secretion phenotype, which may have been informative to discern those residues or specific domains that are potentially not essential for NS1 secretion. Arguably, as we did not sequence those NS1 clones displaying moderate impairment in NS1 secretion efficiency between 35-50% (not shown), additional single substitution mutants that reasonably influence the efficiency of NS1 secretion may have been regrettably overlooked. A more refined and comprehensive mutagenesis approach such as site-saturation mutagenesis (SSM) (Li et al 2018; Wells et al 1985) and a more robust automated approach for screening individual mutants would be required to generate a comprehensive map of mutations that alter NS1 secretion.

From our *in silico* analyses, it was apparent that the majority of these identified NS1 secretion impairing mutations were distinctly mapped to the β -ladder domain which suggest its importance in NS1 secretion (Tan et al 2023). Additionally, based on the multiple sequence alignment of DENV NS1 proteins, several of these mutations corresponded to residues within the β -ladder domain that are highly conserved among the DENV serotypes, indicating their relative importance. Accordingly, a site-directed mutagenesis approach solely focusing on the β -ladder domain itself could potentially help to elucidate the overall network or processes involving the NS1 secretory pathway. By doing so, we could also identify molecular features of this domain that not only influence NS1 secretion but also underlying properties of NS1 folding or maturation that are essential to this and other 'functions' of NS1. As discussed earlier in Chapter 4, we identified Arg-336 as a key determinant of NS1 secretion as the mutation (R336S) impaired NS1 secretion efficiency, corroborated with earlier findings by Plaszczyca et al 2019. Also, Arg-336 has also been described to be essential for viral RNA

replication, highly suggesting that this specific residue is important for multiple functions of NS1 (Scaturro et al 2015).

Also, there were no mutations mapped to the β -roll domain which we hypothesised to be important to NS1 secretion given it is possible that the β -roll domain might not be strongly represented in our relatively small library of mutant, so a larger cohort is needed to fully validate its importance in NS1 secretion activity. Given that the β -roll domain encompasses only 29 residues, there is a higher possibility that these residues are less frequently selected to be mutagenized by the error prone DNA polymerase in comparison to the relatively larger Wing domain and the β -ladder domain. It has also been suggested that the hydrophobic face of the NS1 dimer that is comprised of the β -roll and 'greasy finger' sub-connector domain that mediates its association with the luminal surface of the ER membrane and interacts with other DENV proteins (Plaszczyca et al 2019; Scaturro et al 2015; Akey et al 2014; Youn et al 2013). Accordingly, residues within the β -roll domain might be particularly sensitive to mutation given their potential to alter membrane and lipid cargo association and dimer formation/stability.

Interestingly, several NS1 mutant proteins were difficult to detect by Western blotting using a conformation specific anti-NS1 4G4 antibody. Given these NS1 mutant proteins were readily detected by immunofluorescence using the 4G4 antibody, we hypothesised that these mutant proteins may be much more structurally sensitive than wildtype NS1 to the sample processing steps such as lysis in strong detergents and boiling prior to Western blotting, as compared to the less destructive steps involved in immunofluorescent labelling. However, follow-up studies using an anti-HiBiT peptide tag antibody successfully detected all mutant proteins and validated the secretion-impaired phenotypes of these identified mutants. Thus, future studies involving utilisation of techniques such as native PAGE instead of SDS-PAGE and Western

blotting using a range of different anti-NS1 antibodies (polyclonal or monoclonal) against conformational and linear epitopes could help to elucidate whether the secretion-impaired phenotype of these mutant proteins may be attributable entirely to folding and/or maturation defects. Specifically, as the separation of proteins on native PAGE is based on their size, charge and shape in contrast to SDS-PAGE which relies on the mass of the protein, this could help to determine if these mutant proteins are structurally compromised as a result of their respective point mutations (Arndt et al 2012).

Follow-up characterisation studies involving confocal immunofluorescence analyses of these NS1 secretion impairing mutations also demonstrated no apparent changes in the subcellular localisation of NS1 protein or its colocalisation with the ER (Tan et al 2023). Further colocalisation analysis with other DENV non-structural proteins would be valuable to determine if there are any further distinctive impacts of these mutations on other NS1 interactions. Also, given that *N*-glycosylation of NS1 has been shown to be important in many NS1 functions in the DENV life cycle and associated pathogenesis, it would be interesting to investigate whether *N*-glycosylation and glycan trimming is compromised by these NS1 secretion impairing mutations. This could be investigated by experiments involving PNGase F and N-glycosidase treatment of supernatant protein samples prior to Western blotting experiments and analysis of changes in the apparent molecular weight between wildtype and mutant NS1 proteins due to deglycosylation (Wang and Voglmeir 2014; Norris et al 1994). However, prior to acquisition of the anti-HiBiT antibody, we were unable to probe the given *N*-glycosylation status of these mutant proteins due to the inability to detect several of these mutant proteins by Western blotting using the anti-NS1 4G4 antibody.

Next, we investigated the impact of these NS1 secretion impairing mutations on the roles of NS1 in the DENV life cycle (Tan et al 2023). We selected the two NS1 mutants with the

greatest effects on NS1 secretion, V220D and A248V, from our NS1 mutant panel and for comparison, also investigated two *N*-glycosylation mutants, N130A and N207A, to assess their influences on viral RNA replication and infectious virus production. By incorporating these mutations individually into full-length or sub-genomic DENV constructs, we discovered that both V220D and A248V mutants prevented RNA replication and infectious virus production. In contrast, both *N*-glycosylation mutants displayed virus particle production levels and replication kinetics that were comparable to that of the wildtype virus, which is largely consistent with previous related studies (Crabtree et al 2005; Fan et al 2014). Follow-up investigation on these selected NS1 mutants utilising a T7-based replication independent NS polyprotein expression system revealed no apparent changes to the NS1 localisation profiles and colocalisation with the ER and NS4B protein (Cerikan et al 2020). Due to unforeseen challenges in cloning and time constraints, the remaining 8 NS1 secretion impairing mutations in our panel were not further investigated for their impacts on roles of NS1 in viral RNA replication and infectious virus production. Although it is tempting to speculate that majority of these mutations would not support RNA replication and infectious virus production given their relatively high conservation among DENV serotypes and their apparent impact via detection using a conformation specific antibody, it would be ideal to validate their potential impacts in future studies.

Given successful establishment of the workflow which involves employing random point mutagenesis and luciferase reporter-based assays to identify NS1 secretion impairing mutations at a small-scale level, we could potentially proceed to conduct even larger scale experiments to identify mutations that would lead to an impairment in NS1 secretion. Furthermore, as with the generation of the library of NS1-HiBiT point mutants was conducted using a lentiviral expression vector, this library could be pooled and packaged into lentiviral vectors to transduce cells *en masse*. Following antibiotic selection and single cell sorting,

intracellular and extracellular NS1 level of the respective cell lines could then be assessed for their NS1 secretion efficiency based on extracellular-to-intracellular NS1 luminescence ratios. For those clones displaying a significant decrease in their NS1 secretion efficiency, Sanger sequencing could then be utilised to identify the mutation(s) associated with this given phenotype. Those mutations could then be incorporated into the established infectious DENV-2 clone to evaluate their influences on NS1 secretion, RNA replication, infectious virus production and NS1 localisation profiles performed in the present study. Alternatively, a more targeted approach based on our understanding of the critical features and the domains of the NS1 crystal structure and their relative conservation across all DENV serotypes could be performed before subjecting these selected residues to alanine scanning mutagenesis and functional analysis to identify residues that might be essential for NS1 secretion (Plaszczyca et al 2019; Scaturro et al 2015).

Concurrently, we also developed tools and experimental pipelines involving an APEX2-based proximity biotinylation labelling method coupled with quantitative LC-MS/MS approach towards identification of novel or currently known host factors associated with NS1 *N*-glycosylation, given its importance in various NS1 functions throughout the DENV life cycle (Hafirassou et al 2017; Hung et al 2016; Fan et al 2014). We have successfully validated the APEX2-biotinylation of NS1 proximal protein for our wildtype APEX2-NS1, and two of our APEX2-NS1 glycosylation mutants of interest, N130A and N207A via immunofluorescence and Western blotting analysis. Confocal immunofluorescence demonstrated strong colocalisation of NS1 and biotinylated NS1 proximal proteins in juxtannuclear foci where the formation of replication complex is proposed to occur. Subsequent Western blotting experiments showed comparable biotinylation levels and banding patterns between the wildtype and mutants, indicating the incorporation of these *N*-glycosylation mutations did not compromise APEX2 biotinylation activity. However, these mutations markedly attenuated the

viral fitness of both APEX2 NS1 glycosylation mutants which complicated the intended downstream proteomics experiments involving these infectious virus constructs. Accordingly, we pivoted to utilise the pIRO expression system for our APEX2-NS1 biotinylation experiments. As expected, wildtype and mutant pIROD-APEX2-NS1 constructs displayed strong and similar biotinylation activity supporting the employment of these constructs for downstream proteomics experiments. Furthermore, substantial efforts were made to optimise efficient and non-toxic large scale transfections conditions to enable streptavidin-mediated purification of large amounts of the APEX2-NS1 proximity biotinylated proteins for quantitative analysis by LC-MS/MS. These large-scale biotinylated protein lysates have been prepared for streptavidin-mediated pulldowns and label free quantitative proteomics analysis by other laboratory members and proteomics facility collaborators. It is expected that these future studies will identify known and novel NS1-interacting proteins for wildtype APEX2-NS1 samples and, through comparison to *N*-glycosylation APEX2-NS1 mutants, changes to the host factor microenvironment of NS1 proteins potentially associated with NS1 glycosylation and glycan trimming such as the OST complex, which has been identified as a critical host factor complex that interacts with NS1 (Hafirassou et al 2017) and novel host factor interactions of NS1 that are dependent on its correct glycosylation. Given that there are two known OST complexes in mammalian cells, we proposed that the catalytic subunits (STT3A and STT3B) and encompassing subunits of the complexes (RPN1, RPN2, DDOST DAD1) could be detected and identified as host factors associated with NS1 *N*-glycosylation (Hafirassou et al 2017; Cherepanova et al 2016). Also, there is a possibility that two important subunits of STT3B of the OST complex, TUSC3 and MagT1 could be potentially identified in this study as the loss of both subunits have been associated with inactivity of the OST complex and alterations of ER homeostasis (Cherepanova et al 2016; Horak et al 2014). As OST complex-mediated *N*-glycosylation has been demonstrated to be essential for DENV replication, there is also a possibility that we could identified several host factors associated

with NS1 *N*-glycosylation and OST complex, independent of DENV replication in the context of the replication-independent pIRO expression system (Marceau et al 2016).

In summary of this overall study, random mutagenesis and luciferase reporter-based assay approaches were successfully employed to elucidate and identify the residues within DENV NS1 that are essential for its secretion. By utilising these approaches, we have identified 10 single point mutations demonstrating a NS1 secretion-impairing phenotype, with the majority of these mutations mapping to the β -ladder domain. We have also demonstrated that these mutations did not appear to compromise NS1 localisation profiles and NS1 colocalisation with the ER but may impact upon correct NS1 folding and/or maturation. Follow-up studies utilising established DENV reporter virus genome constructs showed that two mutants of interest, V220D and A248V prevented RNA replication and infectious virus production. In another subsequent related aim involving identification of host factors associated with NS1 *N*-glycosylation activity utilising APEX2 proximity biotinylation labelling approach, we have successfully validated the biotinylation of NS1 proximal proteins in wildtype and NS1 glycosylation mutant pIROD APEX2 NS1 groups of interest. Despite the need to conclude experimental work in the interest of time, we have optimised and employed an experimental workflow for large scale pulldowns of biotinylated NS1 proximal proteins for upcoming proteomics analyses. Taken together, this project has identified and characterised residues within NS1 that are essential for its secretion and developed a powerful approach to identify novel NS1-associated proteins, including those that are related to its *N*-glycosylation. We hope that this will pave the way for future studies to elucidate viral and host factor determinants of DENV NS1 secretion that may be targeted in future novel antiviral strategies.

Appendices

Appendix I: Buffers, Media and Solutions

1X Phosphate Buffered Saline (PBS)

1M Sodium Ascorbate solution

1M Sodium Azide solution (Toxic!!)

1M Tris (pH 8)

10% SDS

10X Tris-Glycine SDS (TGS) Running Buffer

100X Streptomycin-Penicillin

20% D-Glucose Solution

80% Glycerol Solution

20X Phosphate Buffered Saline (PBS)

20X Tris Acetate EDTA Buffer

4M Sodium Chloride

62.5mM Tris-HCL (pH6.7)

Acetone-Methanol fixative solution

Agar Plates supplemented with Ampicillin Sodium Salt

Ampicillin at various concentrations (100mg/mL)

Biotin phenol solution

Dulbecco's Phosphate Buffered Saline (DPBS)

Dimethyl sulfoxide (DMSO)

Foetal Calf Serum (FCS)

Hydrogen Peroxide solution

MilliQ water (Autoclaved)

Kanamycin (12.5mg/mL)

LB Lennox Media with agarose

LB Lennox Media (100mL, 250mL, 500mL)

Super Optimal Broth (SOB) (10mL, 20mL)

Trolox solution

Trypan Blue

Trypsin-EDTA

Agarose Gel Electrophoresis Reagents and Solutions

1kb DNA ladder (New England BioLabs) (500 μ L)	100 μ L of 1Kb ladder 83 μ L of 6X loading dye (no SDS) 317 μ L of nuclease-free H ₂ O
Gel Loading Dye (6X), Blue/Purple (New England Biolabs)	2.5% Ficoll® -40010 mM EDTA 3.3 mM Tris-HCl (pH 8.0 at 25°C) 0.08% SDS 0.02% Dye 1 (pink/red) 0.0008% Dye 2 (blue) for Purple / 0.015% bromophenol blue for Blue

Tris-Acetate-EDTA (TAE)	40 mM Tris (pH 7.6) 20 mM acetic acid, 500mM EDTA (pH 8.0)
1% Agarose gel	1g of pure Agarose powder 100 mL of 1X TAE buffer

Cloning and Transformation

LB agar plates + Ampicillin (pre-made)	Ampicillin sodium salt in LB Lennox Broth 1.5% agar (w/v)
Ampicillin plates	250 mL of LB Lennox Media with agarose 25mg/mL of Ampicillin
LB Lennox Media	1% bacto-tryptone 0.5% bacto-yeast extract 10mM of 0.5% sodium chloride
Super Optimal Broth with Catabolite Repression (SOC) Media	0.5% bacto-yeast extract 2% tryptone 10 mM NaCl 2.5 mM KCl 10mM magnesium chloride 10 mM MgSO ₄ 20 mM D-Glucose (100 μ L of 20% D-Glucose per 10 mL)

Cell Culture Buffers and Solutions

1% Bovine Serum Albumin (BSA) Solution	1g of BSA 100 mL of 1X PBS
5% Bovine Serum Albumin (BSA) Solution	5g of BSA 100 mL of 1X PBS

Acetone: Methanol Fixative solution (10 mL)	5 mL of 100% Methanol 5 mL of 100 % Acetone
NP-40 Lysis Buffer (40 mL)	1M Tris-HCl (pH8) (2 mL of 1M Tris) 150mM of NaCl (1.5 mL of 4M NaCl) 0.4 mL of 1% NP-40 36.1 mL of MilliQ water (1: 100) Protease Inhibitor Cocktail (400 μ L in 40 mL)
30 % Hydrogen peroxide	10 μ L 30% H ₂ O ₂ + 990 μ L DPBS
Quencher Solution	1M Sodium Ascorbate 500mM Trolox 1M Sodium Azide DPBS
RIPA Lysis Buffer (25 mL)	1M Tris-HCL (1mL of 1M Tris) 4M NaCl (0.9375 mL of 4M NaCl) 10% SDS (0.25 mL of 10% SDS) Sodium Deoxycholate (0.125g) Triton X-100 (0.25 mL) 22.4 mL of MilliQ H ₂ O (1:100) Protease Inhibitor Cocktail (250 μ L in 25 mL)
Trypsin-EDTA	0.25% Trypsin (w/v) 0.02% EDTA (w/v)

General Buffers and Solutions

Phosphate Buffered Saline (PBS)	2.97 mM Na ₂ HPO ₄ -7H ₂ O (pH 7.4) 1.06 mM KH ₂ PO ₄ 155.17 mM NaCl,
Tris-Buffered Saline (TBS) (10X)	24g Tris-Base 88g NaCl 1 mL of MilliQ H ₂ O (pH 7.6)
Tris-EDTA (TE) Buffer	1 mM EDTA 10 mM Tris (pH 7.5)

Western Blot Buffers and Solutions

Running Buffer (TGS) (10X)	30.2g Tris 144.2g Glycine 100 mL 10% SDS 900 mL MilliQ H ₂ O (pH 8.8)
SDS PAGE 4X Non-Reducing Buffer	10% SDS 80% glycerol 250mM Tris HCl 0.5% bromophenol blue dye (pH6.8)
SDS PAGE 4X Reducing Buffer	10% SDS, 500mM dithiothreitol (DTT) 80% glycerol 250mM Tris-HCl 0.5% bromophenol blue dye (pH6.8)
Stripping Buffer	2% SDS 62.5mM Tris-HCl (pH6.7) 100mM 2-mercaptoethanol
Transfer Buffer (1L)	3.03 g of 25mM Tris, 14.4 g of 192mM Glycine 200 mL of 100% Methanol 800 mL of MilliQ water
Wash Buffer (TBS-T) (1L)	1 mL of 0.1% Tween 20, 1L of 1X TBS
5% Skim Milk	5g of instant skim milk powder 100 mL of TBS-T

Appendix II: Primers

Primers for cloning of the HiBiT tag into the pLenti6 expression construct

Primer Name	Oligonucleotide sequences (5' to 3')
HiBiT TOP FWD	CTCGAGGGATCAGTGAGCGGCTGGCGGCTGTTCAAGAAGATTAGCTAGA
HiBiT BOT REV	CGCGTCTAGCTAATCTTCTTGAACAGCCGCCAGCCGCTCACTGATCCC

Primers for PCR-based random point mutagenesis (Agilent) application of DENV-2 NS1 via Gibson Assembly

Primer Name	Oligonucleotide sequences (5' to 3')
pLenti6 NS1 FWD	TAGAAGACACCGACTCTAGACCACCATGAGCACCTCACTGTCTGTG
pLenti6 NS1 REV	GCCAGCCGCTCACTGATCCCCCAGCTGTGACCAAGGAGTTG

Primers for incorporation of the Δ NS1 into the pFKDVs-R2A or pFK sgDVs-R2A via Gibson Assembly. Also, primers to include the 'GND' mutation (negative control) into the DENV NS5 gene sequence within pFKDVs-R2A- Δ NS1 and pFKsgDVs-R2A- Δ NS1 via Gibson Assembly

Primer Name	Oligonucleotide sequences (5' to 3')
pFKsgDVs dNS1 FWD	GGA ATC CGC TCA GTA ACG CGT CTG GAG AAT CTG ATG TGG A
pFKsgDVs dNS1 REV	GTC ATC CGT CAT AGT GGC GCC TAC CAT AAC CAT CAC TCT TCC
pFK dNS1GND FWD	CTT AGA GTT TGA AGC CCT AGG ATT CTT AAA TGA AGA TCA CTG GT
pFK dNS1GND REV	ACT AAA GGG ACT AGT TCT AGA ACC TGT TGA TTC AAC AGC A

Primers for site-directed mutagenesis of E139K, V220D, A248V, N130A or N207A point mutations into pFKDVs, pFKDVs-R2A, pFKsgDVs-R2A and pIRO-D

Primer Name	Oligonucleotide sequences (5' to 3')
<i>MluI</i> ext FWD	TTT GTG GAA TCC GCT CAG TA ACGCGT CT
<i>KasI</i> ext REV	CCT ATG TCA TCC GTC ATA GT GGCGCC TAC CAT AAC C
pIRO-D SDM FWD (<i>MluI</i>)	GGA ATC CGC TCA GTA ACGCGT CTG GAG AAT CTGA TGT GGA
pIRO-D SDM REV (<i>XhoI</i>)	CCT CAC CCA TCT CCA CTCGAG TTG AGA TGT ATC CTC TAG CT
NS1 N130A FWD	GCTCTCTACAGAGTCTCAT GCCC CAGACCTTTCTCATTGATGGCCC
NS1 N130A REV	CCATCAATGAGAAAGGCTGG GC CATGAGACTCTGTAGAGAGCAT
NS1 E139K FWD	CAGACCTTTCTCATTGATGGCCCC AAA ACAGCAGAATGCCCAACACAAA
NS1 E139K REV	TTGTGTTGGGGCATTCTGCTGTTT T GGGGCCATCAATGAGAA
NS1 S152L FWD	AACACAAATAGAGCTTGGAATTTGTTGGAAGTTGAAGACTATGG
NS1 S152L REV	ATAGTCTTCAACTTCCAACAAATTCCAAGCTCTATTTGTGTT
NS1 N207A FWD	TGGATAGAAAGTGCACT CGCT GACACATGGAAGATAGAGAAAGCCTC
NS1 N207A REV	TCTCTATCTCCATGTGTC AGCG GAGTGCACTTTCTATCCAATAACC

NS1 V220D FWD	AAAGCCTCTTTCATTGAAGAATAAAAACTGCCACTGGCCAA
NS1 V220D REV	TGGCCAGTGGCAGTTTTTATCTTCAATGAAAGAGGCTTTCT
NS1 A248V FWD	ATAATTCCAAAGAATCTCGTTGGACCAGTGTCTCAACACAACATA
NS1 A248V REV	GTGTTGAGACACTGGTCCAACGAGATTCTTTGGAATTATCATCT

Primers for Sanger sequencing of expression constructs

Primer Name	Oligonucleotide sequences (5' to 3')
CMVseq FP	CGC AAA TGG GCG GTA GGC GTG
pLenti6seq RP	CAA ACT CAT TAC TAA CCG GTA C
pFKDVs seq FWD	ATA GGA ATG AAT TCA CGC AG
pFKDVs seq REV	GTA GGG CAA GAT AAG TCA CG
pFKDVsGND seq FP	CCT ATG GAC TCA ATA CTT TC
pFKDVsGNDseq REV	GTC TTT CAT GAT TAA CTC ATG
APEX2 seq FP	ATT CAC CAC CAA TAT ATG GC
APEX2 seq RP	CCG CTG ACA TGA GTT TTG AG
sgDVs seq FP	CGT TGT GAG CTG GAA AAA CA
sgDVs seq RP	GGC TGC TAG TAG GGC AAG ATA
pIRO-D FP seq	GGA CAG AAC AAT ACA AGT TC
pIRO-D RP seq	CTA CCA TAA CCA TGA CTC TTC

Appendix III: Antibodies and Dyes

1° antibodies

Antibody	Specificity	Dilution factor	Incubation	Manufacturer
Mouse monoclonal IgG1 (4G4) hybridoma supernatant	flavivirus NS1	1:10 (WB) 1:5 (IF)	4°C overnight	Mozzy Mabs, Queensland MMABS 4G4
Mouse anti β -actin (8H10D10)	Mouse β -actin	1:1000 (WB)	4°C overnight	Cell Signalling Technology (#3700)
Rabbit anti β -actin (13E5)	Rabbit β -actin	1:1000 (WB)	4°C overnight	Cell Signalling Technology (#4970)
Mouse anti-capsid monoclonal antibody (6F3.1)	Mouse anti-capsid	1:5 (IF)	4°C overnight	Prof John Aaskov (QUT, Brisbane, Australia)
Mouse IgG2a anti-NS1 (GT4212)	DENV NS1	1:1000 (WB)	4°C overnight	GeneTex (GTX630556)
Mouse anti β -actin (AC-15)	Mouse β -actin	1: 10 000 (WB)	4°C overnight	Sigma-Aldrich (A1978-200UL)
Mouse IgG1 anti-NS3 (GT2811)	DENV NS3	1: 1000 (WB)	4°C overnight	GeneTex (GTX629477)
Mouse IgG anti-NS4B	DENV NS4B	1: 200 (IF)	4°C overnight	GeneTex (GTX124250)
DENV-2 NS1 Polyclonal Antibody	Rabbit DENV-2 NS1	1: 2000 (WB)	4°C overnight	Thermo Fisher (PA5-32207)
Mouse anti-HiBiT mAb Clone (30E5)	HiBiT tag	1:1000 (WB)	4°C overnight	Promega (Early Access)

2° antibodies

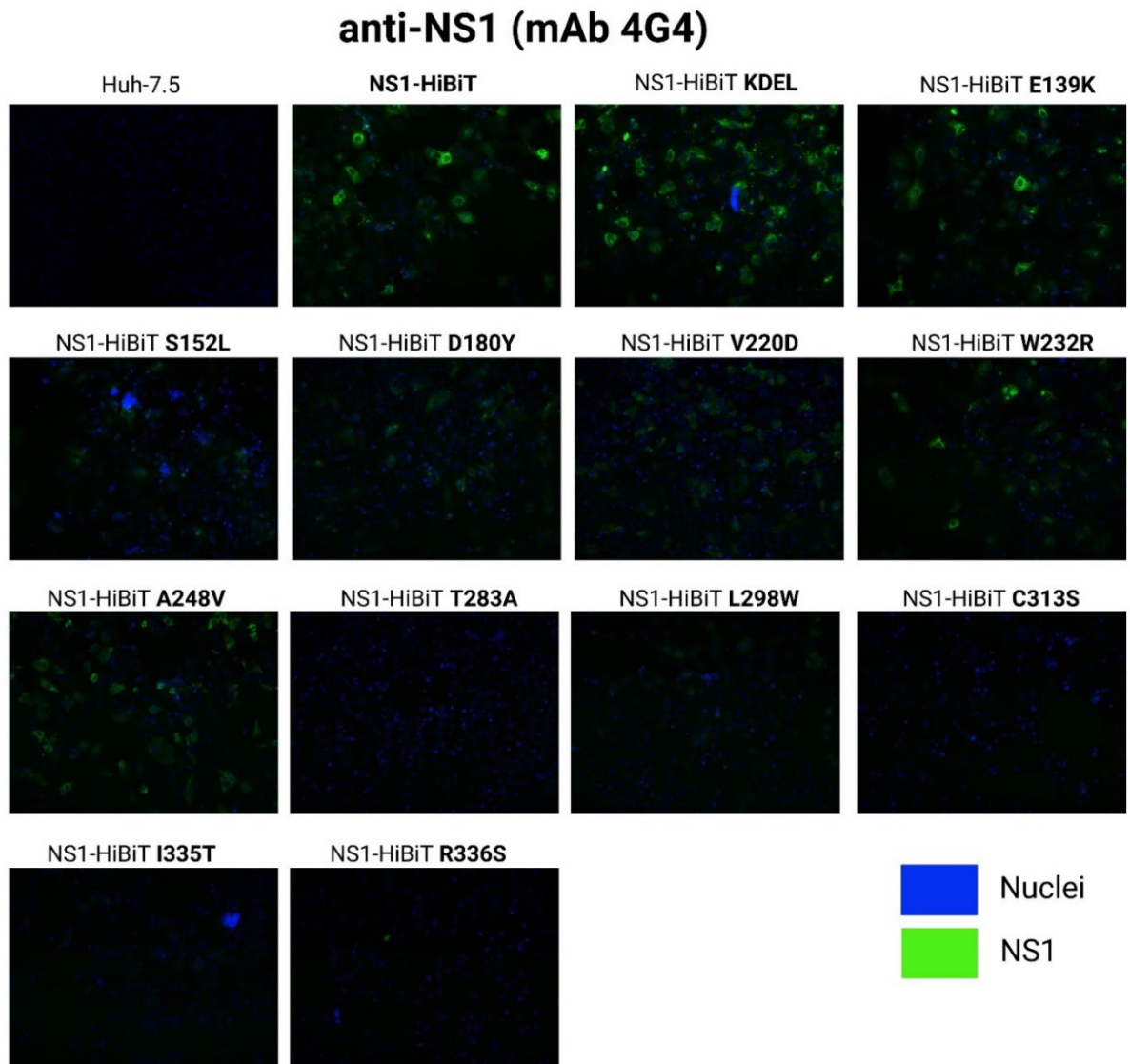
Name	Specificity	Dilution factor	Incubation	Manufacturer
Goat anti-mouse. HRP conjugate	Mouse IgG (H + L)	1:40 000	RT 1hr dark	Invitrogen (A16066)
Goat anti-mouse IgG, Alexa Fluor 488	Mouse IgG (H+L)	1:200 (IF)	4°C 2hr dark	Invitrogen (A11001)
Goat anti-rabbit IgG Alexa Fluor 488	Rabbit IgG (H+L)	1:200 (IF)	4°C 2hr dark	Invitrogen (A11008)
Goat anti-rabbit IgG Alexa Fluor 555	Rabbit IgG	1:200 (IF)	4°C 2hr dark	Invitrogen (A21428)
IR®Dye 800CW goat anti-mouse	Mouse IgG	1:10 000 (WB)	RT 1hr dark with gentle agitation	LI-COR (926-32210)
IR®Dye 680RD goat anti-rabbit	Rabbit IgG	1: 10 000 (WB)	RT 1hr dark with gentle agitation	LI-COR (926-68071)
IR®Dye 800CW Streptavidin	Biotin	1: 4000 (WB)	RT 1hr dark with gentle agitation	LI-COR (926-32230)
Cy3-Streptavidin	Biotin	1: 100 (IF)	2hr in the dark at 4°C	Jackson ImmunoResearch Laboratories (016-160-084)

Fluorescent dyes

Name	Specificity	Dilution factor/ Incubation	Manufacturer
DAPI	Nucleic acid	1/1000 (1 µg/mL) (IF) RT 10 min, dark	Sigma Aldrich (D9542-5MG)
IRaZolve-ER Blue®	Endoplasmic reticulum	1/400 (10mM) (IF) RT 30 min, dark	REZOLVE Scientific (1101026)

Abbreviations: HRP- horseradish peroxidase, WB-Western Blotting, IF-Immunofluorescence

Appendix IV: Supplementary Figures



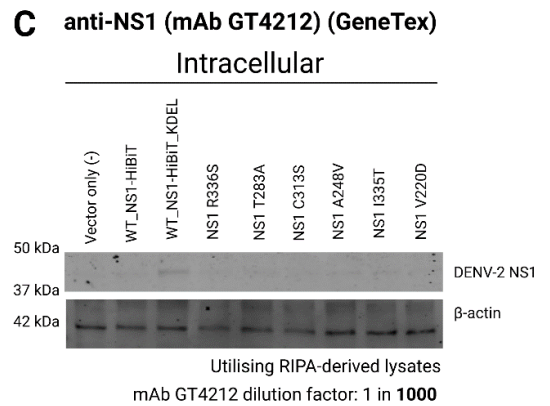
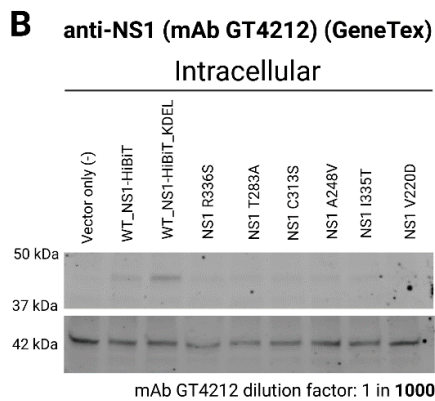
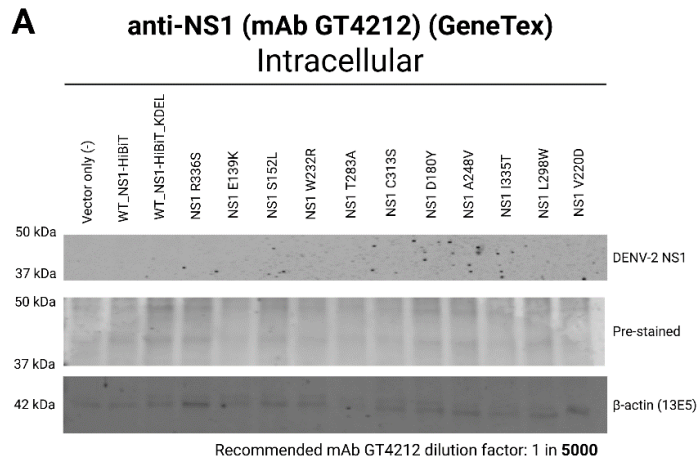
SF4.1 Immunofluorescence staining with an anti-NS1 ‘4G4’ antibody revealed reasonable expression of wildtype NS1 and NS1 mutant proteins. Seeded Huh7.5 cells were transiently transfected with NS1 expression constructs containing indicated point mutations and cultured overnight. Following 24-hours post-transfection, transfected Huh-7.5 cells were fixed and immunolabelled with both DAPI staining dye (nuclei;blue) and the anti-NS1 ‘4G4’ antibody (NS1; green) before being imaged as shown.

SF4.2 Brief overview depicting the outcomes of the detection of wildtype NS1 or NS1 mutant proteins with the anti-NS1 4G4 monoclonal antibody in either immunofluorescence or Western blotting studies

anti-NS1 (mAb 4G4)

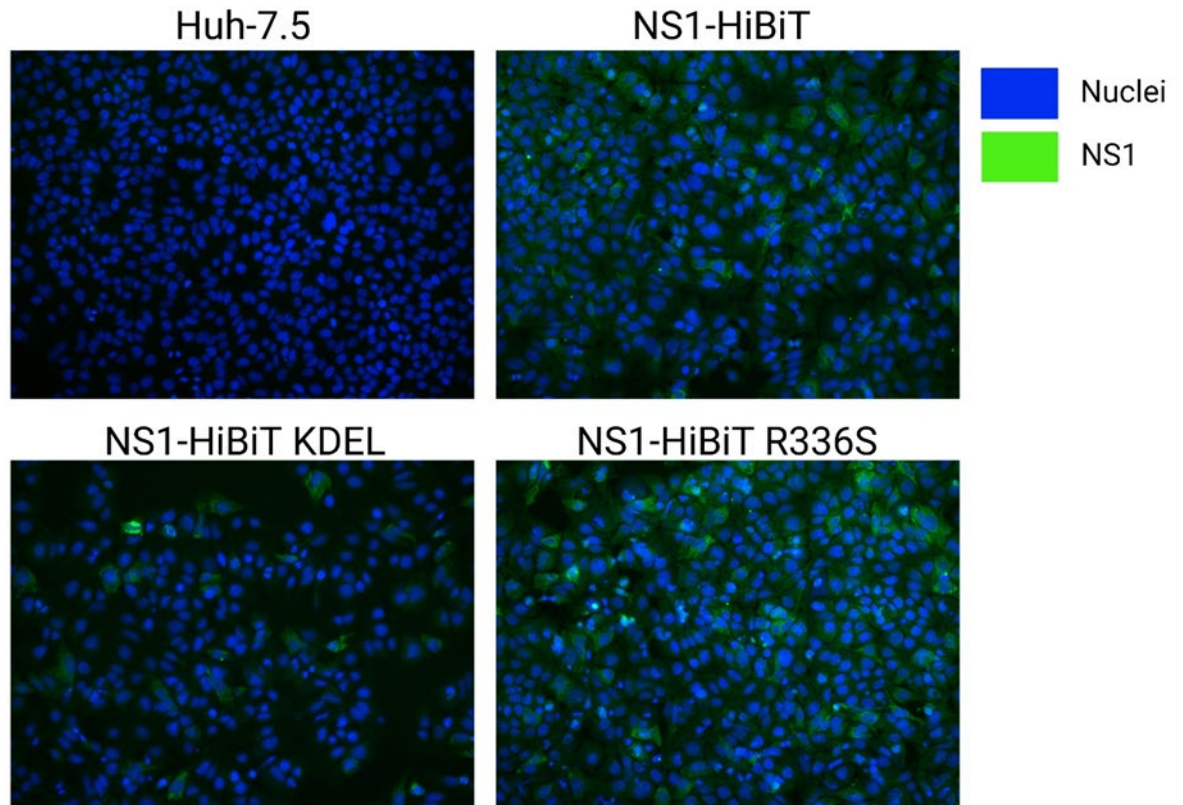
	Immunofluorescence	Western Blotting
wildtype NS1-HiBiT	✓	✓
wildtype NS1-HiBiT KDEL	✓	✓
NS1-HiBiT E139K	✓	✓
NS1-HiBiT S152L	✓	✓
NS1-HiBiT D180Y	✓	✓
NS1-HiBiT V220D	✓	✓
NS1-HiBiT W232R	✓	✓
NS1-HiBiT A248V	✓	✓
NS1-HiBiT T283A	✓	✗
NS1-HiBiT L298W	✓	✓
NS1-HiBiT C313S	✓	✗
NS1-HiBiT I335T	✓	✓
NS1-HiBiT R336S	✓	✗

✓	Detected
✗	Not Detected



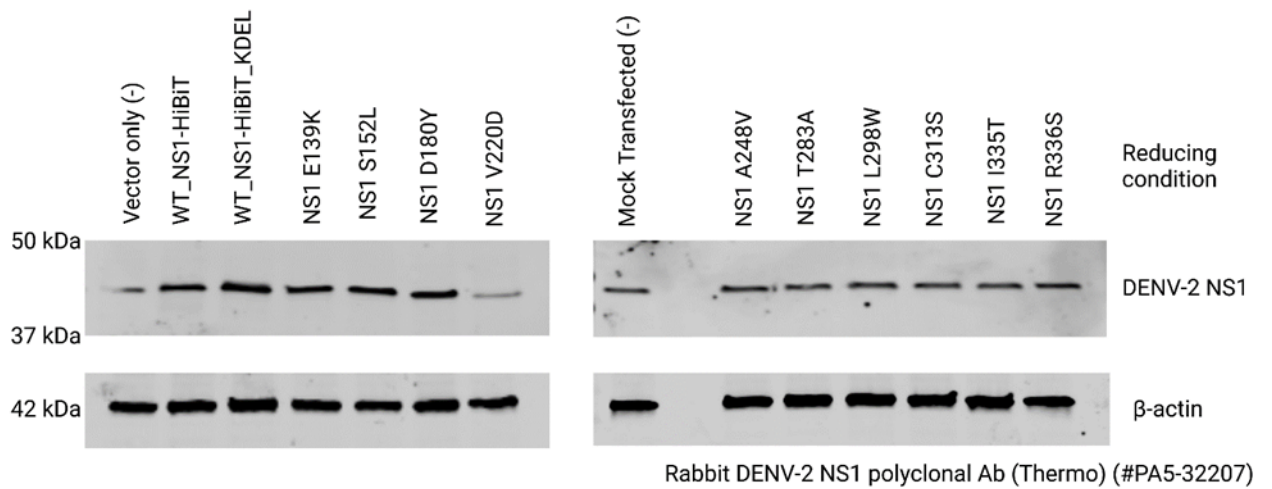
SF4.3 Utilisation of an alternative anti-NS1 monoclonal antibody did not enable reliable detection of NS1 mutant proteins. (A,B,C) Huh-7.5 cells were transiently transfected with NS1 expression constructs containing the indicated point mutations. At 48-hours post transfection, supernatants were collected and lysates were harvested using either NP-40 (A,B) or RIPA lysis buffer (C). Supernatants and lysates were subsequently subjected to SDS PAGE and Western blotting to detect DENV NS1 using an anti-NS1 monoclonal antibody (GeneTex) at recommended dilution factor of 1 in 5000 (A) or 1 in 1000 (B,C). (A) Prior to the blocking step, membranes were also stained with a total-protein fluorescent stain (LI-COR). β -actin was also detected as a loading control for lysate samples only.

anti-NS1(mAb GT4212)



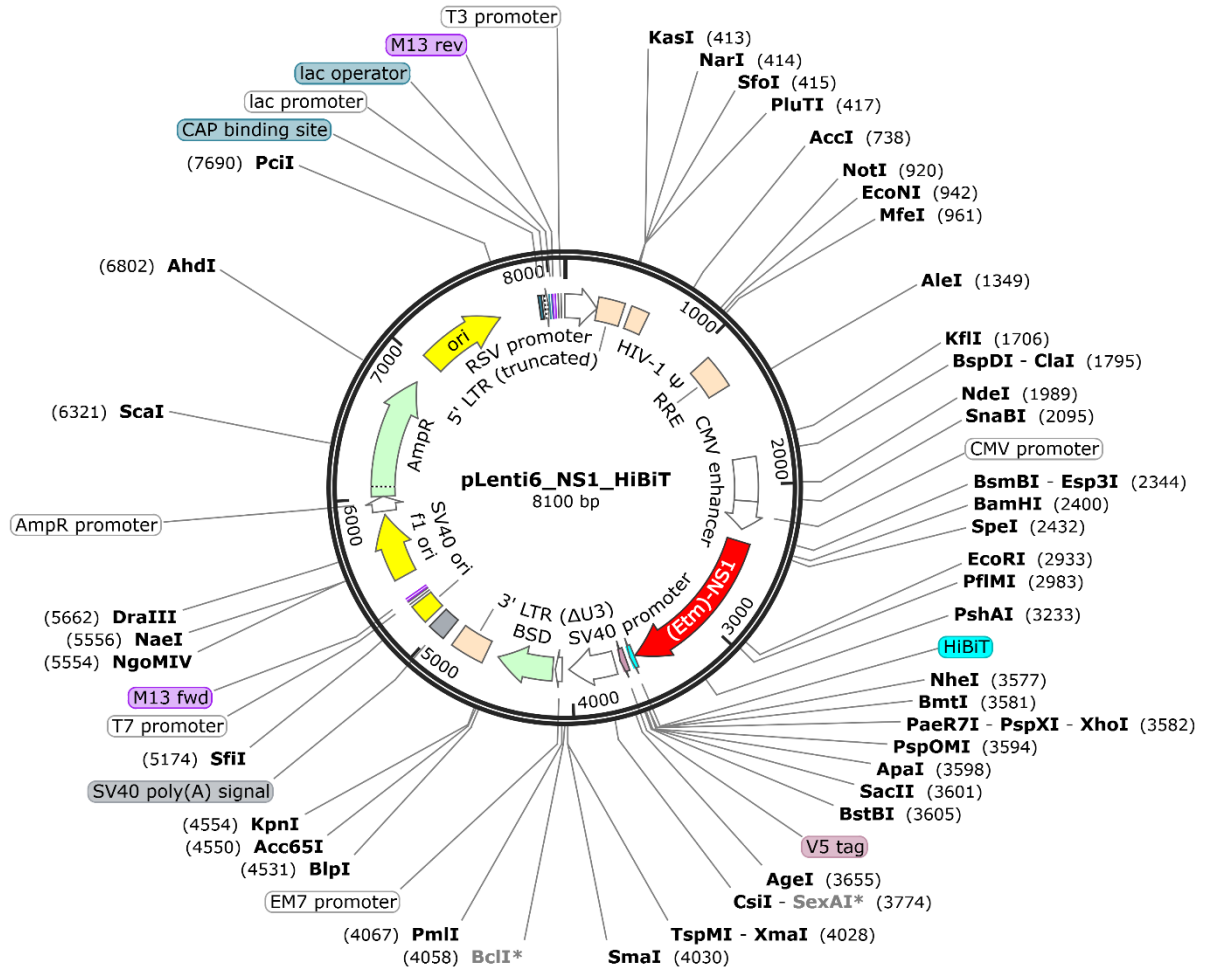
SF4.4 Immunofluorescent labelling of Huh-7.5 cells that were transfected with NS1 expression constructs using the DENV anti-NS1 monoclonal antibody ‘GT4212’ (GeneTex). NS1 expression constructs (wildtype NS1-HiBiT, wildtype KDEL-tagged NS1-HiBiT and a mutant NS1-HiBiT R336S) were transiently transfected into Huh-7.5 cells. At 24-hours post transfection, transfected cells were washed before fixation and immunolabelling with an anti-NS1 monoclonal antibody ‘GT4212’ (GeneTex) (DENV NS1; green) and DAPI staining dye (nuclei; blue).

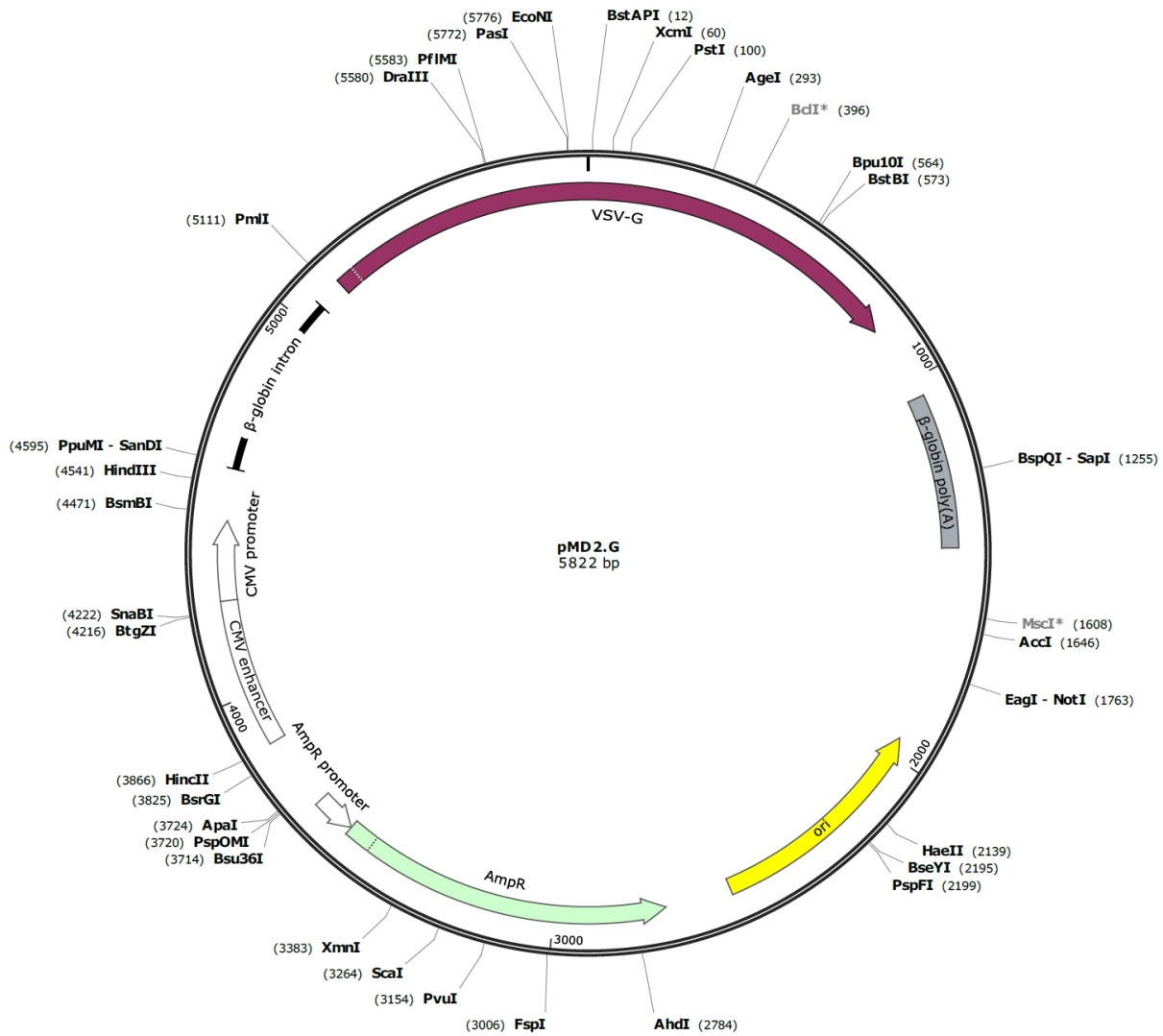
anti-NS1 (pAb Thermo) Intracellular

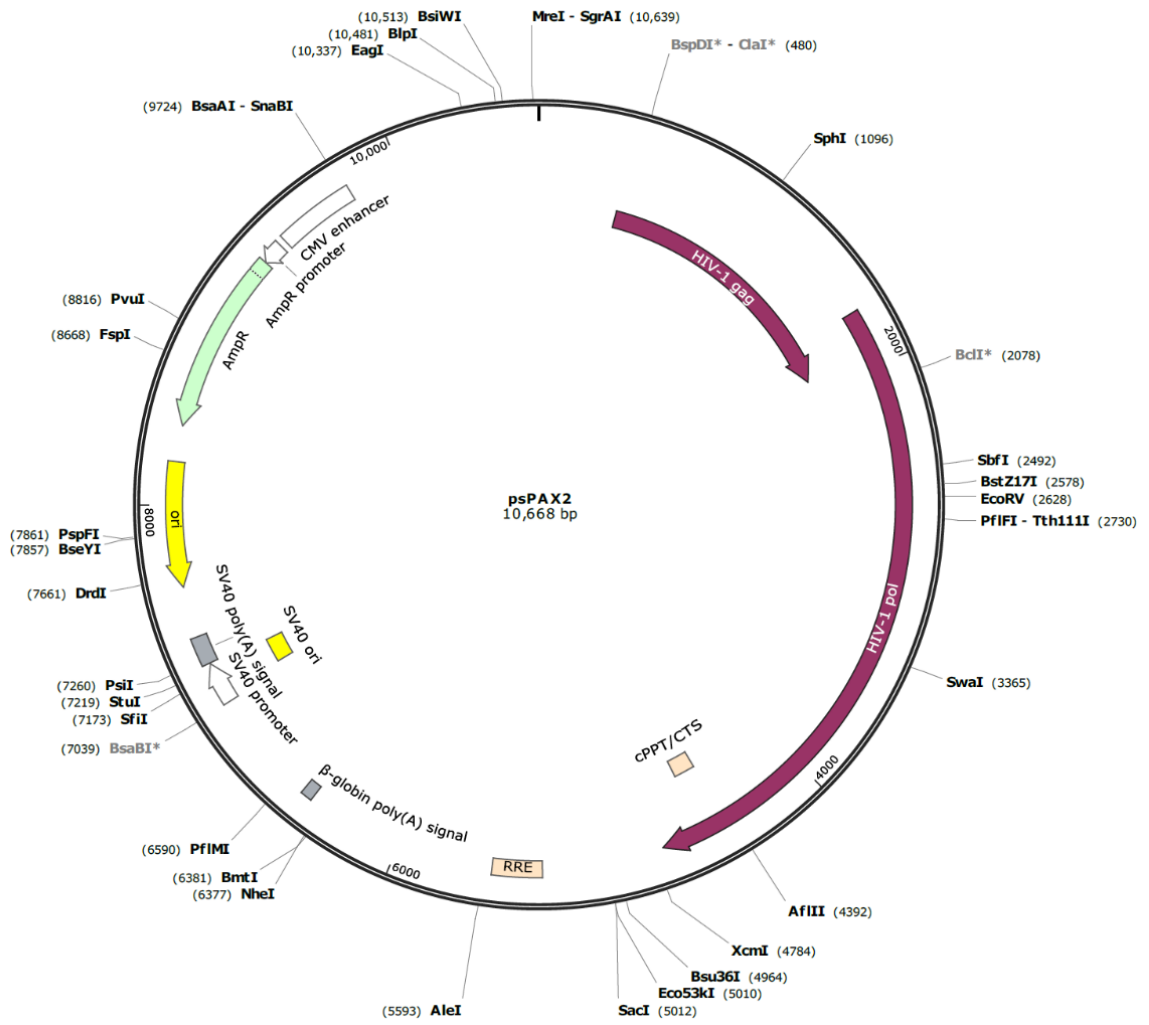


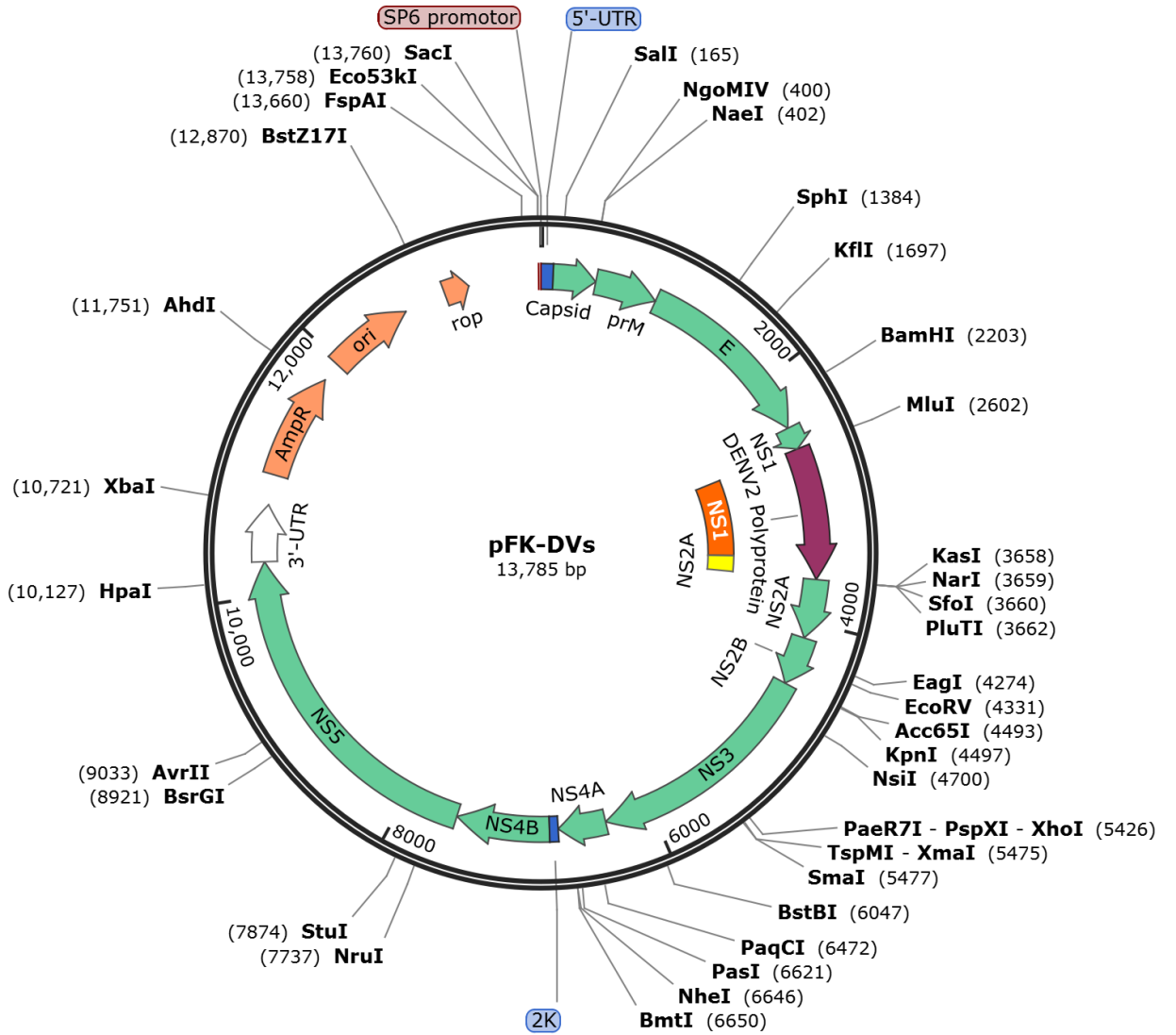
SF4.5 Detection of non-specific similar bands in all mock-transfected and transfected cell lysates samples by Western blotting using a rabbit polyclonal anti-NS1 antibody. Seeded Huh-7.5 cells were transiently transfected with respective expression constructs, before subjecting cell lysate samples to SDS PAGE and Western blotting to detect DENV2 NS1 using a rabbit polyclonal anti-NS1 antibody (Thermo). β -actin was also detected in parallel as a loading control for the lysate samples.

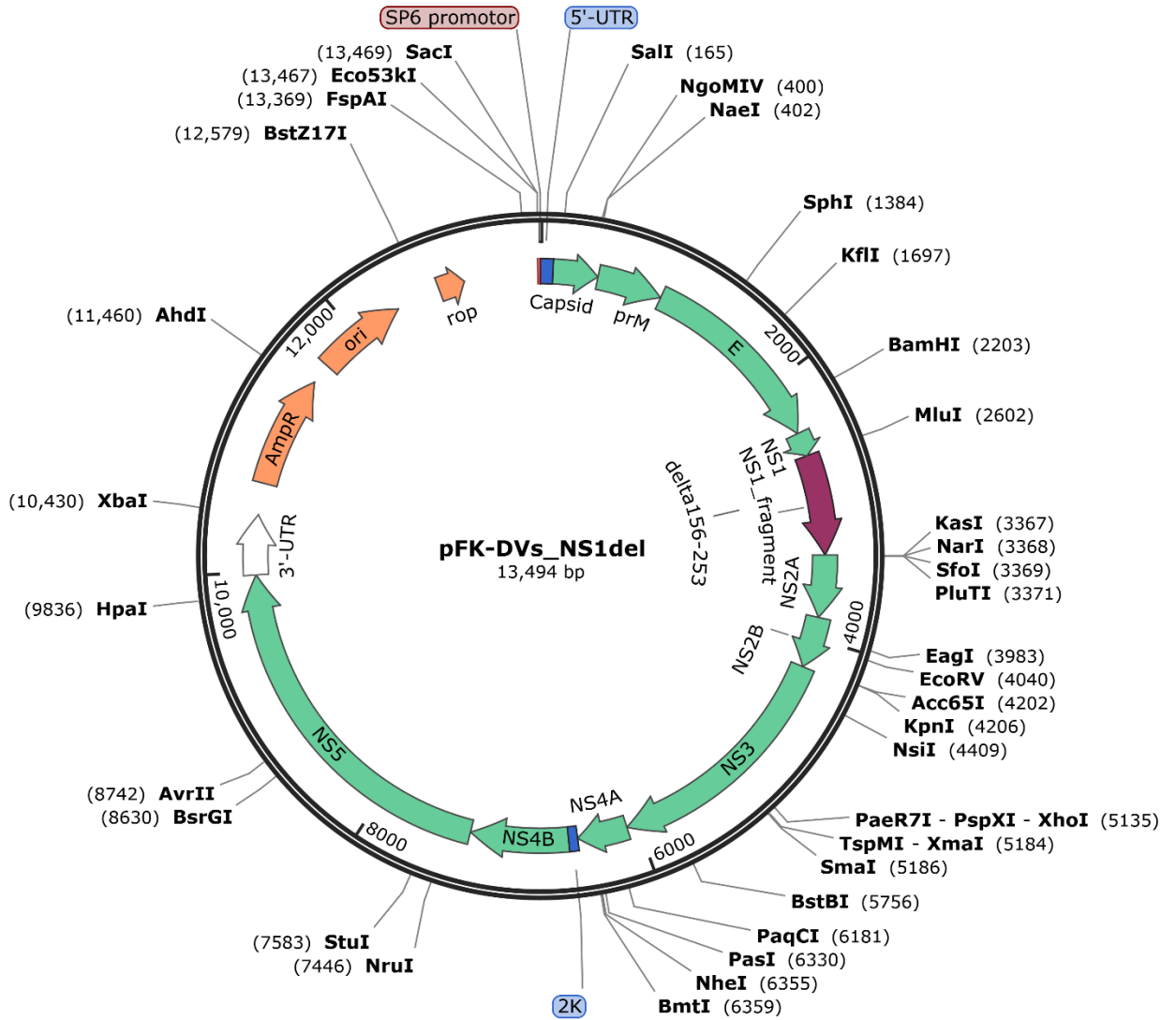
Appendix V: Plasmid Maps

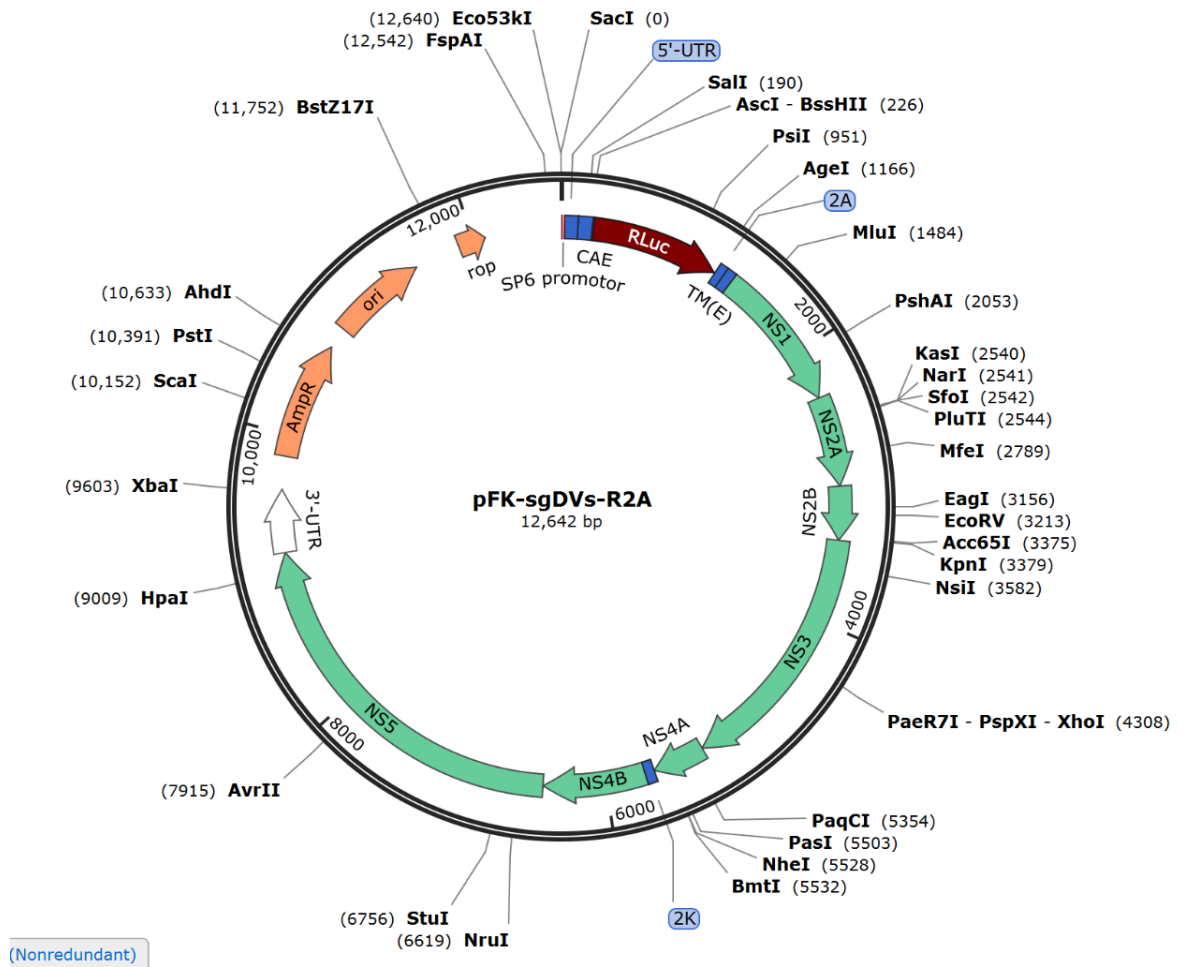


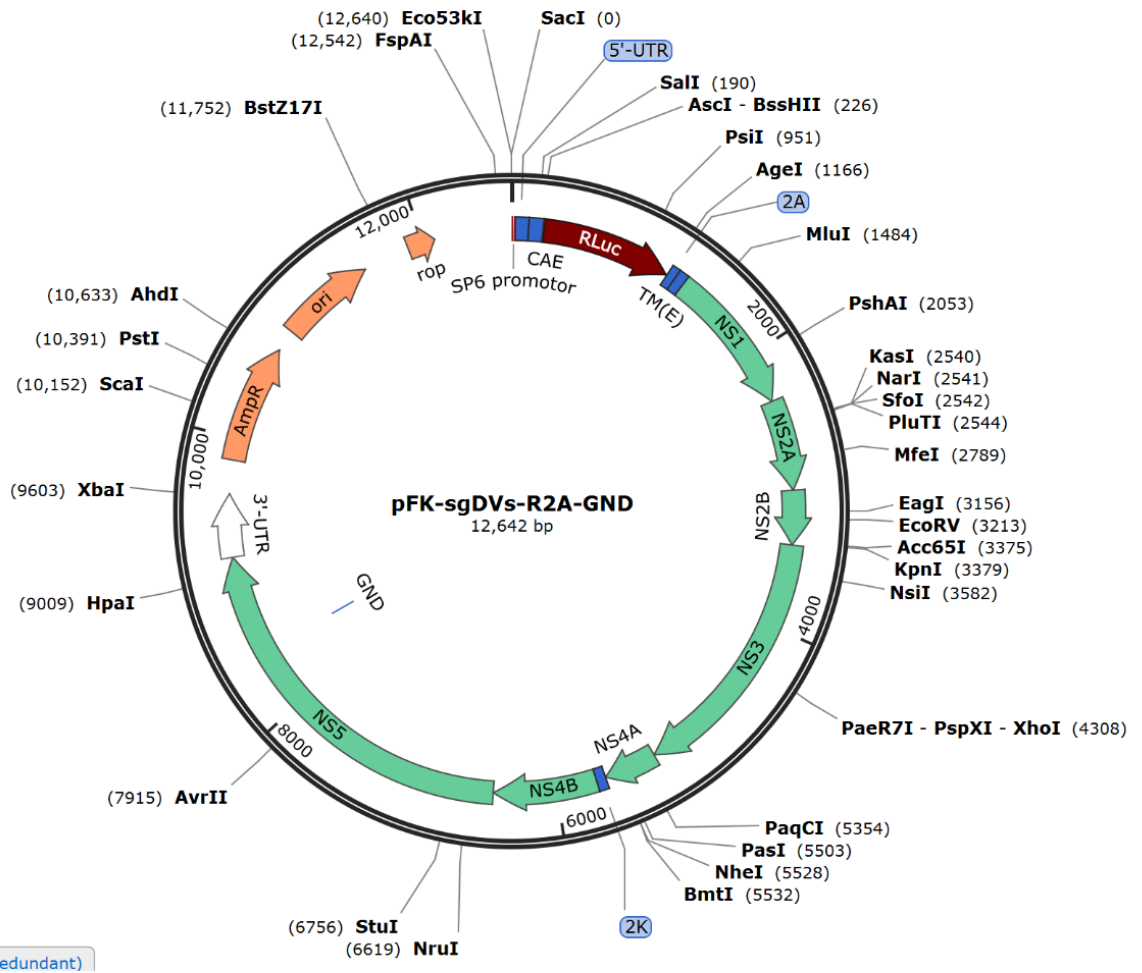




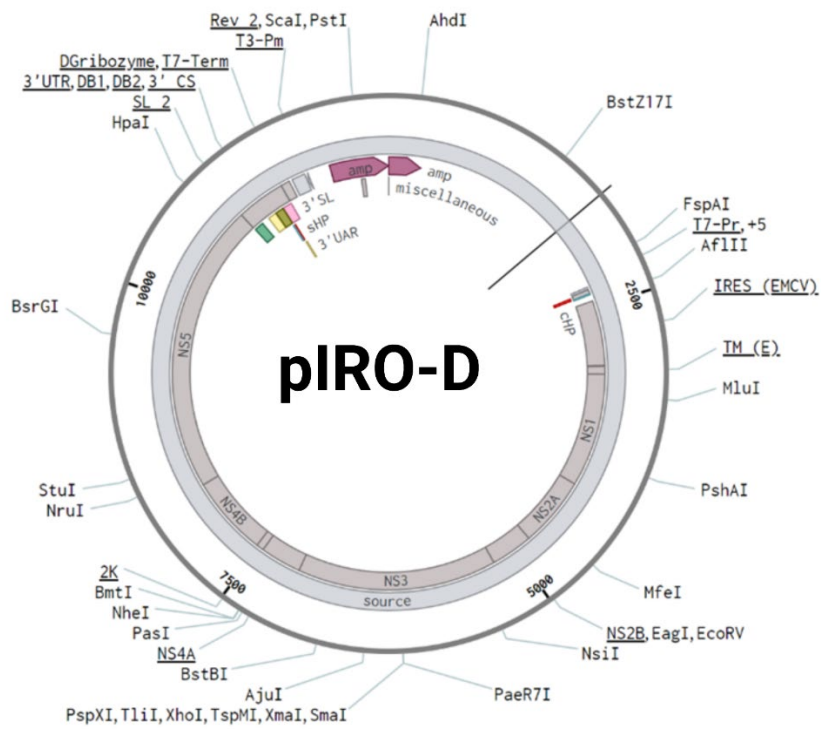


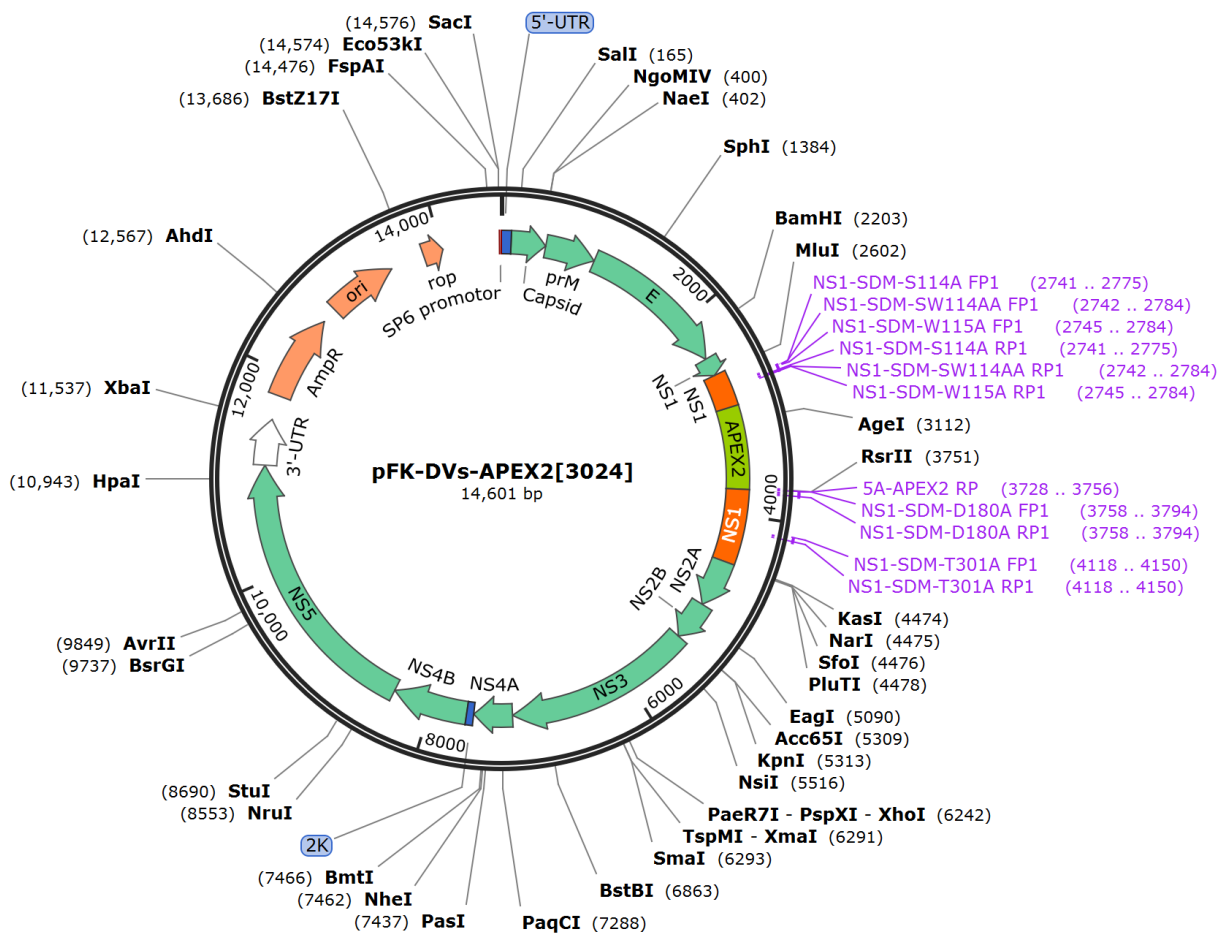






(Nonredundant)





Appendix VI: DENV-2 NS1 processed DNA/peptide sequences

DENV-2 NS1

1- ATGAGCACCTCACTGTCTGTGACACTAGTATTGGTGGGAATTGTGACACTGTATTTGGGA -60
1- M S T S L S V T L V L V G I V T L Y L G -20
61- GTCATGGTGCAGGCCGATAGTGGTTGCGTTGTGAGCTGGAAAAACAAAGAACTGAAATGT -120
21- V M V Q A D S G C V V S W K N K E L K C -40
121- GGCAGTGGGATTTTCATCACAGACAACGTGCACACATGGACAGAACAATACAAGTTCCAA -180
41- G S G I F I T D N V H T W T E Q Y K F Q -60
181- CCAGAATCCCCTTCAAACTAGCTTCAGCTATCCAGAAAGCCCATGAAGAGGGCATTGT -240
61- P E S P S K L A S A I Q K A H E E G I C -80
241- GGAATCCGCTCAGTAACGCGTCTGGAGAATCTGATGTGGAAACAATAACACCAGAATTG -300
81- G I R S V T R L E N L M W K Q I T P E L -100
301- AATCACATTCTATCAGAAAATGAGGTGAAGTTGACTATTATGACAGGAGACATCAAAGGA -360
101- N H I L S E N E V K L T I M T G D I K G -120
361- ATCATGCAGGCAGGAAAACGATCTCTGCGGCCTCAGCCCACTGAGCTGAAGTATTCATGG -420
121- I M Q A G K R S L R P Q P T E L K Y S W -140
421- AAAACATGGGGCAAAGCAAAAATGCTCTCTACAGAGTCTCATAACCAGACCTTTCTCATT -480
141- K T W G K A K M L S T E S H N Q T F L I -160
481- GATGGCCCCGAAACAGCAGAATGCCCAACACAAATAGAGCTTGAATTCGTTGGAAGTT -540
161- D G P E T A E C P N T N R A W N S L E V -180
541- GAAGACTATGGCTTTGGAGTATTCACCACCAATATATGGCTAAAATTGAAAGAAAAACAG -600
181- E D Y G F G V F T T N I W L K L K E K Q -200
601- GATGTATTCTGCGACTCAAACTCATGTCAGCGGCCATAAAAGACAACAGAGCCGTCCAT -660

201- D V F C D S K L M S A A I K D N R A V H -220
 661- GCCGATATGGGTTATTGGATAGAAAAGTGCCTCAATGACACATGGAAGATAGAGAAAGCC -720
 221- A D M G Y W I E S A L N D T W K I E K A -240
 721- TCTTTCATTGAAGTTAAAACTGCCACTGGCCAAAATCACACACCCTCTGGAGCAATGGA -780
 241- S F I E V K N C H W P K S H T L W S N G -260
 781- GTGCTAGAAAAGTGAGATGATAATTCCAAAGAATCTCGCTGGACCAGTGTCTCAACACAAC -840
 261- V L E S E M I I P K N L A G P V S Q H N -280
 841- TATAGACCAGGCTACCATAACAAAATAACAGGACCATGGCATCTAGGTAAGCTTGAGATG -900
 281- Y R P G Y H T Q I T G P W H L G K L E M -300
 901- GACTTTGATTTCTGTGATGGAACAACAGTGGTAGTGACTGAGGACTGCGGAAATAGAGGA -960
 301- D F D F C D G T T V V V T E D C G N R G -320
 961- CCCTCTTTGAGAACAACCACTGCCTCTGGAAAACATATAACAGAATGGTGTGCCGATCT -1020
 321- P S L R T T T A S G K L I T E W C C R S -340
 1021- TGCACATTACCACCGCTAAGATACAGAGGTGAGGATGGGTGCTGGTACGGGATGGAAATC -1080
 341- C T L P P L R Y R G E D G C W Y G M E I -360
 1081- AGACCATTGAAGGAGAAAGAAGAGAATTTGGTCAACTCCTTGGTCACAGCTGGATCAGTG -1140
 361- R P L K E K E E N L V N S L V T A G S V -380

Linker
 1141- AGCGGCTGGCGGCTGTTCAAGAAGATTAGCTAG
 381- S G W R L F K K I S *
 -----HiBiT tag-----STOP

Appendix VII: Published experimental manuscript

Statement of Authorship

Title of Paper	Identification of Key Residues in Dengue virus NS1 Protein That Are Essential for Its Secretion
Publication Status	<input checked="" type="checkbox"/> Published <input type="checkbox"/> Accepted for Publication <input type="checkbox"/> Submitted for Publication <input type="checkbox"/> Unpublished and Unsubmitted work written in manuscript style
Publication Details	Dengue virus (DENV) non-structural protein 1 (NS1) is involved in multiple aspects of the DENV lifecycle. Importantly, it is secreted from infected cells as a hexameric lipoparticle that mediates vascular damage that is a hallmark of severe dengue. Although the secretion of NS1 is known to be important in DENV pathogenesis, the exact molecular features of NS1 that are required for its secretion from cells are not fully understood. In this study, we employed random point mutagenesis in the context of an NS1 expression construct encoding a C-terminal HIV1 luciferase reporter tag to identify residues within NS1 that are essential for its secretion. Together, these studies demonstrate that combination of a fluorescently tagged NS1 expression system with random point mutagenesis enables rapid identification of mutations that alter NS1 secretion.

Principal Author

Name of Principal Author (Candidate)	TAN ENG KUAN BRANDON
Contribution to the Paper	Conceptualization Methodology Formal Analysis Data curation Writing of original draft preparation Writing - review and editing Intellectual input
Overall percentage (%)	80%
Certification:	This paper reports on original research I conducted during the period of my Higher Degree by Research candidature and is not subject to any obligations or contractual agreements with a third party that would constrain its inclusion in this thesis. I am the primary author of this paper.
Signature	Date 28/6/23

Co-Author Contributions

By signing the Statement of Authorship, each author certifies that:

- the candidate's stated contribution to the publication is accurate (as detailed above);
- permission is granted for the candidate to include the publication in the thesis; and
- the sum of all co-author contributions is equal to 100% less the candidate's stated contribution.




Name of Co-Author	Michael Beard
Contribution to the Paper	<ul style="list-style-type: none"> Resources acquisition Supervision Funding acquisition
Signature	Date 29/06/23

Name of Co-Author	NICHOLAS EMRE
Contribution to the Paper	<ul style="list-style-type: none"> Methodology Supervision Funding acquisition Resources acquisition Intellectual input
Signature	Date 4/7/23

Please cut and paste additional co-author panels here as required.

Article

Identification of Key Residues in Dengue Virus NS1 Protein That Are Essential for Its Secretion

Brandon E. K. Tan ¹, Michael R. Beard ¹ and Nicholas S. Eyre ^{2,*}

¹ Research Centre of Infectious Diseases, School of Biological Sciences, University of Adelaide, Adelaide, SA 5005, Australia

² College of Medicine and Public Health (CMPH), Flinders University, Bedford Park, SA 5042, Australia

* Correspondence: nicholas.eyre@flinders.edu.au

Abstract: Dengue virus (DENV) non-structural protein 1 (NS1) is involved in multiple aspects of the DENV lifecycle. Importantly, it is secreted from infected cells as a hexameric lipoparticle that mediates vascular damage that is a hallmark of severe dengue. Although the secretion of NS1 is known to be important in DENV pathogenesis, the exact molecular features of NS1 that are required for its secretion from cells are not fully understood. In this study, we employed random point mutagenesis in the context of an NS1 expression vector encoding a C-terminal HiBiT luminescent peptide tag to identify residues within NS1 that are essential for its secretion. Using this approach, we identified 10 point mutations that corresponded with impaired NS1 secretion, with *in silico* analyses indicating that the majority of these mutations are located within the β -ladder domain. Additional studies on two of these mutants, V220D and A248V, revealed that they prevented viral RNA replication, while studies using a DENV NS1-NS5 viral polyprotein expression system demonstrated that these mutations resulted in a more reticular NS1 localisation pattern and failure to detect mature NS1 at its predicted molecular weight by Western blotting using a conformation-specific monoclonal antibody. Together, these studies demonstrate that the combination of a luminescent peptide tagged NS1 expression system with random point mutagenesis enables rapid identification of mutations that alter NS1 secretion. Two such mutations identified via this approach revealed residues that are essential for correct NS1 processing or maturation and viral RNA replication.



Citation: Tan, B.E.K.; Beard, M.R.; Eyre, N.S. Identification of Key Residues in Dengue Virus NS1 Protein That Are Essential for Its Secretion. *Viruses* 2023, 15, 1102. <https://doi.org/10.3390/v15051102>

Academic Editors: Carlos A. Sariol, Mariana Leguia and Daniela Weiskopf

Received: 24 February 2023

Revised: 21 April 2023

Accepted: 25 April 2023

Published: 30 April 2023



Copyright: © 2023 by the authors. Licensee MDPI, Basel, Switzerland. This article is an open access article distributed under the terms and conditions of the Creative Commons Attribution (CC BY) license (<https://creativecommons.org/licenses/by/4.0/>).

Keywords: dengue virus; NS1; NS1 secretion; mutagenesis; HiBiT; N-glycosylation

1. Introduction

Dengue virus (DENV) is a mosquito-borne (+) RNA virus of the *Flavivirus* genus within the *Flaviviridae* family. Epidemiological modelling has indicated that there are approximately 390 million DENV infections annually [1]. DENV infection is normally asymptomatic but can potentially lead to a wide range of clinical manifestations ranging from mild fever to severe forms of dengue, formerly categorized as dengue haemorrhagic fever (DHF) and life-threatening dengue shock syndrome (DSS) [2,3]. No specific antiviral therapies are currently available and the only licensed dengue vaccine available is only recommended for administration in individuals that are 9–45 years of age, and most importantly have at least one prior history of dengue infection [1,4]. Thus, there remains an urgent need for the development of safe and effective antiviral strategies, particularly in the form of vaccines and treatments, to effectively counteract the rise in dengue infection.

Following virus internalization into permissive host cells via clathrin-mediated endocytosis, the DENV nucleocapsid dissociates in the cytosol, liberating the positive-sense single-stranded RNA DENV genome, which is translated by host ribosomes at the rough endoplasmic reticulum (ER) [5]. The nascent 3400-amino-acid-long polyprotein is co- and post-translationally cleaved into three structural proteins (capsid, prM, and envelope) and seven non-structural proteins (NS1, NS2A, NS2B, NS3, NS4A, NS4B, and NS5) by host

proteases and the viral DENV NS2B/NS3 protease complex [6]. The non-structural proteins promote endoplasmic reticulum (ER) membrane rearrangements, including the induction of disordered membranes, known as convoluted membranes (CMs), whose functions are unclear, and clusters of spherular invaginations of the ER, known as vesicle packets (VPs), which often remain connected to the cytoplasm via 10 nm pores and are the proposed sites of viral RNA replication [5–9]. Viral replication complexes (RC), constituting an incompletely defined collection of host cell factors, viral non-structural proteins and viral RNA, are anchored within these membranous compartments to enable efficient DENV replication mediated by the NS5 RNA-dependent RNA polymerase in a microenvironment that is shielded from host defence mechanisms [9,10]. The formation of viral nucleocapsids that contain newly synthesized viral RNA is proposed to occur in close proximity to viral replication sites and this is followed by nucleocapsid budding into envelope and prM enriched-ER membranes, acquiring a lipid envelope in the process. Virus assembly is thought to take place in close proximity to VPs, with assembled virions being stored in ER cisternae in ordered arrays encased by “virion bags” [9,11]. Individual virions are transported to the trans-Golgi network via secretory vesicles, where virion maturation occurs through cleavage of the prM protein by host resident protease, Furin, before the release of infectious mature viral particles via the conventional secretory pathway [6].

Flavivirus NS1 is a 48-kDa non-structural multi-functional glycoprotein that can be identified either as a membrane-associated (mNS1) species associated with vesicular compartments within the cell and the plasma membrane or a secreted extracellular NS1 species (sNS1) [12–14]. Intracellular mNS1 is essential in virus replication and has been observed to co-localize with components of viral replication complexes in mammalian cells and insect cells [7,15–22]. The sNS1 is a soluble lipoprotein particle forming an open-barrel hexamer exterior, with its central internal channel tightly packed with lipid components resembling those of plasma high-density lipoproteins (HDLs) that are involved in systemic lipid traffic and vascular homeostasis [23]. Interestingly, a recent cryo-EM study has indicated that NS1 hexamers interact with and collapse upon HDLs, and that this interaction of sNS1 with lipoproteins is important for the ability of sNS1 to induce inflammatory cytokine production by macrophages [24]. Another high-resolution cryo-EM study has also recently demonstrated that, in addition to hexamers, the majority of sNS1 is found in either ‘loose’ or ‘stable’ tetrameric forms, which are differentially susceptible to the antibody mediated blockade of vascular damage [25]. The DENV NS1 dimer 3D structure has been successfully resolved, revealing that NS1 comprises three main domains: a small N-terminal β -roll domain (amino acids position 1 to 29) formed by disulphide linkage of two β -hairpins, the Wing domain (amino acids position 38–151) flanked by connector subdomains (amino acids position 30–37 and 152–180), and finally, a core β -ladder domain (amino acids position 181–352) that stretches along the whole length of the dimer via its 18-antiparallel β -strands that are arranged like rungs of a ladder [22,26,27]. The β -roll domain and the connector subdomain of the Wing domain form a protrusion that causes one face of the dimer to be hydrophobic such that is thought to mediate the association of the NS1 dimer with the inner leaflet of the ER membrane. In its hexameric form, three β -rolls face the interior of the hexamer, interacting with the central lipid cargo. In both mNS1 and sNS1 forms, the distal tips of the β -ladder and the Wing domain disorientated loops contain N-glycosylation sites (amino acids position 130 and 207) that protrude outwards, enabling them to be exposed to the external environment.

Following the cleavage of the NS1-NS2A junction by an undefined protease in the ER, glycosylation of DENV NS1 occurs whereby high mannose carbohydrate moieties are added to asparagine residues 130 and 207 [12,28]. In the Golgi, additional NS1 glycan modification occurs, where a complex-type sugar is incorporated onto the N130 glycan, while the high mannose moiety on N207 remains [28]. N-glycosylation on NS1 has been demonstrated to be essential in many NS1 functions throughout the DENV life cycle. Mutating either the N130 or N207 glycosylation site within DENV NS1 appeared to impede virus growth, thus reducing DENV neurovirulence in a mouse model [29]. The alteration of

both N-linked NS1 glycosylation sites interestingly resulted in the generation of relatively unstable mutant viruses, indicating that the glycosylation of these sites is important for viral replication. Additionally, it was demonstrated that the DENV NS1 N130 glycan is essential for the stabilisation of secreted NS1, whereas the N207 glycan promotes the stability of the extracellular NS1 protein and its secretion [30]. Recently, a related study by Wang et al. (2019) indicated that the DENV NS1 N130 glycan is essential for NS1 protein secretion, whereas the N207 glycan is dispensable for both NS1 stability and secretion, contrasting with the results from the earlier study by Somnuk et al. 2011 [30,31]. Regardless, these N-glycans appeared to be intimately involved in NS1 secretion and the stability of the NS1 dimer.

sNS1 has been strongly associated with the pathogenesis of severe DENV infections since early studies reported its detection at significantly elevated levels in the serum of DENV-infected patients [32–35]. Highly immunogenic sNS1 and plasma-membrane-associated NS1 are known to be essential in immune evasion through a range of mechanisms, including the activation or inhibition of complement pathways and the elicitation of autoantibodies that cross-react with platelets and endothelial cells leading to endothelial dysfunction; one of the distinctive hallmarks of flavivirus disease pathogenesis [14,35–39].

In addition to its roles in triggering endothelial permeability via complement and auto-antibodies, sNS1 has also been recognized as a pathogen-associated molecular pattern (PAMP) that promotes the release of vasoactive chemokines and cytokines from human peripheral blood mononuclear cells (PBMCs) via TLR-4 activation, subsequently leading to vascular leakage [40,41]. Importantly, pre-treatment of endothelial cells with anti-TLR-4 antibody effectively inhibited sNS1-mediated vascular leakage, further demonstrating that sNS1-mediated TLR-4 activation in endothelial cells directly contributes to vascular leakage. In addition, sNS1 has been shown to promote the disruption of the endothelial glycocalyx-like layer (EGL) of human pulmonary endothelial cells, which are responsible for endothelial barrier function. The sNS1-mediated activation of cellular enzymes, including heparinase, sialidases and cathepsin L, has been shown to induce the degradation and shedding of components of the EGL-layer, subsequently leading to the disruption of its integrity and endothelial hyperpermeability [42]. More recently, a cohort of flavivirus NS1 proteins, including DENV NS1, was examined for their ability to induce endothelial barrier dysfunction *in vitro* and hyperpermeability *in vivo* in a tissue-specific manner, thus reflecting the unique pathogenesis, disease, and dissemination of respective flavivirus infections [43].

Several recent comprehensive mutagenesis studies have investigated which NS1 residues are critical to its roles in viral RNA replication, infectious virus particle production, NS1 secretion, and the pathogenic effects of sNS1 [22,44,45]. Despite this and the recognized importance of NS1 secretion to DENV disease pathogenesis, the molecular features of NS1 that are important to its secretion remain incompletely understood. In this study, we have employed random mutagenesis of NS1 in combination with the HiBiT luminescent peptide tagging system to identify mutations that disrupt its secretion activity from transfected cells. This led to the identification of 10 point mutations that resulted in markedly impaired NS1 secretion, with most of these mutations mapping to the β -ladder domain. Subsequent analyses of these mutants by confocal microscopy revealed similar localization patterns to that of the wildtype NS1, while initial Western blotting indicated that many of these mutant NS1 proteins may be inherently unstable and/or improperly folded. In support of this interpretation, repetition of these Western blotting experiments using an anti-HiBiT tag antibody revealed ready detection of all of the mutant NS1-HiBiT proteins and enabled confirmation of the secretion-impaired phenotypes of these mutants. Follow-up studies of two of these mutants, V220D and A248V, revealed that they prevented viral RNA replication and, when expressed in the context of an NS1-NS5 polyprotein, exhibited an ER-like localization pattern and were once again not detectable by Western blotting, implying that these mutant NS1 proteins may prevent viral RNA replication as a result of failing to mature properly.

2. Materials and Methods

2.1. Cell Culture, Antibodies, Conjugates, and Fluorescent Dyes

The Huh-7.5 human hepatocellular carcinoma cell line was kindly provided by Charles M. Rice (Rockefeller University, New York, NY, USA). Human embryonic kidney-derived 293FT cells were purchased from Thermo Fisher Scientific. Huh-7.5 cells stably expressing T7 RNA polymerase (Huh-7.5 + T7RNA pol) have been previously described [46]. All of these cell lines were cultured and maintained in a 37 °C, 5% CO₂ humidifier incubator in complete Dulbecco's modified Eagle medium (DMEM) with HEPES (Invitrogen, USA) supplemented with 1% penicillin-streptomycin (Sigma) and 10% foetal bovine serum (FBS), referred to henceforth as complete DMEM. Huh-7.5 + T7 RNApol cells were cultured, as above, with puromycin (Sigma-Aldrich) added to a final concentration of 3 µg/mL.

Mouse anti-flavivirus NS1 protein '4G4' monoclonal antibody was kindly provided by Dr Jody Peters and Prof. Roy Hall (University of Queensland, Australia) or purchased from Mozzy Mabs (University of Queensland, Australia). Mouse monoclonal antibody recognizing β-actin (AC-15) was purchased from Sigma-Aldrich. Mouse anti-NS3 monoclonal antibody (GT2811) was purchased from GeneTex, USA. Mouse anti-HiBiT monoclonal antibody (30E5) was purchased from Promega. Mouse anti-capsid monoclonal antibody '6F3.1' was kindly obtained from Professor John G. Aaskov (Queensland University of Technology, Australia). IRDye[®] 800 CW goat anti-mouse IgG secondary antibody for Western Immunoblotting was purchased from LI-COR Biosciences, USA). AlexaFluor 488- and 555-conjugated anti-mouse IgG and anti-rabbit IgG secondary antibodies were purchased from Thermo Fisher Scientific.

Fluorescent stain 4',6-diamidino-2-phenylindole (DAPI) was purchased from Sigma-Aldrich. Double-stranded DNA dye, DRAQ5[®], was purchased from Thermo Fisher Scientific. A cell permeant stain that labels the endoplasmic reticulum, Irazolve-ER Blue[®], was purchased from REZOLVE Scientific (Australia) or kindly provided by Dr Sally Plush (UniSA, Adelaide, Australia). Additional details about antibodies and dyes, including catalogue numbers, are detailed in Supplementary Table S1.

2.2. Cloning of Plasmid DNA Constructs

A synthetic version of the full length DENV-2 strain 16681 (pFK-DVs), a derivative full-length reporter construct that encodes a *Renilla* luciferase reporter gene (R2A) (pFK-DVs-R2A) and a *Renilla* luciferase-encoding sub-genomic replicon construct (pFK-sgDVs-R2A) were kindly provided by Prof. Ralf Bartenschlager (University of Heidelberg, Germany) [47]. For site-directed mutagenesis (N130A, N207A, V220D, A248V), external primers (*Mlu*I ext FWD and *Kas*I ext REV) were used in combination with internal mutation-encoding primers (see Supplementary Table S2 for oligonucleotide sequences) to generate two PCR-derived fragments featuring 10–20 bp overlaps using Q5 DNA polymerase (New England Biolabs). These fragments were gel-purified before being assembled into *Mlu*I/*Kas*I-digested pFK-DVs plasmid based on a 2-fragment Gibson Assembly reaction using NEBuilder[®] HiFi DNA Assembly (New England Biolabs). Sequences of manipulated DNA regions within plasmids were confirmed by automated DNA Sanger sequencing (Australian Genome Research Facility; AGRF, Australia).

2.3. Generation of DENV-2 NS1 Expression Constructs with Point Mutation (s)

To generate a library of NS1 expression plasmids featuring 1 point mutation in each clone on average, PCR-based random point mutagenesis using the GeneMorphII Random Mutagenesis Kit (Agilent Technologies) was carried out using a forward primer encoding an N-terminal start codon and the first 6 codons of the C-terminal of the envelope (E) protein coding region (pLenti6 NS1 FWD) and a reverse primer encoding a C-terminal HiBiT tag and stop codon (pLenti6 NS1 REV) (see Supplementary Table S2 for oligonucleotide sequences). PCR-based random point mutagenesis reactions were set up in 50 µL volumes containing 150 ng of pFK-DVs plasmid DNA as template, 250 ng of each forward/reverse primer and dNTPs, reaction buffer and DNA polymerase as per the manufacturer's rec-

ommendations. Samples were amplified via 30 cycles of PCR as per the manufacturer's instructions. PCR products were *DpnI*-treated for 2 h at 37 °C and gel-purified before cloning into a *Bam*HI/*Xho*I digested lentiviral expression plasmid construct (pLenti6-V5-D-TOPO) (Thermo Fisher, USA) using NEBuilder® HiFi DNA Assembly (NEB). Colony PCR was performed to verify the presence of potentially mutagenized NS1 cDNA before proceeding to subsequent HiBiT luciferase reporter-based assays (Promega). Out of 300 bacterial colonies randomly selected for colony PCR, 173 clones were confirmed to possess a potentially mutagenized NS1 insert.

2.4. HiBiT Luciferase Reporter-Based Assays

Huh-7.5 cells were seeded into 24-well plates and cultured overnight before transient transfection with purified uncharacterized NS1 expression clones using Lipofectamine 2000 (Thermo Fisher Scientific), according to the manufacturer's instructions. At 48 h post-transfection, supernatant samples were collected, cleared by centrifugation and mixed with an equal volume of 2X Passive Lysis Buffer (Promega). 1X Passive Lysis Buffer was added to the remaining transfected cell monolayers, pipetting (10×) before harvesting the lysate samples. Supernatant and lysates of respective samples were then probed for their luciferase signals using a Nano-Glo HiBiT Lytic Detection System (Promega) and a GloMax® Discover Microplate Reader (Promega) as per the manufacturer's instructions.

2.5. SDS-PAGE and Western Blotting

Supernatant and cell lysate samples were harvested and prepared from transfected Huh-7.5/293FT cells using NP-40 lysis buffer (1% NP-40, 50 mM Tris-HCl [pH 8], 150 mM NaCl) containing protease inhibitor cocktail (Sigma-Aldrich), as described previously [46]. Samples were mixed with non-reducing sample buffer for anti-NS1 (mAb 4G4) Western blotting or reducing sample buffer for Western blotting using all other antibodies, boiled for 5 min at 95 °C, separated via SDS-PAGE and transferred to nitrocellulose membranes (Bio-Rad). Following blocking for 1 h using 5% (*w/v*) skim milk in TBS, membranes were incubated with anti-NS1 primary antibody (1:10) (See Supplementary Table S2 key reagent resources) in TBS containing 0.1% (*v/v*) Tween-20 (Sigma-Aldrich) and 1% (*w/v*) skim milk at 4 °C overnight. Following stringent washing, membranes were incubated with IRDye® 800 CW goat anti-mouse IgG secondary antibody (1:10,000) for an hour in the dark at room temperature (RT) before being washed and imaged using a LI-COR Odyssey imaging system (Flinders Proteomics Facility, Flinders University, Australia).

2.6. Immunofluorescence Analyses

Huh-7.5 cells were seeded into 8-well coverslip bottomed chamber slides (ibidi GmbH, Germany) that were pre-coated with 0.2% (*w/v*) gelatin. Following overnight culture, cells were transiently transfected with NS1 expression plasmid constructs of interest using Lipofectamine 3000 (Thermo Fisher Scientific), according to the manufacturer's instructions. At 24–30 h post-transfection, cells were fixed with ice-cold acetone:methanol (1:1) fixative for 15 min at 4 °C, washed once with PBS and blocked with 5% (*w/v*) BSA in PBS at RT for 30 min.

For DENV NS1 staining, mouse anti-NS1 monoclonal antibody '4G4' was utilized in combination with goat anti-mouse IgG AlexaFluor 488 conjugated secondary antibody (Thermo Fisher Scientific). Nuclear DNA was stained with DAPI dye (Sigma Aldrich) diluted to 1 µg/mL in PBS for 10 min in the dark. Alternatively, nuclei were stained with DRAQ5 (Invitrogen) by incubating fixed samples for 15 min at RT with 0.5 µM DRAQ5 in PBS. IRaZolve-ER Blue® dye (REZOLVE Scientific, Australia) was used for endoplasmic reticulum staining by incubating fixed samples in the dark at RT with IraZolve-ER at 25 µM in PBS. The samples were then washed with PBS prior to imaging. Z-stacks of respective samples (with 0.2 µm step-size) were acquired using a ZEISS LSM 880 Fast Airyscan confocal fluorescence microscope system using a C Plan-Apochromat 63X oil immersion objective (NA:1.4) and 2.5× zoom (Flinders Microscopy and Microanalysis,

Flinders University, Australia). Appropriate laser lines (405, 488, 561 and 633 nm) were used at 2% of maximal power, adjusting master gain settings to enable signal visualisation with minimal saturation. Pinhole sizes were set to 1.0 Airy units for the longest-wavelength fluorophore and matched for all tracks. Images were acquired at 1024×1024 pixels, with an xy pixel size of 50 nm. The images were processed and analysed using ZEN Blue (version 3.2) software (ZEISS). Colocalization analysis was performed by measurement of Pearson's correlation coefficients for each cell (>20 cells/group) following drawing Bezier regions of interest around each cell using ZEN Blue. Highlighting of colocalized pixels was performed using the 'Colocalization' tool of ZEN Blue following setting conservative thresholds that were consistent across all images for a given experiment.

2.7. Multiple Sequence Alignments and In Silico Analyses

Sequence alignments of NS1 protein sequences were performed using Jalview software ver.2.11.1.4, with the following isolates (UniprotKB [Swiss-Prot accession no.]), as detailed: DENV-1 Brazil/97011/1997 strain (P27909); DENV-2 Thailand/16681-PDK-53 strain (P29991); DENV-3 Martinique/1243/1999 strain (Q6YMS3); DENV-4 Thailand/0348/1991 strain (Q2YHF0); West Nile virus (P06935), and Yellow Fever virus Ivory Coast/1999 (Q6J3PI) using the in-built ClustalW scoring algorithm. In silico analyses were conducted using the UCSF[®] Chimera software ver.1.13.1. on the established DENV-2 NS1 crystal structure derived from Protein Data Bank accession 4O6B.

2.8. In Vitro RNA Transcription and RNA Transfection

A total of 5 µg of plasmid DNA of interest was linearized overnight at 37 °C with *Xba*I before being purified using a Nucleospin[®] Gel and PCR Clean-up kit (Macherey-Nagel). In vitro RNA transcription was carried out via SP6 RNA polymerase reactions using a mMessage mMachine[®] Kit (Thermo Fisher Scientific) as per the manufacturer's instructions. Samples were treated with 1 µL of TURBO Dnase (Thermo Fisher Scientific) before proceeding to RNA isolation. In vitro RNA transcripts were purified using TRIreagent (Sigma-Aldrich), as per the manufacturer's instructions, and RNA pellets were resuspended in nuclease free water. The integrity of RNA transcripts was validated by agarose gel electrophoresis. For RNA transfection, cells were transfected with RNA transcripts using DMRIE-C transfection reagent (Thermo Fisher Scientific) in reduced serum Opti-MEM medium (Thermo Fisher Scientific) as per the manufacturer's instructions. The transfection medium was replaced by complete DMEM at 3–4 h post-transfection.

2.9. Infectivity Assays

Prior to conducting focus-forming unit (FFU) assays, virus-containing supernatants were collected at respective timepoints, cleared of cells and debris by centrifugation, and stored at -80 °C. To determine the viral titers, Huh-7.5 target cells were seeded into 96-wells plates at 2×10^4 cells/well a day prior to the infection. The cells were inoculated with 40 µL/well of serially diluted virus-containing supernatants. The cells were then cultured for 3 h before washing with PBS and returning to culture for 72 h. At 72 h post-infection, the cells were fixed with ice-cold acetone: methanol (1:1) for 15 min at 4 °C. The infected cell foci were enumerated following the indirect immunofluorescent labelling of the DENV capsid protein using the mouse anti-capsid monoclonal antibody (6F3.1, diluted 1:5 in 1% BSA/PBS) and the conjugated secondary antibody (Alexa Fluor 488, diluted 1:400 in 1% BSA/PBS). Virus infectivity was expressed as focus-forming units (FFU)/mL.

2.10. Graphics and Statistical Analyses

Several diagrams were created using the online tool platform, BioRender[®]. All graphs were generated using GraphPad Prism 9 software.

3. Results

3.1. Identification of DENV-2 NS1 Residues That Are Essential for Its Secretion via Random Point Mutagenesis and Luminescent Peptide Reporter Assays

A recent study identified a cluster of several highly conserved amino acid residues within the β -ladder domain of NS1, which are essential for NS1 secretion [44]. To further elucidate the molecular determinants of NS1 that are essential for its secretion, we generated a library of expression plasmid constructs encoding random NS1 point mutations and bearing a C-terminal HiBiT luminescent peptide tag. To screen for NS1 mutations that impact NS1 secretion, NS1 expression clones that resulted from PCR-based random point mutagenesis were transfected into cells prior to the measurement of extracellular and intracellular NS1-associated luminescence activities (Figure 1A). In this system, HiBiT-tagged proteins can be readily detected with the addition of the complementary binding partner “LgBiT”, which auto-associates with HiBiT-tagged proteins to generate a strong luminescence signal [48]. Thus, the luminescence signal generated is directly proportional to the amount of the HiBiT-tagged protein in the samples.

We prepared a collection of 173 potentially mutagenised NS1-HiBiT expression constructs, and an analysis of these constructs by HiBiT luciferase assays revealed numerous mutagenised NS1 expression clones with altered ratios of extracellular-to-intracellular NS1 luminescence activities (Figure 1B). As many of these constructs contained multiple mutations that complicated interpretations, only clones with a single coding point mutation and a >50% decrease in extracellular-to-intracellular luciferase activity ratios are depicted. Wildtype NS1-HiBiT generated an almost equivalent luciferase activity in intracellular and extracellular samples across each independent luciferase experiment. The NS1-SmBiT construct (negative control) yielded negligible levels of luminescence, which were similar to those of untransfected parental Huh-7.5 cells, consistent with the SmBiT peptide’s weak association with the LgBiT protein [48,49]. An NS1-HiBiT construct with an ER-retention motif, KDEL, displayed intracellular NS1 luminescence activity that was markedly higher than that of the corresponding extracellular NS1 samples. This indicated that the KDEL motif attached to the carboxy terminus of the NS1-mediated ER retention of the NS1-HiBiT protein, as anticipated, supporting its utility as a positive control for the inhibition of NS1 secretion. Extracellular-to-intracellular NS1 luminescence ratios were subsequently determined for each NS1 clone to identify clones bearing mutation(s) that impact NS1 secretion activity (Figure 1C). Several NS1 mutant clones displayed a greater than 50% decrease in NS1 secretion efficiency, and were submitted for Sanger sequencing.

Sanger sequencing revealed varying mutation frequencies among these NS1 mutant clones. To simplify interpretations, only those NS1 clones bearing single coding mutation(s) were considered for subsequent experiments. Accordingly, the identified mutants, E139K, S152L, D180Y, V220D, A248V, T283A, L298W, C313S, I335T, and R336S, were selected for *in silico* analyses. Although W210L and W232R were shown to exhibit a greater than 50% decrease in NS1 secretion efficiency, they were excluded from this study, given that their luminescence activities closely resembled those of the wild-type NS1-HiBiT-expressing cells and parental Huh-7.5 cells, respectively.

3.2. *In Silico* Analyses Indicate That the Majority of NS1 Secretion-Impairing Mutations Are Located within the Carboxy-Terminal Region of the β -Ladder

In silico modelling analyses were conducted to map and visualise the locations of NS1 secretion-impairing mutations on the established NS1 dimer crystal structure (Figure 2A,B). Interestingly, most of the NS1 secretion-impairing mutations identified in this study localised to the β -ladder domain (V220D, A248V, T283A, L298W, C313S, I335T, R336S), while two mutations flanking the second connector sub-domain (S152L and D180Y) interconnecting the Wing domain and β -ladder domain and one mutation within the Wing domain (E139K) were also identified (Figure 2C). Additionally, an alignment of NS1 amino acid residues of all DENV serotypes, as well as those of the West Nile virus (WNV) and Yellow

Fever virus (YFV), was conducted, revealing the position of each NS1 secretion-impaired mutation and their relative conservation across various NS1 protein sequences (Figure 3).

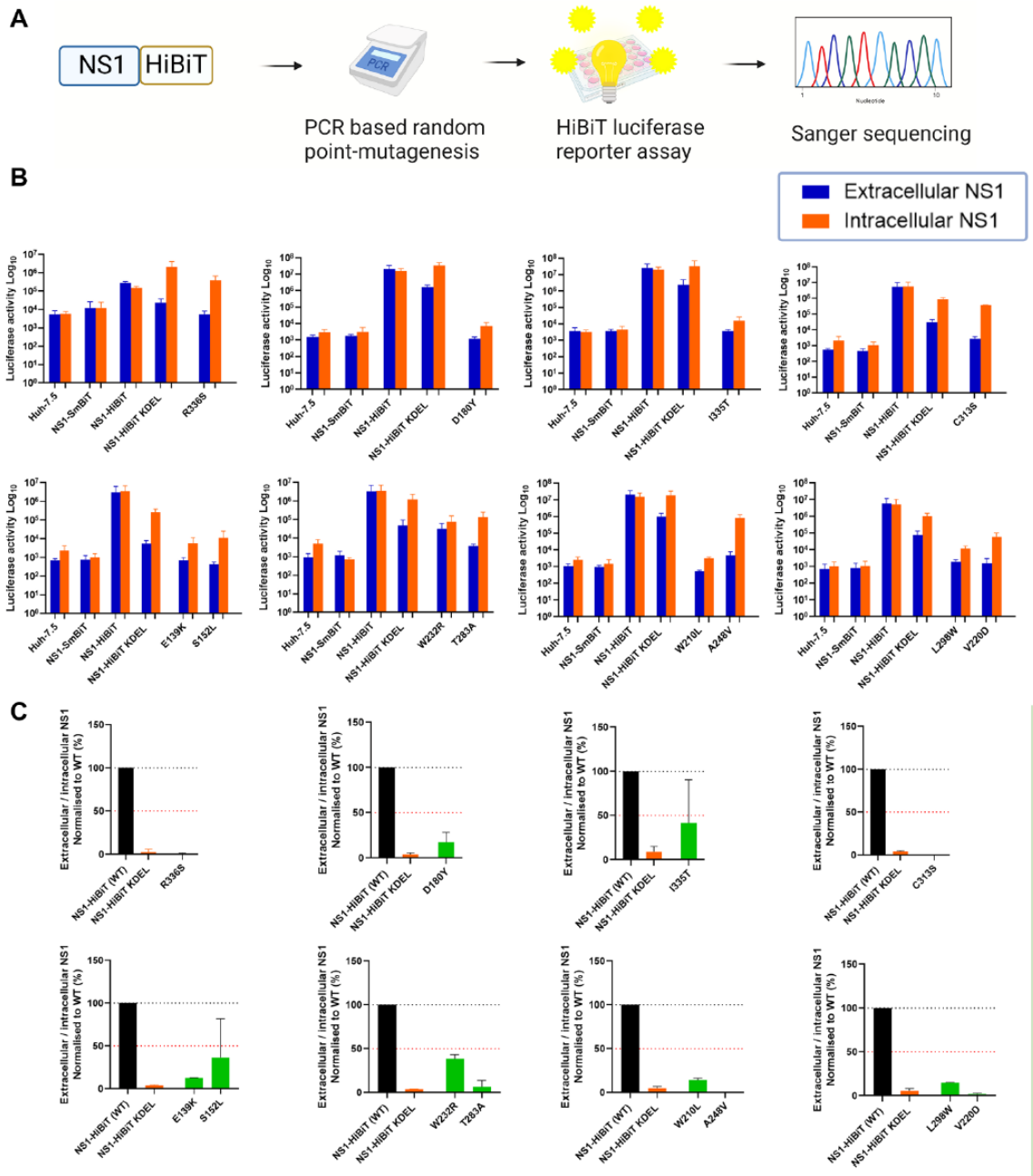


Figure 1. Identification of NS1 mutant clones with impaired NS1 protein secretion. (A) Schematic diagram of the experimental approach. Wild-type DENV-2 NS1 was subjected to PCR-based random point mutagenesis before incorporating the mutagenized NS1 into an expression plasmid construct containing the C-terminal HiBiT tag. Seeded Huh-7.5 cells were transiently transfected with the indicated NS1 expression plasmids, and supernatants and lysates were harvested at 48 h post-transfection. (B) Supernatants and lysates were collected from cells that were transfected with

NS1-SmBiT (negative control), NS1-HiBiT (wildtype), NS1-HiBiT KDEL (positive control for intracellular NS1 retention) or mutagenized NS1-HiBiT expression clones, as indicated, and probed for their luciferase activity via the Nano-Glo[®] HiBiT Lytic Detection System. Orange bars represent intracellular (lysate) samples, while blue bars represent extracellular (supernatant) samples. Data for mutagenized clones are only depicted for those clones that encoded a single amino acid substitution and displayed a >50% reduction in the ratio of the extracellular-to-intracellular luciferase activity. Data are presented as raw luciferase activity (relative light units [RLU]) means \pm SD of duplicates for each group, from two independent experiments. (C) Extracellular-to-intracellular NS1 luminescence ratios were determined for each sample in (B), and expressed as a percentage of wildtype NS1-HiBiT values. Black bars represent wildtype NS1-HiBiT, orange bars represent NS1-HiBiT KDEL, while green bars represent NS1-HiBiT point mutants, as indicated. A black dotted line is indicated at 100%, while a red dotted line is indicated at 50%. Data are means \pm SD of duplicates for each group from two independent experiments.

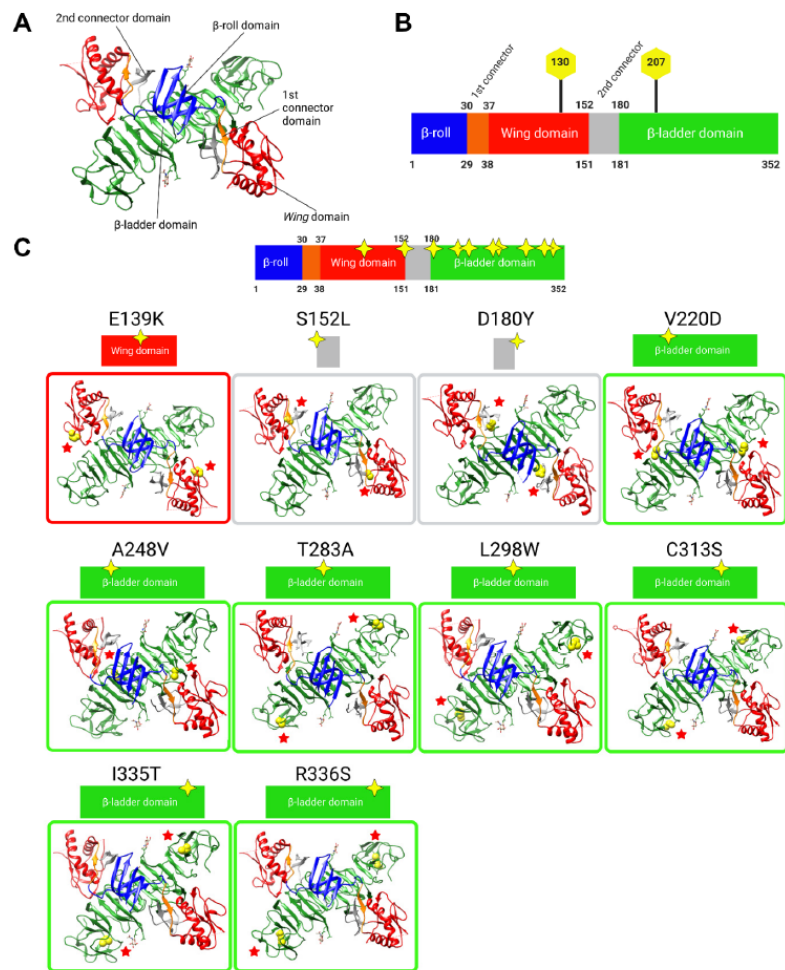


Figure 2. In silico analyses of the identified NS1 secretion-impaired mutants. (A) Three-dimensional structure of the NS1 dimer. (B) Schematic diagram representation of NS1 protein domains, which

have been color-coded to match those of the 3D dimer structure in (A). The residue locations of junctions between domains and N-glycosylation sites are indicated. (C) Overall in silico analyses of the 10 selected NS1 secretion-impaired mutants identified from Figure 1. Homology model of the 3D structure of NS1 dimer retrieved from Protein Data Bank entry 4O6B, with mutated residues portrayed as van der Waals spheres in yellow and indicated with red stars for easier visualisation. From left to right, the β -roll, 1st connector, Wing, 2nd connector, and β -ladder are highlighted in blue, orange, red, grey and green, respectively (A), and this color-coding is also maintained in the diagrams in (B) and graphics (C). Yellow stars indicate the approximate amino acid positions in each domain. In silico analyses were carried out using the UCSF[®] Chimera software ver.1.13.1.

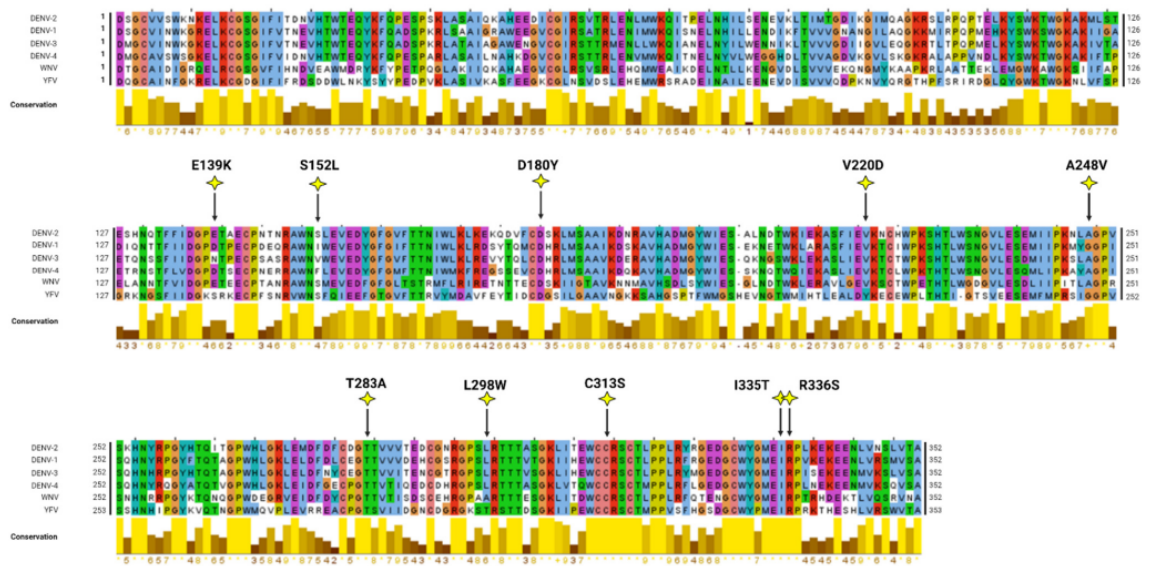


Figure 3. Multiple sequence alignment of various NS1 proteins. Alignment of NS1 amino acid sequences of different DENV serotypes and two related flaviviruses (West Nile virus [WNV], Yellow Fever virus [YFV]) was performed using the in-built ClustalW algorithm in Jalview. The graphical displays below the alignments show the relative amino acid conservation across the various NS1 sequences with yellow, indicating the highest degree of conservation across the sequences. The positions of the mutated residues are indicated as yellow stars within the NS1 amino acid sequence alignment.

3.3. Western Blot Analysis of Putative Secretion-Impairing NS1 Mutations

Given that our identification of NS1 secretion-impairing mutants was exclusively based on luciferase readout values (Figure 1), we further investigated the impairment of NS1 secretion activity by these NS1 mutants via Western blotting using a conformation-specific anti-NS1 antibody (mAb 4G4) (Figure 4A). Intracellular DENV-2 NS1 was strongly detected for wildtype (WT) NS1-HiBiT and KDEL-tagged NS1-HiBiT in cell lysates, while E139K, D180Y, and V220D NS1-HiBiT mutants were also readily detected in transfected cell lysates. Other NS1 mutants, including S152L, A248V, L298W, and I335T, appeared to be weakly expressed, while T283A, C313S, and R336S NS1 mutants could not be detected by Western blotting using this antibody. The extracellular DENV-2 NS1 protein was only detected in WT, E139K, S152L, and D180Y NS1 supernatant samples, while, as expected, NS1-HiBiT KDEL was not detected in supernatant samples, consistent with its expected retention in the ER.

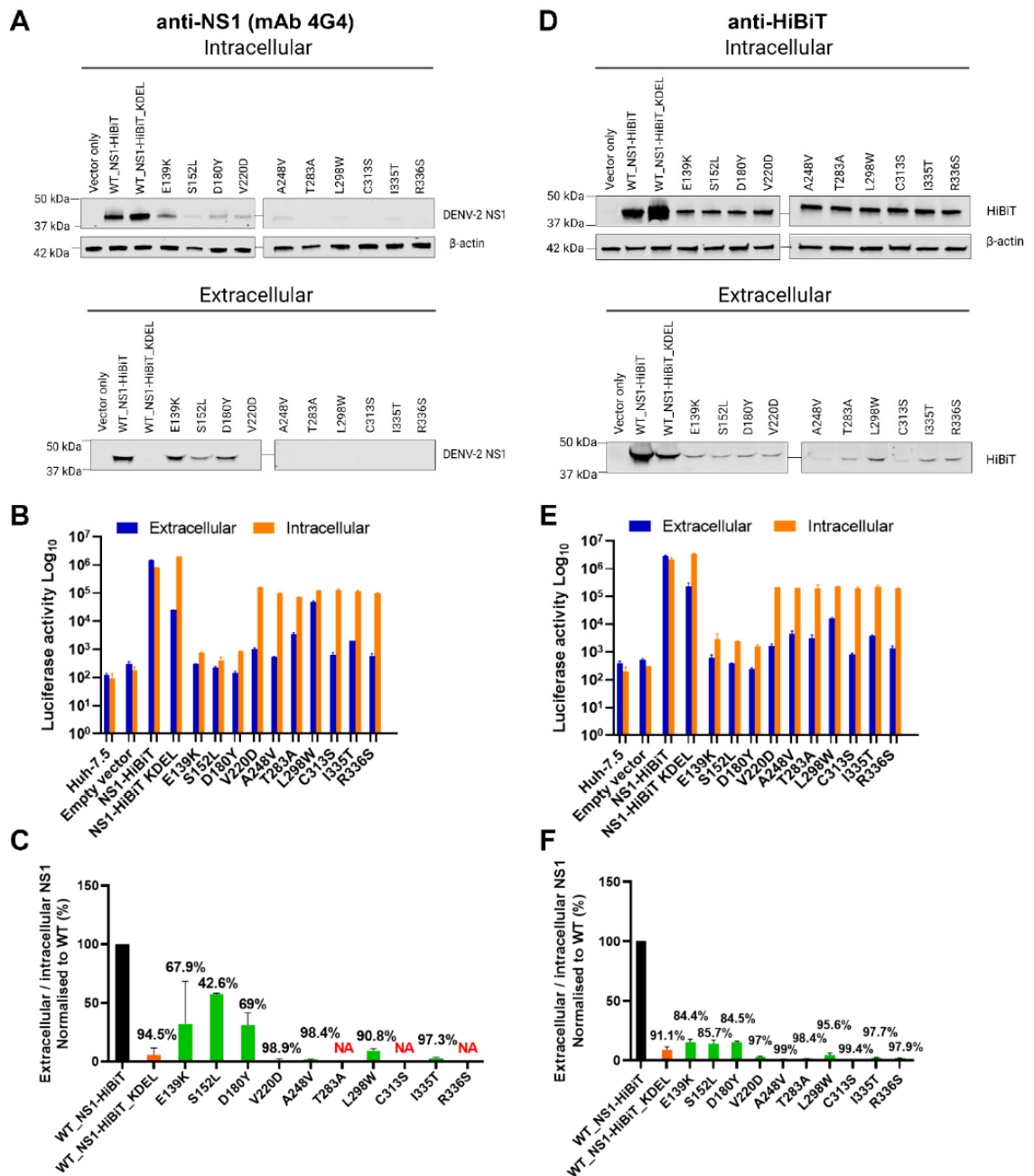


Figure 4. Western blot analysis of NS1 protein secretion efficiencies for putative NS1 secretion-defective mutants. (A,D) At 48 h post-transfection, supernatants (‘extracellular’) and cell lysates (‘intracellular’) were harvested from Huh-7.5 cells that were transfected with the indicated expression constructs, before subjecting samples to SDS-PAGE and Western blotting to detect DENV NS1 using a conformation-specific anti-NS1 antibody (A) or an anti-HiBiT tag antibody (D). β -actin was also detected in parallel as a loading control for lysate samples (A,D). (B,E) Lysate and supernatant

samples that were used in Western blotting (A,D) were also analysed via HiBiT luciferase assays (B,E). Orange bars represent intracellular (lysate) samples, while blue bars represent extracellular (supernatant) samples. (C,F) Quantitative analysis of Western blotting data obtained using anti-NS1 and anti-HiBiT antibodies (A,D, respectively). Extracellular-to-intracellular NS1-HiBiT mutant protein levels were expressed as a percentage of values for the respective wildtype control samples. Black bars represent wildtype NS1-HiBiT, orange bars represent NS1-HiBiT KDEL, while green bars represent NS1-HiBiT point mutants, as indicated. Data are means \pm SD from two independent replicates, with the values above each error bar indicating %-decrease in NS1 secretion efficiency compared to wildtype values. Note that NS1 mutants, T283A, C313S, and R336S were excluded from quantification analyses in (C) (NA; not assessed), given the inability to detect them by Western blotting (A).

To investigate whether the weak or undetectable expression of NS1 mutants in these Western blotting experiments could be attributed to inefficient transfection, lysates and supernatant samples from these experiments were also tested for intracellular and extracellular NS1 levels, respectively, via HiBiT luciferase reporter-based assays (Figure 4B). Intracellular NS1-associated luciferase activities were markedly higher than their corresponding extracellular values for the majority of these mutants, including V220D, A248V, T283A, L298W, C313S, I335T, and R336S, indicating that difficulties in detecting the expression of these mutants by anti-NS1 Western blotting cannot be attributed simply to low transfection efficiency (Figure 4B). DENV-2 NS1 Western blotting signals for each NS1 mutant, with the exception of T283A, C313S, and R336S, were also quantified before determining the extracellular-to-intracellular NS1 luminescence ratio (Figure 4C). The selected NS1 mutants displayed an impairment in the NS1 secretion efficiency, which is largely consistent with the results from the HiBiT-based luciferase reporter assays (Figure 1B,C).

Given difficulties in the detection of several NS1 mutant proteins using the conformation-specific anti-NS1 antibody, additional Western blotting studies using an anti-HiBiT peptide tag antibody were also performed. This revealed the ready detection of wildtype, KDEL-tagged, and mutant NS1-HiBiT proteins in intracellular lysate samples, although mutant constructs appeared to be expressed at lower levels than their wildtype and KDEL-tagged counterparts (Figure 4D). As expected, wildtype NS1-HiBiT was strongly detected in supernatants samples, while KDEL-tagged NS1-HiBiT was detected at an appreciably lower level in supernatant samples (Figure 4D). All NS1-HiBiT point mutants were detected at markedly reduced levels in supernatant samples (Figure 4D), with parallel analysis of HiBiT luciferase activity in lysate and supernatant samples largely reflecting the phenotypes that were observed via Western blot analysis (Figure 4E). A quantitative analysis of the NS1-HiBiT Western blot signals and an expression of these signals as normalised extracellular-to-intracellular NS1-HiBiT ratios was then performed (Figure 4F), and this largely confirmed the phenotypes that were observed in the original and Western-blot-parallel HiBiT luciferase assays (Figures 1C and 4E). Surprisingly, in some instances, there were moderate inconsistencies between the strength of the HiBiT signals between Western blots and luciferase assays performed using the same samples (Figure 4A,B,D,E). It is possible that this is attributable to mutation-induced changes in the accessibility of the HiBiT peptide to its complementary LgBiT partner in the HiBiT luciferase assays. Taken together, these studies confirm the secretion-impaired phenotypes of all 10 NS1-HiBiT point mutants and indicate that at least some of these mutations may impact the ability of NS1 to be recognised by a conformation-specific anti-NS1 monoclonal antibody.

3.4. NS1 Secretion-Impaired Mutants and Wildtype NS1 Display Strong Colocalisation with the ER

NS1 is thought to participate in the membrane rearrangements of the ER to form VPs that house viral RNA replication events [7,9,21,22]. We, therefore, sought to investigate whether the secretion-defective NS1 mutants that we identified also displayed altered localisation with regard to the ER. To this end, we transiently transfected Huh-7.5 cells

with NS1 expression constructs bearing their single point mutations, and assessed the localisation of NS1 with respect to the ER by high-resolution confocal imaging.

All of the mutants, including the positive control for intracellular retention, NS1-HiBiT KDEL, and the negative control NS1-SmBiT utilised in the HiBiT luciferase reporter assays (Figure 1) displayed DENV-2 NS1 staining patterns that were highly similar to those of the wildtype NS1-HiBiT (Figure 5A–C). NS1 and an ER-specific fluorescent dye were strongly colocalised in all groups, as highlighted by a separate visualisation of colocalised signals, as shown (white; right panels) (Figure 5A–C). Additionally, colocalization analysis across a large number of cells revealed no significant differences between the groups (Figure 5D), indicating that none of the mutations appeared to disrupt the localisation of NS1 to the ER.

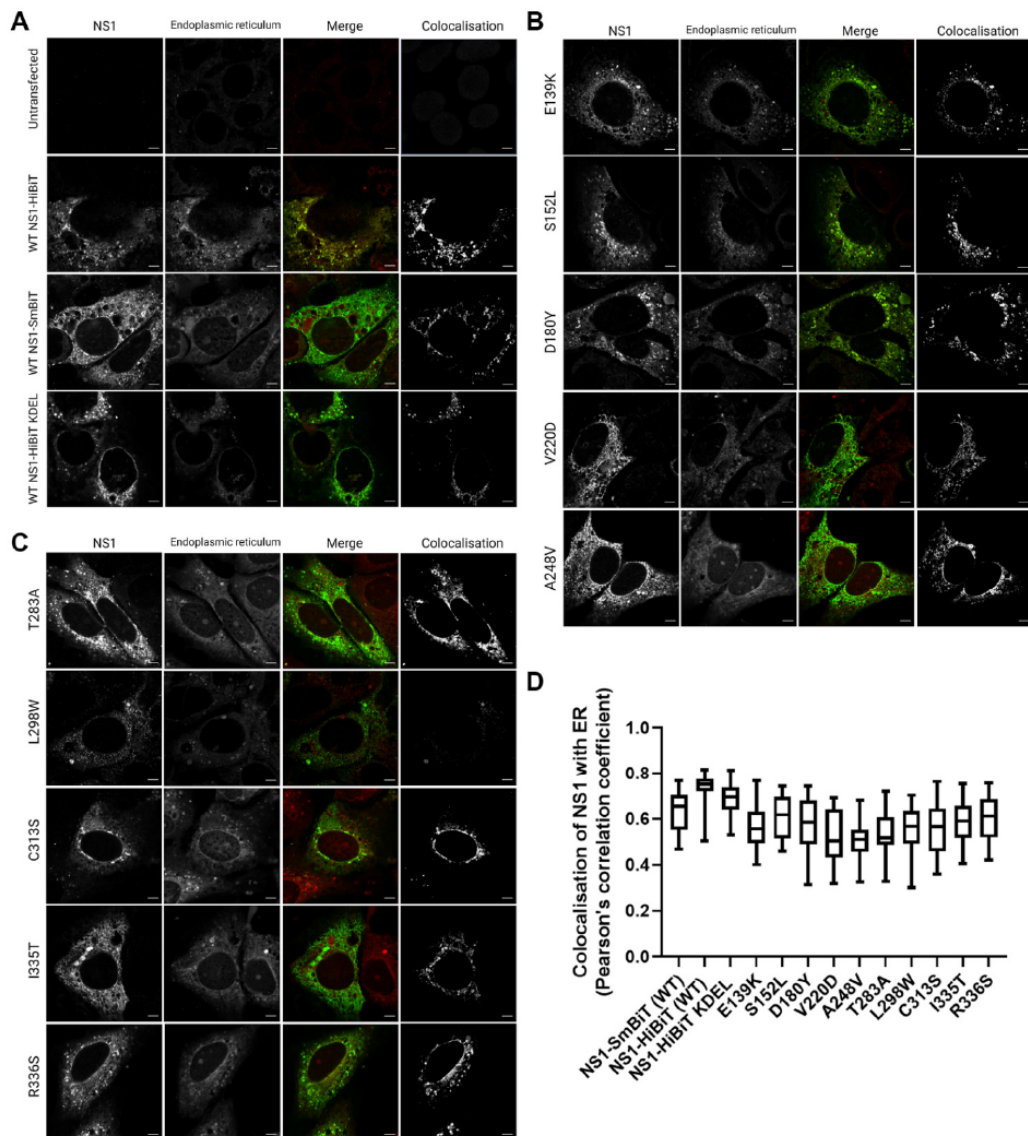


Figure 5. Identified secretion-improving mutations within DENV NS1 do not impact its localisation to the ER. Huh-7.5 cells were transiently transfected with DENV NS1 expression constructs bearing

respective NS1 secretion-impairing mutations and cultured overnight prior to fixation and fluorescent labelling. NS1 proteins (white, left column), endoplasmic reticulum (white, second column from the left), merged images (third column, with NS1 and ER staining pseudocolored green and red, respectively) and NS1-ER colocalised pixels (white, fourth column) are displayed in (A–C); (scale bars, 5 μ M). (D) Colocalization between ER and NS1 signals (Pearson’s correlation coefficient) was measured for 20–25 cells per sample group. Box and whiskers plot indicates median values, 25th to 75th percentiles, maximum and minimum values (n = 20–25 cells/group).

3.5. Effect of NS1 Secretion-Impairing Mutations on the DENV Replication Cycle

Given their strong impact on NS1 secretion, we next investigated the influence of V220D and A248V mutations on the DENV replication cycle. We also chose to compare the effects of these mutations to those of two glycosylation mutations, N130A and N207A, which have been previously shown to impact NS1 secretion [30,31,50]. *In vitro* RNA transcripts of full-length constructs were transfected into Huh-7.5 cells, and culture supernatants were harvested at 24, 48, 72, 96, and 120 h post-transfection for measurement of viral infectivity by focus-forming unit (FFU) assays (Figure 6A). As shown, V220D and A248V mutations prevented infectious virus production across all timepoints. Interestingly, both N130A and N207A mutants were associated with marked increases in infectious virus production. In this particular context, a previous study showed that an N130Q mutation resulted in infectious virus titres that were similar to those of wildtype DENV [29].

To determine if the phenotypes observed for the V220D and A248V mutants were due to an impairment of viral RNA replication rather than a defect in infectious viral particle production, we also assessed the effects of these mutations on viral RNA replication. To this end, we incorporated these mutations into a sub-genomic replicon construct (sgDV_s-R2A) that encodes a Renilla luciferase reporter [47]. Huh-7.5 cells were transfected with *in vitro* RNA transcripts for respective replicon constructs, and lysates were harvested at 4, 24, 48, and 72 h timepoints for measurement of luciferase activity as a readout of viral RNA replication/translation, compared to wildtype sgDV_s-R2A and a replication-defective ‘GND’ control replicon (Figure 6B). While N130A and N207A mutant replicons displayed replication kinetics that were similar to that of the wildtype sub-genomic replicon, V220D and A248V mutants displayed steadily declining luciferase activities that reflected those of the replication-defective GND control. Together, this indicates that V220D and A248V mutations in NS1 prevent DENV-2 RNA replication, while mutations to N-glycosylation sites, N130A and N207A, were associated with unchanged viral RNA replication levels but moderated the elevated production of the infectious virus.

3.6. Utilisation of a Replication-Independent Expression System (pIRO) to Further Characterise Selected NS1 Secretion-Impaired Mutants

Given that the NS1 secretion-impaired mutants V220D and A248V were also replication-defective, we also further investigated the impact of these mutations using a recently established replication-independent expression system termed “pIRO” (plasmid-induced replication organelle formation) that induces the biogenesis of VPs that morphologically resemble conventional VPs generated in infected cells [51]. For this, we individually incorporated our mutations of interest, N130A, N207A, V220D, and A248V, into the pIRO expression construct using site-directed mutagenesis. To determine if these mutations induce any distinctive changes in the colocalization staining pattern between NS1 and NS4B, we transfected Huh-7.5 cells with the wildtype and mutant pIRO expression constructs 24 h prior to fixation, immunofluorescent staining of NS1 and NS4B, and high-resolution confocal imaging analyses (Figure 7A).

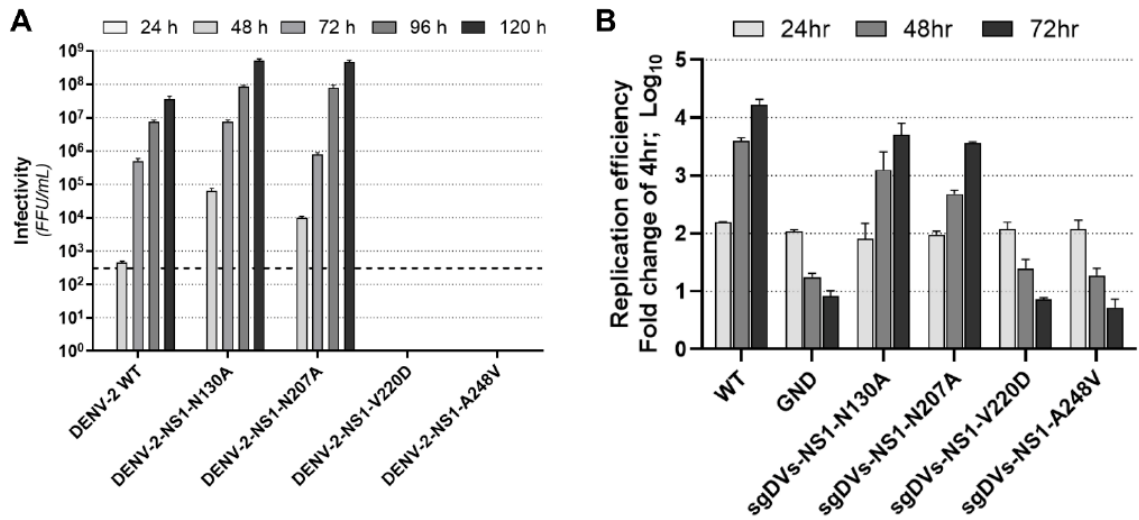


Figure 6. NS1 secretion-impairing mutations V220D and A248V prevent viral RNA replication and infectious virus production. (A) Infectious virus production by Huh-7.5 cells following transfection with wildtype (WT) DENV-2 RNA transcripts or derivatives containing NS1 secretion-impairing mutations (V220D or A248V) or N-linked glycosylation mutations (N130A or N207A), as indicated. Culture supernatants were harvested at indicated timepoints from 24 to 120 h post-transfection. Infectivity of viral particles within supernatants was determined by focus-forming unit (FFU) assay. Data are presented as means \pm SD from three independent replicates. The dashed line indicates the limit of detection for the assay. (B) Replicative fitness of NS1 mutants in the context of a Renilla luciferase reporter encoding sub-genomic replicon construct (sgDVs-R2A). NS1 mutations in (A) were incorporated into sgDVs-R2A and in vitro transcribed RNA for each construct was transfected into Huh-7.5 cells. Luciferase activities were measured for lysates harvested at 4, 24, 48, and 72 h post-transfection. For each construct, raw luciferase values were expressed as a fold change relative to the average values for the 4 h timepoint (a measurement of input RNA) to determine replication efficiency. A replication-deficient lethal mutation within NS5 (GND) that disrupts NS5 RNA-dependent RNA polymerase activity was included as a negative control. Data are presented as means \pm S.D from three independent replicates ($n = 3$).

The pIRO-D mutants dictated similar NS1 and NS4B staining patterns in comparison to WT pIRO-D, although typical juxtannuclear NS1- and NS4B-positive foci were less frequently observed for N130A, V220D, and A248V mutants compared to wildtype. Colocalization analyses revealed no significant difference in NS1-NS4B colocalization (Figure 7B), suggesting that none of these mutations alter the association between NS1 and NS4B. However, NS1 in pIRO-D V220D and pIRO-D A248V lysates was not readily detected by Western blotting (Figure 7C), which was unexpected given our earlier results demonstrating that the same mutant NS1 proteins were detectable, albeit at low levels, when expressed in the context of NS1-HiBiT expression constructs (Figure 4A). In contrast, intracellular NS1 was strongly detected for WT, pIROD-N130A and pIROD-N207A. Extracellular NS1 was also detected in supernatants for WT, pIROD-N130A and pIROD-N207A, while NS3 was detected at a similar level in lysates of WT and all four pIRO-D mutants, indicating similar transfection efficiencies and NS protein expression levels across all pIRO-D transfected samples.

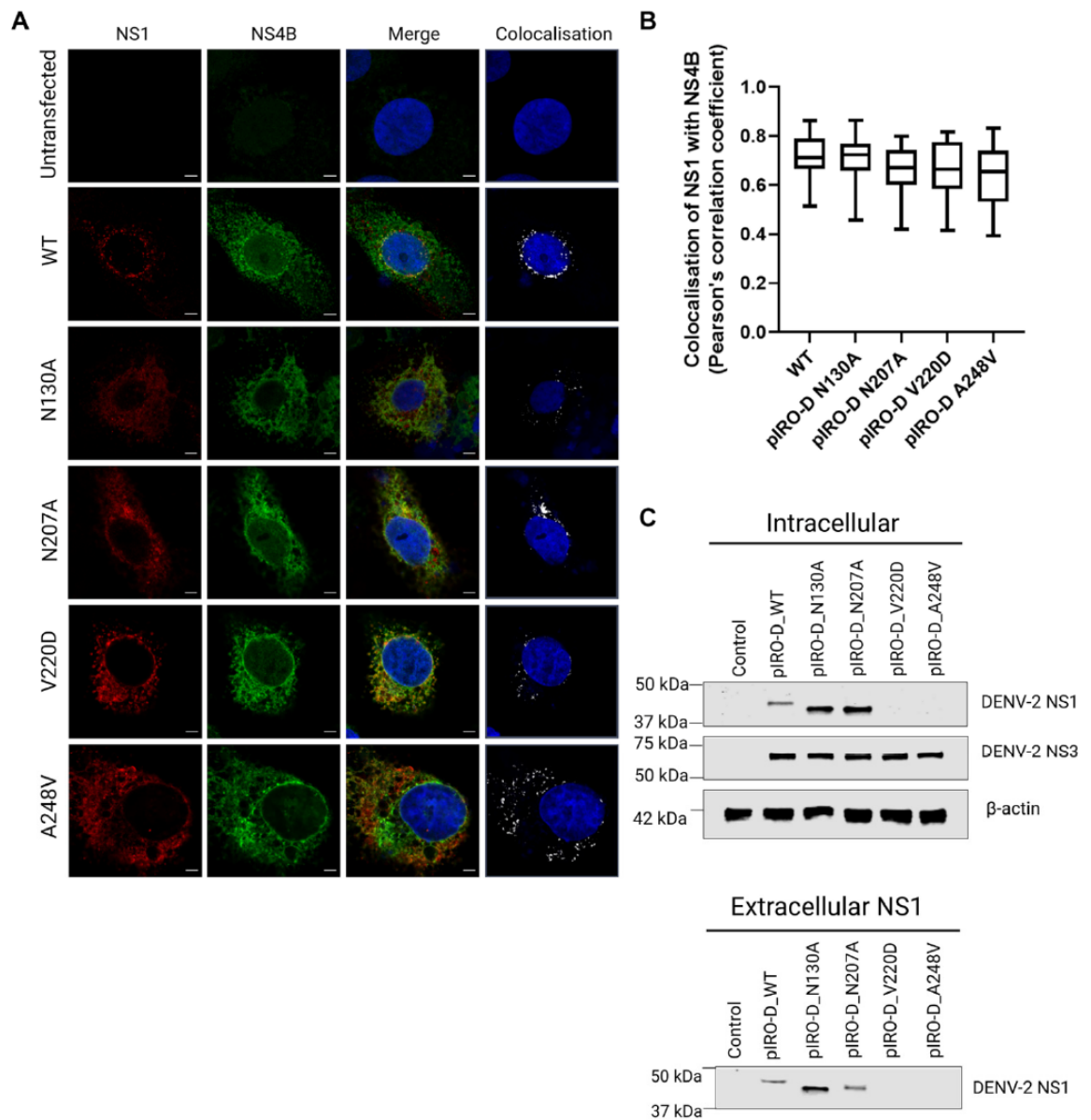


Figure 7. Characterisation of NS1 mutants using a replication-independent expression system (pIRO). (A) Near-confluent Huh-7.5 cells were transfected with pIRO expression constructs containing the indicated NS1 mutations (N130A/ N207A/ V220D/ A248V) and cultured overnight prior to fixation and immunolabelling. Confocal images of NS1 protein (red, left column), NS4B proteins (green, second column from the left), nuclei (blue), colocalization between NS1 and NS4B proteins in merge images (yellow, third column) or colocalization panels (white, fourth column) are depicted. Scale bars are 5 μ m. (B) Quantification of colocalization between NS1 and NS4B for >30 identified cells/group. Box and whiskers plot indicates median values, 25th to 75th percentiles, maximum and minimum values ($n = 30$ – 32 cells/group). (C) Huh-7.5 were transiently transfected with the indicated pIRO expression constructs 48 h prior to collection of cell lysates and supernatants for Western blotting using antibodies NS1-, NS3- and β -actin, as indicated.

4. Discussion

Since its initial identification and characterisation in the 1970s, NS1 has been one of the most heavily studied flaviviral proteins. Over the years, it has emerged that this enigmatic viral non-structural protein is essential for viral RNA replication and infectious virus production, while the secreted form of NS1 is involved in a variety of extracellular functions strongly linked with flaviviral disease pathogenesis. Despite this, the exact molecular features of NS1 that are essential for its secretion remain unclear.

In this study, we applied random point mutagenesis, sensitive luciferase-based expression assays, and molecular virology approaches to identify NS1 residues that are required for NS1 secretion, and subsequently investigated the impact of two of these identified mutations on aspects of the DENV life cycle. There are several advantages and disadvantages of our chosen random point mutagenesis-coupled HiBiT luciferase assay screening approach in which we only sequenced clones with a >50% reduction in NS1 secretion efficiency. While this approach enables a simple, rapid, unbiased, and relatively inexpensive identification of secretion-defective NS1 mutants, despite attempts to carefully control PCR-based mutagenesis rates to result in one mutation per clone, many of the secretion-defective NS1 clones contained several or multiple mutations that could not be disentangled from one another without subsequent site-directed mutagenesis and follow-up experimentation. Conversely, as we chose not to sequence and characterise clones that displayed near-normal NS1 secretion, it is arguable that we missed the opportunity to identify residues and regions of NS1 that are not involved in its secretion. Furthermore, while our NS1-HiBiT expression approach enabled a simple and relatively rapid screening of approximately 170 clones for changes in the efficiency of NS1 secretion, mutations that specifically disrupted NS1 secretion could not be readily distinguished from mutations that indirectly affected NS1 secretion, as might be the result of NS1 mis-folding or failure to dimerise. For these given reasons, it remains important to consider that there are several potential reasons that a given NS1 mutant may display altered secretion and that detailed analysis in the context of a full-length infectious virus is essential to fully appreciate the underlying impact of a given mutation.

Relevant to our study, Plaszczyca et al. (2019) identified an NS1 secretion-impairing mutation, D136A, within the Wing domain, as well as a series of NS1 secretion-impairing mutations, W311A, P319A, P320A, E334A, and R336A within the C-terminal β -ladder domain [44]. Consistent with that study, our analyses also identified Arg-336 as an important determinant of NS1 secretion as its mutation (R336S) similarly inhibited NS1 secretion in our HiBiT-tagged expression system. Of note, Arg-336 has also been shown to be essential for viral RNA replication, indicating that this residue is important for multiple functions of NS1, and perhaps correct NS1 maturation and/or interactions may be disrupted by its mutation [22]. It is also noteworthy that several of the NS1 secretion-defective mutations that we identified, E139K, C313S, and I335T, mapped in close proximity to NS1 secretion-defective mutations that were identified by Plaszczyca et al.; namely, D136A, W311A, E334A and R336A [44]. This supports the interpretation that these sub-domains are important for NS1 secretion, and that the solvent-exposed nature of these sites within the C-terminus of the β -ladder and, to a lesser extent, the Wing domain may mediate NS1 interactions that are important for its secretion.

Intriguingly, NS1 protein was not readily detected in transfected cell lysates or supernatants for several NS1 mutants when analysed by Western blotting using a conformation-specific anti-NS1 antibody. This could not be simply attributed to inefficient transfection, as many of the mutant NS1 proteins that could not be detected by Western blotting nonetheless displayed robust HiBiT luciferase assay values in the same lysates. The inability to detect NS1 mutants in several lysate and supernatant samples using the conformation-specific anti-NS1 antibody could be potentially attributed to mutation-mediated disruption of residues that are involved in the binding of this antibody or impairment of correct NS1 folding and/or maturation, such that the protein cannot be recognised by the antibody. In support of this possibility, Western blot studies using an anti-HiBiT peptide tag antibody

revealed ready detection of all mutant proteins and confirmed the secretion-impaired phenotypes of these mutants that were indicated by HiBiT luciferase assays.

Interestingly, the mutations that altered NS1 secretion efficiency did not cause dramatic changes in the localisation of NS1 protein or its colocalization with the ER. This indicates that the impaired secretion of these NS1 mutant proteins cannot be easily attributed to the gross mislocalisation of the protein, although more detailed analyses are required to determine whether these mutations induce more subtle changes in NS1 localisation. In regard to the discrepancies between the detection of many of these NS1 mutant proteins by immunofluorescence but not Western blotting using the same antibody, it is possible that the mutant proteins are much more sensitive than wildtype NS1 to sample the processing steps involved in Western blotting, such as lysis in strong detergents and boiling, as compared to less destructive steps involved in immunofluorescent labelling. Future studies of the localization of these NS1 mutant proteins using anti-NS1 antibodies that recognize linear epitopes may help to clarify whether the secretion-impairing mutations indeed alter NS1 localization within cells.

Given that N-glycans within DENV NS1 are likely involved in NS1 secretion and NS1 dimer stability, we decided to include two N-glycosylation mutants, N130A and N207A, in our studies [29–31]. Both V220D and A248V mutants did not support DENV RNA replication or infectious virus production, indicating that these relatively highly conserved residues are critical to multiple NS1 functions. In contrast, both N-glycosylation mutants displayed RNA replication and virus particle production levels that were similar to those of the wildtype virus, which is largely consistent with previous reports [29,50].

Taken together, our findings suggest that mutating the relatively highly conserved residues V220 and A248 may lead to conformational changes in the NS1 structure resulting in its inherent instability or improper folding. For example, the introduction of a charged aspartate residue in place of the hydrophobic valine residue in the V220D mutant may disrupt intramolecular or intermolecular interactions within this ‘spaghetti loop’ region of the β -ladder to disrupt folding and conformation. In contrast, the conservative A248V substitution in the same domain is perhaps less likely to greatly alter NS1 conformation. It was initially considered that these mutations may cause NS1 mislocalisation, thereby disrupting viral replication and viral particle production in the process. However, heterologously expressed NS1-V220D and NS1-A248V displayed localisation profiles and colocalization with the endoplasmic reticulum that were similar to those of heterologously expressed wildtype NS1. Additionally, both NS1 mutants colocalised with NS4B when expressed via T7 RNA polymerase in the context of an NS1-NS5 polyprotein, which suggests that their interaction with NS4B is not overtly affected or compromised. This possibility was investigated, given the previous demonstration that NS1 may play a role in the stabilisation of membranous viral replication complexes, via its interaction with NS4B [19,20,22].

In summary, this study has demonstrated the utility of combining the random mutagenesis of NS1 and the HiBiT luminescent peptide tagging system in the rapid and simple identification of NS1 secretion-impairing mutants. Using this system, we have identified ten point mutations associated with an impairment in NS1 secretion, with two mutations (V220D and A248V) shown to also be critical for viral RNA replication. We suggest that future identification of mutations that prevent NS1 secretion but do not markedly attenuate viral fitness will reveal new details about dengue virus biology and may represent a promising strategy towards the development of an attenuated vaccine to combat DENV.

Supplementary Materials: The following supporting information can be downloaded at: <https://www.mdpi.com/article/10.3390/v15051102/s1>. Table S1: Antibodies and Dyes [52]; Table S2: Oligonucleotide sequences (5' to 3').

Author Contributions: Conceptualization, N.S.E., M.R.B. and B.E.K.T.; Methodology, N.S.E. and B.E.K.T.; Formal analysis, B.E.K.T.; Resources, N.S.E. and M.R.B.; Data curation, B.E.K.T.; Writing—original draft preparation, B.E.K.T.; Writing—review and editing, N.S.E., M.R.B. and B.E.K.T.; Super-

vision, N.S.E. and M.R.B.; Funding acquisition, N.S.E. and M.R.B. All authors have read and agreed to the published version of the manuscript.

Funding: This research was funded by a grant from the National Health and Medical Research Council (NHMRC, Australia) (1163662) N.S.E.

Institutional Review Board Statement: The study was approved by the Institutional Biosafety Committee of Flinders University (approval number 2021-05).

Informed Consent Statement: Not applicable.

Data Availability Statement: Original data files are available on request.

Acknowledgments: We thank the following people for generously providing reagents (as detailed in Material and Methods): Ralf Bartenschlager (University of Heidelberg); Charles Rice (Rockefeller University); Roy Hall (University of Queensland); Jody Peters (University of Queensland); John Aaskov (Queensland University of Technology); Sally Plush (University of South Australia). The authors acknowledge the facilities, and the scientific and technical assistance of Microscopy Australia and the Australian National Fabrication Facility (ANFF) under the National Collaborative Research Infrastructure Strategy, at the South Australian Regional Facility, Flinders Microscopy and Microanalysis (FMMA), Flinders University.

Conflicts of Interest: All authors declare no conflicts of interest. The funding sponsors had no direct and specific roles in the design of the study, interpretation of the data, manuscript writing, and the decision to publish the results.

References

- Bhatt, S.; Gething, P.W.; Brady, O.J.; Messina, J.P.; Farlow, A.W.; Moyes, C.L.; Drake, J.M.; Brownstein, J.S.; Hoen, A.G.; Sankoh, O. The global distribution and burden of dengue. *Nature* **2013**, *496*, 504–507. [[CrossRef](#)] [[PubMed](#)]
- WHO. *Dengue Guidelines for Diagnosis, Treatment, Prevention and Control*, 3rd ed.; World Health Organisation and the Special Programme for Research and Training in Tropical Diseases (TDR): Geneva, Switzerland, 2009; pp. 1–147.
- Narvaez, F.; Gutierrez, G.; Pérez, M.A.; Elizondo, D.; Nuñez, A.; Balmaseda, A.; Harris, E. Evaluation of the traditional and revised WHO classifications of dengue disease severity. *PLoS Negl. Trop. Dis.* **2011**, *5*, e1397. [[CrossRef](#)] [[PubMed](#)]
- WHO. *Dengue and Severe Dengue Facts Sheets*; World Health Organization: Geneva, Switzerland, 2020.
- Acosta, E.G.; Kumar, A.; Bartenschlager, R. Revisiting dengue virus–host cell interaction: New insights into molecular and cellular virology. *Adv. Virus Res.* **2014**, *88*, 1–109. [[CrossRef](#)] [[PubMed](#)]
- Bartenschlager, R.; Miller, S. Molecular aspects of Dengue virus replication. *Future Microbiol.* **2008**, *3*, 155–165. [[CrossRef](#)] [[PubMed](#)]
- Mackenzie, J.M.; Jones, M.K.; Young, P.R. Immunolocalization of the dengue virus nonstructural glycoprotein NS1 suggests a role in viral RNA replication. *Virology* **1996**, *220*, 232–240. [[CrossRef](#)] [[PubMed](#)]
- Grief, C.; Galler, R.; Côrtes, L.; Barth, O. Intracellular localisation of dengue-2 RNA in mosquito cell culture using electron microscopic in situ hybridisation. *Arch. Virol.* **1997**, *142*, 2347–2357. [[CrossRef](#)] [[PubMed](#)]
- Welsch, S.; Miller, S.; Romero-Brey, I.; Merz, A.; Bleck, C.K.; Walther, P.; Fuller, S.D.; Antony, C.; Krijnse-Locker, J.; Bartenschlager, R. Composition and three-dimensional architecture of the dengue virus replication and assembly sites. *Cell Host Microbe* **2009**, *5*, 365–375. [[CrossRef](#)]
- Novoa, R.R.; Calderita, G.; Arranz, R.; Fontana, J.; Granzow, H.; Risco, C. Virus factories: Associations of cell organelles for viral replication and morphogenesis. *Biol. Cell* **2005**, *97*, 147–172. [[CrossRef](#)]
- Gillespie, L.K.; Hoenen, A.; Morgan, G.; Mackenzie, J.M. The endoplasmic reticulum provides the membrane platform for biogenesis of the flavivirus replication complex. *J. Virol.* **2010**, *84*, 10438–10447. [[CrossRef](#)]
- Winkler, G.; Randolph, V.B.; Cleaves, G.R.; Ryan, T.E.; Stollar, V. Evidence that the mature form of the flavivirus non-structural protein NS1 is a dimer. *Virology* **1988**, *162*, 187–196. [[CrossRef](#)]
- Mason, P.W. Maturation of Japanese encephalitis virus glycoproteins produced by infected mammalian and mosquito cells. *Virology* **1989**, *169*, 354–364. [[CrossRef](#)] [[PubMed](#)]
- Muller, D.A.; Young, P.R. The flavivirus NS1 protein: Molecular and structural biology, immunology, role in pathogenesis and application as a diagnostic biomarker. *Antivir. Res.* **2013**, *98*, 192–208. [[CrossRef](#)]
- Lindenbach, B.D.; Rice, C.M. trans-Complementation of yellow fever virus NS1 reveals a role in early RNA replication. *J. Virol.* **1997**, *71*, 9608–9617. [[CrossRef](#)] [[PubMed](#)]
- Khromykh, A.A.; Kenney, M.T.; Westaway, E.G. trans-Complementation of flavivirus RNA polymerase gene NS5 by using Kunjin virus replicon-expressing BHK cells. *J. Virol.* **1998**, *72*, 7270–7279. [[CrossRef](#)] [[PubMed](#)]
- Khromykh, A.A.; Sedlak, P.L.; Guyatt, K.J.; Hall, R.A.; Westaway, E.G. Efficient trans-complementation of the flavivirus kunjin NS5 protein but not of the NS1 protein requires its coexpression with other components of the viral replicase. *J. Virol.* **1999**, *73*, 10272–10280. [[CrossRef](#)] [[PubMed](#)]

18. Khromykh, A.A.; Sedlak, P.L.; Westaway, E.G. cis-and trans-acting elements in flavivirus RNA replication. *J. Virol.* **2000**, *74*, 3253–3263. [[CrossRef](#)]
19. Youn, S.; Li, T.; McCune, B.T.; Edeling, M.A.; Fremont, D.H.; Cristea, I.M.; Diamond, M.S. Evidence for a genetic and physical interaction between nonstructural proteins NS1 and NS4B that modulates replication of West Nile virus. *J. Virol.* **2012**, *86*, 7360–7371. [[CrossRef](#)] [[PubMed](#)]
20. Youn, S.; Ambrose, R.L.; Mackenzie, J.M.; Diamond, M.S. Non-structural protein-1 is required for West Nile virus replication complex formation and viral RNA synthesis. *Virol. J.* **2013**, *10*, 339. [[CrossRef](#)] [[PubMed](#)]
21. Eyre, N.S.; Johnson, S.M.; Eltahla, A.A.; Aloji, M.; Aloia, A.L.; McDevitt, C.A.; Bull, R.A.; Beard, M.R. Genome-Wide Mutagenesis of Dengue Virus Reveals Plasticity of the NS1 Protein and Enables Generation of Infectious Tagged Reporter Viruses. *J. Virol.* **2017**, *91*, e01455-17. [[CrossRef](#)]
22. Scaturro, P.; Cortese, M.; Chatel-Chaix, L.; Fischl, W.; Bartenschlager, R. Dengue Virus Non-structural Protein 1 Modulates Infectious Particle Production via Interaction with the Structural Proteins. *PLoS Pathog.* **2015**, *11*, e1005277. [[CrossRef](#)]
23. Gutsche, I.; Coulibaly, F.; Voss, J.E.; Salmon, J.; d’Alayer, J.; Ermonval, M.; Larquet, E.; Charneau, P.; Krey, T.; Megret, F.; et al. Secreted dengue virus nonstructural protein NS1 is an atypical barrel-shaped high-density lipoprotein. *Proc. Natl. Acad. Sci. USA* **2011**, *108*, 8003–8008. [[CrossRef](#)] [[PubMed](#)]
24. Benfrid, S.; Park, K.H.; Dellarole, M.; Voss, J.E.; Tamiotti, C.; Pehau-Arnaudet, G.; Raynal, B.; Brûlé, S.; England, P.; Zhang, X. Dengue virus NS1 protein conveys pro-inflammatory signals by docking onto high-density lipoproteins. *EMBO Rep.* **2022**, *23*, e53600. [[CrossRef](#)] [[PubMed](#)]
25. Shu, B.; Ooi, J.; Tan, A.; Ng, T.-S.; Dejnirattisai, W.; Mongkolsapaya, J.; Fibriansah, G.; Shi, J.; Kostyuchenko, V.; Screaton, G. CryoEM structures of the multimeric secreted NS1, a major factor for dengue hemorrhagic fever. *Nat. Commun.* **2022**, *13*, 6756. [[CrossRef](#)] [[PubMed](#)]
26. Akey, D.L.; Brown, W.C.; Dutta, S.; Konwerski, J.; Jose, J.; Jurkiw, T.J.; DelProposto, J.; Ogata, C.M.; Skinotis, G.; Kuhn, R.J.; et al. Flavivirus NS1 structures reveal surfaces for associations with membranes and the immune system. *Science* **2014**, *343*, 881–885. [[CrossRef](#)]
27. Akey, D.L.; Brown, W.C.; Jose, J.; Kuhn, R.J.; Smith, J.L. Structure-guided insights on the role of NS1 in flavivirus infection. *Bioessays* **2015**, *37*, 489–494. [[CrossRef](#)]
28. Pryor, M.J.; Wright, P.J. Glycosylation mutants of dengue virus NS1 protein. *J. Gen. Virol.* **1994**, *75*, 1183–1187. [[CrossRef](#)]
29. Crabtree, M.; Kinney, R.; Miller, B. Deglycosylation of the NS1 protein of dengue 2 virus, strain 16681: Construction and characterization of mutant viruses. *Arch. Virol.* **2005**, *150*, 771–786. [[CrossRef](#)]
30. Somnuk, P.; Hauhart, R.E.; Atkinson, J.P.; Diamond, M.S.; Avirutnan, P. N-linked glycosylation of dengue virus NS1 protein modulates secretion, cell-surface expression, hexamer stability, and interactions with human complement. *Virology* **2011**, *413*, 253–264. [[CrossRef](#)]
31. Wang, C.; Puerta-Guardo, H.; Biering, S.B.; Glasner, D.R.; Tran, E.B.; Patana, M.; Gomberg, T.A.; Malvar, C.; Lo, N.T.; Espinosa, D.A. Endocytosis of flavivirus NS1 is required for NS1-mediated endothelial hyperpermeability and is abolished by a single N-glycosylation site mutation. *PLoS Pathog.* **2019**, *15*, e1007938. [[CrossRef](#)]
32. Young, P.R.; Hilditch, P.A.; Bletchly, C.; Halloran, W. An antigen capture enzyme-linked immunosorbent assay reveals high levels of the dengue virus protein NS1 in the sera of infected patients. *J. Clin. Microbiol.* **2000**, *38*, 1053–1057. [[CrossRef](#)]
33. Libraty, D.H.; Young, P.R.; Pickering, D.; Endy, T.P.; Kalayanarooj, S.; Green, S.; Vaughn, D.W.; Nisalak, A.; Ennis, F.A.; Rothman, A.L. High circulating levels of the dengue virus nonstructural protein NS1 early in dengue illness correlate with the development of dengue hemorrhagic fever. *J. Infect. Dis.* **2022**, *186*, 1165–1168. [[CrossRef](#)] [[PubMed](#)]
34. Avirutnan, P.; Punyadee, N.; Noisakran, S.; Komoltri, C.; Thiemmecca, S.; Auethavornanan, K.; Jairungsri, A.; Kanlaya, R.; Tangthawornchaikul, N.; Puttikhunt, C. Vascular leakage in severe dengue virus infections: A potential role for the nonstructural viral protein NS1 and complement. *J. Infect. Dis.* **2006**, *193*, 1078–1088. [[CrossRef](#)]
35. Avirutnan, P.; Fuchs, A.; Hauhart, R.E.; Somnuk, P.; Youn, S.; Diamond, M.S.; Atkinson, J.P. Antagonism of the complement component C4 by flavivirus nonstructural protein NS1. *J. Exp. Med.* **2010**, *207*, 793–806. [[CrossRef](#)] [[PubMed](#)]
36. Falconar, A. The dengue virus nonstructural-1 protein (NS1) generates antibodies to common epitopes on human blood clotting, integrin/adhesin proteins and binds to human endothelial cells: Potential implications in haemorrhagic fever pathogenesis. *Arch. Virol.* **1997**, *142*, 897–916. [[CrossRef](#)] [[PubMed](#)]
37. Falconar, A.K. Antibody responses are generated to immunodominant ELK/KLE-type motifs on the nonstructural-1 glycoprotein during live dengue virus infections in mice and humans: Implications for diagnosis, pathogenesis, and vaccine design. *Clin. Vaccine Immunol.* **2007**, *14*, 493–504. [[CrossRef](#)]
38. Avirutnan, P.; Hauhart, R.E.; Somnuk, P.; Blom, A.M.; Diamond, M.S.; Atkinson, J.P. Binding of flavivirus nonstructural protein NS1 to C4b binding protein modulates complement activation. *J. Immunol.* **2011**, *187*, 424–433. [[CrossRef](#)]
39. Yin, Y.; Jiang, L.; Fang, D.; Jiang, L.; Zhou, J. Differentially expressed genes of human microvascular endothelial cells in response to anti-dengue virus NS1 antibodies by suppression subtractive hybridization. *Viral Immunol.* **2013**, *26*, 185–191. [[CrossRef](#)]
40. Beatty, P.R.; Puerta-Guardo, H.; Killingbeck, S.S.; Glasner, D.R.; Hopkins, K.; Harris, E. Dengue virus NS1 triggers endothelial permeability and vascular leak that is prevented by NS1 vaccination. *Sci. Transl. Med.* **2015**, *7*, 304ra141. [[CrossRef](#)]

41. Modhiran, N.; Watterson, D.; Muller, D.A.; Panetta, A.K.; Sester, D.P.; Liu, L.; Hume, D.A.; Stacey, K.J.; Young, P.R. Dengue virus NS1 protein activates cells via Toll-like receptor 4 and disrupts endothelial cell monolayer integrity. *Sci. Transl. Med.* **2015**, *7*, 304ra142. [[CrossRef](#)]
42. Puerta-Guardo, H.; Glasner, D.R.; Harris, E. Dengue virus NS1 disrupts the endothelial glycocalyx, leading to hyperpermeability. *PLoS Pathog.* **2016**, *12*, e1005738. [[CrossRef](#)]
43. Puerta-Guardo, H.; Glasner, D.R.; Espinosa, D.A.; Biering, S.B.; Patana, M.; Ratnasiri, K.; Wang, C.; Beatty, P.R.; Harris, E. Flavivirus NS1 triggers tissue-specific vascular endothelial dysfunction reflecting disease tropism. *Cell Rep.* **2019**, *26*, 1598–1613. [[CrossRef](#)] [[PubMed](#)]
44. Plaszczyca, A.; Scaturro, P.; Neufeldt, C.J.; Cortese, M.; Cerikan, B.; Ferla, S.; Brancale, A.; Pichlmair, A.; Bartenschlager, R. A novel interaction between dengue virus nonstructural protein 1 and the NS4A-2K-4B precursor is required for viral RNA replication but not for formation of the membranous replication organelle. *PLoS Pathog.* **2019**, *15*, e1007736. [[CrossRef](#)] [[PubMed](#)]
45. Wessel, A.W.; Dowd, K.A.; Biering, S.B.; Zhang, P.; Edeling, M.A.; Nelson, C.A.; Funk, K.E.; DeMaso, C.R.; Klein, R.S.; Smith, J.L. Levels of circulating NS1 impact West Nile virus spread to the brain. *J. Virol.* **2021**, *95*, e00844-21. [[CrossRef](#)] [[PubMed](#)]
46. Eyre, N.S.; Hampton-Smith, R.J.; Aloia, A.L.; Eddes, J.S.; Simpson, K.J.; Hoffmann, P.; Beard, M.R. Phosphorylation of NS5A Serine-235 is essential to hepatitis C virus RNA replication and normal replication compartment formation. *Virology* **2016**, *491*, 27–44. [[CrossRef](#)] [[PubMed](#)]
47. Fischl, W.; Bartenschlager, R. High-throughput screening using dengue virus reporter genomes. *Methods Mol. Biol.* **2013**, *1030*, 205–219. [[CrossRef](#)] [[PubMed](#)]
48. Schwinn, M.K.; Machleidt, T.; Zimmerman, K.; Eggers, C.T.; Dixon, A.S.; Hurst, R.; Hall, M.P.; Encell, L.P.; Binkowski, B.F.; Wood, K.V. CRISPR-mediated tagging of endogenous proteins with a luminescent peptide. *ACS Chem. Biol.* **2018**, *13*, 467–474. [[CrossRef](#)] [[PubMed](#)]
49. Dixon, A.S.; Schwinn, M.K.; Hall, M.P.; Zimmerman, K.; Otto, P.; Lubben, T.H.; Butler, B.L.; Binkowski, B.F.; Machleidt, T.; Kirkland, T.A.; et al. NanoLuc Complementation Reporter Optimized for Accurate Measurement of Protein Interactions in Cells. *ACS Chem. Biol.* **2016**, *11*, 400–408. [[CrossRef](#)]
50. Fan, J.; Liu, Y.; Yuan, Z. Critical role of Dengue Virus NS1 protein in viral replication. *Virol. Sin.* **2014**, *9*, 162–169. [[CrossRef](#)]
51. Cerikan, B.; Goellner, S.; Neufeldt, C.J.; Haselmann, U.; Mulder, K.; Chatel-Chaix, L.; Cortese, M.; Bartenschlager, R. A Non-Replicative Role of the 3' Terminal Sequence of the Dengue Virus Genome in Membranous Replication Organelle Formation. *Cell Rep.* **2020**, *32*, 107859. [[CrossRef](#)]
52. Clark, D.C.; Lobigs, M.; Lee, E.; Howard, M.J.; Clark, K.; Blitvich, B.J.; Hall, R.A. In situ reactions of monoclonal antibodies with a viable mutant of Murray Valley encephalitis virus reveal an absence of dimeric NS1 protein. *Gen. Virol.* **2007**, *88*, 1175–1183. [[CrossRef](#)]

Disclaimer/Publisher's Note: The statements, opinions and data contained in all publications are solely those of the individual author(s) and contributor(s) and not of MDPI and/or the editor(s). MDPI and/or the editor(s) disclaim responsibility for any injury to people or property resulting from any ideas, methods, instructions or products referred to in the content.

References

- Acosta, E. G., Kumar, A., & Bartenschlager, R. (2014). Revisiting dengue virus–host cell interaction: new insights into molecular and cellular virology. *Advances in virus research*, 88, 1-109. <https://doi.org/10.1016/B978-0-12-800098-4.00001-5>
- Aguirre, S., Maestre, A. M., Pagni, S., Patel, J. R., Savage, T., Gutman, D., Maringer, K., Bernal-Rubio, D., Shabman, R. S., & Simon, V. (2012). DENV inhibits type I IFN production in infected cells by cleaving human STING. <https://doi.org/10.1371/journal.ppat.1002934>
- Aguirre, S., Luthra, P., Sanchez-Aparicio, M. T., Maestre, A. M., Patel, J., Lamothe, F., Fredericks, A. C., Tripathi, S., Zhu, T., & Pintado-Silva, J. (2017). Dengue virus NS2B protein targets cGAS for degradation and prevents mitochondrial DNA sensing during infection. *Nature microbiology*, 2(5), 1-11. <https://doi.org/10.1038/nmicrobiol.2017.37>
- Aizaki, H., Lee, K.J., Sung, V.M.H., Ishiko, H. and Lai, M.M., 2004. Characterization of the hepatitis C virus RNA replication complex associated with lipid rafts. *Virology*, 324(2), pp.450-461. doi: <https://doi.org/10.1016/j.virol.2004.03.034>
- Akey, D.L.; Brown, W.C.; Dutta, S.; Konwerski, J.; Jose, J.; Jurkiw, T.J.; DelProposto, J.; Ogata, C.M.; Skiniotis, G.; Kuhn, R.J.; et al.(2014) Flavivirus NS1 structures reveal surfaces for associations with membranes and the immune system. *Science*,343, 881–885. <https://doi.org/10.1126/science.1247749>
- Akey, D. L., Brown, W. C., Jose, J., Kuhn, R. J., & Smith, J. L. (2015). Structure-guided insights on the role of NS1 in flavivirus infection. *Bioessays*, 37(5), 489-494. <https://doi.org/10.1002/bies.201400182> <https://doi.org/10.1002/bies.201400182>
- Alcon, S., Talarmin, A., Debruyne, M., Falconar, A., Deubel, V., & Flamand, M. (2002). Enzyme-linked immunosorbent assay specific to Dengue virus type 1 nonstructural protein NS1 reveals circulation of the antigen in the blood during the acute phase of disease in patients experiencing primary or secondary infections. *Journal of clinical microbiology*, 40(2), 376-381. <https://doi.org/10.1128/jcm.40.02.376-381.2002>
- Anders, K. L., Nguyet, N. M., Chau, N. V. V., Hung, N. T., Thuy, T. T., Farrar, J., Wills, B., Hien, T. T., & Simmons, C. P. (2011). Epidemiological factors associated with dengue shock syndrome and mortality in hospitalized dengue patients in Ho Chi Minh City, Vietnam. *The American journal of tropical medicine and hygiene*, 84(1), 127. <https://doi.org/10.4269/ajtmh.2011.10-0476>
- Anwar, A., Khan, N., Ayub, M., Nawaz, F., Shah, A., & Flahault, A. (2019). Modeling and predicting dengue incidence in highly vulnerable countries using panel data approach. *International journal of environmental research and public health*, 16(13), 2296. <https://doi.org/10.3390/ijerph16132296>
- Arndt, C., Koristka, S., Bartsch, H., & Bachmann, M. (2012). Native polyacrylamide gels. *Protein electrophoresis: methods and protocols*, 49-53. https://doi.org/10.1007/978-1-61779-821-4_5
- Ashour, J., Laurent-Rolle, M., Shi, P.-Y., & García-Sastre, A. (2009). NS5 of dengue virus mediates STAT2 binding and degradation. *Journal of virology*, 83(11), 5408-5418. <https://doi.org/10.1128/JVI.02188-08>
- Avirutnan, P., Punyadee, N., Noisakran, S., Komoltri, C., Thiemmecca, S., Auethavornanan, K., Jairungsri, A., Kanlaya, R., Tangthawornchaikul, N., & Puttikhunt, C. (2006). Vascular leakage in severe dengue virus infections: a potential role for the nonstructural viral protein NS1 and complement. *The Journal of infectious diseases*, 193(8), 1078-1088. <https://doi.org/10.1086/500949>

- Avirutnan, P.; Fuchs, A.; Hauhart, R.E.; Somnuk, P.; Youn, S.; Diamond, M.S.; Atkinson, J.P. (2010). Antagonism of the complement component C4 by flavivirus nonstructural protein NS1. *J. Exp. Med.* 207, 793–806. <https://doi.org/10.1084/jem.20092545>
- Avirutnan, P.; Hauhart, R.E.; Somnuk, P.; Blom, A.M.; Diamond, M.S.; Atkinson, J.P. (2011). Binding of flavivirus nonstructural protein NS1 to C4b binding protein modulates complement activation. *J. Immunol.* 187, 424–433. <https://doi.org/10.4049/jimmunol.1100750>
- Bartenschlager, R., & Miller, S. (2008). Molecular aspects of Dengue virus replication. <https://doi.org/10.2217/17460913.3.2.155>
- Beatty, P.R.; Puerta-Guardo, H.; Killingbeck, S.S.; Glasner, D.R.; Hopkins, K.; Harris, E. Dengue virus NS1 triggers endothelial permeability and vascular leak that is prevented by NS1 vaccination. *Sci. Transl. Med.* 2015, 7, 304ra141. <https://doi.org/10.1126/scitranslmed.aaa3787>
- Benarroch, D., Selisko, B., Locatelli, G. A., Maga, G., Romette, J.-L., & Canard, B. (2004). The RNA helicase, nucleotide 5'-triphosphatase, and RNA 5'-triphosphatase activities of Dengue virus protein NS3 are Mg²⁺-dependent and require a functional Walker B motif in the helicase catalytic core. *Virology*, 328(2), 208-218. <https://doi.org/10.1016/j.virol.2004.07.004>
- Benfrid, S.; Park, K.H.; Dellarole, M.; Voss, J.E.; Tamietti, C.; Pehau-Arnaudet, G.; Raynal, B.; Brûlé, S.; England, P.; Zhang, X. Dengue virus NS1 protein conveys pro-inflammatory signals by docking onto high-density lipoproteins. *EMBO Rep.* 2022, 23,e53600. <https://doi.org/10.15252/embr.202153600>
- Bhatt, S., Gething, P. W., Brady, O. J., Messina, J. P., Farlow, A. W., Moyes, C. L., Drake, J. M., Brownstein, J. S., Hoen, A. G., & Sankoh, O. (2013). The global distribution and burden of dengue. *Nature*, 496(7446), 504-507. <https://doi.org/10.1038/nature12060>
- Bhatt, S., Weiss, D. J., Mappin, B., Dalrymple, U., Cameron, E., Bisanzio, D., Smith, D. L., Moyes, C. L., Tatem, A. J., & Lynch, M. (2015). Coverage and system efficiencies of insecticide-treated nets in Africa from 2000 to 2017. *Elife*, 4, e09672. <https://doi.org/10.7554/eLife.09672>
- Bhattacharya, M., Bhowmik, D., Tian, Y., He, H., Zhu, F., & Yin, Q. (2023). The Dengue virus protease NS2B3 cleaves cyclic GMP-AMP synthase to suppress cGAS activation. *Journal of Biological Chemistry*, 299(3). <https://doi.org/10.1016/j.jbc.2023.102986>
- Biering, S. B., Akey, D. L., Wong, M. P., Brown, W. C., Lo, N. T., Puerta-Guardo, H., Tramontini Gomes de Sousa, F., Wang, C., Konwerski, J. R., & Espinosa, D. A. (2021). Structural basis for antibody inhibition of flavivirus NS1-triggered endothelial dysfunction. *Science*, 371(6525), 194-200. <https://doi.org/10.1126/science.abc0476>
- Brady, O. J., & Hay, S. I. (2020). The global expansion of dengue: how *Aedes aegypti* mosquitoes enabled the first pandemic arbovirus. *Annual review of entomology*, 65, 191-208. <https://doi.org/10.1146/annurev-ento-011019-024918>
- Brandt, W. E., Chiewsilp, D., Harris, D. L., & Russell, P. K. (1970). Partial purification and characterization of a dengue virus soluble complement-fixing antigen. *The journal of immunology*, 105(6), 1565-1568. <https://doi.org/10.4049/jimmunol.105.6.1565>
- Brinton, M. A. (2002). The molecular biology of West Nile Virus: a new invader of the western hemisphere. *Annual Reviews in Microbiology*, 56(1), 371-402. <https://doi.org/10.1146/annurev.micro.56.012302.160654>
- Brunner, J. E., Nguyen, J. H., Roehl, H. H., Ho, T. V., Swiderek, K. M., & Semler, B. L. (2005). Functional interaction of heterogeneous nuclear ribonucleoprotein C with poliovirus RNA synthesis initiation complexes. *Journal of virology*, 79(6), 3254-3266. <https://doi.org/10.1128/JVI.79.6.3254-3266.2005>
- Byk, L. A., & Gamarnik, A. V. (2016). Properties and functions of the dengue virus capsid protein. *Annual review of virology*, 3, 263-281. <https://doi.org/10.1146/annurev-virology-110615-042334>

- Canyon, D., Hii, J., & Muller, R. (1999). The frequency of host biting and its effect on oviposition and survival in *Aedes aegypti* (Diptera: Culicidae). *Bulletin of entomological research*, 89(1), 35-39. <https://doi.org/10.1017/S000748539900005X>
- Carpp, L. N., Rogers, R. S., Moritz, R. L., & Aitchison, J. D. (2014). Quantitative proteomic analysis of host-virus interactions reveals a role for Golgi brefeldin A resistance factor 1 (GBF1) in dengue infection. *Molecular & Cellular Proteomics*, 13(11), 2836-2854. <https://doi.org/10.1074/mcp.M114.038984>
- Cerikan, B., Goellner, S., Neufeldt, C. J., Haselmann, U., Mulder, K., Chatel-Chaix, L., Cortese, M., & Bartenschlager, R. (2020). A Non-Replicative Role of the 3' Terminal Sequence of the Dengue Virus Genome in Membranous Replication Organelle Formation. *Cell Rep*, 32(1), 107859. <https://doi.org/10.1016/j.celrep.2020.107859>
- Chambers, T. J., Hahn, C. S., Galler, R., & Rice, C. M. (1990). Flavivirus genome organization, expression, and replication. *Annual review of microbiology*, 44(1), 649-688.
- Chen, J., Ng, M. M.-L., & Chu, J. J. H. (2015). Activation of TLR2 and TLR6 by dengue NS1 protein and its implications in the immunopathogenesis of dengue virus infection. *PLoS pathogens*, 11(7), e1005053. <https://doi.org/10.1371/journal.ppat.1005053>
- Cherepanova, N., Shrimal, S., & Gilmore, R. (2016). N-linked glycosylation and homeostasis of the endoplasmic reticulum. *Current opinion in cell biology*, 41, 57-65. <https://doi.org/10.1016/j.celb.2016.03.021>
- Coelho, D. R., Carneiro, P. H., Mendes-Monteiro, L., Conde, J. N., Andrade, I., Cao, T., Allonso, D., White-Dibiasio, M., Kuhn, R. J., & Mohana-Borges, R. (2021). ApoA1 neutralizes proinflammatory effects of dengue virus NS1 protein and modulates viral immune evasion. *Journal of virology*, 95(13), e01974-01920. <https://doi.org/10.1128/JVI.01974-20>
- Coffin III, W. F., Geiger, T. R., & Martin, J. M. (2003). Transmembrane domains 1 and 2 of the latent membrane protein 1 of Epstein-Barr virus contain a lipid raft targeting signal and play a critical role in cytotaxis. *Journal of virology*, 77(6), 3749-3758. <https://doi.org/10.1128/JVI.77.6.3749-3758.2003>
- Colton, Y., Chadee, D., & Severson, D. (2003). Natural skip oviposition of the mosquito *Aedes aegypti* indicated by codominant genetic markers. *Medical and veterinary entomology*, 17(2), 195-204. <https://doi.org/10.1046/j.1365-2915.2003.00424.x>
- Cortese, M., Goellner, S., Acosta, E. G., Neufeldt, C. J., Oleksiuk, O., Lampe, M., Haselmann, U., Funaya, C., Schieber, N., & Ronchi, P. (2017). Ultrastructural characterization of Zika virus replication factories. *Cell reports*, 18(9), 2113-2123. <http://dx.doi.org/10.1016/j.celrep.2017.02.014>
- Cortese, M., Mulder, K., Chatel-Chaix, L., Scaturro, P., Cerikan, B., Plaszczyca, A., Haselmann, U., Bartenschlager, M., Neufeldt, C. J., & Bartenschlager, R. (2021). Determinants in nonstructural protein 4A of dengue virus required for RNA replication and replication organelle biogenesis. *Journal of virology*, 95(21), e01310-01321. <https://doi.org/10.1128/JVI.01310-21>
- Courageot, M.-P., Frenkiel, M.-P., Duarte Dos Santos, C., Deubel, V., & Desprès, P. (2000). α -Glucosidase inhibitors reduce dengue virus production by affecting the initial steps of virion morphogenesis in the endoplasmic reticulum. *Journal of virology*, 74(1), 564-572. <https://doi.org/10.1128/JVI.74.1.564-572.2000>
- Crabtree, M., Kinney, R., & Miller, B. (2005). Deglycosylation of the NS1 protein of dengue 2 virus, strain 16681: construction and characterization of mutant viruses. *Archives of virology*, 150(4), 771-786. <https://doi.org/10.1007/s00705-004-0430-8>
- de los Reyes, A. A., & Escaner IV, J. M. L. (2018). Dengue in the Philippines: model and analysis of parameters affecting transmission. *Journal of biological dynamics*, 12(1), 894-912. <https://doi.org/10.1080/17513758.2018.1535096>
- de Sousa, F. T. G., Biering, S. B., Patel, T. S., Blanc, S. F., Camelini, C. M., Venzke, D., Nunes, R. J., Romano, C. M., Beatty, P. R., & Sabino, E. C. (2022). Sulfated β -glucan from *Agaricus subrufescens*

- inhibits flavivirus infection and nonstructural protein 1-mediated pathogenesis. *Antiviral research*, 203, 105330. <https://doi.org/10.1016/j.antiviral.2022.105330>
- Dechtawewat, T., Paemane, A., Roytrakul, S., Songprakhon, P., Limjindaporn, T., Yenichitsomanus, P.-t., Saitornuang, S., Puttikhunt, C., Kasinrer, W., & Malasit, P. (2016). Mass spectrometric analysis of host cell proteins interacting with dengue virus nonstructural protein 1 in dengue virus-infected HepG2 cells. *Biochimica et Biophysica Acta (BBA)-Proteins and Proteomics*, 1864(9), 1270-1280. <https://doi.org/10.1016/j.bbapap.2016.04.008>
- Dixon, A. S., Schwinn, M. K., Hall, M. P., Zimmerman, K., Otto, P., Lubben, T. H., Butler, B. L., Binkowski, B. F., Machleidt, T., Kirkland, T. A., Wood, M. G., Eggers, C. T., Encell, L. P., & Wood, K. V. (2016). NanoLuc Complementation Reporter Optimized for Accurate Measurement of Protein Interactions in Cells. *ACS Chem Biol*, 11(2), 400-408. <https://doi.org/10.1021/acscchembio.5b00753>
- Doores, K. J. (2015). The HIV glycan shield as a target for broadly neutralizing antibodies. *The FEBS journal*, 282(24), 4679-4691. <https://doi.org/10.1111/febs.13530>
- Dumont, A.-A., Dumont, L., Berthiaume, J., & Auger-Messier, M. (2019). p38 α MAPK proximity assay reveals a regulatory mechanism of alternative splicing in cardiomyocytes. *Biochimica et Biophysica Acta (BBA)-Molecular Cell Research*, 1866(12), 118557. <https://doi.org/10.1016/j.bbamcr.2019.118557>
- Eyre, N. S., Johnson, S. M., Eltahla, A. A., Aloia, M., Aloia, A. L., McDevitt, C. A., Bull, R. A., & Beard, M. R. (2017a). Genome-Wide Mutagenesis of Dengue Virus Reveals Plasticity of the NS1 Protein and Enables Generation of Infectious Tagged Reporter Viruses. *J Virol*, 91(23). <https://doi.org/10.1128/JVI.01455-17>
- Eyre, N. S., Aloia, A. L., Joyce, M. A., Chulanetra, M., Tyrrell, D. L., & Beard, M. R. (2017b). Sensitive luminescent reporter viruses reveal appreciable release of hepatitis C virus NS5A protein into the extracellular environment. *Virology*, 507, 20-31. <https://doi.org/10.1016/j.virol.2017.04.003>
- Falconar, A. The dengue virus nonstructural-1 protein (NS1) generates antibodies to common epitopes on human blood clotting, integrin/adhesin proteins and binds to human endothelial cells: Potential implications in haemorrhagic fever pathogenesis. *Arch. Virol.* 1997, 142, 897–916. <https://doi.org/10.1007/s007050050127>
- Falconar, A.K. Antibody responses are generated to immunodominant ELK/KLE-type motifs on the nonstructural-1 glycoprotein during live dengue virus infections in mice and humans: Implications for diagnosis, pathogenesis, and vaccine design. *Clin. Vaccine Immunol.* 2007, 14, 493–504. <https://doi.org/10.1128/CVI.00371-06>
- Falgout, B., Chanock, R. and Lai, C.J., (1989). Proper processing of dengue virus nonstructural glycoprotein NS1 requires the N-terminal hydrophobic signal sequence and the downstream nonstructural protein NS2a. *Journal of virology*, 63(5), pp.1852-1860. <https://doi.org/10.1128/jvi.63.5.1852-1860.1989>
- Falgout, B., Pethel, M., Zhang, Y.-M., & Lai, C. (1991). Both nonstructural proteins NS2B and NS3 are required for the proteolytic processing of dengue virus nonstructural proteins. *Journal of virology*, 65(5), 2467-2475. <https://doi.org/10.1128/jvi.65.5.2467-2475.1991>
- Fan, J.; Liu, Y.; Yuan, Z. Critical role of Dengue Virus NS1 protein in viral replication. *Virol. Sin.* 2014, 9, 162–169. <https://doi.org/10.1007/s12250-014-3459-1>
- Fang, E., Li, M., Liu, X., Hu, K., Liu, L., Zhang, Z., Li, X., Peng, Q., & Li, Y. (2023). NS1 Protein N-Linked Glycosylation Site Affects the Virulence and Pathogenesis of Dengue Virus. *Vaccines*, 11(5), 959. <https://doi.org/10.3390/vaccines11050959>
- Feingold, K. R. (2015). Introduction to lipids and lipoproteins. *endotext [internet]*. PMID: 26247089
- Ferreira, G. L. (2012). Global dengue epidemiology trends. *Revista do Instituto de Medicina Tropical de São Paulo*, 54, 5-6. <https://doi.org/10.1590/S0036-46652012000700003>

- Fischl, W., & Bartenschlager, R. (2013). High-throughput screening using dengue virus reporter genomes. *Methods Mol Biol*, *1030*, 205-219. https://doi.org/10.1007/978-1-62703-484-5_17
- Flamand, M., Megret, F. o., Mathieu, M., Lepault, J., Rey, F. I. A., & Deubel, V. (1999). Dengue virus type 1 nonstructural glycoprotein NS1 is secreted from mammalian cells as a soluble hexamer in a glycosylation-dependent fashion. *Journal of virology*, *73*(7), 6104-6110. <https://doi.org/10.1128/JVI.73.7.6104-6110.1999>
- Flasche, S., Jit, M., Rodríguez-Barraquer, I., Coudeville, L., Recker, M., Koelle, K., Milne, G., Hladish, T. J., Perkins, T. A., & Cummings, D. A. (2016). The long-term safety, public health impact, and cost-effectiveness of routine vaccination with a recombinant, live-attenuated dengue vaccine (Dengvaxia): a model comparison study. *PLoS medicine*, *13*(11), e1002181. <https://doi.org/10.1371/journal.pmed.1002181>
- Gao, F., Duan, X., Lu, X., Liu, Y., Zheng, L., Ding, Z., & Li, J. (2010). Novel binding between pre-membrane protein and claudin-1 is required for efficient dengue virus entry. *Biochemical and biophysical research communications*, *391*(1), 952-957. <https://doi.org/10.1016/j.bbrc.2009.11.172>
- Gavin, A.-C., Aloy, P., Grandi, P., Krause, R., Boesche, M., Marzioch, M., Rau, C., Jensen, L. J., Bastuck, S., & Dümpelfeld, B. (2006). Proteome survey reveals modularity of the yeast cell machinery. *Nature*, *440*(7084), 631-636. <https://doi.org/10.1038/nature04532>
- Glasner, D. R., Puerta-Guardo, H., Beatty, P. R., & Harris, E. (2018). The good, the bad, and the shocking: the multiple roles of dengue virus nonstructural protein 1 in protection and pathogenesis. *Annual review of virology*, *5*, 227-253. <https://doi.org/10.1146/annurev-virology-101416-041848>
- Goethals, O., Kaptein, S. J., Kesteleyn, B., Bonfanti, J.-F., Van Wesenbeeck, L., Bardiot, D., Verschoor, E. J., Verstrepen, B. E., Fagrouch, Z., & Putnak, J. R. (2023). Blocking NS3–NS4B interaction inhibits dengue virus in non-human primates. *Nature*, *615*(7953), 678-686. <https://doi.org/10.1038/s41586-023-05790-6>
- Grainger, S., Nguyen, N., Richter, J., Setayesh, J., Lonquich, B., Oon, C. H., Wozniak, J. M., Barahona, R., Kamei, C. N., & Houston, J. (2019). EGFR is required for Wnt9a–Fzd9b signalling specificity in haematopoietic stem cells. *Nature cell biology*, *21*(6), 721-730. <https://doi.org/10.1038/s41556-019-0330-5>
- Grief, C., Galler, R., Côrtes, L., & Barth, O. (1997). Intracellular localisation of dengue-2 RNA in mosquito cell culture using electron microscopic in situ hybridisation. *Archives of virology*, *142*(12), 2347-2357. <https://doi.org/10.1007/s007050050247>
- Gubler, D. J. (1997). Dengue and dengue hemorrhagic fever: its history and resurgence as a global public health problem. *Dengue and dengue hemorrhagic fever*, 1-22.
- Gubler, D. J. (2002). The global emergence/resurgence of arboviral diseases as public health problems. *Archives of medical research*, *33*(4), 330-342. [https://doi.org/10.1016/S0188-4409\(02\)00378-8](https://doi.org/10.1016/S0188-4409(02)00378-8)
- Gubler, D. J. (2006). Dengue/dengue haemorrhagic fever: history and current status. *New Treatment Strategies for Dengue and Other Flaviviral Diseases: Novartis Foundation Symposium 277*, <https://doi.org/10.1002/0470058005.ch2>
- Gutsche, I., Coulibaly, F., Voss, J. E., Salmon, J., d'Alayer, J., Ermonval, M., Larquet, E., Charneau, P., Krey, T., Megret, F., Guittet, E., Rey, F. A., & Flamand, M. (2011). Secreted dengue virus nonstructural protein NS1 is an atypical barrel-shaped high-density lipoprotein. *Proc Natl Acad Sci U S A*, *108*(19), 8003-8008. <https://doi.org/10.1073/pnas.1017338108>
- Guzman, M. G., & Harris, E. (2015). Dengue. *The Lancet*, *385*(9966), 453-465. [https://doi.org/10.1016/S0140-6736\(14\)60572-9](https://doi.org/10.1016/S0140-6736(14)60572-9)
- Hafirassou, M. L., Meertens, L., Umana-Diaz, C., Labeau, A., Dejarnac, O., Bonnet-Madin, L., Kummerer, B. M., Delaugerre, C., Roingard, P., Vidalain, P. O., & Amara, A. (2017). A Global

- Interactome Map of the Dengue Virus NS1 Identifies Virus Restriction and Dependency Host Factors. *Cell Rep*, 21(13), 3900-3913. <https://doi.org/10.1016/j.celrep.2017.11.094>
- Harrington, L. C., Edman, J. D., & Scott, T. W. (2001). Why do female *Aedes aegypti* (Diptera: Culicidae) feed preferentially and frequently on human blood? *Journal of medical entomology*, 38(3), 411-422. <https://doi.org/10.1603/0022-2585-38.3.411>
- Horak, P., Tomasich, E., Vaňhara, P., Kratochvílová, K., Anees, M., Marhold, M., Lemberger, C. E., Gerschpacher, M., Horvat, R., & Sibia, M. (2014). TUSC3 loss alters the ER stress response and accelerates prostate cancer growth in vivo. *Scientific reports*, 4(1), 3739. <https://doi.org/10.1038/srep03739>
- Hsieh, S.-C., Zou, G., Tsai, W.-Y., Qing, M., Chang, G.-J., Shi, P.-Y., & Wang, W.-K. (2011). The C-terminal helical domain of dengue virus precursor membrane protein is involved in virus assembly and entry. *Virology*, 410(1), 170-180. <https://doi.org/10.1016/j.virol.2010.11.006>
- Hsieh, S.-C., Wu, Y.-C., Zou, G., Nerurkar, V. R., Shi, P.-Y., & Wang, W.-K. (2014). Highly conserved residues in the helical domain of dengue virus type 1 precursor membrane protein are involved in assembly, precursor membrane (prM) protein cleavage, and entry. *Journal of Biological Chemistry*, 289(48), 33149-33160. <https://doi.org/10.1074/jbc.M114.610428>
- Hung, N. T., Lan, N. T., Lei, H.-Y., Lin, Y.-S., LE BICH, L., Huang, K.-J., Lin, C.-F., DO QUANG, H., Huong, V. T. Q., & My, L. T. (2005). Association between sex, nutritional status, severity of dengue hemorrhagic fever, and immune status in infants with dengue hemorrhagic fever. *The American journal of tropical medicine and hygiene*, 72(4), 370-374.
- Hung, V., Zou, P., Rhee, H.-W., Udeshi, N. D., Cracan, V., Svinkina, T., Carr, S. A., Mootha, V. K., & Ting, A. Y. (2014). Proteomic mapping of the human mitochondrial intermembrane space in live cells via ratiometric APEX tagging. *Molecular cell*, 55(2), 332-341. <https://doi.org/10.1016/j.molcel.2014.06.003>
- Hung, V., Udeshi, N. D., Lam, S. S., Loh, K. H., Cox, K. J., Pedram, K., Carr, S. A., & Ting, A. Y. (2016). Spatially resolved proteomic mapping in living cells with the engineered peroxidase APEX2. *Nature protocols*, 11(3), 456-475. <https://doi.org/10.1038/nprot.2016.018>
- Ikonen, E. (2001). Roles of lipid rafts in membrane transport. *Current opinion in cell biology*, 13(4), 470-477. [https://doi.org/10.1016/S0955-0674\(00\)00238-6](https://doi.org/10.1016/S0955-0674(00)00238-6)
- Kalocsay, M. (2019), “APEX Peroxidase-Catalysed Proximity Labelling and Multiplexed Quantitative Proteomics”, Chapter 4 of Proximity Labelling: Methods and Protocols, Methods in Molecular Biology, vol.2008
- Kaptein, S. J., Goethals, O., Kiemel, D., Marchand, A., Kesteley, B., Bonfanti, J.-F., Bardiot, D., Stoops, B., Jonckers, T. H., & Dallmeier, K. (2021). A pan-serotype dengue virus inhibitor targeting the NS3–NS4B interaction. *Nature*, 598(7881), 504-509. <https://doi.org/10.1038/s41586-021-03990-6>
- Khromykh, A. A., Sedlak, P. L., Guyatt, K. J., Hall, R. A., & Westaway, E. G., 1999. Efficient trans-complementation of the flavivirus kunjin NS5 protein but not of the NS1 protein requires its coexpression with other components of the viral replicase. *Journal of virology*, 73(12), pp.10272–10280. <https://doi.org/10.1128/JVI.73.12.10272-10280.1999>
- Kim, D. I., & Roux, K. J. (2016). Filling the void: proximity-based labeling of proteins in living cells. *Trends in cell biology*, 26(11), 804-817. <https://doi.org/10.1016/j.tcb.2016.09.004>
- Kuhn, R. J., Zhang, W., Rossmann, M. G., Pletnev, S. V., Corver, J., Lenches, E., Jones, C. T., Mukhopadhyay, S., Chipman, P. R., & Strauss, E. G. (2002). Structure of dengue virus: implications for flavivirus organization, maturation, and fusion. *Cell*, 108(5), 717-725. [https://doi.org/10.1016/S0092-8674\(02\)00660-8](https://doi.org/10.1016/S0092-8674(02)00660-8)
- Kumar, R., Singh, N., Abidin, M. Z., Patel, A. H., & Medigeshi, G. R. (2018). Dengue virus capsid interacts with DDX3X—a potential mechanism for suppression of antiviral functions in dengue infection. *Frontiers in cellular and infection microbiology*, 7, 542. <https://doi.org/10.3389/fcimb.2017.00542>

- Lam, S. S., Martell, J. D., Kamer, K. J., Deerinck, T. J., Ellisman, M. H., Mootha, V. K., & Ting, A. Y. (2015). Directed evolution of APEX2 for electron microscopy and proximity labeling. *Nature methods*, *12*(1), 51-54. <https://doi.org/10.1038/nmeth.3179>
- Lee, A., & Cooper, T. (1995). Improved direct PCR screen for bacterial colonies: wooden toothpicks inhibit PCR amplification. *Biotechniques*, *18*(2), 225-226.
- Lee, C. M., Xie, X., Zou, J., Li, S.-H., Lee, M. Y. Q., Dong, H., Qin, C.-F., Kang, C., & Shi, P.-Y. (2015). Determinants of dengue virus NS4A protein oligomerization. *Journal of virology*, *89*(12), 6171-6183. <https://doi.org/10.1128/JVI.00546-15>
- Lescar, J., Soh, S., Lee, L. T., Vasudevan, S. G., Kang, C., & Lim, S. P. (2018). The dengue virus replication complex: from RNA replication to protein-protein interactions to evasion of innate immunity. *Dengue and Zika: Control and antiviral treatment strategies*, 115-129. https://doi.org/10.1007/978-981-10-8727-1_9
- Li, L., Lok, S.-M., Yu, I.-M., Zhang, Y., Kuhn, R. J., Chen, J., & Rossmann, M. G. (2008). The flavivirus precursor membrane-envelope protein complex: structure and maturation. *Science*, *319*(5871), 1830-1834. <https://doi.org/10.1126/science.1153263>
- Li, Y., Li, Q., Wong, Y. L., Liew, L. S. Y., & Kang, C. (2015). Membrane topology of NS2B of dengue virus revealed by NMR spectroscopy. *Biochimica et Biophysica Acta (BBA)-Biomembranes*, *1848*(10), 2244-2252. <https://doi.org/10.1016/j.bbamem.2015.06.010>
- Li, A., Acevedo-Rocha, C. G., & Reetz, M. T. (2018). Boosting the efficiency of site-saturation mutagenesis for a difficult-to-randomize gene by a two-step PCR strategy. *Applied microbiology and biotechnology*, *102*, 6095-6103. <https://doi.org/10.1007/s00253-018-9041-2>
- Libraty, D.H.; Young, P.R.; Pickering, D.; Endy, T.P.; Kalayanarooj, S.; Green, S.; Vaughn, D.W.; Nisalak, A.; Ennis, F.A.; Rothman, A.L. High circulating levels of the dengue virus nonstructural protein NS1 early in dengue illness correlate with the development of dengue hemorrhagic fever. *J. Infect. Dis.* 2002, *186*, 1165–1168. <https://doi.org/10.1086/343813>
- Lin, C.-F., Chiu, S.-C., Hsiao, Y.-L., Wan, S.-W., Lei, H.-Y., Shiau, A.-L., Liu, H.-S., Yeh, T.-M., Chen, S.-H., & Liu, C.-C. (2005). Expression of cytokine, chemokine, and adhesion molecules during endothelial cell activation induced by antibodies against dengue virus nonstructural protein 1. *The journal of immunology*, *174*(1), 395-403. <https://doi.org/10.4049/jimmunol.174.1.395>
- Lindenbach, B. D., & Rice, C. M. (1997). trans-Complementation of yellow fever virus NS1 reveals a role in early RNA replication. *Journal of virology*, *71*(12), 9608-9617. <https://doi.org/10.1128/jvi.71.12.9608-9617.1997>
- Liu, L., Dong, H., Chen, H., Zhang, J., Ling, H., Li, Z., Shi, P.-Y., & Li, H. (2010). Flavivirus RNA cap methyltransferase: structure, function, and inhibition. *Frontiers in biology*, *5*, 286-303. <https://doi.org/10.1007/s11515-010-0660-y>
- Liu, H., Zhang, L., Sun, J., Chen, W., Li, S., Wang, Q., Yu, H., Xia, Z., Jin, X., & Wang, C. (2017). Endoplasmic reticulum protein SCAP inhibits dengue virus NS2B3 protease by suppressing its K27-linked polyubiquitylation. *Journal of virology*, *91*(9), e02234-02216. <https://doi.org/10.1128/JVI.02234-16>
- Lo, N. T., Roodsari, S. Z., Tin, N. L., Wong, M. P., Biering, S. B., & Harris, E. (2022). Molecular Determinants of Tissue Specificity of Flavivirus Nonstructural Protein 1 Interaction with Endothelial Cells. *Journal of virology*, *96*(19), e00661-00622. <https://doi.org/10.1128/jvi.00661-22>
- Lobingier, B. T., Hüttenhain, R., Eichel, K., Miller, K. B., Ting, A. Y., von Zastrow, M., & Krogan, N. J. (2017). An approach to spatiotemporally resolve protein interaction networks in living cells. *Cell*, *169*(2), 350-360. e312. <https://doi.org/10.1016/j.cell.2017.03.022>
- Lu, G., & Gong, P. (2013). Crystal structure of the full-length Japanese encephalitis virus NS5 reveals a conserved methyltransferase-polymerase interface. *PLoS pathogens*, *9*(8), e1003549. <https://doi.org/10.1371/journal.ppat.1003549>

- Ma, L., Jones, C. T., Groesch, T. D., Kuhn, R. J., & Post, C. B. (2004). Solution structure of dengue virus capsid protein reveals another fold. *Proceedings of the National Academy of Sciences*, 101(10), 3414-3419. <https://doi.org/10.1073/pnas.0305892101>
- Mackenzie, J. M., Jones, M. K., & Young, P. R. (1996). Immunolocalization of the dengue virus nonstructural glycoprotein NS1 suggests a role in viral RNA replication. *Virology*, 220(1), 232-240. <https://doi.org/10.1006/viro.1996.0307>
- Mady, B. J., Erbe, D. V., Kurane, I., Fanger, M. W., & Ennis, F. A. (1991). Antibody-dependent enhancement of dengue virus infection mediated by bispecific antibodies against cell surface molecules other than Fc gamma receptors. *The journal of immunology*, 147(9), 3139-3144. <https://doi.org/10.4049/jimmunol.147.9.3139>
- Mañes, S., del Real, G., Lacalle, R.A., Lucas, P., Gómez-Moutón, C., Sánchez-Palomino, S., Delgado, R., Alcamí, J., Mira, E. and Martínez-A, C., 2000. Membrane raft microdomains mediate lateral assemblies required for HIV-1 infection. *EMBO reports*, 1(2), pp.190-196. doi: <https://doi.org/10.1093/embo-reports/kvd025>
- Marceau, C. D., Puschnik, A. S., Majzoub, K., Ooi, Y. S., Brewer, S. M., Fuchs, G., Swaminathan, K., Mata, M. A., Elias, J. E., & Sarnow, P. (2016). Genetic dissection of Flaviviridae host factors through genome-scale CRISPR screens. *Nature*, 535(7610), 159-163. <https://doi.org/10.1038/nature18631>
- Martell, J. D., Deerinck, T. J., Sancak, Y., Poulos, T. L., Mootha, V. K., Sosinsky, G. E., Ellisman, M. H., & Ting, A. Y. (2012). Engineered ascorbate peroxidase as a genetically encoded reporter for electron microscopy. *Nature biotechnology*, 30(11), 1143-1148. <https://doi.org/10.1038/nbt.2375>
- Mason, P.W. Maturation of Japanese encephalitis virus glycoproteins produced by infected mammalian and mosquito cells. *Virology* **1989**, 169, 354–364.
- Medina, R. A., Stertz, S., Manicassamy, B., Zimmermann, P., Sun, X., Albrecht, R. A., Uusi-Kerttula, H., Zagordi, O., Belshe, R. B., & Frey, S. E. (2013). Glycosylations in the globular head of the hemagglutinin protein modulate the virulence and antigenic properties of the H1N1 influenza viruses. *Science translational medicine*, 5(187), 187ra170-187ra170. <https://doi.org/10.1126/scitranslmed.3005996>
- Miller, S., Sparacio, S., & Bartenschlager, R. (2006). Subcellular localization and membrane topology of the dengue virus type 2 non-structural protein 4B. *Journal of Biological Chemistry*, 281(13), 8854-8863. <https://doi.org/10.1074/jbc.M512697200>
- Miller, S., Kastner, S., Krijnse-Locker, J., Buhler, S., & Bartenschlager, R. (2007). The non-structural protein 4A of dengue virus is an integral membrane protein inducing membrane alterations in a 2K-regulated manner. *Journal of Biological Chemistry*, 282(12), 8873-8882. <https://doi.org/10.1074/jbc.M609919200>
- Modhiran, N.; Watterson, D.; Muller, D.A.; Panetta, A.K.; Sester, D.P.; Liu, L.; Hume, D.A.; Stacey, K.J.; Young, P.R. Dengue virus NS1 protein activates cells via Toll-like receptor 4 and disrupts endothelial cell monolayer integrity. *Sci. Transl. Med.* (2015), 7,304ra142. <https://doi.org/10.1126/scitranslmed.aaa3863>
- Modhiran, N., Watterson, D., Blumenthal, A., Baxter, A. G., Young, P. R., & Stacey, K. J. (2017). Dengue virus NS1 protein activates immune cells via TLR4 but not TLR2 or TLR6. *Immunology and cell biology*, 95(5), 491-495. <https://doi.org/10.1038/icb.2017.5>
- Modhiran, N., Song, H., Liu, L., Bletchly, C., Brillault, L., Amarilla, A. A., Xu, X., Qi, J., Chai, Y., & Cheung, S. T. (2021). A broadly protective antibody that targets the flavivirus NS1 protein. *Science*, 371(6525), 190-194. <https://doi.org/10.1126/science.abb9425>
- Modis, Y., Ogata, S., Clements, D., & Harrison, S. C. (2004). Structure of the dengue virus envelope protein after membrane fusion. *Nature*, 427(6972), 313-319. <https://doi.org/10.1038/nature02165>
- Mondotte, J. A., Lozach, P.-Y., Amara, A., & Gamarnik, A. V. (2007). Essential role of dengue virus envelope protein N glycosylation at asparagine-67 during viral propagation. *Journal of virology*, 81(13), 7136-7148. <https://doi.org/10.1128/JVI.00116-07>

- Moyes, C. L., Vontas, J., Martins, A. J., Ng, L. C., Koou, S. Y., Dusfour, I., Raghavendra, K., Pinto, J., Corbel, V., & David, J.-P. (2017). Contemporary status of insecticide resistance in the major *Aedes* vectors of arboviruses infecting humans. *PLoS neglected tropical diseases*, *11*(7), e0005625. <https://doi.org/10.1371/journal.pntd.0005625>
- Mukhopadhyay, S., Kuhn, R. J., & Rossmann, M. G. (2005). A structural perspective of the flavivirus life cycle. *Nat Rev Microbiol*, *3*(1), 13-22. <https://doi.org/10.1038/nrmicro1067>
- Muller, D. A., Landsberg, M. J., Bletchly, C., Rothnagel, R., Waddington, L., Hankamer, B., & Young, P. R. (2012). Structure of the dengue virus glycoprotein non-structural protein 1 by electron microscopy and single-particle analysis. *Journal of General Virology*, *93*(4), 771-779. <https://doi.org/10.1099/vir.0.039321-0>
- Muller, D. A., & Young, P. R. (2013). The flavivirus NS1 protein: molecular and structural biology, immunology, role in pathogenesis and application as a diagnostic biomarker. *Antiviral Res*, *98*(2), 192-208. <https://doi.org/10.1016/j.antiviral.2013.03.008>
- Muñoz-Jordán, J. L., Sánchez-Burgos, G. G., Laurent-Rolle, M., & García-Sastre, A. (2003). Inhibition of interferon signaling by dengue virus. *Proceedings of the National Academy of Sciences*, *100*(24), 14333-14338. <https://doi.org/10.1073/pnas.2335168100>
- Murray, N. E. A., Quam, M. B., & Wilder-Smith, A. (2013). Epidemiology of dengue: past, present and future prospects. *Clinical epidemiology*, 299-309. <https://doi.org/10.2147/CLEP.S34440>
- Muylaert, I. R., Chambers, T. J., Galler, R., & Rice, C. M. (1996). Mutagenesis of the N-linked glycosylation sites of the yellow fever virus NS1 protein: effects on virus replication and mouse neurovirulence. *Virology*, *222*(1), 159-168. <https://doi.org/10.1006/viro.1996.0406>
- Nasar, S., Rashid, N., & Iftikhar, S. (2020). Dengue proteins with their role in pathogenesis, and strategies for developing an effective anti-dengue treatment: A review. *Journal of medical virology*, *92*(8), 941-955. <https://doi.org/10.1002/jmv.25646>
- Neufeldt, C. J., Cortese, M., Acosta, E. G., & Bartenschlager, R. (2018). Rewiring cellular networks by members of the Flaviviridae family. *Nat Rev Microbiol*, *16*(3), 125-142. <https://doi.org/10.1038/nrmicro.2017.170>
- Neufeldt, C. J., Cortese, M., Scaturro, P., Cerikan, B., Wideman, J. G., Tabata, K., Moraes, T., Oleksiuk, O., Pichlmair, A., & Bartenschlager, R. (2019). ER-shaping atlastin proteins act as central hubs to promote flavivirus replication and virion assembly. *Nature microbiology*, *4*(12), 2416-2429. <https://doi.org/10.1038/s41564-019-0586-3>
- Noisakran, S., Sengsai, S., Thongboonkerd, V., Kanlaya, R., Sinchaikul, S., Chen, S.-T., Puttikhunt, C., Kasinrerak, W., Limjindaporn, T., & Wongwiwat, W. (2008a). Identification of human hnRNP C1/C2 as a dengue virus NS1-interacting protein. *Biochemical and biophysical research communications*, *372*(1), 67-72. <https://doi.org/10.1016/j.bbrc.2008.04.165>
- Noisakran, S., Dechtawewat, T., Avirutnan, P., Kinoshita, T., Siripanyaphinyo, U., Puttikhunt, C., Kasinrerak, W., Malasit, P., & Sittisombut, N. (2008b). Association of dengue virus NS1 protein with lipid rafts. *Journal of General Virology*, *89*(10), 2492-2500. <https://doi.org/10.1099/vir.0.83620-0>
- Norris, G. E., Stillman, T. J., Anderson, B. F., & Baker, E. N. (1994). The three-dimensional structure of PNGase F, a glycosyl asparaginase from *Flavobacterium meningosepticum*. *Structure*, *2*(11), 1049-1059.
- Nowak, T., Färber, P. M., Wengler, G., & Wengler, G. (1989). Analyses of the terminal sequences of West Nile virus structural proteins and of the in vitro translation of these proteins allow the proposal of a complete scheme of the proteolytic cleavages involved in their synthesis. *Virology*, *169*(2), 365-376. [https://doi.org/10.1016/0042-6822\(89\)90162-1](https://doi.org/10.1016/0042-6822(89)90162-1)
- Osorio, J. E., Velez, I. D., Thomson, C., Lopez, L., Jimenez, A., Haller, A. A., Silengo, S., Scott, J., Boroughs, K. L., & Stovall, J. L. (2014). Safety and immunogenicity of a recombinant live attenuated tetravalent dengue vaccine (DENVax) in flavivirus-naive healthy adults in Colombia: a randomised,

- placebo-controlled, phase 1 study. *The Lancet Infectious Diseases*, 14(9), 830-838.
[https://doi.org/10.1016/S1473-3099\(14\)70811-4](https://doi.org/10.1016/S1473-3099(14)70811-4)
- Paek, J., Kalocsay, M., Staus, D. P., Wingler, L., Pascolutti, R., Paulo, J. A., Gygi, S. P., & Kruse, A. C. (2017). Multidimensional tracking of GPCR signaling via peroxidase-catalyzed proximity labeling. *Cell*, 169(2), 338-349. e311. <https://doi.org/10.1016/j.cell.2017.03.028>
- Paul, D., & Bartenschlager, R. (2013). Architecture and biogenesis of plus-strand RNA virus replication factories. *World journal of virology*, 2(2), 32. <https://doi.org/10.5501%2Fwjv.v2.i2.32>
- Plaszczycza, A., Scaturro, P., Neufeldt, C. J., Cortese, M., Cerikan, B., Ferla, S., Brancale, A., Pichlmair, A., & Bartenschlager, R. (2019). A novel interaction between dengue virus nonstructural protein 1 and the NS4A-2K-4B precursor is required for viral RNA replication but not for formation of the membranous replication organelle. *PLoS Pathog*, 15(5), e1007736.
<https://doi.org/10.1371/journal.ppat.1007736>
- Pokidysheva, E., Zhang, Y., Battisti, A. J., Bator-Kelly, C. M., Chipman, P. R., Xiao, C., Gregorio, G. G., Hendrickson, W. A., Kuhn, R. J., & Rossmann, M. G. (2006). Cryo-EM reconstruction of dengue virus in complex with the carbohydrate recognition domain of DC-SIGN. *Cell*, 124(3), 485-493.
<https://doi.org/10.1016/j.cell.2005.11.042>
- Potisopon, S., Priet, S., Collet, A., Decroly, E., Canard, B., & Selisko, B. (2014). The methyltransferase domain of dengue virus protein NS5 ensures efficient RNA synthesis initiation and elongation by the polymerase domain. *Nucleic acids research*, 42(18), 11642-11656.
<https://doi.org/10.1093/nar/gku666>
- Pryor, M. J., & Wright, P. J. (1994). Glycosylation mutants of dengue virus NS1 protein. *Journal of General Virology*, 75(5), 1183-1187. <https://doi.org/10.1099/0022-1317-75-5-1183>
- Puerta-Guardo, H.; Glasner, D.R.; Harris, E. Dengue virus NS1 disrupts the endothelial glycocalyx, leading to hyperpermeability. *PLoS Pathog*. (2016), 12, e1005738.
<https://doi.org/10.1371/journal.ppat.1005738>
- Puerta-Guardo, H.; Glasner, D.R.; Espinosa, D.A.; Biering, S.B.; Patana, M.; Ratnasiri, K.; Wang, C.; Beatty, P.R.; Harris, E. Flavivirus NS1 triggers tissue-specific vascular endothelial dysfunction reflecting disease tropism. *Cell Rep*.(2019), 26, 1598–1613.
<https://doi.org/10.1016/j.celrep.2019.01.036>
- Qin, W., Cho, K. F., Cavanagh, P. E., & Ting, A. Y. (2021). Deciphering molecular interactions by proximity labeling. *Nature methods*, 18(2), 133-143. <https://doi.org/10.1038/s41592-020-01010-5>
- Reiter, P. (2007). Oviposition, dispersal, and survival in *Aedes aegypti*: implications for the efficacy of control strategies. *Vector-Borne and Zoonotic Diseases*, 7(2), 261-273.
<https://doi.org/10.1089/vbz.2006.0630>
- Rhee, H.-W., Zou, P., Udeshi, N. D., Martell, J. D., Mootha, V. K., Carr, S. A., & Ting, A. Y. (2013). Proteomic mapping of mitochondria in living cells via spatially restricted enzymatic tagging. *Science*, 339(6125), 1328-1331. <https://doi.org/10.1126/science.1230593>
- Ritchie, S., Gubler, D., Ooi, E., & Vasudevan, S. (2014). Dengue vector bionomics: Why *Aedes aegypti* is such a good vector. Ch. 24. *Dengue and Dengue Hemorrhagic Fever: CAB International*.
- Rocklöv, J., & Tozan, Y. (2019). Climate change and the rising infectiousness of dengue. *Emerging Topics in Life Sciences*, 3(2), 133-142. <https://doi.org/10.1042/ETLS20180123>
- Roy, S. K., & Bhattacharjee, S. (2021). Dengue virus: epidemiology, biology, and disease aetiology. *Canadian Journal of Microbiology*, 67(10), 687-702. <https://doi.org/10.1139/cjm-2020-0572>
- Sampath, A., Xu, T., Chao, A., Luo, D., Lescar, J., & Vasudevan, S. G. (2006). Structure-based mutational analysis of the NS3 helicase from dengue virus. *Journal of virology*, 80(13), 6686-6690.
<https://doi.org/10.1128/JVI.02215-05>
- Savidis, G., McDougall, W. M., Meraner, P., Perreira, J. M., Portmann, J. M., Trincucci, G., John, S. P., Aker, A. M., Renzette, N., & Robbins, D. R. (2016). Identification of Zika virus and dengue virus

- dependency factors using functional genomics. *Cell reports*, 16(1), 232-246. <https://doi.org/10.1016/j.celrep.2016.06.028>
- Scaturro, P., Trist, I. M. L., Paul, D., Kumar, A., Acosta, E. G., Byrd, C. M., Jordan, R., Brancale, A., & Bartenschlager, R. (2014). Characterization of the mode of action of a potent dengue virus capsid inhibitor. *Journal of virology*, 88(19), 11540-11555. <https://doi.org/10.1128/JVI.01745-14>
- Scaturro, P., Cortese, M., Chatel-Chaix, L., Fischl, W., & Bartenschlager, R. (2015). Dengue Virus Non-structural Protein 1 Modulates Infectious Particle Production via Interaction with the Structural Proteins. *PLoS Pathog*, 11(11), e1005277. <https://doi.org/10.1371/journal.ppat.1005277>
- Schröder, M., Baran, M., & Bowie, A. G. (2008). Viral targeting of DEAD box protein 3 reveals its role in TBK1/IKK ϵ -mediated IRF activation. *The EMBO journal*, 27(15), 2147-2157. <https://doi.org/10.1038/emboj.2008.143>
- Schwinn, M. K., Machleidt, T., Zimmerman, K., Eggers, C. T., Dixon, A. S., Hurst, R., Hall, M. P., Encell, L. P., Binkowski, B. F., & Wood, K. V. (2018). CRISPR-mediated tagging of endogenous proteins with a luminescent peptide. *ACS chemical biology*, 13(2), 467-474. <https://doi.org/10.1021/acscchembio.7b00549>
- Scott, J. D., & Pawson, T. (2009). Cell signaling in space and time: where proteins come together and when they're apart. *Science*, 326(5957), 1220-1224. <https://doi.org/10.1126/science.1175668>
- Shrivastava, G., García-Cordero, J., León-Juárez, M., Oza, G., Tapia-Ramírez, J., Villegas-Sepulveda, N., & Cedillo-Barrón, L. (2017). NS2A comprises a putative viroporin of Dengue virus 2. *Virulence*, 8(7), 1450-1456. <https://doi.org/10.1080/21505594.2017.1356540>
- Shu, B.; Ooi, J.; Tan, A.; Ng, T.-S.; Dejnirattisai, W.; Mongkolsapaya, J.; Fibriansah, G.; Shi, J.; Kostyuchenko, V.; Screaton, G. CryoEM structures of the multimeric secreted NS1, a major factor for dengue hemorrhagic fever. *Nat. Commun.* 2022, 13,6756 <https://doi.org/10.1038/s41467-022-34415-1>
- Simmons, C. P., Farrar, J. J., van Vinh Chau, N., & Wills, B. (2012). Dengue. *New England Journal of Medicine*, 366(15), 1423-1432. <https://doi.org/10.1056/NEJMra1110265>
- Simons, K., & Ikonen, E. (1997). Functional rafts in cell membranes. *Nature*, 387(6633), 569-572. <https://doi.org/10.1038/42408>
- Slon Campos, J. L., Poggianella, M., Marchese, S., Mossenta, M., Rana, J., Arnoldi, F., Bestagno, M., & Burrone, O. R. (2017). DNA-immunisation with dengue virus E protein domains I/II, but not domain III, enhances Zika, West Nile and Yellow Fever virus infection. *PloS one*, 12(7), e0181734. <https://doi.org/10.1371/journal.pone.0181734>
- Smaby, J.M., Momsen, M., Kulkarni, V.S. and Brown, R.E., 1996. Cholesterol-induced interfacial area condensations of galactosylceramides and sphingomyelins with identical acyl chains. *Biochemistry*, 35(18), pp.5696-5704. doi: <https://doi.org/10.1021/bi953057k>
- Somnuk, P., Hauhart, R. E., Atkinson, J. P., Diamond, M. S., & Avirutnan, P. (2011). N-linked glycosylation of dengue virus NS1 protein modulates secretion, cell-surface expression, hexamer stability, and interactions with human complement. *Virology*, 413(2), 253-264. <https://doi.org/10.1016/j.virol.2011.02.022>
- Soulat, D., Bürckstümmer, T., Westermayer, S., Goncalves, A., Bauch, A., Stefanovic, A., Hantschel, O., Bennett, K. L., Decker, T., & Superti-Furga, G. (2008). The DEAD-box helicase DDX3X is a critical component of the TANK-binding kinase 1-dependent innate immune response. *The EMBO journal*, 27(15), 2135-2146. <https://doi.org/10.1038/emboj.2008.126>
- Stern, O., Hung, Y.-F., Valdau, O., Yaffe, Y., Harris, E., Hoffmann, S., Willbold, D., & Sklan, E. H. (2013). An N-terminal amphipathic helix in dengue virus nonstructural protein 4A mediates oligomerization and is essential for replication. *Journal of virology*, 87(7), 4080-4085. <https://doi.org/10.1128/JVI.01900-12>
- Tajima, S., Takasaki, T., & Kurane, I. (2008). Characterization of Asn130-to-Ala mutant of dengue type 1 virus NS1 protein. *Virus Genes*, 36, 323-329. <https://doi.org/10.1007/s11262-008-0211-7>

- Tan, B. E., Beard, M. R., & Eyre, N. S. (2023). Identification of Key Residues in Dengue Virus NS1 Protein That Are Essential for Its Secretion. *Viruses*, *15*(5), 1102. <https://doi.org/10.3390/v15051102>
- Teo, C. S. H., & Chu, J. J. H. (2014). Cellular vimentin regulates construction of dengue virus replication complexes through interaction with NS4A protein. *Journal of virology*, *88*(4), 1897-1913. <https://doi.org/10.1128/JVI.01249-13>
- Tian, J.-N., Yang, C.-C., Chuang, C.-K., Tsai, M.-H., Wu, R.-H., Chen, C.-T., & Yueh, A. (2019). A Dengue virus type 2 (DENV-2) NS4B-interacting host factor, SERP1, reduces DENV-2 production by suppressing viral RNA replication. *Viruses*, *11*(9), 787. <https://doi.org/10.3390/v11090787>
- van Cleef, K. W., Overheul, G. J., Thomassen, M. C., Kaptein, S. J., Davidson, A. D., Jacobs, M., Neyts, J., van Kuppeveld, F. J., & van Rij, R. P. (2013). Identification of a new dengue virus inhibitor that targets the viral NS4B protein and restricts genomic RNA replication. *Antiviral research*, *99*(2), 165-171. <https://doi.org/10.1016/j.antiviral.2013.05.011>
- van der Goot, F. G., & Harder, T. (2001). Raft membrane domains: from a liquid-ordered membrane phase to a site of pathogen attack. *Seminars in immunology*, <https://doi.org/10.1006/smim.2000.0300>
- Varki A, Cummings R.D., Esko J.D., Stanley P., Hart G.W., Aebi M., Darvill A.G., Kinoshita T., Packer N.H., Prestegard J.H., Schnaar R.L., Seeberger P.H., 2015. Essentials of Glycobiology [Internet]. 3rd ed. Cold Spring Harbor (NY): Cold Spring Harbor Laboratory Press; pp.2015–2017. PMID: 27010055. <https://doi.org/10.1101/9781621824213>
- Vasilakis, N., Cardoso, J., Hanley, K. A., Holmes, E. C., & Weaver, S. C. (2011). Fever from the forest: prospects for the continued emergence of sylvatic dengue virus and its impact on public health. *Nature Reviews Microbiology*, *9*(7), 532-541. <https://doi.org/10.1038/nrmicro2595>
- Wang, E., Ni, H., Xu, R., Barrett, A. D., Watowich, S. J., Gubler, D. J., & Weaver, S. C. (2000). Evolutionary relationships of endemic/epidemic and sylvatic dengue viruses. *Journal of virology*, *74*(7), 3227-3234. <https://doi.org/10.1128/JVI.74.7.3227-3234.2000>
- Wang, T., & Voglmeir, J. (2014). PNGases as valuable tools in glycoprotein analysis. *Protein and peptide letters*, *21*(10), 976-985. <https://doi.org/10.2174/0929866521666140626111237>
- Wang, C., Puerta-Guardo, H., Biering, S. B., Glasner, D. R., Tran, E. B., Patana, M., Gomberg, T. A., Malvar, C., Lo, N. T., & Espinosa, D. A. (2019). Endocytosis of flavivirus NS1 is required for NS1-mediated endothelial hyperpermeability and is abolished by a single N-glycosylation site mutation. *PLoS pathogens*, *15*(7), e1007938. <https://doi.org/10.1371/journal.ppat.1007938>
- Watterson, D., Modhiran, N., & Young, P. R. (2016). The many faces of the flavivirus NS1 protein offer a multitude of options for inhibitor design. *Antiviral Res*, *130*, 7-18. <https://doi.org/10.1016/j.antiviral.2016.02.014>
- Welsch, S., Miller, S., Romero-Brey, I., Merz, A., Bleck, C. K., Walther, P., Fuller, S. D., Antony, C., Krijnse-Locker, J., & Bartenschlager, R. (2009). Composition and three-dimensional architecture of the dengue virus replication and assembly sites. *Cell host & microbe*, *5*(4), 365-375. <https://doi.org/10.1016/j.chom.2009.03.007>
- Wells, J. A., Vasser, M., & Powers, D. B. (1985). Cassette mutagenesis: an efficient method for generation of multiple mutations at defined sites. *Gene*, *34*(2-3), 315-323. [https://doi.org/10.1016/0378-1119\(85\)90140-4](https://doi.org/10.1016/0378-1119(85)90140-4)
- Whitehead, S. S., Blaney, J. E., Durbin, A. P., & Murphy, B. R. (2007). Prospects for a dengue virus vaccine. *Nature Reviews Microbiology*, *5*(7), 518-528. <https://doi.org/10.1038/nrmicro1690>
- WHO (2009). Dengue Guidelines for Diagnosis, Treatment, Prevention and Control. Third edition. World Health Organisation and the Special Programme for Research and Training in Tropical Diseases (TDR) 1-147
- World Health Organization. Dengue vaccine: WHO position paper - July 2016. *Wkly Epidemiol Rec* (2016);91:349–64.

- WHO. Dengue and Severe Dengue Facts Sheets; World Health Organization: Geneva, Switzerland, (2020).
- Wichmann, O., Vannice, K., Asturias, E. J., de Albuquerque Luna, E. J., Longini, I., Lopez, A. L., Smith, P. G., Tissera, H., Yoon, I.-K., & Hombach, J. (2017). Live-attenuated tetravalent dengue vaccines: the needs and challenges of post-licensure evaluation of vaccine safety and effectiveness. *Vaccine*, 35(42), 5535-5542. <https://doi.org/10.1016/j.vaccine.2017.08.066>
- Wilder-Smith, A., Ooi, E.-E., Vasudevan, S. G., & Gubler, D. J. (2010). Update on dengue: epidemiology, virus evolution, antiviral drugs, and vaccine development. *Current infectious disease reports*, 12, 157-164. <https://doi.org/10.1007/s11908-010-0102-7>
- Winkler, G., Randolph, V. B., Cleaves, G. R., Ryan, T. E., & Stollar, V. (1988). Evidence that the mature form of the flavivirus nonstructural protein NS1 is a dimer. *Virology*, 162(1), 187-196. [https://doi.org/10.1016/0042-6822\(88\)90408-4](https://doi.org/10.1016/0042-6822(88)90408-4)
- Winkler, G., Maxwell, S. E., Rueemler, C., & Stollar, V. (1989). Newly synthesized dengue-2 virus nonstructural protein NS1 is a soluble protein but becomes partially hydrophobic and membrane-associated after dimerization. *Virology*, 171(1), 302-305. [https://doi.org/10.1016/0042-6822\(89\)90544-8](https://doi.org/10.1016/0042-6822(89)90544-8)
- Wu, R.-H., Tsai, M.-H., Tsai, K.-N., Tian, J. N., Wu, J.-S., Wu, S.-Y., Chern, J.-H., Chen, C.-H., & Yueh, A. (2017). Mutagenesis of dengue virus protein NS2A revealed a novel domain responsible for virus-induced cytopathic effect and interactions between NS2A and NS2B transmembrane segments. *Journal of virology*, 91(12), e01836-01816. <https://doi.org/10.1128/JVI.01836-16>
- Xie, X., Gayen, S., Kang, C., Yuan, Z., & Shi, P.-Y. (2013). Membrane topology and function of dengue virus NS2A protein. *Journal of virology*, 87(8), 4609-4622. <https://doi.org/10.1128/JVI.02424-12>
- Xie, X., Zou, J., Wang, Q.-Y., Noble, C. G., Lescar, J., & Shi, P.-Y. (2014). Generation and characterization of mouse monoclonal antibodies against NS4B protein of dengue virus. *Virology*, 450, 250-257. <https://doi.org/10.1016/j.virol.2013.12.025>
- Xie, X., Zou, J., Zhang, X., Zhou, Y., Routh, A. L., Kang, C., Popov, V. L., Chen, X., Wang, Q.-Y., & Dong, H. (2019). Dengue NS2A protein orchestrates virus assembly. *Cell host & microbe*, 26(5), 606-622. e608. <https://doi.org/10.1016/j.chom.2019.09.015>
- Yap, S. S., Nguyen-Khuong, T., Rudd, P. M., & Alonso, S. (2017). Dengue virus glycosylation: what do we know? *Frontiers in microbiology*, 8, 1415. <https://doi.org/10.3389/fmicb.2017.01415>
- Yin, Y., Jiang, L., Fang, D., Jiang, L., & Zhou, J. (2013). Differentially expressed genes of human microvascular endothelial cells in response to anti-dengue virus NS1 antibodies by suppression subtractive hybridization. *Viral immunology*, 26(3), 185-191. <https://doi.org/10.1089/vim.2012.0063>
- Youn, S., Ambrose, R. L., Mackenzie, J. M., & Diamond, M. S. (2013). Non-structural protein-1 is required for West Nile virus replication complex formation and viral RNA synthesis. *Virology journal*, 10(1), 1-14. <https://doi.org/10.1186/1743-422X-10-339>
- Young, P.R.; Hilditch, P.A.; Bletchly, C.; Halloran, W. An antigen capture enzyme-linked immunosorbent assay reveals high levels of the dengue virus protein NS1 in the sera of infected patients. *J. Clin. Microbiol.* (2000), 38, 1053–1057. <https://doi.org/10.1128/jcm.38.3.1053-1057.2000>
- Young, L. B., Balmori Melian, E., & Khromykh, A. A. (2013). NS1' colocalizes with NS1 and can substitute for NS1 in West Nile virus replication. *Journal of virology*, 87(16), 9384-9390. <https://doi.org/10.1128/JVI.01101-13>
- Yu, I.-M., Holdaway, H., Chipman, P., Kuhn, R., Rossmann, M., & Chen, J. (2009). Association of the pr peptides with dengue virus at acidic pH blocks membrane fusion. *Journal of virology*, 83(23), 12101-12107. <https://doi.org/10.1128/JVI.01637-09>
- Yu, C.-Y., Chang, T.-H., Liang, J.-J., Chiang, R.-L., Lee, Y.-L., Liao, C.-L., & Lin, Y.-L. (2012). Dengue virus targets the adaptor protein MITA to subvert host innate immunity. *PLoS pathogens*, 8(6), e1002780. <https://doi.org/10.1371/journal.ppat.1002780>

Zhang, W., Chipman, P. R., Corver, J., Johnson, P. R., Zhang, Y., Mukhopadhyay, S., Baker, T. S., Strauss, J. H., Rossmann, M. G., & Kuhn, R. J. (2003). Visualization of membrane protein domains by cryo-electron microscopy of dengue virus. *Nature Structural & Molecular Biology*, *10*(11), 907-912. <https://doi.org/10.1038/nsb990>

Zou, J., Lee, L. T., Wang, Q. Y., Xie, X., Lu, S., Yau, Y. H., Yuan, Z., Geifman Shochat, S., Kang, C., & Lescar, J. (2015). Mapping the interactions between the NS4B and NS3 proteins of dengue virus. *Journal of virology*, *89*(7), 3471-3483. <https://doi.org/10.1128/JVI.03454-14>